

# Exploring Ultracold Quantum Many-Body Systems with Multi-Layer Multi-Configurational Approaches

Dissertation  
zur Erlangung des Doktorgrades  
an der Fakultät für Mathematik,  
Informatik und Naturwissenschaften,  
Fachbereich Physik  
der Universität Hamburg

vorgelegt von  
Fabian Köhler

Hamburg

2023

---

Gutachter/innen der Dissertation

Prof. Dr. Peter Schmelcher  
Prof. Dr. Michael Potthoff

Zusammensetzung der Prüfungskommission

Prof. Dr. Daniela Pfannkuche  
Prof. Dr. Peter Schmelcher  
Prof. Dr. Michael Potthoff  
Prof. Dr. Henning Moritz  
Dr. Thore Posske

Vorsitzende/r der Prüfungskommission

Prof. Dr. Daniela Pfannkuche

Datum der Disputation

19.01.2024

Vorsitzende/r Fach-Promotionsausschuss Physik

Prof. Dr. Markus Drescher

Leiter/in des Fachbereichs Physik

Prof. Dr. Wolfgang J. Parak

Dekan/in der Fakultät MIN

Prof. Dr.-Ing. Norbert Ritter

Persistent identifier: [urn:nbn:de:gbv:18-ediss-114975](https://nbn-resolving.org/urn:nbn:de:gbv:18-ediss-114975)

# Abstract

QUANTUM gases of ultracold atoms are ubiquitous in modern physics as they offer excellent isolation from the environment as well as fine-grained control over their relevant characteristics such as interparticle interactions. Almost arbitrary spatial arrangements of these particles can be realized and manipulated by employing external potentials. This versatility renders ultracold atoms an ideal platform for the simulation of other quantum system as well as promising candidates in the field of quantum information. However, the corresponding theoretical description usually involves complex many-body problems which can rarely be solved analytically, thus rendering the development of powerful numerical approaches crucial.

The present thesis employs the family of [multi-layer multi-configuration time-dependent Hartree \(ML-MCTDH\)](#) methods in order to simulate ultracold quantum many-body systems. While this class of ab-initio approaches originates from the description of molecular dynamics in quantum chemistry, it was later applied to a plethora of other problems and extended to capture indistinguishable particles such as ultracold atoms. The strength of this class of algorithms stems from the fact that they employ variationally optimal, time-dependent basis functions in order to obtain a compact representation of the many-body wave function. The construction of hierarchical multi-layer ansätze allows for the treatment of large and complex composite quantum systems. The present thesis focuses on the development of methodological and implementational improvements as well as the application of the method to novel scenarios.

Even though [ML-MCTDH](#) methods can often yield compact representations of the many-body wave function, they too cannot escape the exponential scaling of computational complexity as the number of particles increases or when strong correlations in the system require numerous basis functions in order to obtain accurate results. In recent years, various different approaches have been proposed to tackle this problem and reduce the numerical effort. Unfortunately, these schemes cannot be easily transferred to ultracold atom setups or are unable to adapt to non-trivial dynamics. Hence, a novel dynamical pruning approach targeting bosonic particles is developed in the scope of the present thesis. The scheme automatically selects the most relevant many-body states and adapts to the time-evolution of the system. The algorithm is benchmarked using two typical scenarios motivated from ultracold atom physics and found to capture the physics accurately while significantly reducing the computational effort in some cases.

A particularly fascinating aspect of quantum simulation is the emulation ultrafast processes such as electronic dynamics with slower-moving atomic particles. In light of this strategy, controlled collisions of ultracold atoms confined in moving potential wells may serve as a test bed to unravel the fundamental processes in atom-atom collisions by taking on the role of electrons. Furthermore, similar scenarios have been proposed as a means to generate entanglement and implement quantum gates in the context of quantum computing. Therefore, the second focus of the present dissertation is to investigate the nonequilibrium dynamics of bosonic particles in colliding potential wells which can be realized experimentally using optical tweezers. This study illuminates the

---

main signatures of the dynamics such as entanglement build-up as well as the transport and untrapping of particles.

Quantum spin models are relevant in many areas of physics such as quantum information or condensed matter physics and have been realized experimentally using ultracold atoms or in the related field of Rydberg atoms, among others. The theoretical description of these systems is often challenging, especially when disorder comes into play. Disorder can result in a high level of degeneracy in the low-energy spectrum and the violation of the so-called area law of entanglement entropy which is a fundamental assumption of many numerical approaches, such as those based on matrix product states. The present thesis studies how the [ML-MCTDH](#) method can handle such scenarios by computing the ground states of different disordered models and comparing the results with other established numerical approaches. [ML-MCTDH](#) is found to yield accurate results even in the presence of strong disorder and should be considered as another promising approach for the investigation of quantum spin systems.

# Zusammenfassung

ULTRAKALTE atomare Quantengase sind aufgrund ihrer exzellenten Isolation von der Umgebung und der präzisen Kontrollierbarkeit ihrer relevanten Eigenschaften wie der Wechselwirkung zwischen den Teilchen in vielen Bereichen der modernen Physik allgegenwärtig. Unter Verwendung externer Potenziale lassen sich nahezu beliebige räumliche Anordnungen dieser Partikel realisieren und manipulieren. Diese Vielseitigkeit macht ultrakalte Atome zu einer idealen Plattform zur Simulation anderer Quantensysteme und zu vielversprechenden Kandidaten im Bereich der Quanteninformationstechnologie. Eine entsprechende theoretische Beschreibung solcher Systeme beinhaltet jedoch meist komplexe Vielteilchenprobleme, die selten analytisch gelöst werden können. Aus diesem Grund ist die Entwicklung leistungsfähiger numerischer Ansätze von essentieller Bedeutung.

Die vorliegende Arbeit verwendet [multi-layer multi-configuration time-dependent Hartree \(ML-MCTDH\)](#) Methoden, um ultrakalte Vielteilchensysteme zu simulieren. Diese Familie von ab initio Algorithmen stammt aus dem Bereich der Quantenchemie zur Beschreibung molekularer Dynamik, wurde aber später auf eine Vielzahl anderer Probleme ausgeweitet und um die Beschreibung ununterscheidbarer Teilchen erweitert. Die Stärke dieser Methoden beruht auf der Verwendung von variationell optimalen, zeitabhängigen Basisfunktionen, um eine kompakte Repräsentation der Vielteilchenwellenfunktion zu erhalten. Durch die Konstruktion hierarchischer, mehrschichtiger Ansätze lassen sich komplexe zusammengesetzte Quantensysteme mit vielen Freiheitsgraden behandeln. Die vorliegende Thesis setzt sich mit der Entwicklung methodischer und implementierungstechnischer Verbesserungen sowie der Anwendung der Methode auf neuartige System auseinander.

Wenngleich [ML-MCTDH](#) Methoden in vielen Fällen zu einer kompakten Darstellung der Vielteilchenwellenfunktion führen, können auch sie dem exponentiellen Anstieg des numerischen Aufwands nicht entkommen, der mit der Erhöhung der Teilchenzahl einhergeht oder wenn signifikante Korrelationen eine Vielzahl an Basisfunktionen erfordern. In den letzten Jahren wurden verschiedene Ansätze vorgeschlagen, um die Rechenzeit der Methoden weiter zu reduzieren. Allerdings lassen sich diese Schemata nicht ohne weiteres auf ultrakalte Atome übertragen oder sind für nicht-triviale Dynamik ungeeignet. Im Rahmen der vorliegenden Arbeit wird deshalb ein neuartiger Beschneidungsalgorithmus für bosonische Ensembles entwickelt, der die wichtigsten Vielteilchenzustände automatisch selektiert und diese Auswahl dynamisch an die Zeitentwicklung des Systems anpasst. Anhand zweier typischer Szenarien aus dem Feld der ultrakalten Atome wird demonstriert, dass die Methode die Physik akkurat beschreibt und in einigen Fällen den numerischen Aufwand deutlich reduziert.

Ein besonders faszinierender Aspekt der Quantensimulation ist die Möglichkeit ultraschnelle Prozesse wie die Dynamik von Elektronen mit langsameren, atomaren Teilchen zu emulieren. Vor diesem Hintergrund können kontrollierte Kollisionen ultrakalter Atome in bewegten Potentialtöpfen zum Verständnis der fundamentalen Prozesse in Zusammenstößen zwischen Atomen beitragen, in dem sie die Rolle von Elektronen übernehmen.

---

Darüber hinaus wurden ähnliche Szenarien zur Erzeugung von Quantenverschränkung und der Realisierung von Quantengattern im Rahmen der Quanteninformationsverarbeitung vorgeschlagen. Deshalb setzt sich die vorliegende Dissertation in einem zweiten Schwerpunkt mit der Nichtgleichgewichtsdynamik bosonischer Teilchen in kollidierenden Potentialtöpfen auseinander, die experimentell mit optischen Pinzetten realisiert werden können. Diese Studie beleuchtet die wichtigsten Signaturen der Dynamik wie der Erzeugung von Quantenverschränkung, dem Teilchentransport und dem Entkommen der Partikel aus den Potentialen.

Quantenspinmodelle tauchen in vielen Bereichen der Physik wie der Quanteninformation oder der kondensierten Materie auf und wurden experimentell unter anderem mit ultrakalten Quantengasen und Rydberg-Atomen realisiert. Die theoretische Beschreibung dieser Systeme ist anspruchsvoll, insbesondere wenn Unordnung zu einem hohen Ausmaß an Entartung im Niederenergiespektrum führt. Dies kann in einer Verletzung des Flächen-Gesetzes der Verschränkungsentropie resultieren, dessen Gültigkeit eine fundamentale Annahme vieler numerischer Ansätze darstellt, zum Beispiel von Methoden die auf Matrix-Produkt-Zuständen basieren. Aus diesem Grund untersucht die vorliegende Arbeit in einem dritten Fokus, inwiefern [ML-MCTDH](#) solche Szenarien bewältigen kann. Zu diesem Zweck werden die Grundzustände verschiedener ungeordneter Modelle berechnet und die Resultate mit anderen etablierten Methoden verglichen. Es zeigt sich, dass [ML-MCTDH](#) auch in der Gegenwart von starker Unordnung genaue Ergebnisse liefert und daher als ein weiterer vielversprechender Ansatz zur Beschreibung von Quantenspinsystemen in Betracht gezogen werden sollte.

# Contents

<b>Abbreviations</b>	<b>IX</b>
<b>List of Figures</b>	<b>XI</b>
<b>Preface</b>	<b>XIII</b>
<b>1. Ultracold Atom Physics</b>	<b>1</b>
1.1. Overview of Ultracold Atom Physics . . . . .	1
1.2. Theoretical Description of Ultracold Atoms . . . . .	5
<b>2. Theoretical Framework</b>	<b>11</b>
2.1. Time-Dependent Variational Principles . . . . .	12
2.2. The Standard Method . . . . .	13
2.3. The Multi-Configuration Time-Dependent Hartree Method . . . . .	14
2.3.1. Wave Function Ansatz . . . . .	15
2.3.2. Constraint Operator . . . . .	17
2.3.3. Equations of Motion . . . . .	17
2.3.4. Mode Combination . . . . .	20
2.4. The Multi-Layer MCTDH Method . . . . .	21
2.5. Tensor Network States . . . . .	22
2.6. Primitive Bases . . . . .	26
2.6.1. Finite Basis Representation . . . . .	26
2.6.2. Discrete Variable Representation . . . . .	27
2.6.3. Fast Fourier Transform . . . . .	28
2.6.4. Spin Basis . . . . .	29
2.7. The MCTDH Method for Bosons . . . . .	29
2.7.1. Wave Function Ansatz . . . . .	30
2.7.2. Structure of the Hamiltonian . . . . .	31
2.7.3. Equations of Motion . . . . .	32
2.7.4. Multi-Layer MCTDHX . . . . .	33
2.7.5. ML-MCTDH in Second Quantization Representation . . . . .	34
2.8. Relaxation Procedures . . . . .	36
2.8.1. Energy Relaxation . . . . .	36
2.8.2. Improved Relaxation Algorithm . . . . .	37
2.8.3. Relaxation in Second Quantization Representation . . . . .	38
<b>3. Outlines of Scientific Contributions</b>	<b>41</b>
3.1. Dynamical Pruning of the Non-Equilibrium Quantum Dynamics of Trapped Ultracold Bosons . . . . .	41
3.2. Bosonic Quantum Dynamics Following Colliding Potential Wells . . . . .	44
3.3. Exploring Disordered Quantum Spin Models with a Multi-Layer Multi-Configurational Approach . . . . .	46

---

<b>4. Scientific Contributions</b>	<b>49</b>
4.1. Dynamical Pruning of the Non-Equilibrium Quantum Dynamics of Trapped Ultracold Bosons . . . . .	49
4.2. Bosonic Quantum Dynamics Following Colliding Potential Wells . . . . .	64
4.3. Exploring Disordered Quantum Spin Models with a Multi-Layer Multi-Configurational Approach . . . . .	76
<b>5. Conclusion &amp; Outlook</b>	<b>89</b>
5.1. Methodological Perspectives . . . . .	89
5.2. Implementational Improvements . . . . .	91
5.3. Future Applications . . . . .	92
<b>Bibliography</b>	<b>95</b>
<b>A. Multi-Layer MCTDH Details</b>	<b>155</b>
<b>B. Natural Orbital Gauge for MCTDHB</b>	<b>159</b>
<b>C. Diagonalization Gauge for MCTDHB</b>	<b>163</b>
<b>Acknowledgements</b>	<b>165</b>
<b>Eidesstattliche Versicherung/Declaration on Oath</b>	<b>167</b>



# Abbreviations

**BEC** Bose-Einstein condensate

**CMF** constant mean-field

**DMRG** density matrix renormalization group method

**DOF** degree of freedom

**DVR** discrete variable representation

**EOM** equation of motion

**FBR** finite basis representation

**FFT** fast Fourier transform

**MCTDH** multi-configuration time-dependent Hartree

**MCTDHB** multi-configuration time-dependent Hartree method for bosons

**MCTDHF** multi-configuration time-dependent Hartree method for fermions

**MERA** mutli-scale entanglement renormalization ansatz

**ML-MCTDH** multi-layer multi-configuration time-dependent Hartree

**ML-MCTDHX** multi-layer multi-configuration time-dependent Hartree method for mixtures

**MPS** matrix product state

**PEPS** projected entangled pair state

**RAS** restricted active space

**SPF** single particle function

**SQR** second quantization representation

**TDVP** time-dependent variational principle

**TFIM** transverse field Ising model

**VMF** variable mean-field



# List of Figures

1.1. Examples of protocols to trigger nonequilibrium dynamics. . . . .	6
2.1. Tree diagram for the standard wave packet ansatz. . . . .	13
2.2. Illustration of the concept of an active space. . . . .	15
2.3. Tree diagram of a <b>MCTDH</b> wave function. . . . .	16
2.4. Tree diagram of a <b>MCTDH</b> wave function with mode combination. . . . .	21
2.5. Exemplary tree diagram of a <b>ML-MCTDH</b> wave function. . . . .	22
2.6. Diagrams of different tensor network states. . . . .	25
2.7. Tree diagram for the <b>MCTDHB</b> wave function ansatz. . . . .	31
2.8. Tree diagram of the <b>ML-MCTDHX</b> wave function for a binary mixture. . . . .	34
2.9. Convergence behavior of (improved) relaxation. . . . .	36
3.1. Partitioning of the Hamiltonian in dynamical pruning of <b>MCTDHB</b> . . . . .	42
3.2. Dynamical scenarios for benchmarking dynamical pruning of <b>MCTDHB</b> . . . . .	43
3.3. Sketch of the dynamical setup studied in [FK2]. . . . .	45
5.1. Collision between a moving projectile well loaded with ultracold bosons and a lattice of multiple stationary wells. . . . .	93
A.1. Detailed tree diagram of a <b>ML-MCTDH</b> wave function. . . . .	156



# Preface

## Publications of the Present Cumulative Dissertation

The present cumulative dissertation is based on the following publications:

- [FK1] F. Köhler et al. “Dynamical Pruning of the Non-Equilibrium Quantum Dynamics of Trapped Ultracold Bosons”. In: *J. Chem. Phys.* 151.5 (Aug. 5, 2019), p. 054108. ISSN: 0021-9606. DOI: [10.1063/1.5104344](https://doi.org/10.1063/1.5104344).
- [FK2] F. Köhler and P. Schmelcher. “Bosonic Quantum Dynamics Following Colliding Potential Wells”. In: *Phys. Rev. A* 103.4 (Apr. 20, 2021), p. 043326. DOI: [10.1103/PhysRevA.103.043326](https://doi.org/10.1103/PhysRevA.103.043326).
- [FK3] F. Köhler, R. Mukherjee, and P. Schmelcher. “Exploring Disordered Quantum Spin Models with a Multilayer Multiconfigurational Approach”. In: *Phys. Rev. Res.* 5.2 (May 30, 2023), p. 023135. DOI: [10.1103/PhysRevResearch.5.023135](https://doi.org/10.1103/PhysRevResearch.5.023135).

## Declaration of Personal Contributions

When I joined the group of Prof. Dr. P. Schmelcher in 2017, the research community around the [ML-MCTDH](#) family of methods was actively exploring approaches to lower the computational cost by employing various truncation and pruning schemes. Since most of these schemes are not suited for the dynamics of trapped bosonic systems with [MCTDHB](#), ideas to develop new approaches to select the most relevant many-body configurations were discussed within the group. Inspired by these meetings, I proposed a straightforward scheme based on simple selection rules of the important bosonic number states. The implementation, numerical studies, and data analysis were conducted by me. Dr. S. Mystakidis and Dr. K. Keiler contributed by suggesting the model systems to benchmark the method and good choices for the involved parameters as well as discussing the involved physics with me. Prof. Dr. H.-D. Meyer provided valuable feedback and helped to formalize parts of the approach. The manuscript [[FK1](#)] was prepared by me with subsequent edits and improvements by all co-authors.

The idea of studying bosonic particles trapped in colliding potential wells [[FK2](#)] was suggested to me by Prof. Dr. P. Schmelcher. The development of the model system, implementation, numerical studies, and data analysis were performed by me. The manuscript was also prepared by me with subsequent edits and improvements by Prof. Dr. P. Schmelcher.

The idea for the simulation of quantum spin models with [ML-MCTDH](#) [[FK3](#)] was developed by me during my implementation of the [SQR](#) feature in our code for the simulation of bosonic lattice systems. Prof. Dr. P. Schmelcher encouraged me to pursue this direction due to the growing interest in quantum spin systems within the group in the context of quantum computing with Rydberg atoms. Dr. R. Mukherjee joined the group later and proposed to push the project much further by studying challenging,

---

disordered models. The implementation, numerical studies, and data analysis were performed by me. Dr. R. Mukherjee and I closely collaborated on the preparation of the manuscript which was subsequently edited and improved by Prof. Dr. P. Schmelcher.

All three projects were closely accompanied by Prof. Dr. P. Schmelcher who provided valuable feedback and guidance at all times.

## Structure of the Present Dissertation

The present cumulative dissertation is structured as follows: Chapter 1 provides an overview of the field of ultracold atom physics and the theoretical methods that can be employed to solve the involved quantum many-body problems. Chapter 2 reviews the theoretical framework of [multi-layer multi-configuration time-dependent Hartree \(ML-MCTDH\)](#) methods which are applied to bosonic systems and spin models in the present thesis. Chapter 3 outlines the scientific contributions [[FK1–FK3](#)] and Chapter 4 includes the corresponding complete manuscripts. Finally, Chapter 5 summarizes the results and provides an outlook on future perspectives.

# Ultracold Atom Physics

ULTRACOLD atoms are a ubiquitous tool in modern physics and the subject of a vast number of experimental as well as theoretical studies. Section 1.1 provides a brief history of the development of the field and highlights some of the most important milestones as well as prominent applications. Section 1.2 introduces the different theoretical and numerical approaches that can be used to study the involved many-body problems.

## 1.1. Overview of Ultracold Atom Physics

Inspired by Bose's work [1] on Planck's law of black body radiation [2], Einstein developed a quantum theory of an ideal gas of indistinguishable particles with integer spin also known as bosons [3, 4]. One of the most striking predictions of this theory is the existence of a peculiar state of matter at extremely low temperatures, the [Bose-Einstein condensate \(BEC\)](#), which is characterized by an occupation of the lowest quantum state by a macroscopic number of particles. In this phase, the atoms condense into a single quantum state and exhibit a coherent matter wave behavior that can be described by a single macroscopic wave function. Early on, the formation of [BECs](#) was suspected to play a crucial role for the understanding of superfluidity in liquid  $^4\text{He}$  [5] as well as in the so-called BCS theory [6, 7] that explains conventional superconductivity by the condensation of bosonic quasiparticles called Cooper pairs.

Even though the theory of Bose gases was developed in the 1920s, it took until 1995 before the first experimental realizations of [BECs](#) were achieved in gases of ultracold sodium atoms in the group of Ketterle [8] and rubidium atoms in the group of Cornell and Wiemann [9] for which they have been awarded the 2001 Nobel Prize in physics<sup>1</sup>. The preparation of such systems required the development of experimental techniques to cool atoms to very low temperatures which includes evaporative cooling [15–18] as well as optical cooling such as Doppler [19, 20], Sisyphus [21] or Raman [22, 23] cooling. In order to prevent the atomic cloud from dispersing, external potentials are used to confine the particles. Over the years, scientists have devised different trapping methods such as magnetic [24] or magneto-optical [25–30] traps. For their contributions to the development of cooling and trapping techniques for neutral atoms, the 1997 Nobel Prize in physics was awarded to Chu, Cohen-Tannoudji and Phillips [31–33].

Nowadays, ensembles of ultracold atoms can be realized with a controlled number of particles [34–36] in almost arbitrarily shaped external potentials [37] including optical lattices [38–41] or harmonic [42] and ring traps [43]. Tuning the confinement of the particles allows the creation of one- [44–47], two- [44, 48, 49] or three-dimensional [50,

---

<sup>1</sup>Since then, [BECs](#) have been realized in various other physical systems including photons in microcavities [10] or quasi particles such as polaritons [11–13] and magnons [14].

[51] systems. Optical tweezers allow for the manipulation of atomic clouds [52–56] as well as individual atoms [36, 57] while tweezer arrays [54, 58, 59] allow for the design of complex spatial arrangements of particles. Quantum gas microscopy provides a tool for the high-resolution imaging of the spatial distribution [60–66] of ultracold atoms. Furthermore, this technique enables access to correlation properties [67–69] as well as the detection of single particles [70, 71]. Feshbach [72, 73] and confinement-induced [74–77] resonances provide fine-grained control over the interparticle interactions, thus providing access to different physical regimes.

Inspired by this experimental progress, the fundamental properties of ultracold bosons have been studied in great detail, including elementary excitations [78] such as solitons [79–82] and vortices [81, 83], as well as collective modes of the whole gas [78, 84–87]. The dynamics and static features of ultracold atoms in various different trapping potentials are the subject of many experimental and theoretical studies. For example, the dynamics of bosons in a double-well exhibits interesting effects such as correlated pair tunneling [88–90], self trapping [91–93] or the Josephson effect [91, 94] originally known from superconductors [95]. Another common scenario is the investigation of bosons trapped in an optical lattice which can undergo a transition from a superfluid to a Mott insulating phase [50, 96] and exhibit phenomena like unconventional, multi-orbital superfluidity as well [97–99]. The nonequilibrium dynamics of lattice setups poses interesting questions regarding thermalization [47, 100–103], ballistic versus diffusive expansion of an atomic cloud [104, 105] and other peculiar transport processes [106–109]. Strong repulsive interactions between the particles can lead to the formation of a so called Tonks-Girardeau gas of fermionized bosons [110, 111] which has been observed experimentally in optical lattices [46, 112]. The phenomenon of superfluidity was a large driving force for the development of the field of ultracold atoms and lead to the discovery of other exotic states of matter in recent times. One example is the formation of quantum droplets [113] in dipolar dysprosium [114–120] and erbium [121] BECs. Here, the competition between long-range dipole-dipole attraction and a stabilizing repulsion induced by quantum fluctuations [122] leads to the formation of self-bound droplets. Very recently, supersolids, i.e., spatially ordered matter with superfluid properties, have been observed in BECs of atoms with large magnetic dipole moments [123–125]. Their existence has been conjectured for many decades [126–128], but their realization remained elusive for a long time [129–131]. The control over the particle number in ultracold atom experiments allows for the realization of few-body systems. While the physical behavior of such microscopic ensembles can serve as an ingredient for our understanding of many-body physics [132–136], they exhibit a rich phenomenology of their own [137]. For example, ultracold few-body systems serve as a test bed for Efimov physics [138] that predicts the existence of three-body bound states [139, 140] which have been confirmed experimentally with ultracold cesium [141, 142], potassium [143] and lithium [144] atoms.

The realization of mixtures of different, distinguishable atomic species is of great interest in the research of ultracold atoms as they provide a rich landscape of physical phenomena. By employing different elements [145–150], isotopes [151–156] or hyperfine states [157–165] binary Bose-Bose [166, 167], Fermi-Fermi [168, 169], and Bose-Fermi mixtures [170–173] have been prepared in the laboratory. The fundamental properties of atomic mixtures including collective [160, 174, 175] and elementary excitations, such as solitary waves [161, 162, 176], have been examined in experimental and theoretical studies. By controlling the interactions between and within the different atomic species in



a Bose-Bose mixture, different physical regimes can be realized [177]. Especially scenarios involving a sizeable interspecies interaction are of great interest. The entangled composite fermionization regime [178–180] occurs for weak intraspecies interactions in which the two gases segregate as a whole. Strong interactions within both species lead to full fermionization [181–183] in which the system can be mapped to an ideal Fermi gas [177], analogue to the Tonks-Girardeau gas [110, 111]. One of the key features of composite mixtures is that they can undergo a miscible-immiscible transition as the interspecies interaction is tuned while one of the intraspecies interactions is weak [157, 158, 184–190] providing control over the phase separation. This phenomenon is closely linked to the dynamical formation of domains [191–193] and certain vortex patterns [191, 194]. Furthermore, control of the phase separation is of immediate experimental relevance in the context of sympathetic cooling [195, 196] where the cooling of an atomic gas is affected by the presence of a second species.

Other highlights in the exploration of binary mixtures include the formation of deeply bound dipolar molecules [197–199] or the formation of quantum droplets [164, 165] based on a competition between attractive interspecies and repulsive intraspecies interactions [113]. Similar to scenarios considering a single atomic species, the few-body regime of binary mixtures exhibits a rich phenomenology. For example, the highly particle number imbalanced case of a few impurity particles immersed in a bath of majority particles, serves as a test bed for polaron physics [169, 200–208] which plays a key role in semiconductors [209–212] and superconducting materials [213–216]. Furthermore, heteronuclear Efimov states have been observed in ultracold atoms [217–219], extending the previously studied homonuclear setups [141–144]. More recently, mixtures comprising more than two components such as triple mixtures have been realized as well [220–223].

Their excellent tunability and isolation from the environment renders ultracold atoms an ideal platform to simulate a plethora of other quantum systems [224–226]. Recent experiments have linked them to interesting questions in condensed matter physics [227–231] including topological matter [232, 233] and high temperature superconductivity [234]. By exploiting the fact that dynamical processes of atoms occur on much slower time scales compared to electron dynamics, ultra-fast processes such as molecular dynamics [235] or light-matter interaction [236–238] have been emulated. Applications inspired from elementary particle physics cover among others the zitterbewegung of Dirac particles [239, 240], Schwinger pair production [241] or quarks [242, 243]. Furthermore, ultracold Fermionic atoms have been employed to model the low-density crusts of neutron stars [244, 245] and analogues to black holes have been discovered in BECs [246, 247]. The field of atomtronics [248, 249] focuses on the development of atomic analogues for electronic devices such as transistors and diodes by employing ultracold atoms. Furthermore, the link between ultracold neutral atoms and topological matter has been established [233, 250] by creating artificial gauge fields in optical lattices. Historically, laser-induced tunneling [38, 251] has been proposed to create synthetic magnetic fields [252, 253] or spin-orbit couplings [254–257] leading to the realization of topological band structures [257–260]. Other approaches rely on exploiting internal states of atoms such as hyperfine states to implement synthetic dimensions [261–263] where the different sublevels serve as fictitious lattice sites, potentially allowing to study topological effects associated with higher dimensions, such as the four-dimensional quantum Hall effect [264]. A different direction, coined Floquet engineering, employs time-periodic modulations of quantum systems to create topological band structures [265–267]. For example, artificial gauge fields can be induced by shaking optical lattices containing

ultracold atoms [232, 268–270].

Ultracold neutral atoms are a promising platform for the rapidly emerging field of quantum technologies that encompasses quantum communication, computing, simulation and sensing. In this domain, academic researchers and commercial stakeholders strive to exploit the unique properties of quantum physics in order to develop applications that could directly impact many areas of industry and everyday life. In the realm of quantum sensing and metrology, ultracold atoms have been used successfully to develop different kinds of very precise sensors [271] such as gravimeters [272, 273], motion detectors [274], gyroscopes [275] and sensors for electromagnetic fields [276, 277]. Optical clocks based on ultracold neutral atoms in free fall [278, 279] or trapped in optical lattices [280] have already reached excellent accuracy, closing in on cesium fountain clocks. Various ways of implementing quantum spin models using ultracold neutral atoms have been proposed, rendering them an interesting platform for the field of quantum simulation and computing [51, 226, 281].

Many of the advances regarding the preparation and control of neutral atom systems, benefited the further development of the related field of Rydberg physics which is concerned with the study of Rydberg atoms [282], i.e., neutral atoms with one or more valence electrons excited to a very high principal quantum number  $n$ . Nowadays, experimentalists are able to realize states with  $n \approx 300$  in the laboratory [283] while astronomical measurements have discovered carbon atoms with  $n \approx 1000$  in the remnants of supernovae [284]. Rydberg states are equipped with a rather long radiative lifetimes that scale as  $n^3$  and which are typically in the order of  $100 \mu\text{s}$  for  $n \approx 50$  [285]. Throughout most of the 20th century, researchers focused on the fundamental properties of Rydberg atoms such as their spectra [286, 287], interactions with electromagnetic fields [288, 289] as well as their collisional behavior [290–294].

Compared to ground state atoms, Rydberg states exhibit exaggerated characteristics. The extent of the electronic cloud scales as  $n^2$  with the principal quantum number and the large distance between the Rydberg electron and the atomic core leads to significant electric and magnetic dipole moments. The resulting susceptibility of Rydberg atoms to electromagnetic fields was exploited by Haroche et al. in their experiments investigating the creation and annihilation of photons in cavities, which was awarded with the 2012 Nobel Prize in Physics [295]. The development of refined cooling and trapping techniques for ultracold neutral atoms [31–33] culminating in the first realizations of BECs [8, 9] further accelerated the development of Rydberg physics. In this context, the year of 2000 is of particular significance as the publication of three seminal papers marked a turning point for the importance of Rydberg atoms for modern physics. Firstly, the blockade mechanism [296] suppresses the excitation of additional Rydberg atoms in the vicinity of an already excited atom [297–302]. Secondly, in a similar spirit laser coupling to a Rydberg level allows control over the interaction between two ground state atoms [303], a process known as Rydberg dressing [304–308]. Finally, a novel molecular binding mechanism between Rydberg and ground state atoms was predicted [309] which leads to the formation ultra-long-range Rydberg molecules [310–313].

In recent years, Rydberg atoms have become a promising platform for the development of quantum technologies. Due to their high sensitivity to external fields, caused by their large dipole moments, Rydberg atoms are useful for the development of sensors for electric and magnetic fields [277] in the context of quantum sensing [314]. The implementation of single-photon switches [315–317] and transistors [318] renders Rydberg atoms a potential building block of complex quantum networks in the context of quan-

tum communication. In a similar spirit, photon-photon gates have been realized using Rydberg atoms [319–321] and can serve as component in the design of photonic quantum computers and simulators [322–324]. Additionally, Rydberg atoms pose a promising platform for the implementation of quantum simulators [224, 325] and computers [285, 326–329] in their own right. Arrays of optical tweezers have already been employed to achieve large numbers of Rydberg qubits [330–335]. The excellent control over the spatial atom arrangement intrinsic to this approach lends itself to the solution of combinatorial optimization problems [328, 336] in the context of variational quantum algorithms such as the quantum approximate optimization algorithm [337]. In this light, disordered spin models such as the ones studied in [FK3] are of particular interest [338–341].

## 1.2. Theoretical Description of Ultracold Atoms

The indisputable success in the experimental preparation of ultracold atom systems necessitates a theoretical many-body description of interacting atoms in the low-energy regime. Unfortunately, the involved many-body problems are not easily solvable, especially when taking realistic atom-atom interactions into account. Therefore, most approaches have to rely on approximations and simplifications. In the following, an overview of the different theoretical approaches is provided.

In general, a quantum system can be described in terms of its density matrix  $\rho(t)$  whose time-evolution is governed by the von Neumann equation. This formalism can capture both pure, and mixed states, such as thermal ensembles. Furthermore, it is useful for the description of open quantum systems<sup>2</sup> [344] which are also relevant for ultracold atom physics [345, 346]. As the present thesis focuses on closed quantum systems in the ultracold regime, i.e., extremely low temperatures  $T \approx 0$ , the system is typically assumed to be in a pure state that can be captured in terms of a wave function  $|\Psi(t)\rangle$ . The time-dependent Schrödinger equation<sup>3</sup> [347]

$$i\partial_t |\Psi(t)\rangle = \hat{H}(t) |\Psi(t)\rangle \quad (1.1)$$

determines the time-evolution of  $|\Psi(t)\rangle$  driven by the generally time-dependent Hamiltonian  $\hat{H}(t)$ . When considering a constant Hamiltonian  $\hat{H}(t) = \hat{H}$ , the solution of the initial value problem given by Eq. (1.1) with respect to some initial state  $|\Psi(0)\rangle$  is given by

$$|\Psi(t)\rangle = e^{-i\hat{H}t} |\Psi(0)\rangle = \sum_i \langle E_j | \Psi(0) \rangle e^{-iE_j t} |E_i\rangle. \quad (1.2)$$

The dynamics is then governed by the eigenenergies  $E_j$  and the eigenstates  $|E_j\rangle$  of  $\hat{H}$  which can be obtained by solving the eigenproblem given by the stationary Schrödinger equation

$$\hat{H} |E_j\rangle = E_j |E_j\rangle. \quad (1.3)$$

While the solutions of Eq. (1.3) provide access to static properties, often the nonequilibrium dynamics of a system is of interest which can be triggered by a variety of protocols (see Fig. 1.1). For example, the system can be prepared in a state that is not an eigenstate

<sup>2</sup>To this end, the von Neumann equation is then extended by dissipative terms that account for the interactions with environment, arriving at master equations such as the famous Lindblad equation [342, 343].

<sup>3</sup>In this work, the convention  $\hbar = 1$  is used.

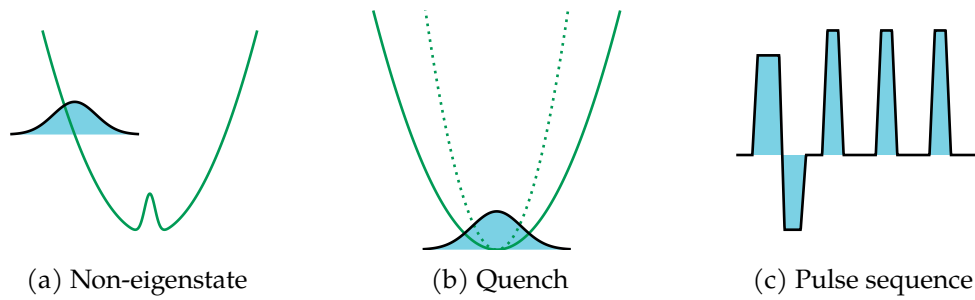


Figure 1.1.: Examples of protocols to trigger nonequilibrium dynamics in a quantum system. (a) The system is initially prepared in a state that is not an eigenstate of the underlying Hamiltonian. (b) A parameter of the system is suddenly changed (quenched), triggering a dynamical response of the system. (c) The system is driven using a time-dependent Hamiltonian. This example shows a sequence of pulses changing one of the parameters of the system, e.g., the strength of an external field.

of the underlying Hamiltonian (see Fig. 1.1a), a physical parameter such as the interaction strength or the shape of the external trap can be changed rapidly in a so-called quantum quench (see Fig. 1.1b) or the system can be driven by a time-dependent Hamiltonian, e.g., a sequence of laser pulses (see Fig. 1.1c). In this context, many interesting questions arise such as the thermalization of the system [102, 348], the build-up of correlations and entanglement as well as the design of optimal control schemes [349, 350].

Solving the Schrödinger Eqs. (1.1) and (1.3) is a formidable task, and analytical solutions are only available for a limited number of systems. Especially when considering many-body systems, approximations and simplifications are inevitable. In typical ultracold atom setups, the scattering length is much smaller than the average interparticle distance and collisions occur at low momenta. Therefore, it is reasonable to assume  $s$ -wave scattering to be the dominant interaction process [78, 351], which can be modeled using a  $\delta$ -potential in one-spatial dimension while regularized potentials have to be employed in higher dimensions [352–359]. Under this assumption, the Schrödinger equation of two bosons subject to a spherically symmetric harmonic potential has been solved analytically [353]. However, this result is of limited usefulness since usually many more atoms are involved. The Lieb-Liniger model [360, 361] employs a Bethe ansatz [362, 363] to describe spinless bosons in one spatial dimension while also considering short-range contact interactions. As it assumes periodic boundary conditions and does not incorporate an external potential, it is not applicable to trapped atoms. In most cases, analytical solutions are not available, rendering the development of powerful numerical approaches crucial.

Exact diagonalization employs numerical algorithms to compute the eigenenergies and eigenstates of the Hamiltonian, thus providing a full description of the quantum system under consideration. It relies on choosing a suitable finite basis set in order to obtain a matrix representation of the Hamiltonian which subsequently can be diagonalized. The computational complexity of solving the full eigenproblem given by an  $n \times n$  matrix scales as  $\mathcal{O}(n^3)$  [364, 365], rendering it a costly operation. Since the number of basis states usually grows exponentially with the number of particles when treating many-body problems, exact diagonalization quickly becomes prohibitively expensive both in terms of required memory and computational time. When studying the static properties of

a system, it is often the case that only a few of the energetically lowest eigenstates are of interest. In this case, iterative methods to compute extremal eigenvalues such as the implicitly restarted Lanczos method [366] or the Davidson algorithm [367] can treat larger systems than general full diagonalization routines. Another advantage of these methods is that they can be implemented matrix-free, i.e., do not require the explicit construction of the Hamiltonian matrix but rather rely on a function that computes the action of the Hamiltonian on a given state vector. In the context of ultracold atoms, exact diagonalization is typically limited to a handful of particles [177, 180, 368–370] such that more advanced tools are required that can represent the wave function in a compact manner when larger many-body systems are of interest.

Another powerful class of numerical schemes for the simulation of ultracold many-body systems that should not go unmentioned, are quantum Monte Carlo methods. A variety of specialized approaches have been developed to describe ground state systems [371–374], finite temperature ensembles [375–379], and real-time dynamics [380, 381]. Fundamentally, these methods all rely on some sort of stochastic sampling of the quantum many-body state or the expectation values of observables. Consequently, they are subject to statistical errors that have to be mitigated by employing sufficiently large sample sizes. Furthermore, most quantum Monte Carlo algorithms can fail to describe fermionic systems due to the so-called sign problem, causing the simulation runtime to increase exponentially with the number of particles [382]. Despite these drawbacks, quantum Monte Carlo methods have seen remarkable success in the description of various quantum systems that are inaccessible to other approaches.

It is often the case that mean-field approaches provide a reasonable approximation of the underlying many-body problem. The Hartree-Fock [383–386] method provides a mean-field description of indistinguishable particles by starting from a single number state given in an initial basis which is subsequently optimized in order to minimize the energy functional, i.e., by solving the stationary Schrödinger equation iteratively. For fermions, the Pauli exclusion principle [387] dictates that every particle has to occupy a different single-particle state, thus uniquely determining the number state of the mean-field ansatz. Bosons on the other hand are not subject to any such constraint and multiple particles can occupy the same single-particle state. Consequently, it is not clear a priori which bosonic number state yields the best mean-field description. A particularly famous Hartree-Fock ansatz for bosons is employed in the framework of the Gross-Pitaevskii equation [388–390] which provides a description of bosons subject to an external potential and contact interactions. In the ultracold regime, a gas of weakly interacting bosons is assumed to be condensed [391], i.e., all particles occupy the same single particle state, i.e.,

$$\Psi(x_1, \dots, x_N, t) = \prod_{i=1}^N \varphi(x_i, t). \quad (1.4)$$

The Gross-Pitaevskii equation can then be derived from this ansatz by applying the variational principle to the corresponding energy functional and reads

$$i\partial_t \Psi(x, t) = \left[ -\frac{1}{2m} \partial_x^2 + V(x) + g|\Psi(x, t)|^2 \right] \Psi(x, t), \quad (1.5)$$

where  $V(x)$  denotes the external potential and  $m$  the particle mass. The nonlinear term  $|\Psi(x, t)|^2 \Psi(x, t)$  accounts for the interaction between the bosons, strength of which is given by  $g = 4\pi a_s/m$  with respect to the  $s$ -wave scattering length  $a_s$ . Equation (1.5)

resembles a nonlinear Schrödinger equation describing an effective one-body problem that can be solved numerically [392]. The Bogoliubov approach [78, 393, 394] can be employed on top of the Gross-Pitaevskii equation in order to describe weak perturbations of the condensate. To this end, one performs a suitable transformation which leads to a description in a picture of quasi-particles, phonons, which represent the elementary excitations of the condensate. The mean-field description provided by the Gross-Pitaevskii framework works remarkably well in the limit of many particles and has been successfully applied to the description of particular BEC excitations [78] such as dark [82, 395, 396] and bright [397, 398] solitons as well as vortices in higher dimensions [399, 400]. By accounting for quantum fluctuations by means of the Lee-Huang-Yang correction [122, 401] an extended Gross-Pitaevskii equation can be derived [114, 121, 402, 403] that is useful for the description of supersolids [123–125] and self-bound quantum droplets [117, 123]. The Gross-Pitaevskii can be generalized to multi-component BECs straightforwardly where it can describe phenomena such as dark-bright solitons [162, 404–406]. Due to its construction, the Gross-Pitaevskii ansatz cannot describe scenarios in which a significant depletion of the condensate occurs, i.e., additional states come into play. Such a fragmentation is usually driven by the build up of substantial interparticle correlations or entanglement and can manifest in defects such as symmetry breaking [407]. The Gross-Pitaevskii description breaks down when considering sizeable interactions among the bosons, e.g., when treating a Tonks-Girardeau gas of fermionized bosons [110, 111] or the Mott insulating phase of bosons trapped in an optical lattice [50, 408]. While in some cases an adequate mean-field description can be obtained by considering multi-orbital ansätze [409–415], more sophisticated beyond-mean-field approaches are essential for the description of correlated systems.

Nowadays, experimentalists possess excellent control over the number of particles [34–36] and scenarios with few particles exhibit rich physics [137] such as the formation of Efimov three-body bound states [138] or impurity physics in the context of atomic mixtures [204, 205, 207, 208]. It is often the case that the system is governed by strong correlations and significant entanglement, especially when investigating non-trivial nonequilibrium dynamics, for example after sizeable quantum quenches [416–419]. In this case, the mean-field picture does not provide an adequate description of the physics and the development of powerful numerical approaches that provide a beyond-mean-field description of many-body systems becomes crucial. The framework of **multi-layer multi-configuration time-dependent Hartree (ML-MCTDH)** [420–423] provides a set of powerful ab initio methods towards the dynamics of many-body wave functions that can take the relevant correlations within the system into account. This family of algorithms originates in quantum chemistry where it was employed to treat high-dimensional molecular dynamics problems [420, 424–428]. The fundamental idea is to employ small sets of time-dependent, variationally optimal basis functions in order to obtain a compact representation of the many-body wave function. The concept of multi-layering [421, 422, 429] is then used to construct complex wave function ansätze that can be tailored towards the underlying problem. Later extensions allow for the treatment of indistinguishable particles, i.e., bosons [430–432] and fermions [430, 433–442], which is fundamental for the description of ultracold atom systems. The present thesis employs **ML-MCTDH** methods for the description of quantum spin models as well as bosonic ensembles. Therefore, Chapter 2 provides a thorough introduction of the theoretical framework of **ML-MCTDH** and its variants.

Fundamentally, **ML-MCTDH** relies on a hierarchical decomposition of the many-body

wave function closely linking it to another powerful class of numerical approaches, tensor network states [443–445]. The most prominent example in this family of wave function ansätze are [matrix product states \(MPS\)](#) [446–449] which have been extremely successful in the description of one-dimensional systems due to the availability of powerful algorithms such as the [density matrix renormalization group method \(DMRG\)](#) [450–453]. Other approaches are more tailored to the description of quantum critical [454–458] or multidimensional systems [459–469]. Section 2.5 provides a more detailed overview over the different methods and their relation to [ML-MCTDH](#).





## Theoretical Framework

THE present thesis investigates the static properties and nonequilibrium dynamics of quantum many-body systems focusing on bosonic ensembles and spin models. To this end, the framework of **ML-MCTDH** methods is employed in order to obtain a beyond-mean-field description that captures all relevant correlations. Originally developed for the numerical treatment of high-dimensional problems<sup>1</sup> in quantum chemistry comprising many distinguishable **degrees of freedom (DOFs)**, these approaches rely on variationally optimized basis functions in order to obtain a compact representation of the many-body wave function. Later extensions allow for the simulation of indistinguishable particles, namely bosons, fermions, and mixtures thereof, rendering them attractive for applications in ultracold atom physics.

The present chapter provides an in-depth overview over this theoretical framework, starting in Section 2.1 with the underlying **time-dependent variational principles (TD-VPs)** that determine the time evolution of the different wave function ansätze. Section 2.2 introduces the standard approach to multi-configurational wave packet dynamics, which is then extended to the **multi-configuration time-dependent Hartree (MCTDH)** method in Section 2.3 by introducing an additional layer of time-dependent basis functions, yielding a more compact representation of the wave function and thus allowing for the description of larger systems. The **ML-MCTDH** approach discussed in Section 2.4 uses a recursive construction consisting of **MCTDH** wave functions, rendering even higher-dimensional problems tractable. Section 2.5 highlights the relation between the **ML-MCTDH** formalism and tensor network states, which are a powerful tool for the description of quantum many-body systems. A commonality of all **ML-MCTDH** methods is that they rely on a time-independent, primitive basis in order to construct the respective wave function ansätze as well as the involved operators. The choice of these basis functions ultimately relies on the physical scenario under consideration and Section 2.6 describes the most common strategies. Section 2.7 shifts the focus towards indistinguishable particles by introducing the **multi-configuration time-dependent Hartree method for bosons (MCTDHB)** method and briefly discusses its multi-layer extension as well as the alternative approach of **ML-MCTDH** in **second quantization representation (SQR)**. Finally, Section 2.8 shows how the **ML-MCTDH** family of methods for wave packet dynamics can be employed in order to access the static properties of quantum many-body systems by switching to imaginary time propagation.

---

<sup>1</sup>In this context, “high-dimensional” refers to the large number of involved **DOFs** and not to physical problems taking place in a high-dimensional Euclidean space.

## 2.1. Time-Dependent Variational Principles

The time-evolution of a wave function  $|\Psi(t)\rangle$  is determined by the time-dependent Schrödinger equation [347]

$$i\partial_t |\Psi(t)\rangle = \hat{H}(t) |\Psi(t)\rangle \quad (2.1)$$

where  $\hat{H}(t)$  is the (potentially time-dependent) Hamiltonian that describes the system at all times  $t$ . In a mathematically rigorous treatment of quantum mechanics, the wave function is represented by state vectors residing in an infinitely dimensional Hilbert space [470]. Consequently, numerical approaches to quantum dynamics have to resort to truncating this space and employing a wave function ansatz  $\Psi(t) = \Psi(t; \{\alpha_i(t)\})$  with a finite number of parameters  $\{\alpha_i(t)\}$ <sup>2</sup> [471]. The TDVP [472, 473] can be applied to obtain equations of motion (EOMs) for these parameters such that the approximate wave function is as close to the exact solution of the time-dependent Schrödinger equation as possible in the given constrained space. The TDVP can be viewed as an alternative formulation of the Schrödinger equation Eq. (2.1) through the variation of an action functional. By introducing the Lagrangian

$$L(\Psi(t), \Psi^*(t)) = \langle \Psi(t) | H - i\partial_t | \Psi(t) \rangle \quad (2.2)$$

and demanding that the variation of the action functional vanishes, i.e.,

$$\delta S = \delta \int_{t_1}^{t_2} L(\Psi(t), \Psi^*(t)) dt \stackrel{!}{=} 0 \quad (2.3)$$

with  $\delta\Psi(t_1) = \delta\Psi(t_2) = 0$ ,

the time-dependent Schrödinger equation can be recovered<sup>3</sup>. It should be noted that other TDVPs can be found in the literature, namely the Dirac-Frenkel [474, 475]

$$\langle \delta\Psi(t) | H - i\partial_t | \Psi(t) \rangle = 0 \quad (2.4)$$

and McLachlan variational principle [476]

$$\delta \|\theta(t) - H\Psi(t)\|^2 = 0 \quad (2.5)$$

where  $\theta(t) = i\partial_t \Psi(t)$  is varied. As long as the parameters  $\{\alpha_i(t)\}$  of the wave function ansatz are complex analytic, the three TDVPs are equivalent<sup>4</sup> [420, 477, 478]. Therefore, the Dirac-Frenkel TDVP (2.4) is employed throughout the remainder of the present thesis since it is the simplest and the one most commonly used in the literature.

It can be shown [420, 423], that the TDVPs conserve the norm of the wave function

$$\frac{d}{dt} \|\Psi(t)\|^2 = 0 \quad (2.6)$$

and, as long as the Hamiltonian is Hermitian and time-independent, the total energy of

---

<sup>2</sup>In the following, we refrain from explicitly denoting these variational parameters for the sake of brevity.

<sup>3</sup>Here, the wave function is assumed to be normalized, i.e.,  $\langle \Psi(t) | \Psi(t) \rangle = 1$ . See References [472, 473] for a more detailed discussion.

<sup>4</sup>It can be shown that the Lagrangian TDVP (2.3) is then equivalent to the real part and the McLachlan TDVP (2.5) to the imaginary part of the Dirac-Frenkel TDVP (2.4).

the system,

$$\frac{d}{dt} \langle \Psi(t) | H | \Psi(t) \rangle = 0. \quad (2.7)$$

## 2.2. The Standard Method

The pure state of a closed quantum system with  $N$  DOFs  $x_1, \dots, x_N$  is described at all times  $t$  by the many-body wave function  $|\Psi(t)\rangle = |\Psi(x_1, \dots, x_N, t)\rangle$ . Depending on the physical scenario under consideration, DOFs could for example be the real-space coordinates of particles, internal degrees of freedom of an atom, or the orientation of a molecule. As mentioned when discussing the TDVP in Section 2.1, the numerical treatment requires the truncation of the Hilbert space to some finite dimension. The traditional approach to this problem employs a finite, time-independent basis

$$\{\chi_{j_\kappa}^{(\kappa)}(x_\kappa)\} \quad j_\kappa = 1, \dots, n_\kappa \quad (2.8)$$

for each DOF. Here,  $n_\kappa$  denotes the finite number of basis functions associated with the DOF  $x_\kappa$ . The many-body wave function is then expanded as a superposition of all possible combinations of basis functions

$$|\Psi(t)\rangle = \sum_{j_1=1}^{n_1} \cdots \sum_{j_N=1}^{n_N} A_{j_1 \dots j_N}(t) \bigotimes_{\kappa=1}^N |\chi_{j_\kappa}^{(\kappa)}(x_\kappa)\rangle \quad (2.9)$$

using time-dependent coefficients  $A_{j_1 \dots j_N}(t)$ . This construction is illustrated as a tree diagram in Fig. 2.1, similar to the graphical notation used for tensor network states (see Section 2.5) and will come in handy later when considering the more complex ansätze used in MCTDH and ML-MCTDH.

The notation can be greatly simplified by introducing a multi-index

$$J = (j_1, j_2, \dots, j_N) \quad (2.10)$$

that provides a single unique index for all possible values of the individual indices  $j_\kappa$ .

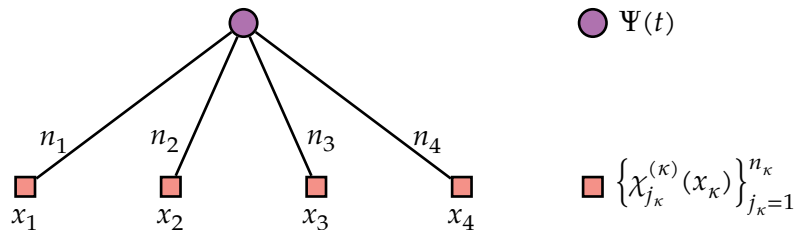


Figure 2.1.: Tree diagram for the standard wave packet ansatz Eq. (2.9) for  $N = 4$  DOFs. Time-independent bases  $\{\chi_{j_\kappa}^{(\kappa)}(x_\kappa)\}$  containing  $n_\kappa$  basis functions are employed for each DOF  $x_\kappa$ . The many-body wave function  $\Psi(t)$  then takes all possible combinations of basis states into account.

Every multi-index  $J$  is associated with a specific combination of basis functions

$$|\Phi_J\rangle = \bigotimes_{\kappa=1}^N |\chi_{j_\kappa}^{(\kappa)}(x_\kappa)\rangle \quad (2.11)$$

which is also referred to as a configuration or Hartree product. The wave function ansatz (2.9) can then be written as the time-dependent superposition

$$|\Psi(t)\rangle = \sum_J A_J(t) |\Phi_J\rangle \quad (2.12)$$

comprising  $N_C = \prod_{\kappa=1}^N n_\kappa$  possible configurations.

If only a single basis function is used for each DOF, i.e.,  $n_\kappa = 1 \quad \forall \kappa = 1, \dots, N$ , the ansatz contains a single Hartree product, and only provides a mean-field description of the system that does not take correlations effects into account. In this case, interaction terms can be reduced to terms acting on individual DOFs by integrating the remaining DOFs out. While in some scenarios, for example when considering weak interactions, such a mean-field description might be sufficient or at least provide some insight into the system, it fails to describe many exciting physical phenomena that are driven by strong correlations and entanglement, for example the dynamics after strong quantum quenches. For a beyond-mean-field description, at least two basis functions are required for each DOF such that  $N_C \geq 2^N$  scales exponentially with respect to the number of DOFs  $N$  rendering the standard ansatz only feasible for small systems.

Finally, the EOM governing the time evolution of the coefficients  $A_J(t)$ ,

$$i\partial_t A_J(t) = \sum_L \langle \Phi_J | \hat{H} | \Phi_L \rangle A_L(t), \quad (2.13)$$

can be obtained by applying the Dirac-Frenkel TDVP (2.4) to Eq. (2.12)

### 2.3. The Multi-Configuration Time-Dependent Hartree Method

The standard approach to wave packet dynamics presented in Section 2.2 provides a beyond-mean-field description of quantum many-body dynamics by employing a time-independent, i.e., fixed, basis. However, in many physical scenarios a much smaller number of *time-dependent* basis functions is sufficient to describe the physics accurately providing a much more compact representation of the wave function and rendering the treatment of larger systems feasible.

In order to motivate this concept, it is instructive to introduce the notion of an *active space* which is defined as a hyperplane embedded in the complete Hilbert space and is spanned by a set of time-dependent basis functions. Now, as time evolves, the active space may move and rotate within the full Hilbert space such that it best describes the wave function at all times. In general, its dimension  $d(t)$ , and therefore the number of required basis functions may change over time. However,  $d(t)$  is typically bounded by a finite upper value  $d_{\max} = \max_t d(t)$  when considering a finite time interval  $t \in [0, T]$  such that  $d_{\max}$  time-dependent basis functions are sufficient at all times. Figure 2.2 visualizes the concept of an active space using an example where the state of the system resides in an instantaneous, two-dimensional active space moving through a three-dimensional Hilbert space.

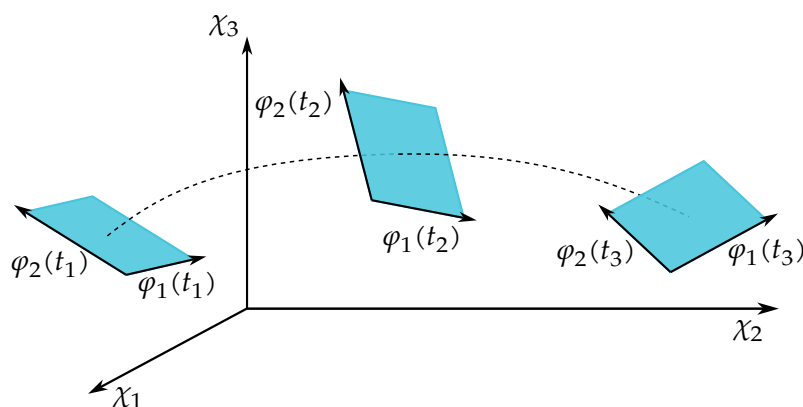


Figure 2.2.: Illustration of the concept of an active space. In this example, the wave function can be fully described by two basis functions  $\varphi_1(t)$  and  $\varphi_2(t)$  at all times during the evolution. If a fixed basis  $\{\chi_i\}$  is employed instead, three basis vectors are required to capture the wave function at all times highlighting that often a time-dependent, optimized basis can yield a more compact representation.

The idea of employing a time-dependent basis is actually quite old. The time-dependent Hartree method [383–385, 474, 479] employed a single time-dependent basis function per DOF and was used to provide a mean-field description of simple molecular problems [479–484]. By additionally incorporating time-dependent, unitary transformations in the wave function, the time-dependent rotated Hartree approach [485, 486] is able to take correlations between the DOFs into account. Inspired by the standard ansatz for wave packet dynamics (2.12), multi-configurational approaches were developed for a beyond-mean-field treatment of quantum dynamics. Early approaches [487–489] relied on employing problem-dependent projection operators, the choice of which is not always obvious and impacts the results significantly. The MCTDH method [420, 424–428] does not suffer from this drawback and provides a general framework for ab-initio quantum dynamics using a multi-configurational ansatz. It can be viewed as the dynamical extension of the multi-configurational self-consistent field theory for stationary quantum chemistry problems and has been applied to wide range of problems that are inaccessible to other methods [490–505].

In the following sections, the MCTDH method is described in detail. Section 2.3.1 introduces the underlying wave function ansatz while Section 2.3.2 outlines the constraints that have to be imposed in order to lift its ambiguity. Section 2.3.3 explains the EOMs that drive the time-evolution of the many-body wave function. Finally, Section 2.3.4 establishes the concept of mode combination, i.e., the combination of multiple physical DOFs into logical coordinates, which is crucial for the application of the MCTDH method to large systems and serves as the foundation for its multi-layer extension (see Section 2.4).

### 2.3.1. Wave Function Ansatz

The MCTDH method employs a time-dependent basis  $\{\varphi_i(x_\kappa, t)\}_{i=1}^{m_\kappa}$  of so-called **single particle functions (SPFs)** or orbitals for each DOF  $\kappa$ . These basis functions are defined

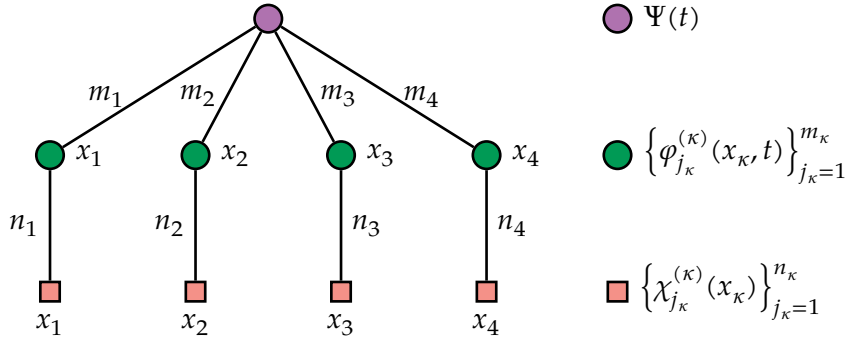


Figure 2.3.: Tree diagram of a **MCTDH** ansatz with  $N = 4$  degrees of freedom. The wave function is spanned by time-dependent **single particle functions (SPFs)** on the layer below, which in turn are represented in the time-independent, primitive bases on the lowest layer.

with respect to the underlying, time-independent (primitive) basis

$$|\varphi_i^{(\kappa)}(x_{\kappa}, t)\rangle = \sum_{j=1}^{n_{\kappa}} c_{ij}^{(\kappa)}(t) |\chi_j^{(\kappa)}(x_{\kappa})\rangle. \quad (2.14)$$

They are typically chosen to be orthonormal, i.e.,

$$\langle \varphi_i^{(\kappa)}(x_{\kappa}, t) | \varphi_j^{(\kappa)}(x_{\kappa}, t) \rangle = \delta_{ij}, \quad (2.15)$$

a property which is preserved throughout the time-evolution. Instead of expanding the many-body wave function directly in the underlying primitive basis as in the standard approach in Section 2.2, the wave function is now written in terms of the **SPFs** as

$$|\Psi(t)\rangle = \sum_{j_1=1}^{m_1} \cdots \sum_{j_N=1}^{m_N} A_{j_1 \dots j_N}(t) \bigotimes_{\kappa=1}^N |\varphi_{j_{\kappa}}^{(\kappa)}(x_{\kappa}, t)\rangle. \quad (2.16)$$

For the further discussion, it is instructive to rewrite (2.16) in terms of configurations  $|\Phi_J(t)\rangle$  which are now time-dependent as they contain products of **SPFs** instead of primitive basis functions (see Eq. (2.12)):

$$|\Psi(t)\rangle = \sum_J A_J(t) |\Phi_J(t)\rangle. \quad (2.17)$$

As with the standard ansatz (2.12), the **MCTDH** ansatz can be illustrated using a tree diagram, see Fig. 2.3. A comparison with Fig. 2.1 highlights that the addition of the **SPFs** introduces a new layer to the wave function expansion hierarchy.

In a many physical scenarios, the number of **SPFs** is much smaller than the number of primitive basis functions, i.e.,

$$\prod_{\kappa=1}^N m_{\kappa} \ll \prod_{\kappa=1}^N n_{\kappa}, \quad (2.18)$$

exploiting that the dynamics typically only takes place in a small subspace of the Hilbert space. If this is the case, the **MCTDH** ansatz contains much fewer configurations com-

pared to an equivalent ansatz that employs a time-independent basis. When applying **MCTDH** to a many-body problem, it is important to ensure its convergence with respect to the number of **SPFs** in order to ensure that they span a large enough space. By following the same line of reasoning as in Section 2.2, at least two **SPFs** per **DOF** are required for a beyond-mean-field description, i.e.,  $m_\kappa \geq 2$ . Consequently, even though **MCTDH** typically yields a much more compact wave function than the standard, time-independent approach, the number of configurations still grows exponentially as the number of **DOFs**  $N$  increases, i.e.,

$$\prod_{\kappa=1}^N m_\kappa \geq 2^N. \quad (2.19)$$

Even though this behavior again limits the feasible system size, **MCTDH** has been successfully applied to molecular problems that included 12–14 correlated coordinates [421, 506–509]. The mode combination of multiple physical **DOFs** into logical coordinates presented Section 2.3.4 further increases the tractable number of coordinates.

### 2.3.2. Constraint Operator

The wave function ansatz given by Eq. (2.16) is not unique. An equivalent wave function  $|\tilde{\Psi}(t)\rangle = \sum_J \tilde{A}_J(t) |\tilde{\Phi}_J(t)\rangle$  can be obtained by performing a unitary transformation  $\mathbf{U}^{(\kappa)}(t)$  of the **SPFs**, i.e.,

$$|\tilde{\varphi}_j^{(\kappa)}(t)\rangle = \sum_{\ell=1}^{m_\kappa} U_{j\ell}^{(\kappa)}(t) |\varphi_\ell^{(\kappa)}(t)\rangle \quad (2.20)$$

and undoing it by applying the inverse transformation to the coefficients,

$$\tilde{A}_{j_1 \dots j_N}(t) = \sum_{\ell_1 \dots \ell_N} (U^{(1)}(t))_{\ell_1 j_1}^{-1} \dots (U^{(N)}(t))_{\ell_N j_N}^{-1} A_{\ell_1 \dots \ell_N}(t). \quad (2.21)$$

The ambiguity can be lifted by imposing additional constraints which have to be chosen such that the variational space is not narrowed down. By fixing

$$i \langle \varphi_j^{(\kappa)}(x_{\kappa'}, t) | \partial_t | \varphi_\ell^{(\kappa)}(x_{\kappa'}, t) \rangle = \langle \varphi_j^{(\kappa)}(x_{\kappa'}, t) | \hat{g}^{(\kappa)} | \varphi_\ell^{(\kappa)}(x_{\kappa'}, t) \rangle = g_{j\ell}^{(\kappa)}(t) \quad (2.22)$$

the representation becomes unique [420]. Here, a constraint operator  $\hat{g}^{(\kappa)}$  for each **DOF**  $\kappa$  is introduced that can be chosen arbitrarily as long as it is Hermitian in order to ensure orthonormality of the **SPFs**<sup>5</sup>.

### 2.3.3. Equations of Motion

Applying the Dirac-Frenkel **TDVP** (2.4) to the wave function ansatz Eq. (2.17) yields **EOMs** for the coefficients  $A_J$  and the **SPFs**  $\varphi_\ell^{(\kappa)}(x, t)$ . From the variation with respect to the coefficients, one obtains the equation

$$i \partial_t A_J(t) = \sum_L \langle \Phi_J(t) | \hat{H}(t) | \Phi_L(t) \rangle A_L(t) - \sum_{\kappa=1}^N \sum_{\ell=1}^{m_\kappa} g_{j_\kappa \ell}^{(\kappa)}(t) A_{J_\ell^\kappa}(t) \quad (2.23)$$

<sup>5</sup>The operator  $\hat{g}^{(\kappa)}(t)$  defines the transformation to transform the **SPFs** computed with  $\hat{g}^{(\kappa)}(t) = 0$  to the ones computed with a given  $\hat{g}^{(\kappa)}(t)$ . The evolution of the corresponding unitary transformation matrix  $\mathbf{U}^{(\kappa)}(t)$  is given by  $i \partial_t \mathbf{U}^{(\kappa)}(t) = \mathbf{g}^{(\kappa)\top} \mathbf{U}^{(\kappa)}(t)$  with the solution  $\mathbf{U}^{(\kappa)}(t) = \mathcal{T} \exp(-i \int_0^t \mathbf{g}^{(\kappa)\top}(t') dt')$  where  $\mathcal{T}$  is the time-ordering operator. See Ref. [423] for details.

that governs their time-evolution. Here,  $J_\ell^\kappa = (j_1, \dots, j_{\kappa-1}, \ell, j_{\kappa+1}, \dots, N)$  denotes the multi-index  $J$  with the  $\kappa$ th index fixed to  $\ell$ . Compared to the EOM of the standard ansatz (see Eq. (2.13)), Eq. (2.23) contains an additional term that incorporates the constraint operator discussed in Section 2.3.2 in order to lift the ambiguity in the ansatz. If  $\hat{g}^{(\kappa)} = 0$  is chosen, both sets of EOMs are identical. Similarly, a variation with respect to the SPFs yields the corresponding EOMs for the SPFs which takes the form<sup>6</sup>

$$i\partial_t |\varphi_j^{(\kappa)}\rangle = \hat{P}^{(\kappa)} \sum_{k=1}^{m_\kappa} g_{jk}^{(\kappa)} |\varphi_k^{(\kappa)}\rangle + (1 - \hat{P}^{(\kappa)}) \sum_{k,\ell=1}^{m_\kappa} (\rho^{(\kappa,-1)})_{jk} \langle H \rangle_{k\ell}^{(\kappa)} |\varphi_\ell^{(\kappa)}\rangle. \quad (2.24)$$

The projector

$$\hat{P}^{(\kappa)}(t) = \sum_{j=1}^{m_\kappa} |\varphi_j^{(\kappa)}(t)\rangle \langle \varphi_j^{(\kappa)}(t)| \quad (2.25)$$

projects onto the instantaneous SPF basis. In order to define the remaining ingredients to the SPF EOM, it is instructive to introduce the single-hole functions

$$\begin{aligned} |\Psi_\ell^{(\kappa)}\rangle &= \langle \varphi_\ell^{(\kappa)} | \Psi \rangle \\ &= \sum_{j_1=1}^{m_1} \dots \sum_{j_{\kappa-1}=1}^{m_{\kappa-1}} \sum_{j_{\kappa+1}=1}^{m_{\kappa+1}} \dots \sum_{j_N=1}^{m_N} A_{j_1 \dots j_{\kappa-1} \ell j_{\kappa+1} \dots j_N} |\varphi_{j_1}^{(1)}\rangle \dots |\varphi_{j_{\kappa-1}}^{(\kappa-1)}\rangle |\varphi_{j_{\kappa+1}}^{(\kappa+1)}\rangle \dots |\varphi_{j_N}^{(N)}\rangle \end{aligned} \quad (2.26)$$

given by the overlap of the total wave function  $|\Psi\rangle$  with the  $\ell$ th SPF of the  $\kappa$ th DOF. These functions define the mean-field elements

$$\langle H \rangle_{ij}^{(\kappa)}(t) = \langle \Psi_i^{(\kappa)}(t) | \hat{H}(t) | \Psi_j^{(\kappa)}(t) \rangle. \quad (2.27)$$

In order to ensure a performant evaluation of these elements, the Hamiltonian is generally assumed to be in a sum-of-product form, where each term is written as a product of single-particle operators acting on different DOFs, i.e.,

$$\hat{H}(t) = \sum_r c_r \bigotimes_{\kappa=1}^N \hat{h}_r^{(\kappa)}(x_\kappa, t). \quad (2.28)$$

Then, each term in the Hamiltonian is composed of operators that act on different DOFs and can be treated independently. Otherwise, the costly and cumbersome numerical evaluation of multidimensional integrals would be required. This particular Hamiltonian structure still covers a wide range of physical systems and is a typical assumption for various of numerical methods, especially ones that rely on hierarchical tensor decompositions [510–513]. Often, the POTFIT algorithm [423, 428, 514, 515] can be used to approximate terms that are not in this product form by employing a Tucker decomposition [516, 517]. It should be noted that more involved schemes exist [518–521] that perform better on very large product spaces.

Finally, the reduced one-body density matrix is defined as

$$\rho_{ij}^{(\kappa)}(t) = \langle \Psi_i^{(\kappa)}(t) | \Psi_j^{(\kappa)}(t) \rangle. \quad (2.29)$$

<sup>6</sup>It should be noted that all objects occurring in Eq. (2.24) are time-dependent, but their time-dependence is omitted for brevity.



It should be noted that the inverse of the matrix given by the elements (2.29) enters the SPF EOM (2.24) which can be problematic when  $\rho$  becomes singular, i.e., any of its eigenvalues becomes zero. In order to resolve this issue,  $\rho$  is usually replaced by a regularized density matrix  $\rho_{\text{reg}}^{(\kappa)}$  with  $\lim_{\varepsilon \rightarrow 0} \rho_{\text{reg}}^{(\kappa)} = \rho^{(\kappa)}$  such as [420, 522]

$$\rho_{\text{reg}}^{(\kappa)}(t) = \rho^{(\kappa)}(t) + \varepsilon \exp(-\rho^{(\kappa)}(t)/\varepsilon). \quad (2.30)$$

Here,  $\varepsilon$  is a small regularization parameter, typically  $\varepsilon \leq 10^{-8}$ , that controls the error introduced by the regularization. By varying  $\varepsilon$ , convergence with respect to this parameter can be checked in order to ensure that the regularization does not lead to unphysical results.

The EOMs (2.23) and (2.24) are typically simplified to

$$i\partial_t A_J(t) = \sum_L \langle \Phi_J(t) | \hat{H}(t) | \Phi_L(t) \rangle A_L(t) \quad (2.31)$$

and

$$i\partial_t \left| \varphi_j^{(\kappa)}(t) \right\rangle = (1 - \hat{P}^{(\kappa)}(t)) \sum_{k,\ell=1}^{m_\kappa} \left( \rho^{(\kappa),-1}(t) \right)_{jk} \langle H \rangle_{k\ell}^{(\kappa)}(t) \left| \varphi_\ell^{(\kappa)}(t) \right\rangle \quad (2.32)$$

by employing the standard gauge  $\hat{g}^{(\kappa)} = 0$  for all DOFs  $\kappa$ . In this representation, the effect of the projection operator  $\hat{P}^{(\kappa)}$  becomes more evident. The expression  $(1 - \hat{P}^{(\kappa)})$  ensures that any change to the current SPF basis stems from a rotation outside the subspace spanned by the current basis, thus preventing unnecessary rotations within the currently spanned space. Another common choice of constraints is the natural orbital gauge [420, 523–525], where the SPFs coincide with the natural orbitals, i.e., the eigenfunctions of the one-body density matrix (2.29). Choosing  $\hat{g}^{(\kappa)}$  to be identical to the one-body Hamiltonian acting on the  $\kappa$ th DOF [420] can reduce the numerical effort for certain applications [420, 526] since the mean-fields (2.27) are evaluated only using interaction terms.

The most straightforward way of implementing the MCTDH method is to directly solve the EOMs (2.23) and (2.24) using standard numerical integration techniques for ordinary differential equations [365, 527, 528] which includes linear multistep methods, the Bulirsch-Stoer algorithm or embedded Runge-Kutta formulae. This approach is referred to as variable mean-field (VMF) integration in the literature. However, it is often the case that the matrix elements  $\langle \Phi_J(t) | \hat{H}(t) | \Phi_L(t) \rangle$  in (2.23) and the products  $\rho^{(\kappa),-1}(t) \langle H \rangle^{(\kappa)}(t)$  change much slower than the underlying SPFs and coefficients. For this reason, constant mean-field (CMF) integration schemes have been devised [420, 522, 529] that update the aforementioned quantities less frequently in order to reduce the computational effort while only introducing a small loss in accuracy. The basic principle is to keep the slowly changing ingredients of the EOMs constant before updating them according to the current values of the coefficients and SPFs. Particularly, when many coefficients or terms in the Hamiltonian have to be considered, constant mean-field (CMF) integration can lead to a significant reduction in the simulation runtime. In practice, the computational cost can further be reduced by exploiting the linear nature of Eq. (2.31) and updating the coefficients using specialized algorithms [530] such as split-operator [531–533], Chebyshev [534] or Lanczos [535] methods.

### 2.3.4. Mode Combination

The **MCTDH** method is efficient if a smaller number of time-dependent functions compared to the size of the primitive basis can be employed to capture the dynamics of the system accurately. In the discussion so far, the **SPFs** were assumed to be one-dimensional functions of a single physical coordinate. Often, however, it is favorable to combine multiple coordinates (*modes*) and effectively introduce multidimensional **SPFs** [536–538], e.g., grouping the euclidean coordinates of a particle into a single logical vector coordinate. A combined treatment of correlated **DOFs** can greatly reduce the number of required **SPFs**. Another situation in which mode combination can be helpful, is the treatment of **DOFs** with small primitive basis sizes. Here, the space spanned by the time-dependent **SPFs** cannot be much smaller than the one spanned by the primitive basis size and cannot yield a significant reduction of the computational effort. The combined Hilbert space of multiple **DOFs** is much larger and offers more potential for compression than the individual Hilbert spaces. Using mode combination, **MCTDH** has been shown to be able to simulate molecular scenarios comprising 15–24 correlated coordinates [490, 495, 496, 539] or system-bath setups with up to 100 correlated **DOFs** [491, 492, 538], thus drastically increasing the feasible system size.

In order to formally introduce the concept of mode combination, we define  $\tilde{N}$  logical coordinates  $q_\lambda$ , with  $\lambda = 1, \dots, \tilde{N}$ , containing  $p_\lambda$  physical coordinates each, i.e.,

$$\begin{aligned} q_1 &= (x_1, \dots, x_{p_1}) \\ q_2 &= (x_{p_1+1}, \dots, x_{p_1+p_2}) \\ &\vdots \end{aligned} \quad (2.33)$$

It is instructive to use a shorthand notation  $\alpha(\lambda) = 1 + \sum_{i=1}^{\lambda-1} p_i$  for the first and  $\beta(\lambda) = \sum_{i=1}^{\lambda} p_i$  for the last **DOF** associated with the  $\lambda$ th logical coordinate such that the **SPFs** can be rewritten as

$$\left| \varphi_i^{(\lambda)}(q_\lambda, t) \right\rangle = \sum_{j_{\alpha(\lambda)}=1}^{n_{\alpha(\lambda)}} \dots \sum_{j_{\beta(\lambda)}=1}^{n_{\beta(\lambda)}} c_{i; j_{\alpha(\lambda)} \dots j_{\beta(\lambda)}}^{(\lambda)}(t) \bigotimes_{\kappa=\alpha(\lambda)}^{\beta(\lambda)} \left| \chi_{j_\kappa}^{(\kappa)}(x_\kappa) \right\rangle. \quad (2.34)$$

The **SPFs**  $\left| \varphi_i^{(\lambda)}(q_\lambda, t) \right\rangle$  are now functions of the logical coordinates  $q_\lambda$ , i.e. multidimensional with respect to the physical coordinates  $x_\kappa$ . Even though they reside in the product space of the Hilbert space spanned by the individual primitive bases, they might span only a subspace in which the dynamics takes place, thus reducing the numerical effort. Figure 2.4 shows a tree representation of a **MCTDH** wave function that employs the combination of 5 physical **DOFs** into 2 logical coordinates.

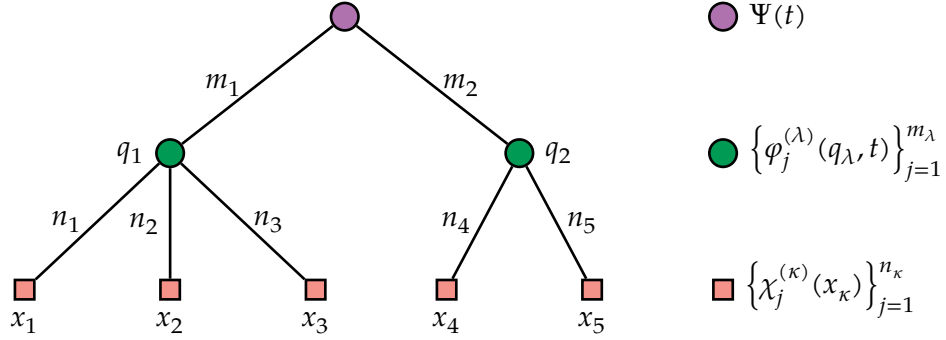


Figure 2.4.: Tree diagram of a **MCTDH** wave function with  $N = 5$  degrees of freedom that uses mode combination in order to introduce two logical coordinates  $q_1$  and  $q_2$ . The first logical coordinate combines  $p_1 = 3$  physical **DOFs** starting from  $\alpha(1) = 1$  and ending at  $\beta(1) = 3$ . The second logical coordinate comprises the remaining  $p_2 = 2$  physical **DOFs** starting from  $\alpha(2) = 4$  and ending at  $\beta(2) = 5$ .

## 2.4. The Multi-Layer MCTDH Method

The **multi-layer multi-configuration time-dependent Hartree (ML-MCTDH)** [421, 422, 429] method extends **MCTDH** by introducing additional layers to the wave function ansatz. This is achieved by applying the concept of mode combination described in Section 2.3.4 to the logical coordinates, grouping them to higher-level logical coordinates with associated **SPFs**. By repeating this construction, intricate wave function ansätze with many layers can be designed. While this approach adds more complexity to the method, it can drastically improve the compactness of the wave function representation as each new set of **SPFs** offers potential for further truncation. Hence, **ML-MCTDH** has been successfully applied to a variety of problems including dynamics calculations of hundreds or thousands of correlated **DOFs** [FK3, 429, 540–546] which are beyond the reach of **MCTDH**. Due to the recursive nature of the wave function ansatz, the notation of the **ML-MCTDH** formalism is rather involved. In the present section, the basic concepts of the method are introduced with the help of an example and simplified notation. For a full general description of the method including the **EOMs**, the reader is referred to Appendix A as well as the literature [421, 422, 547].

Figure 2.5 shows the diagrammatic representation of a **ML-MCTDH** wave function for a system comprising five physical **DOFs**,  $x_1, \dots, x_5$ , which contains one additional layer compared to **MCTDH**. In practice, **ML-MCTDH** wave function ansätze usually involve more **DOFs** and layers, but the fundamental concepts remain the same. Furthermore, highly imbalanced trees with varying depths of each subtree can be designed as well. As before, the leaves of the tree correspond to the physical **DOFs** that are each associated with a set of time-independent, primitive basis functions which are used to represent the **SPFs** on the layer above  $\varphi_i^{(\lambda)}(q_\lambda, t)$ . In this example, the **SPFs** are one-dimensional, i.e.,  $q_\lambda = x_\lambda$ , but more involved ansätze may additionally employ mode combination of the physical coordinates. The conceptually new step of **ML-MCTDH** is to introduce another layer of **SPFs**  $\Phi_i^{(\gamma)}(Q_\gamma, t)$  which are spanned by the **SPFs** of the layer below. The many-body wave function  $\Psi(t)$  is then written as a **MCTDH** wave function in terms of product states of the higher-level **SPFs**, each of which can also be understood as a **MCTDH** wave

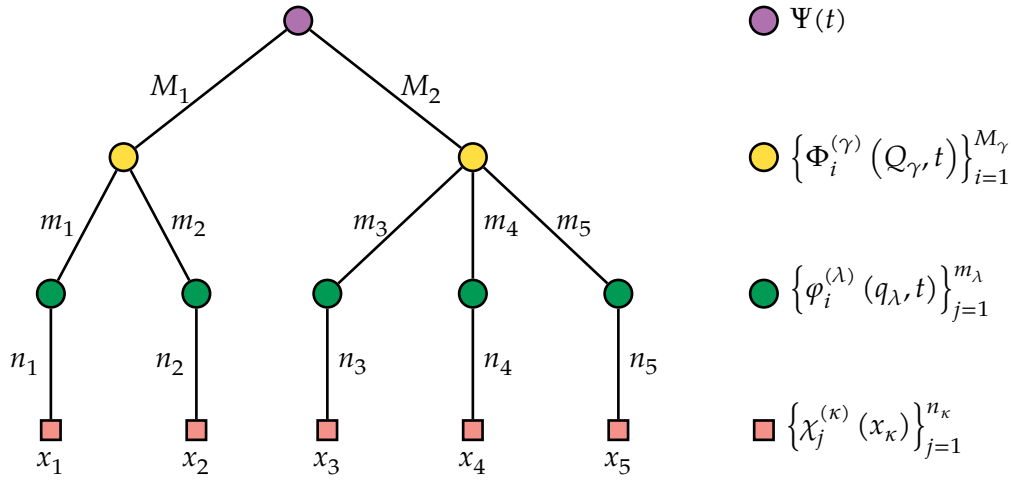


Figure 2.5.: Tree diagram of a **ML-MCTDH** wave function. Compared to **MCTDH**, this example employs one additional layer of **SPFs** to describe a system comprising five physical **DOFs**.

function with respect to the **SPFs** of the layer below highlighting the recursivity of the method. The **EOMs** governing the time-evolution of the various expansion coefficients of the ansatz can be derived using the **TDVPs** discussed in Section 2.1 and exhibit a similar structure to those of **MCTDH**.

A priori, it is not necessarily clear which tree structure is best suited to describe a given problem. Different topologies can result in vastly different simulation runtimes while usually yielding comparable results as long as proper convergence with respect to the number of **SPFs** is ensured. Furthermore, tree transformations allow switching between equivalent tree structures [548] by changing which node is the root of the tree. Compared to **MCTDH**, checking for convergence of the **ML-MCTDH** method is complicated by the presence of many nodes in the tree structure, each associated with a **SPF** number that has to be chosen large enough. Tree diagrams such as the one shown in Fig. 2.5 provide a clear and convenient way to visualize the often very complex tree structure. By labeling the edges with the numbers of **SPFs** and primitive basis functions, the wave function ansatz is uniquely determined.

## 2.5. Tensor Network States

Tensor network states [443–445] play a crucial role in the theoretical description of quantum many-body systems by performing various kinds of tensor decompositions of the full wave function. Since the ansätze used for **MCTDH** method and its multi-layer extension can also be classified as tensor network states, a brief overview of this subject is provided in the following. The Penrose diagrammatic notation [549] for tensor network states is employed throughout this section. Ref. [550] provides a detailed introduction into this graphical formalism using many examples of tensor network states and associated algorithms.

The pure state of a composite quantum system consisting of  $N$  subsystems associated with local Hilbert spaces  $\mathcal{H}_1, \dots, \mathcal{H}_N$  resides in the product Hilbert space  $\mathcal{H} = \mathcal{H}_1 \otimes \dots \otimes$

$\mathcal{H}_N$  and is given by a rank- $N$  tensor  $A_{j_1 j_2 \dots j_N}$  as

$$|\Psi\rangle = \sum_{j_1=1}^{d(\mathcal{H}_1)} \sum_{j_2=1}^{d(\mathcal{H}_2)} \dots \sum_{j_N=1}^{d(\mathcal{H}_N)} A_{j_1 j_2 \dots j_N} |j_1\rangle \otimes |j_2\rangle \otimes \dots \otimes |j_N\rangle, \quad (2.35)$$

see Fig. 2.6a. The total dimension of the full Hilbert space  $d(\mathcal{H}) = d(\mathcal{H}_1) \cdot d(\mathcal{H}_2) \cdot \dots \cdot d(\mathcal{H}_N)$  determines the number of coefficients of  $A_{j_1 j_2 \dots j_N}$  which grows exponentially with the number of subsystems  $N$ . Comparing (2.35) with Eq. (2.9), shows that the standard ansatz for wave packet dynamics presented in Section 2.2 is equivalent to a propagation of the full coefficient tensor. In order to make a numerical treatment of large systems feasible, various approximations have been developed.

Mathematically, the MCTDH wave function ansatz (2.16) corresponds to a Tucker decomposition [551–554] of the full rank- $N$  coefficient tensor, factorizing it into a much smaller core tensor and a set of low-rank auxiliary tensors [516, 555] (see Fig. 2.6b). It can also be understood as a higher-order singular value decomposition [516]. The special case of a Tucker decomposition into two auxiliary tensors is equivalent to the Schmidt decomposition of the system into two subsystems [556] and provides easy access to the entanglement entropy between the two parts. ML-MCTDH constructs the wave function ansatz by repeating this decomposition, introducing a new layer in each step, in a scheme which is also known as the hierarchical or H-Tucker format [557–559]. The resulting recursive tensor structure is also known as a tree tensor network state in the literature [560–564], see Fig. 2.6c for an exemplary diagram.

Matrix product states (MPS) [446–449] also known as tensor trains [565] are another particularly popular and powerful class of tensor network states. Here, the coefficient tensor is factorized into a sequence of rank-3 tensors<sup>7</sup>, see Fig. 2.6d. MPS are extremely useful for the investigation of spin chains and other one-dimensional systems such as the Bose-Hubbard model due to the availability of efficient algorithms. The most prominent example is the DMRG method [450–453] to compute eigenstates of the Hamiltonian. DMRG has proven to be a powerful tool to compute the eigenstates of various one-dimensional lattice models [566–571], but also continuous systems in the context of quantum chemistry [572–578] and higher-dimensional lattices [579–582]. The dynamics of the system can be studied with the time-evolving block-decimation [463, 583–586] that relies on the Trotter-Suzuki decomposition [587, 588] of the time-evolution operator up to some finite order. This approach is most efficient for nearest-neighbor interactions by exploiting that certain parts of the Hamiltonian commute with each other [589] but can also be extended to incorporate long-range interactions by introducing SWAP gates [590]. Recently, other schemes to access the dynamics have been developed by applying TDVP to MPS [591–595]. A MCTDH method for MPS has been devised as well [596] where, in contrast to the other aforementioned methods, the bond dimension (the size of each tensor) is kept fixed during the time-evolution, similar to the fixed number of SPFs in (ML)-MCTDH. Consequently, some of these algorithmic ideas for MPS have also been transferred to tree tensor network states such as TDVP-based time evolution scheme [597, 598]. Larsson demonstrated in the context of a quantum chemistry application [513] how a DMRG-like algorithm for tree tensor network states can be employed to compute many eigenstates efficiently, exceeding the capabilities of the relaxation schemes available to ML-MCTDH (see Section 2.8).

<sup>7</sup>When considering non-periodic boundary conditions, the first and last tensor are of rank-2.

PEPS (projected entangled pair states) [459–469] are the natural extension of MPS to systems that reside in more than one spatial dimension. The coefficient tensor is decomposed into a network of low-rank tensors according to the underlying lattice geometry that are each contracted with their neighbors. Figure 2.6e shows an example for a 2D square lattice, where the many-body state is factorized into rank-5 tensors. The given example does not employ periodic boundary conditions, such the tensors at the edges and corners are of rank-3 and rank-4.

More involved and specialized types of tensor network states have also been developed. One particularly noteworthy example is the [mutli-scale entanglement renormalization ansatz \(MERA\)](#) [454–458] (see Fig. 2.6f) that is tailored towards the description of ground states at quantum critical points. When treating a  $d$ -dimensional system, the corresponding MERA describes a  $d + 1$ -dimensional holographic geometry with the additional dimension corresponding to the length scale.

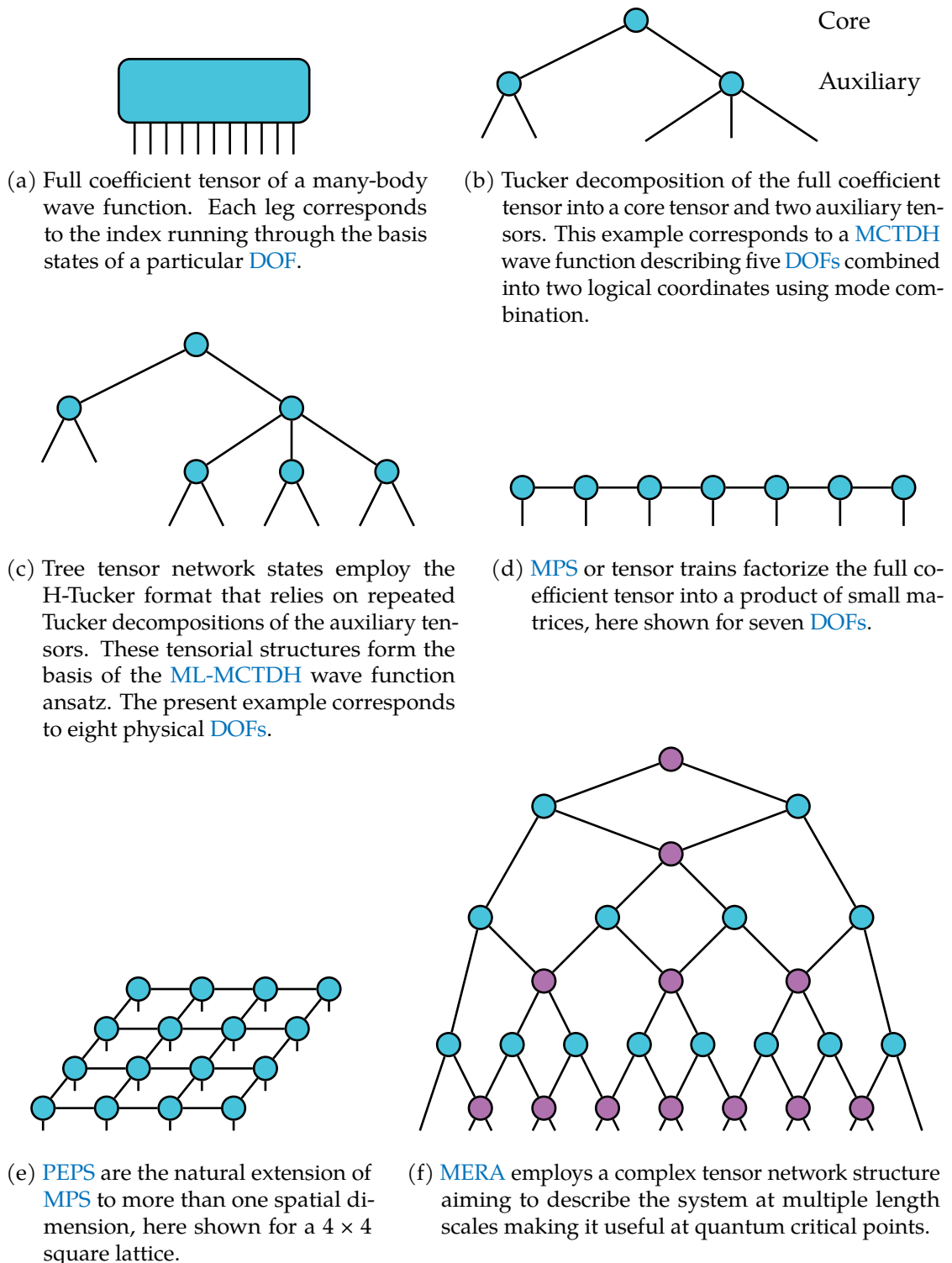


Figure 2.6.: Diagrammatic Penrose representation [549] of different kinds of tensor network states obtained by decomposing the full coefficient tensor. The nodes correspond to tensors, connecting edges to contractions and legs to uncontracted indices.

## 2.6. Primitive Bases

The numerical approaches discussed in Sections 2.2 to 2.4 rely on a primitive, time-independent basis for each physical DOF in order to construct the wave function ansatz and to represent operators like the many-body Hamiltonian. So far, the basis functions were not further specified since their choice depends on the physical problem at hand. In the following, common ways of constructing the primitive basis are presented. Section 2.6.1 introduces the **finite basis representation (FBR)** that employs a finite set of basis functions motivated by analytically solvable single-particle problems. The **discrete variable representation (DVR)** discussed in Section 2.6.2 is based on the FBR and diagonalizes the position operator. Thereby, it allows for a more efficient computation of matrix elements of the potential energy operator compared to FBR. The **fast Fourier transform (FFT)** scheme outlined in Section 2.6.3 exploits transformations to momentum space to reduce the numerical effort of applying differential operators to the wave function. This approach is particularly useful when large numbers of grid points are considered. Finally, Section 2.6.4 describes how internal DOFs can be taken into account using the example of spin- $1/2$  DOFs.

### 2.6.1. Finite Basis Representation

The FBR [599–607] is a straightforward approach to provide primitive basis functions for spatial DOFs and employs the analytical eigenfunctions of well-known one-body problems. Several examples relevant to the present thesis are listed below<sup>8</sup>:

- Quantum harmonic oscillator

$$\chi_j(x) = \frac{1}{\sqrt{2^j j!}} \left( \frac{m\omega}{\pi} \right)^{1/4} H_j(\sqrt{m\omega}(x - x_0)) e^{-\frac{1}{2}m\omega(x-x_0)^2} \quad (2.36)$$

$$j = 0, \dots, n - 1$$

- Periodic exponential functions (Fourier)

$$\chi_j(x) = \frac{1}{\sqrt{L}} \exp\left(i \frac{2\pi j}{L} (x - x_0)\right) \quad (2.37)$$

$$-n' \leq j \leq n'$$

$$n = 2n' + 1$$

- Particle in a box

$$\chi_j(x) = \begin{cases} \sqrt{\frac{2}{L}} \sin\left(\frac{j\pi(x-x_0)}{L}\right) & \text{for } x_0 \leq x \leq x_{N+1} \\ 0 & \text{elsewhere} \end{cases} \quad (2.38)$$

$$j = 1, \dots, n$$

It should be noted that these basis sets impose certain boundary conditions on the problem, e.g., periodic boundary conditions  $\chi_j(x + L) = \chi_j(x)$  in the case of Eq. (2.37) or

---

<sup>8</sup>More examples, especially for angular DOFs, can be found in Refs. [420, 423].



hard-wall boundary conditions  $\chi_j(x_0) = \chi_j(x_0 + L) = 0$  in the case of Eq. (2.38) which are reflected in the resulting many-body wave function and operators.

In the FBR, it is assumed that the matrix elements of the position operator  $x$  as well as of the first two derivative operators,  $\partial_x$  and  $\partial_x^2$ ,

$$\begin{aligned} Q_{ij} &= \langle \chi_i | \hat{x} | \chi_j \rangle, \\ D_{ij}^{(1)} &= \langle \chi_i | \partial_x | \chi_j \rangle, \\ D_{ij}^{(2)} &= \langle \chi_i | \partial_x^2 | \chi_j \rangle, \end{aligned} \quad (2.39)$$

are known analytically [420]. Hence, the evaluation of the kinetic energy operator is straightforward when computing matrix elements of the Hamiltonian. Computing the matrix elements of the potential operator, which is a function of the position operator  $\hat{V} = V(\hat{x})$ , is in general non-trivial and relies on numerical integration that can take a considerable amount of computing time to the point of being infeasible. Instead, to achieve an efficient evaluation of matrix elements of the potential operator, one assumes the potential to be a function of the matrix representation  $\mathbf{Q}$  of  $\hat{x}$ , i.e.,  $V^{\text{FBR}} = V(\mathbf{Q})$  [608]. The potential matrix elements can then be evaluated diagonalizing  $\mathbf{Q} = \mathbf{U}\mathbf{X}\mathbf{U}^\dagger$  with  $X_{ij} = \delta_{ij}x_i$  and are given by

$$V_{ij}^{\text{FBR}} = \sum_{k=1}^n U_{ik} V(x_k) U_{kj}^*. \quad (2.40)$$

However, the assumption of the potential being a function of the position operator matrix instead of the operator itself would only be exact when operating in a complete basis set. While  $\langle \chi_i | V(\hat{x}) | \chi_j \rangle \neq V_{ij}^{\text{FBR}}$  in general,  $V^{\text{FBR}}$  still provides a useful and efficient approximation that can yield accurate results if  $n$  large enough.<sup>9</sup> It has been shown that the FBR of the potential (2.40) is equivalent to a Gaussian quadrature formula [609] when the representation of the position operator is tridiagonal. This property can be used for an efficient computation of the matrix representation of the potential operator in the FBR as well as the DVR introduced in the next section.

### 2.6.2. Discrete Variable Representation

In the aforementioned FBR approach, the wave function is represented with respect to the eigenstates of some one-body problem. The DVR [471, 600, 607–609] takes an additional conceptual step by transforming to a new primitive basis,

$$\tilde{\chi}_i(x) = \sum_{j=1}^n \chi_j(x) U_{ji}, \quad (2.41)$$

which diagonalizes the position operator by construction, using the matrix  $\mathbf{U}$  from the previous section. The wave function is then represented with respect to a set of grid points, i.e., the eigenvalues of the position operator. In the newly defined DVR basis, the evaluation of the often complicated potential operator becomes straightforward as the position operator becomes diagonal [599–603, 605, 607, 610–612] showcasing

<sup>9</sup>Ref. [420] includes a very illustrative example on why this construction is not exact using a harmonic potential.

why the **DVR** approach is favorable for a numerical simulation. However, the representation of differential operators is problematic. Local interpolation would lead to finite-difference formulae which are not very accurate [423]. Instead, one switches back to the **FBR** representation (2.39) where the matrix elements of the differential operators are known analytically and transforms into the new **DVR** basis using the matrix  $\mathbf{U}$  (from Section 2.6.1).

It should be noted that advanced **DVR** approaches have been devised as well which are more commonly used in quantum chemistry applications. For example, Manthe refined the **DVR** scheme to the so-called correlated **DVR** or **CDVR** [613–615] that employs time-dependent primitive basis functions and aims to provide an accurate description with fewer basis functions by treating separable parts of the potential exactly instead of by quadrature. The **DVR** can be classified as a collocation method, which are typical approaches for the solution of partial differential equations [616] and commonly used for the numerical solution of the Schrödinger equation [617–622]. Recently, other collocation-based approaches have been devised within the framework of **MCTDH** [623–626] that aim at obviating the need for a sum-of-product form for the potential but have not yet seen wide-spread adoption. Compared to the complex potential energy surfaces in quantum chemistry problems, that motivate the development of such refined approaches, the trapping potentials encountered in ultracold atom setups are rather simple and low-dimensional. Hence, for these physical scenarios one typically applies the traditional **DVR** scheme.

### 2.6.3. Fast Fourier Transform

The **DVR** introduced in Section 2.6.2 allows for an efficient application of potential operators requiring only  $\mathcal{O}(n)$  operations since the corresponding matrix representations are diagonal. However, when many grid points, of the order of  $\mathcal{O}(10^2)$  [420], are used<sup>10</sup>, the application of the non-diagonal kinetic energy operator, or any other differential operator for that matter, can become computationally expensive due to the  $\mathcal{O}(n^2)$  complexity of matrix-vector multiplications. This numerical effort can be drastically reduced by performing a Fourier transformation, i.e., by switching from real space to momentum space [488, 599, 610]. In momentum space, the non-local differential operators become local expressions, e.g.,

$$\begin{aligned} \partial_x \varphi(x) &\xrightarrow{\mathcal{F}} ik\tilde{\varphi}(k) \\ \partial_x^2 \varphi(x) &\xrightarrow{\mathcal{F}} -k^2\tilde{\varphi}(k), \end{aligned} \tag{2.42}$$

which can be applied with a complexity of  $\mathcal{O}(n)$  to a state vector, the result of which is then transformed back to real space. In practice, the **FFT** algorithm [627, 628] allows to apply these transformations efficiently with a complexity of  $\mathcal{O}(n \log n)$ . Except for the modified application of differential operators, this **FFT** scheme is equivalent to a **DVR** based on periodic exponential functions (2.37) and imposes the same periodic boundary conditions on the problem. Typically, the exponential **DVR** performs faster for small grids ( $n \lesssim 16$  grid points) while the **FFT** scheme is considerably more performant for large grids ( $n \gtrsim 100$ ) [420].

---

<sup>10</sup>For example in Ref. [FK2]

### 2.6.4. Spin Basis

The previous Sections 2.6.1 to 2.6.3 introduced approaches to construct primitive bases for continuous spatial DOFs and how to represent the corresponding kinetic as well as potential operators. In many physical scenarios, however, one encounters DOFs that are already described by a finite number of states such as internal DOFs of atoms. For example, if the  $\kappa$ th DOF is a spin- $1/2$  DOF, we can employ the z-basis as the primitive basis

$$\begin{aligned} |\chi_1^{(\kappa)}\rangle &= |\uparrow\rangle \\ |\chi_2^{(\kappa)}\rangle &= |\downarrow\rangle \end{aligned} \quad (2.43)$$

and represent the Hamiltonian using the Pauli matrices [629]

$$\sigma^0 = \begin{pmatrix} 1 & 0 \\ 0 & 1 \end{pmatrix} \quad \sigma^x = \begin{pmatrix} 0 & 1 \\ 1 & 0 \end{pmatrix} \quad \sigma^y = \begin{pmatrix} 0 & -i \\ i & 0 \end{pmatrix} \quad \sigma^z = \begin{pmatrix} 1 & 0 \\ 0 & -1 \end{pmatrix}. \quad (2.44)$$

In [FK3] this primitive basis is applied to treat a variety of intricate quantum spin models. The extension to higher total spins is straightforward, only requiring a matrix representation of the involved operators. The flexibility of the (ML)-MCTDH approach also allows for the simultaneous treatment of discrete internal and continuous motional DOFs which is of great importance in many physical scenarios such as in the presence of spin-orbit coupling [630–632].

## 2.7. The MCTDH Method for Bosons

In order to simulate the dynamics of ultracold atoms, numerical approaches are required that can describe indistinguishable particles, i.e., fermions and bosons. The many-body wave function of an ensemble of such identical particles must be symmetric under the exchange of two bosons and antisymmetric under the permutation of fermions. While the MCTDH method and its multi-layer extension have proven to be powerful and versatile tools to treat the dynamics of quantum many-body systems, they assume the DOFs/particles to be distinguishable and do not take any particle exchange symmetry into account. Even though it is, in principle, possible to manually symmetrize the coefficient vector of MCTDH [135], specialized approaches, namely the multi-configuration time-dependent Hartree method for fermions (MCTDHF) [430, 433–442] and MCTDHB [430–432] have been developed. They directly take the particle exchange symmetry into account when constructing the many-body wave function and allow for a much more efficient treatment of indistinguishable particles. Since the present thesis focuses on the bosonic problems, only the MCTDHB method is discussed in the following. This method has been employed to explore a variety of different physical setups including optical lattices [416, 418, 419, 633–636], harmonic potentials [633, 637–639] and double-well traps [432, 639–641].

First, in Section 2.7.1, the underlying many-body wave function ansatz is introduced. Section 2.7.2 describes the Hamiltonian structure that is typically assumed when applying MCTDHB and leads to the EOMs presented in Section 2.7.3. Section 2.7.4 provides a brief overview of the multi-layer extension of MCTDHB which allows treating Bose-Bose mixtures and was recently extended to Bose-Fermi as well as Fermi-Fermi mixtures by incorporating MCTDHF. Finally, in Section 2.7.5, MCTDHB is compared to the SQR of ML-MCTDH, which is an alternative approach to treat indistinguishable particles.

### 2.7.1. Wave Function Ansatz

The development of **MCTDHB** was inspired by earlier works that employed two time-dependent orbitals for description of bosonic dynamics [642, 643] as well as by the development of **MCTDHF** for fermionic systems [433, 434, 436, 437, 644]. Like **MCTDH**, **MCTDHB** employs a basis  $\{\varphi_i(t)\}_{i=1}^m$  of  $m$  variationally optimal, time-dependent **SPFs** or orbitals which are represented with respect to an underlying primitive basis (see Eq. (2.14)). Instead of employing Hartree products as in **MCTDH**, **MCTDHB** spans the many-body wave function with respect to bosonic number states or permanents [645] constructed from the instantaneous **SPF** basis, thus directly taking the particle exchange symmetry into account. In contrast to fermions, which are subject to the Pauli exclusion principle [387], multiple bosons may occupy the same orbital, resulting in

$$N_C = \binom{N + m - 1}{N} \quad (2.45)$$

possible ways of distributing  $N$  bosonic particles over  $m$  orbitals. Each of these combinations can be associated with a number state vector

$$\mathbf{n} = (n_1 \ n_2 \ \dots \ n_m)^\top \in \mathbb{N}_0^m \quad \text{with} \quad \sum_{i=1}^m n_i = N \quad (2.46)$$

of integer numbers, which denote the occupation numbers of the different single particle states. The corresponding number states are given by

$$|\mathbf{n}; t\rangle = \left( \prod_{i=1}^m \frac{(\hat{b}_i^\dagger(t))^{n_i}}{\sqrt{n_i!}} \right) |\text{vac}\rangle \quad (2.47)$$

where  $|\text{vac}\rangle$  denotes the vacuum state.  $\hat{b}_i^\dagger(t)$  and  $\hat{b}_i(t)$  are the bosonic creation and annihilation operators with respect to the  $i$ th **SPF** that obey the commutation relations [646]

$$\begin{aligned} [\hat{b}_i(t), \hat{b}_j^\dagger(t)] &= \delta_{ij} \\ \text{and } [\hat{b}_i(t), \hat{b}_j(t)] &= [\hat{b}_i^\dagger(t), \hat{b}_j^\dagger(t)] = 0. \end{aligned} \quad (2.48)$$

Finally, the wave function ansatz of the **MCTDHB** method reads

$$|\Psi(t)\rangle = \sum_{\mathbf{n}|N} C_{\mathbf{n}}(t) |\mathbf{n}; t\rangle, \quad (2.49)$$

where the sum runs over all possible  $N$ -particle number states. Figure 2.7 shows the graphical representation of this ansatz.

It should be noted that **MCTDHB** provides a mean-field description when considering a single orbital, i.e.,  $m = 1$ . If additionally contact interactions [78, 351] are considered between the particles, the method is then equivalent to solving the Gross-Pitaevskii equation (1.5). In general, the number of coefficients (2.45) increases exponentially with a growing number of particles  $N$  or orbitals  $m$ . The amount of correlation in the system dictates how many **SPFs** are required to accurately describe the physics and therefore limits the number of bosons. The stronger the correlations, the more orbitals are required, and the fewer particles can be treated. In the low excitation regime, where only few

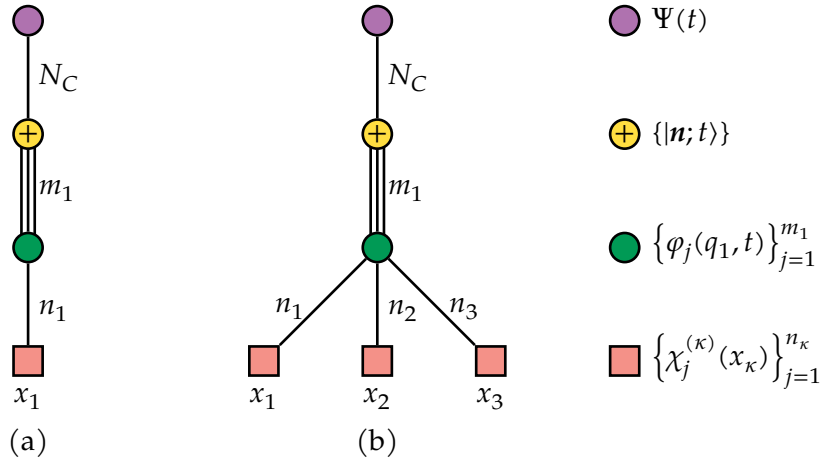


Figure 2.7.: (a) Tree diagram for the **MCTDHB** wave function ansatz of bosons in one spatial dimension. The plus sign indicates a bosonic node containing bosonic number states built from the **SPFs** of the node below, highlighted with a triple line. (b) Mode-combination (see Section 2.3.4) allows treating particles in more spatial dimensions as well, here shown for three dimensions, by combining multiple primitive bases.

orbitals are sufficient, up to  $\mathcal{O}(10^4)$  particles have been considered [637, 640, 647, 648]. In other cases the method is limited to a few particles when significant correlations are present [649–651], rendering many orbitals necessary.

## 2.7.2. Structure of the Hamiltonian

In order to derive the **MCTDHB EOMs**, one usually assumes a Hamiltonian of the form

$$\hat{H} = \sum_{i=1}^N \hat{h}(x_i, t) + \sum_{\substack{i=1 \\ j>i}}^N \hat{W}(x_i, x_j, t) \quad (2.50)$$

that consists of both one-body terms  $\hat{h}(x_i, t)$ <sup>11</sup> and two-body interactions  $\hat{W}(x_i, x_j, t)$  covering a wide range of physical systems. However, it should be noted that in general the **MCTDHB** method can be extended to handle higher order interaction terms. This opportunity is of relevance in light of the increased interest in three-body [132, 652–659] and even four-body [660–663] physics in recent years which includes fascinating topics such as Efimov physics [138, 141, 664] or the continuum limit of certain anyonic models [665].

In order to apply the Hamiltonian Eq. (2.50) to a **MCTDHB** wave function on the level of the number states, it can be expressed in second quantization [646, 666, 667] as

$$\hat{H} = \sum_{a,b=1}^m h_{ij} \hat{b}_i^\dagger \hat{b}_j + \frac{1}{2} \sum_{i,j,k,l=1}^m W_{ijkl} \hat{b}_i^\dagger \hat{b}_j^\dagger \hat{b}_k \hat{b}_l \quad (2.51)$$

with respect to the bosonic creation and annihilation operators (see Eq. (2.48)). The

<sup>11</sup>Such as an external potential  $V(x_i, t)$  or the kinetic energy operator proportional to  $-\partial_{x_i}^2$ .

matrix elements  $h_{ab}$  and  $W_{abcd}$  are determined by the integrals

$$h_{ab} = \langle \varphi_a | h(x) | \varphi_b \rangle = \int \varphi_a^*(x) \hat{h}(x) \varphi_b(x) dx \quad (2.52)$$

and

$$W_{abcd} = \langle \varphi_a \varphi_b | \hat{W}(x, x') | \varphi_c \varphi_d \rangle = \iint \varphi_a^*(x) \varphi_b^*(x') W(x, x') \varphi_c(x) \varphi_d(x') dx dx' \quad (2.53)$$

which are typically evaluated by exploiting the quadrature property of the DVR basis (see Section 2.6.2).<sup>12</sup>

The aforementioned operator structure allows for one-body terms and two-body interactions. In the ultracold regime,  $s$ -wave scattering is the dominant interaction process between particles [78, 351]. The interaction term is then given by a contact interaction  $W(x_i, x_j) = g\delta(x_i - x_j)$  which simplifies the integral (2.53). However, while the assumption of a  $\delta$ -potential is a valid approach in one spatial dimension, it breaks down in two or three dimensions [668–670] due to ultraviolet divergence such that effectively no scattering occurs [671]. A regularized  $\delta$ -interaction [352, 354–357, 359] has been employed to overcome this problem in analytical studies [353, 358] though it is not useful for numerical methods that operate in second quantization like MCTDHB [671]. Other approaches like the introduction of high-momentum cut-offs [669, 672–676] also cannot be easily transferred. Instead, it has been shown that carefully chosen Gaussian model potentials are the most suitable approach for mimicking the short-range interactions of ultracold bosons within the MCTDHB framework [671]. The POTFIT algorithm [514, 515] can then be used to obtain a sum-of-product form of such potentials which often leads to a numerical bottleneck as the number of terms in the Hamiltonian increases substantially.

### 2.7.3. Equations of Motion

The EOMs for the coefficients  $C_n(t)$  and the SPFs  $|\varphi_j(t)\rangle$  are derived by applying the Dirac-Frenkel TDVP (2.4) to the wave function ansatz (2.49) while usually assuming the structure of the Hamiltonian given in Eq. (2.51). Variation with respect to the coefficients  $C_n(t)$  yields the corresponding EOM

$$i\partial_t C_n(t) = \sum_m \langle n; t | (\hat{H}(t) - \hat{G}) | m; t \rangle C_m(t). \quad (2.54)$$

Here,

$$\hat{G} = g_{ab} \hat{b}_a^\dagger \hat{b}_b \quad (2.55)$$

is the constraint operator that lifts the ambiguity of the wave function ansatz (see Section 2.3.2), expressed in second quantization. As before, the time-dependence of the bosonic operators is not explicitly shown for the sake of readability. By varying with respect to the SPFs, one obtains the respective EOM<sup>13</sup>

$$i\partial_t |\varphi_j\rangle = \hat{P} \hat{g} |\varphi_j\rangle + (1 - \hat{P}) \left[ \hat{h} |\varphi_j\rangle + \sum_{k,\ell,p,q=1}^m (\rho^{(1)})_{jk}^{-1} \rho_{k\ell pq}^{(2)} \hat{W}_{\ell q} |\varphi_q\rangle \right]. \quad (2.56)$$

---

<sup>12</sup>The time-dependence of the matrix elements, SPFs and bosonic operators has been omitted for the sake of brevity.

<sup>13</sup>Omitting the time-dependence of all ingredients as in the MCTDH EOMs.

Here,  $\hat{P}$  denotes the projection operator on the instantaneous SPFs basis, see Eq. (2.25). Similar to MCTDH, the inverse of the one-body density matrix

$$\rho_{ij}^{(1)}(t) = \langle \Psi(t) | \hat{b}_i^\dagger \hat{b}_j | \Psi(t) \rangle, \quad (2.57)$$

enters the SPF EOM and needs to be regularized, see (2.30). Additionally, due to the assumption of two-body interactions, the reduced two-body density matrix

$$\rho_{ijpq}^{(2)}(t) = \langle \Psi(t) | \hat{b}_i^\dagger \hat{b}_j^\dagger \hat{b}_p \hat{b}_q | \Psi(t) \rangle \quad (2.58)$$

and the mean-field interaction

$$\hat{W}_{ab}(x, t) = \langle \varphi_a | \hat{W}(x, x', t) | \varphi_b \rangle = \int \varphi_a^*(x', t) \hat{W}(x, x', t) \varphi_b(x', t) dx' \quad (2.59)$$

appear in Eq. (2.56). When deriving the MCTDHB EOMs for Hamiltonians that contain more than two-body interactions, the corresponding higher-order density matrices and mean-fields will enter the corresponding SPF EOM.

Usually, the standard gauge  $\hat{g} = 0$  is chosen, leading to the simplified EOMs

$$i\partial_t C_n(t) = \sum_m \langle \mathbf{n}; t | \hat{H}(t) | \mathbf{m}; t \rangle C_m(t) \quad (2.60)$$

and

$$i\partial_t |\varphi_j\rangle = (1 - \hat{P}) \left[ \hat{h} |\varphi_j\rangle + \sum_{k,\ell,p,q=1}^m (\rho^{(1),-1})_{jk} \rho_{k\ell pq}^{(2)} \hat{W}_{\ell q} |\varphi_q\rangle \right]. \quad (2.61)$$

#### 2.7.4. Multi-Layer MCTDHX

The realization of mixtures of distinguishable atomic species such as different elements, isotopes or hyperfine states is of great interest in the field of ultracold quantum gases as it exhibits a rich variety of intriguing phenomena (see Section 1.1). In order to provide a theoretical description of such systems, schemes have been developed to describe Bose-Bose, Bose-Fermi or Fermi-Fermi mixtures by unifying the MCTDHB and MCTDHF methods. Early approaches [441, 677, 678] relied on expanding the wave function with respect to products of the number states for each species, i.e.,  $|\mathbf{n}^A; t\rangle \otimes |\mathbf{n}^B; t\rangle$ . However, such a construction quickly becomes intractable due to the enormous number of coefficients involved. The multi-layer multi-configuration time-dependent Hartree method for mixtures (ML-MCTDHX) approach achieves a much more compact representation by introducing multi-layering to the wave function ansatz. Originally developed for the description of bosonic mixtures [679, 680], the method was later extended to include fermionic species by incorporating MCTDHF [681]. Since the present thesis is concerned with the description of a single bosonic species, only the wave function ansatz of ML-MCTDHX will be briefly reviewed here for the sake of completeness. Ref. [681] provides an excellent review of the method including the EOMs. ML-MCTDHX has been successfully applied to a variety of problems such as impurity physics [208, 682, 683], breathing dynamics [370, 638] and solitons [684, 685].

For a two-component mixture, the many-body wave function is expanded in the first

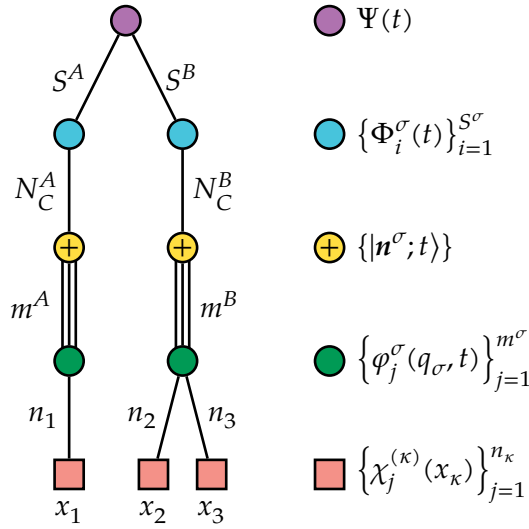


Figure 2.8.: Tree diagram of the **ML-MCTDHX** wave function to describe a binary mixture of two bosonic species  $\sigma \in \{A, B\}$ . The ansatz can be understood as employing multiple **MCTDHB** wave functions, often referred to as species basis functions, for each species and combining them in the **ML-MCTDH** sense.

layer as a superposition

$$|\Psi(t)\rangle = \sum_{i=1}^{S^A} \sum_{j=1}^{S^B} A_{ij}(t) |\Phi_i^A(t)\rangle |\Phi_j^B(t)\rangle \quad (2.62)$$

of so-called species basis states  $|\Phi_i^\sigma(t)\rangle$  where  $\sigma \in \{A, B\}$  denotes the species. For each species, a time-dependent **SPF** basis is employed, and the species basis states are given as superpositions of the corresponding number states

$$|\Phi_i^\sigma(t)\rangle = \sum_{n^\sigma | N^\sigma} C_{i,n^\sigma}(t) |n^\sigma; t\rangle. \quad (2.63)$$

Consequently, the species basis states be understood as **MCTDHB** or **MCTDHF** wave functions. Figure 2.8 shows a tree diagram representing a **ML-MCTDHX** ansatz for a binary mixture. The flexibility of **ML-MCTDH** allows to extend this construction further by including additional species, as done recently for triple mixtures [208, 686], or coupling to other types of distinguishable **DOFs**.

### 2.7.5. ML-MCTDH in Second Quantization Representation

The **second quantization representation (SQR)** of **ML-MCTDH** [687, 688] provides an alternative to **MCTDHB** and **MCTDHF** for the description of indistinguishable particles and has been successfully applied to charge transport processes [545, 687, 689–692]. In the following, a brief introduction of **ML-MCTDH-SQR** for bosons is provided, but the method can be readily applied to fermions as well [688]. Instead of incorporating the particle exchange symmetry by spanning the many-body wave function with respect to permanents or determinants, **ML-MCTDH-SQR** directly operates in the occupation



number basis. When considering a bosonic model comprising  $L$  orbitals or sites, the **ML-MCTDH-SQR** method treats the occupation number of each orbital as a **DOF**. The occupation number basis

$$|\chi_1^{(\kappa)}\rangle = |0\rangle \quad |\chi_2^{(\kappa)}\rangle = |1\rangle \quad \dots \quad |\chi_{N+1}^{(\kappa)}\rangle = |N\rangle, \quad (2.64)$$

allowing zero to  $N$  particles to occupy each orbital, provides the corresponding primitive basis. Operators are then given as a sum of products of bosonic creation, annihilation and number operators. The corresponding matrix elements read

$$\begin{aligned} \langle \chi_i^{(\kappa)} | \hat{b}_\kappa^\dagger | \chi_j^{(\kappa)} \rangle &= \sqrt{j} \delta_{i,j+1} \\ \langle \chi_i^{(\kappa)} | \hat{b}_\kappa | \chi_j^{(\kappa)} \rangle &= \sqrt{j-1} \delta_{i,j-1} \\ \langle \chi_i^{(\kappa)} | \hat{n}_\kappa | \chi_j^{(\kappa)} \rangle &= (j-1) \delta_{i,j} \end{aligned} \quad (2.65)$$

in the occupation number basis<sup>14</sup>.

In contrast to **MCTDHB** and **MCTDHF**, which consider only number states with a fixed total number of particles, **ML-MCTDH-SQR** contains configurations of different particle numbers. Notably, the ansatz spans the full Fock space [667] of zero to  $N^L$  particles when considering  $L$  orbitals each containing up to  $N$  particles. Therefore, **ML-MCTDH-SQR** provides a more general description, allowing to describe models that do not conserve the particle number and which are inaccessible to **MCTDHB** and **MCTDHF**. However, when systems that are restricted by particle number conservation are considered, the method is often at a disadvantage due to the large number of irrelevant configurations in the wave function ansatz. During the derivation of the **MCTDHB** and **MCTDHF** EOMs, one assumes a certain structure of the Hamiltonian (see Eq. (2.51)) thus limiting the kinds of terms that may occur, typically one- and two-body operators. **ML-MCTDH-SQR** on the other hand treats the occupation of the different orbitals as **DOFs** and can straightforwardly incorporate higher order terms as long as they can be written in a sum of product form.

It should be noted that the creation and annihilation operators of the original **ML-MCTDH-SQR** approach given by (2.65) are time-independent. The recently developed, optimized second quantization representation (OSQR) [694, 695] improves this approach by employing variationally optimal, time-dependent operators  $\hat{b}_\kappa^\dagger(t)$ . These operators are represented with respect to time-independent, primitive operators  $a_\mu^\dagger$  as

$$\hat{b}_\kappa^\dagger(t) = \sum_{\mu=1}^n c_{\mu\kappa}(t) a_\mu^\dagger. \quad (2.66)$$

This construction can reduce the number of coefficients in the wave function ansatz significantly, when fewer time-dependent than primitive operators are required to describe the system accurately.

<sup>14</sup>The matrix representations of the equivalent fermionic operators are not as straightforward. In order to capture the particle exchange symmetry correctly, the creation and annihilation operators acting on the  $i$ th site accumulate a phase factor that depends on the occupation of all previous sites 1 to  $i-1$  resulting in  $i$ -body operators. The treatment can be significantly simplified [687, 693] by employing the Jordan-Wigner transformation [666].

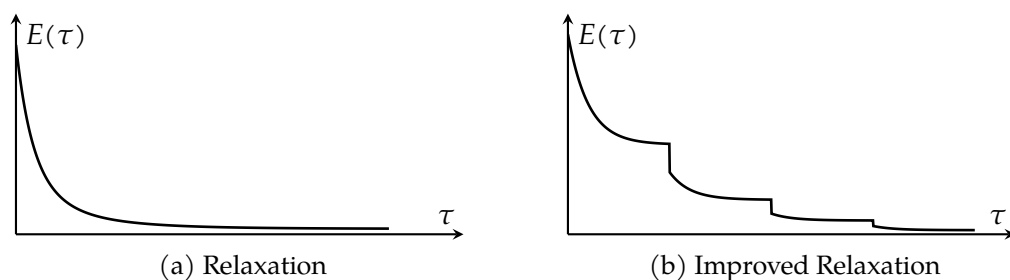


Figure 2.9.: Typical convergence behavior of the total energy  $E(\tau)$  as a function of the imaginary propagation time  $\tau$  using (a) normal relaxation and (b) improved relaxation. The jumps in the total energy seen in panel (b) correspond to the updating of the top-level coefficients via exact diagonalization.

## 2.8. Relaxation Procedures

The **MCTDH** family of methods introduced in Sections 2.3, 2.4 and 2.7 is a set of algorithms to study the quantum dynamics of many-body systems by computing the time evolution of a given initial state. However, by switching to propagation in imaginary time  $\tau = it$ , they can also be applied to obtain eigenstates of the Hamiltonian by means of energy relaxation [420, 423]. This is particularly useful for large systems where an exact diagonalization of the Hamiltonian matrix [696–700] is prohibitive due to the involved computational effort and memory requirements. Obtaining eigenstates of the Hamiltonian allows studying static properties of the system or providing initial states for the propagation in real time. For example, it is common practice to compute the interacting ground state of an ultracold bosonic system starting from a configuration where all particles occupy the same **SPF**. The result can then serve as an initial state to study real time dynamics.

First, in Section 2.8.1, the principle of energy relaxation is introduced. Section 2.8.2 discusses a more advanced relaxation algorithm that has been developed in the framework of the **ML-MCTDH** family of methods and combines imaginary time propagation with exact diagonalization in order to achieve faster convergence and allows computing excited states as well. Section 2.8.3 describes how to handle a pitfall when treating particle number conserving systems of indistinguishable particles using **ML-MCTDH** in **SQR**.

### 2.8.1. Energy Relaxation

The goal of energy relaxation is to compute the ground state of the Hamiltonian starting from some initial trial state  $|\Psi(0)\rangle$ . By propagating the wave function according to the time-dependent Schrödinger equation in imaginary time, i.e.,

$$\partial_\tau |\Psi(\tau)\rangle = -\hat{H} |\Psi(\tau)\rangle, \quad (2.67)$$

it will evolve towards the ground state [601]. This behavior becomes more apparent when formulating the solution of Eq. (2.67) in the eigenbasis  $\{|E_n\rangle\}$  of the Hamiltonian:

$$|\Psi(\tau)\rangle = \sum_n A_n e^{-\tau E_n} |E_n\rangle. \quad (2.68)$$

The coefficients  $A_n = \langle E_n | \Psi(0) \rangle$  depend on the initial conditions and are determined by the overlap of  $|\Psi(0)\rangle$  with the eigenstates of the Hamiltonian. The contribution of each eigenstate to the instantaneous wave function decays exponentially according to the corresponding energy eigenvalue such that after a sufficiently long propagation time, the lowest energy state becomes the dominant component (see Fig. 2.9a). If the overlap between the initial state and the ground state is finite, i.e.,  $A_0 > 0$ ,  $\Psi(\tau)$  converges arbitrarily close to the ground state after long enough imaginary propagation times. It should be noted, that the norm of the wave function given by Eq. (2.68) is not conserved. The norm can be restored by manually renormalizing the wave function or employing the modified Schrödinger equation

$$\partial_\tau |\Psi(\tau)\rangle = - \left( \hat{H} - \langle \Psi(\tau) | \hat{H} | \Psi(\tau) \rangle \right) |\Psi(\tau)\rangle, \quad (2.69)$$

instead of Eq. (2.67) [420].

The convergence speed of the energy relaxation is dictated by the overlap between the ground state and the initial state as well as its energetic separation from the excited states. A large overlap as well as a large energetic gap lead to faster convergence while the opposite situation can be detrimental to the efficiency. In the case that the ground state is degenerate, the wave function will converge to an arbitrary linear combination of the degenerate states.

In principle, it is possible to compute excited states using energy relaxation by ensuring that the wave function is orthogonal to energetically lower lying states. However, this approach is very cumbersome in practice since it first requires to compute the lower states and then continuously projecting them out, which is challenging as the involved **SPF** bases might differ. A better approach is to employ the improved relaxation algorithm discussed in Section 2.8.2. In many scenarios, improved relaxation also converges faster than energy relaxation when computing the ground state.

### 2.8.2. Improved Relaxation Algorithm

Computing the ground state of a Hamiltonian using energy relaxation as described in Section 2.8.1 relies on the exponential damping of the excited states which is an inherently slow process often requiring long propagation times to achieve adequate accuracy. The improved relaxation algorithm [423, 426, 688, 701] often achieves faster convergence by combining imaginary time propagation with exact diagonalization into a hybrid approach that provides access to excited states as well.

In order to obtain the working equations of the improved relaxation algorithm, the time-independent variational principle is applied to the **ML-MCTDH** ansatz (A.1) [688, 701]. The variation with respect to the top-level coefficients  $A_J^{(1)}$  yields an eigenvalue equation,

$$\sum_K \underbrace{\langle \Phi_J^{(1)} | \hat{H} | \Phi_K^{(1)} \rangle}_{H_{JK}} A_K^{(1)} = E A_J^{(1)}, \quad (2.70)$$

which can be solved by diagonalizing the matrix  $\mathbf{H} = (H_{JK})$  to obtain the eigenenergies as well as the eigenvectors in the current **SPF** basis. Variation with respect to the **SPFs** then yields highly non-linear equations which could be solved iteratively but are difficult to converge [688, 701] similar to early multi-configuration self-consistent field theory [702]. Instead, the improved relaxation algorithm alternates between updating the top-level coefficients via diagonalization and then rotating the **SPFs** via imaginary

time propagation while keeping the top-level coefficients fixed. By always choosing the  $n$ th eigenstate when performing the diagonalization, the wave function converges towards the  $n$ th eigenstate of the Hamiltonian as long as there exist significant overlap between the initial state and the relevant low-energy spectrum. To this end, it can be beneficial to add random noise to the initial state to ensure that it contains contributions from all important eigenstates. Figure 2.9b shows the convergence behavior of the improved relaxation algorithm exhibiting jumps in energy due to the sudden update of the top-level coefficients while the timespans of energy relaxation show a smooth exponential decay similar to the standard relaxation algorithm (see Fig. 2.9). Typically, one is interested in obtaining one of the lowest energetic eigenstates such that algorithms to compute extremal eigenvalues are applicable. These methods have the advantage that they only require to compute the action of the Hamiltonian on a vector instead of its full matrix representation and can treat much larger problems than algorithms which compute the full spectrum at once. Examples for such numerical methods are the implicitly restarted Lanczos method [366] provided by ARPACK [703] or the Davidson algorithm [367].

### 2.8.3. Relaxation in Second Quantization Representation

When treating particle number conserving Hamiltonians such as the Bose-Hubbard model [38, 96, 704], one is routinely interested in computing ground states that correspond to a specific particle number which might not necessarily be the state with overall lowest energy. The wave function ansatz of the ML-MCTDH method in SQR allows for all possible particle numbers from 0 to  $N^L$  when considering  $L$  sites that may contain up to  $N$  bosons each (see Section 2.7.5). In the absence of numerical errors, this would not constitute a problem since the particle number is a constant of motion under the time evolution with a particle number conserving Hamiltonian, and it would be sufficient to choose an initial state with the correct number of bosons. However, inaccuracies like the regularization of the one-body density matrix (see Eq. (2.30)) or the overall inexactness of floating point arithmetic can lead to small contributions of configurations with a different particle number. If the corresponding states exhibit lower energies than the desired state, they are enhanced under imaginary time evolution and can become the dominant contributions to the wave function. It should be emphasized that these inaccuracies do not pose an issue for real time propagation as they remain small due to the norm conservation of the wave function, leading only to negligible contributions from undesired states to the final state.

In order to overcome the issue with energy relaxation and enforce the numerical stability of the method, a penalty term is usually added to the Hamiltonian which penalizes and suppresses configurations with a different particle number than the desired one. An intuitive choice is a quadratic penalty term which increases the energy of unwanted states

$$\hat{H}_{\text{penalty}} = \lambda \left( \sum_{i=1}^L \hat{n}_i - N \right)^2 \quad (2.71)$$

according to some large parameter  $\lambda > 0$ . To be used in the ML-MCTDH method,

Eq. (2.71) can be written in a sum-of-products form as

$$\hat{H}_{\text{penalty}} = \lambda \sum_{i,j=1}^L \hat{n}_i \hat{n}_j - 2\lambda N \sum_{i=1}^L \hat{n}_i + \lambda N^2. \quad (2.72)$$

In this form, it becomes evident that  $\hat{H}_{\text{penalty}}$  generates  $L^2 + L + 1$  additional terms in the Hamiltonian which becomes quite costly for large systems. To overcome this poor scaling behavior, Ref. [695] suggests using the term

$$\hat{H}_{\text{penalty};2} = \frac{2\lambda}{\zeta^2} \cosh \left( \zeta \left( \sum_{i=1}^L \hat{n}_i - N \right) \right) \quad (2.73)$$

with large positive parameter  $\lambda$  and a small positive parameter  $\zeta$  instead. When written in a sum-of-product form,

$$\hat{H}_{\text{penalty};2} = \frac{\lambda}{\zeta^2} e^{-\zeta N} \prod_{i=1}^L e^{\zeta \hat{n}_i} + \frac{\lambda}{\zeta^2} e^{\zeta N} \prod_{i=1}^L e^{-\zeta \hat{n}_i} - \frac{2\lambda}{\zeta^2}, \quad (2.74)$$

only three additional terms are added to the Hamiltonian, one of which is a constant that may be omitted. A Taylor expansion of Eq. (2.73) in the parameter  $\zeta$ ,

$$\hat{H}_{\text{penalty};2} \approx \underbrace{\lambda \left( \sum_{i=1}^L \hat{n}_i - N \right)^2}_{\hat{H}_{\text{penalty}}} + \frac{\zeta^2 \lambda}{12} \left( \sum_{i=1}^L \hat{n}_i - N \right)^4 + \mathcal{O}(\zeta^4) \quad (2.75)$$

highlights that Eq. (2.71) and Eq. (2.73) are asymptotically equivalent for  $\zeta \rightarrow 0$ . Despite its obvious advantages when it comes to the number of terms added to the Hamiltonian, we found the second penalty term to perform worse with respect to the simulation runtimes, most likely due to an increase in stiffness of the EOMs, and also much harder to control due the presence of two parameters.



## Outlines of Scientific Contributions

THE present cumulative dissertation is based on the scientific contributions published in the References [FK1], [FK2] and [FK3] which are summarized in this chapter. More detailed explanations can be found in the included manuscripts provided in Chapter 4.

### 3.1. Dynamical Pruning of the Non-Equilibrium Quantum Dynamics of Trapped Ultracold Bosons

The **MCTDHB** method presented in Section 2.7 has proven to be a powerful and versatile ab-initio approach for the investigation of the nonequilibrium dynamics of bosonic many-body systems that provides a beyond-mean-field description. Like other numerical approaches, **MCTDHB** faces the challenge of an exponentially growing dimension of the Hilbert space when studying large systems. The number of configurations that are taken into account grows rapidly as the number of particles and/or **SPFs** increases, see Eq. (2.45). Various approaches in the scope of the **MCTDH** family of methods have been devised in the literature in order to tackle this issue and reduce the computational effort. For instance, configuration selection schemes for **MCTDH** [705, 706] as well as **restricted active space (RAS)** schemes for **MCTDHF** [707–710] and **MCTDHB** [711] have been developed. These procedures try to exploit the observation that not all configurations are equally important for the description of the dynamics and rely on considering only the most relevant Hartree products/number states. Since this selection is static and does not adapt to the dynamics, these approaches are not able to account for the fact that the importance of a configuration may change over time. Furthermore, the a priori removal of important configurations may restrict the evolution of the system artificially leading to unphysical results. Hence, a good selection is crucial for the success of these approaches, often requiring in-depth knowledge of the underlying physics. Therefore, in order to apply such schemes to arbitrary setups, the development of dynamical methods that can adapt on-the-fly is desirable.

In the context of molecular dynamics with distinguishable **DOFs**, such dynamical approaches have been applied successfully in the framework of **MCTDH**. The runtime of simulations can be greatly reduced by pruning the primitive basis [712, 713] or the coefficients of the wave function [713]. However, ultracold atoms are typically subject to external trapping potentials, such that there rarely exist large regions of unoccupied real space rendering the pruning of the primitive basis less lucrative. Additionally, the neighborhood criterion proposed for the wave function coefficients in [713] cannot be easily transferred to bosonic number states, thus requiring development of specialized approaches for indistinguishable particles.

In [FK1], a general dynamical pruning approach for **MCTDHB** is presented that adapts

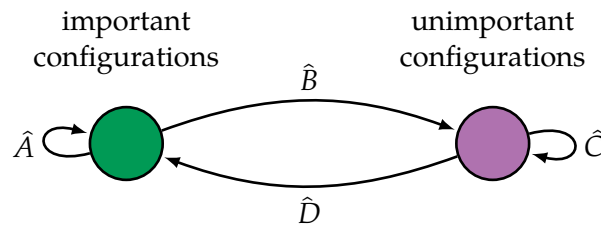


Figure 3.1.: Sketch of the partitioning of the Hamiltonian  $\hat{H} = \hat{A} + \hat{B} + \hat{C} + \hat{D}$  exploited in the dynamical pruning of MCTDHB in [FK1]. The first, Hermitian pruning approach deactivates the coupling among the inactive configurations  $\hat{C}$ , while the second, non-Hermitian scheme additionally removes the scattering from inactive to active configurations  $\hat{D}$ .

during the time evolution of the system. As a first step, a pruning criterion is introduced that is used to classify the configurations as either important or unimportant according to a fixed threshold, which is a parameter of the algorithm. Here, two different pruning criteria are proposed, one based on the magnitude of the coefficients and another one based on their relative contribution to the total energy. The selection of the important configurations can adapt to the dynamics of the system and is updated in regular time intervals, the size of which is another parameter of the algorithm.

Next, in order to exploit the partitioning of the configuration space, the Hamiltonian is reinterpreted as consisting of four parts that couple the two disjoint sets of configurations (see Fig. 3.1). Based on this representation two different modifications of the MCTDHB EOM for the coefficients (2.60) are proposed. The first approach is to neglect couplings among the unimportant configurations ( $\hat{C}$ ) thus reducing the computational complexity of the coefficient EOM. It should be noted, that in this protocol configurations that have previously been deemed to be unimportant may become active again due to scattering from active configurations by part  $\hat{B}$  of the Hamiltonian, allowing the configuration selection to adapt to the dynamics of the system. A second pruning approach additionally removes the coupling  $\hat{D}$  that mediates scattering from the unimportant to the important configurations, thus further reducing the computational effort. The resulting Hamiltonian of this scheme is strictly speaking non-Hermitian, but the numerical results indicate that the many-body dynamics can still accurately be captured.

In order to benchmark the performance of the dynamical pruning approach two typical dynamical scenarios motivated from ultracold atom physics are considered. It is a common setup to subject the particles to a periodic optical lattice [38] which can be realized experimentally by forming a standing wave from interfering two counter-propagating laser beams. The system is prepared in the interacting ground state of a five well lattice (see Fig. 3.2a) and then subjected to a sudden change of the interaction strength which can be achieved experimentally via Feshbach [72, 73] or confinement induced resonances [74–77]. Similar scenarios have been extensively investigated with MCTDHB in the literature [416, 418, 419, 633–636]. The second scenario starts from the interacting ground state of bosons confined in an external harmonic potential that is suddenly disturbed by a central, Gaussian barrier (see Fig. 3.2b) forming what is known in the literature as a dimple trap [714]. A similar scheme employing a continuous ramping of the barrier has already been investigated with MCTDHB in Ref. [431]. In the literature, many studies of both Harmonic [633, 637–639] and double-well [432, 639–641]



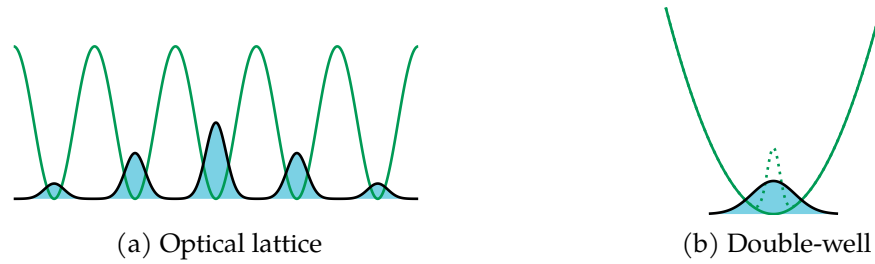


Figure 3.2.: Sketch of the two dynamical scenarios considered when benchmarking the dynamical pruning approach for **MCTDHB** in [FK1]. (a) The system is prepared in the interacting ground state of a five well optical lattice. Then the dynamics is triggered by suddenly increasing the interaction strength between the particles. (b) The interacting ground state of a harmonic potential is suddenly disturbed by ramping up a central, Gaussian barrier (dotted line) effectively forming a double-well potential.

trapping potentials have been conducted with **MCTDHB**, rendering this a common scenario.

In both scenarios, all combinations of configuration selection criteria and modifications to the coefficient **EOM** are considered. The accuracy of the approach is assessed by comparing a variety of quantities to full, unpruned **MCTDHB** simulations. For this purpose, fundamental properties of the wave function such as the energy conservation, normalization and the orthonormality of the **SPFs** as well as the reduced one- and two-body density matrices are analyzed. As long as the pruning threshold and the update time are chosen appropriately, the dynamical pruning approach is found to describe the underlying dynamics accurately only introducing small errors. For a detailed discussion of all quantities the reader is referred to the manuscript in Section 4.1 and only some particularly interesting observations are highlighted here.

Except for the natural populations, where the energy criterion yields slightly better results, both configuration selection criteria perform equally well. The non-Hermitian scheme yields only to slightly larger errors than the Hermitian scheme. The only exception is the norm of the wave function where the Hermitian modification of the **EOMs** is on par with unpruned **MCTDHB** while the other approach introduces some slight deviation from unity. The efficiency of the dynamical pruning of **MCTDHB** is found to be strongly dependent on the particular system under investigation. In the case of the optical lattice, more than 97% of the configurations can be classified as unimportant at all times, which results in a speed-up by a factor of up to seven compared to unpruned **MCTDHB** when considering large particle numbers and the non-Hermitian modification of the **EOMs**. For the same regime, the Hermitian pruning scheme still leads to a speed-up by more than a factor of four. When simulating the harmonic trap setup, only about half of the configurations can be pruned during most of the time evolution which drastically reduces the speed-up that can be achieved to 1.4 for the Hermitian and 1.8 for the non-Hermitian scheme. Finally, the long-time evolution of the approach as well as the impact of the pruning parameters are investigated. Using the example of the total energy, it is shown that most of the error builds early in the dynamics before growing very slowly afterwards, almost saturating. The pruning threshold is found to influence the accuracy of the dynamical pruning approach in a controlled manner which converges towards the full **MCTDHB** calculation as the threshold is lowered. By varying

the update time for the coefficient selection it is shown that too large values, i.e., too infrequent updates, can lead to incorrect results. This behavior highlights the importance of the development of dynamical pruning schemes that can adapt to the evolution of the system.

### 3.2. Bosonic Quantum Dynamics Following Colliding Potential Wells

Ever since the first experimental realization of Bose-Einstein condensates [8, 9, 715], ultracold atomic gases have been the subject of an abundance of theoretical and experimental studies. Due to their excellent isolation from the environment and the possibility to tune the relevant characteristics of the system such as interactions, particle number, dimensionality and external potentials, they provide a versatile platform to simulate a plethora of different quantum many-body systems [102, 224, 229]. A particularly interesting direction of research is to investigate fast physical processes such as electron dynamics [235–238, 716] by emulating them with much slower-moving atomic particles, a process sometimes referred to as temporal magnification [716]. In light of these studies, colliding clouds of ultracold atoms could be employed to mimic electrons during atom-atom or atom-ion collisions, potentially providing deep insights into the fundamental processes such as projectile ionization [717, 718] or charge transfer [719, 720]. Another intriguing application of ultracold atoms is quantum information processing [229]. In this context, controlled collisions of cold neutral atoms have been proposed as an efficient mechanism to create highly entangled states as well as to implement two-qubit gates [38, 721], two essential building blocks of a quantum computer [722, 723].

Experimentally, collisions of ultracold atomic clouds can be realized using optical tweezers. Originally developed for the manipulation of micrometer sized particles [724, 725] using highly focused laser beams, optical tweezers have been refined to operate at a variety of length scales ranging from individual atoms [726, 727] to bacteria and viruses [728]. By trapping and accelerating ultracold atomic clouds in optical tweezers [53, 54], fundamental properties of quantum scattering processes like partial wave interference have already been studied, effectively building an “optical collider” [52, 55, 56]. Furthermore, Rydberg atoms trapped in arrays of optical tweezers are an auspicious platform quantum computing and simulation [285, 326–329].

In [FK2], we study the collisions of two Gaussian potential wells containing two interacting bosons using the MCTDHB method described in Section 2.7. While the computational approach is able to handle more particles easily, the main signatures of the dynamics can be most clearly identified in this few-body scenario. Initially, the system is prepared in the interacting ground state of both bosons contained in the resting left well. Starting from a large initial separation (Fig. 3.3a), the wells are then accelerated towards each other forming a transient double structure (Fig. 3.3b). After the wells penetrated each other, they separate again, moving in opposite directions (Fig. 3.3c) until they reach their initial separation again.

The one-body density [729] provides insight in the spatial distribution of the particles at all times and unravels the main signatures of the dynamics of the system. During the first stage of the time evolution, the particles follow the trajectory of the left well. As the wells come into proximity an effective, transient double-well structure forms which drives oscillatory transport of the particles. Afterwards, the wells separate from each

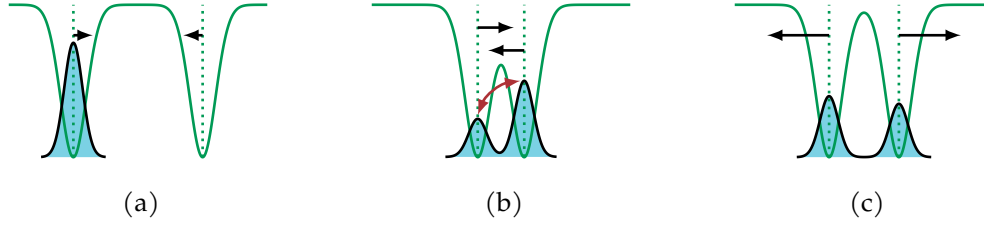


Figure 3.3.: Sketch of the dynamical setup studied in [FK2]. (a) Initially, the particles are prepared in the interacting ground state of the left well. The wells then start to accelerate towards each other. (b) In proximity the two wells form a transient double-well structure that changes over time. (c) The potential wells pass through each other and separate again.

other again, taking a fraction of particles with them. The final distribution of particles depends on the acceleration of the wells. For certain values of the acceleration, the particles are localized in one of the wells while for others we observe a distribution over both wells. Within each well a sloshing motion of the particles around the well center is visible, which can be characterized as a dipole mode [78, 351]. Additionally, a less pronounced, periodic widening and narrowing of the atomic clouds within each well takes place, resembling an intrawell breathing mode. The amplitudes of both of these collective excitations are larger the more evenly the particles are distributed over both wells and vanish when the particles are localized in a single well after the separation. For high values of the acceleration, a density halo outside the potential wells indicates a partial deconfinement of the initially trapped particles. All of these phenomena are then analyzed in greater detail using more involved observables.

By employing the center of mass position of the particles, the particle transfer between the wells can be quantified. The final, average position of the bosons oscillates as a function of  $v_f^{-1} \propto a^{-1/2}$ , i.e., the inverse final speed or the inverse square root of the acceleration. Modified center of mass observables allow to determine the frequency and amplitude of the dipole modes and unravel a  $90^\circ$  phase shift between the two wells.

As a next step, the many-body wave function is projected onto the instantaneous eigenbasis of the one-body Hamiltonian in order to develop an understanding of the most relevant single particle states. In the beginning, the two energetically lowest states are predominantly occupied. As the wells approach each other, the oscillatory particle transport starts as soon as these states turn into over-barrier states such that the transport can be classified as an over-barrier process in this single particle picture. During the last stage of the time evolution for fast collisions, a significant occupation of untrapped single particle states becomes apparent. By comparing to simulations where the second, initially empty well is absent, two distinct mechanisms for this deconfinement are identified. Firstly, we observe a steady increase of particle deconfinement with increasing acceleration due to the inertia of the bosons that already sets on early during the time evolution. Secondly, a sudden increase in the occupation of untrapped single particle states during the last stage of the dynamics at certain values of  $v_f^{-1}$  indicates another deconfinement mechanism, which is not present when only a single well is considered. Using a more involved many-body analysis with respect to number states constructed from the instantaneous eigenbasis of the one-body Hamiltonian, this phenomenon can be analyzed in greater detail, confirming that indeed the particle untrapping is enhanced in the presence of two wells around certain values of  $v_f^{-1}$  which is reminiscent of an

ionization spectrum.

Finally, the entanglement of the final state is analyzed by means of the von Neumann entanglement entropy [730]. For specific intermediate values of  $v_f^{-1}$ , which correspond to an even density distribution over both wells, strong entanglement between the particles builds up, reaching almost 75% of the maximum possible value. If both bosons are localized in the same well, the entanglement entropy is significantly reduced becoming almost negligible. While the entanglement entropy drops to zero as the acceleration increases, it remains finite for slow collisions, highlighting the importance of the transient double-well structure for the entanglement generation.

### 3.3. Exploring Disordered Quantum Spin Models with a Multi-Layer Multi-Configurational Approach

Historically, quantum spin models have been proposed to explain the magnetic properties of materials [362, 731–734]. Nowadays, they play a crucial role in many areas of physics such as quantum information processing [556]. The possibility of realizing quantum spin models in Rydberg atom arrays [285, 325, 330, 338] and ultracold atoms trapped in optical lattices [51, 226, 735], renders them of immediate interest for the research of ultracold atom systems. Several numerical methods have been developed to study the properties of quantum spin models. For small system sizes, exact diagonalization [696] provides access to eigenstates of the Hamiltonian. Methods based on MPS [446–449] such as DMRG [450–453], time evolving block decimation [584–586, 736] or TDVP-based approaches [591, 594, 595] can treat much larger numbers of spins and are particularly successful in describing one-dimensional geometries. More advanced tensor network state methods such as PEPS [459–469] are tailored towards more than one spatial one-dimensions or in the case of MERA [454–458] are designed to describe systems at quantum critical points.

Often, when investigating quantum many-body systems, disordered systems are of particular interest. Inhomogeneities may be introduced due to imperfect, experimental realizations of the system, such as due to dislocations or impurities in crystals [737–739]. In other scenarios, the role of disorder is the central object of interest, for example when studying the fractional quantum Hall effect [740–742], glassy systems [743–745] or Anderson [746–748] as well as many-body localization [749–755]. The numerical treatment of such non-translationally invariant systems is often particularly challenging due to the high amount of degeneracy in the low energy spectrum that results in many cases in a violation of the so-called area law of entanglement. In  $D$  spatial dimensions, the area or boundary law [756–763] states that the entanglement entropy [730] between a subsystem  $A$  with a size proportional to  $L$  in each dimension and the remainder of the system grows at most proportionally to the size  $|\partial A|$  of its boundary  $\partial A$  [443], i.e.,

$$S(A) \propto |\partial A| \propto L^{D-1}. \quad (3.1)$$

Consequently, in a one-dimensional geometry, the entanglement entropy of a block as a function of its size is bounded by some constant value  $S(A) \leq S_0$ . However, a variety of critical models have been discovered, that exhibit a weak area law violation [583, 763–777] that require logarithmic corrections of Eq. (3.1) [778–780], i.e.,

$$S(A) \propto L^{D-1} \log(L). \quad (3.2)$$

While in  $D = 1$  the validity of the boundary law has been linked to the presence of an energy gap, this connection is less clear for  $D > 1$  [443]. Furthermore, research in recent years has shown that quantum systems exhibiting even stronger violations of the area law are more common than previously expected [781–787]. In the presence of area law violations, the merits of MPS based algorithms have to be questioned and the development of new methods that fare well when treating such challenging setups is of great interest.

In Ref. [FK3], the ML-MCTDH method presented in Section 2.4 is applied to the study of the ground states of disordered quantum spin models for the first time. In order to benchmark this approach, the ground state energy, connected correlation functions [463, 788] and the von Neumann entanglement entropy [730] of different setups are studied, starting from a translationally invariant system and then moving to models that exhibit weak or strong violations of the area law. The accuracy of the ML-MCTDH results is assessed by comparison with exact diagonalization [696] and DMRG [450–453] calculations.

The ubiquitous *transverse field Ising model* (TFIM) [789–791] forms the starting point of the analysis since it is a well studied and fundamental spin model that also has been realized experimentally with trapped ions [792–795], single crystals [796], and Rydberg atoms [325, 330, 797, 798]. Both short-range, nearest neighbor and long-range interactions are considered when treating this homogeneous system. The ground state of the TFIM obeys the area law and the ground state energy as well as correlations are captured accurately by all three methods under consideration. However, exact diagonalization is limited to treating a few spins as it relies on the diagonalization of the Hamiltonian matrix while both ML-MCTDH and DMRG are shown to scale to much larger system sizes, here demonstrated for up to 512 spins. Furthermore, by studying the TFIM with short-range interactions on a square lattice, the ML-MCTDH method is shown to be capable of treating two-dimensional systems.

After demonstrating that ML-MCTDH can describe quantum spin models accurately, the focus is shifted to disordered systems. The first of which is a XY spin glass [799–801] which has been shown to exhibit weak violation of the area law [786, 787]. The corresponding Hamiltonian is characterized by random long-range interactions that render the system non-translationally invariant. Due to the stochastic nature of the model, multiple disorder realizations are considered<sup>1</sup>. The disorder of the spin couplings leads to many near-degeneracies in the low energy spectrum of the Hamiltonian which are not well resolved in the DMRG algorithm. Consequently, DMRG usually locks on to one of the first excited states and therefore cannot reproduce the correlations among the spins correctly or achieve the same accuracy of the ground state energy as for the TFIM. The ML-MCTDH method, on the other hand, shows excellent agreement with exact diagonalization.

The last model analyzed in Ref. [FK3] is motivated by the strong disorder renormalization group framework [781, 802–805]. The Hamiltonian is defined on a chain and employs nearest-neighbor interactions with a strength that decays like a Gaussian with increasing distance from the central bond, thus breaking the translational invariance of the system. The model has been shown to exhibit a strong violation of the area law [781] characterized by a linear growth of the entanglement with respect to the system size. As in the XY spin glass, DMRG does not achieve the same accuracy of the ground state

---

<sup>1</sup>For this purpose, particularly challenging realizations are chosen that exhibit large deviations between the exact diagonalization and DMRG results.

energy as in the [TFIM](#), but this time succeeds in capturing the correlations correctly except for a small deviation in one of the data points. Again, [ML-MCTDH](#) shows excellent agreement with exact diagonalization and also captures the linear growth of the entanglement entropy, enabled by its flexibility of constructing the wave function tree. [DMRG](#) cannot reproduce this scaling behavior due to the formation of distant singlet states, which the algorithm is struggling to entangle.

# 4

## Scientific Contributions

**T**HE present chapter includes the manuscripts of the scientific contributions published in References [FK1–FK3] which have been summarized in Chapter 3.

### 4.1. Dynamical Pruning of the Non-Equilibrium Quantum Dynamics of Trapped Ultracold Bosons

# Dynamical pruning of the non-equilibrium quantum dynamics of trapped ultracold bosons

Cite as: *J. Chem. Phys.* **151**, 054108 (2019); doi: [10.1063/1.5104344](https://doi.org/10.1063/1.5104344)

Submitted: 26 April 2019 • Accepted: 16 July 2019 •

Published Online: 5 August 2019



F. Köhler,<sup>1,2,a)</sup> K. Keiler,<sup>1</sup> S. I. Mistakidis,<sup>1</sup> H.-D. Meyer,<sup>3</sup> and P. Schmelcher<sup>1,2</sup>

## AFFILIATIONS

<sup>1</sup>Center for Optical Quantum Technologies, Department of Physics, University of Hamburg, Luruper Chaussee 149, 22761 Hamburg, Germany

<sup>2</sup>Hamburg Center for Ultrafast Imaging, University of Hamburg, Luruper Chaussee 149, 22761 Hamburg, Germany

<sup>3</sup>Theoretische Chemie, Physikalisch-Chemisches Institut, Universität Heidelberg, Im Neuenheimer Feld 229, 69120 Heidelberg, Germany

<sup>a)</sup>Electronic mail: [fkoeehler@physnet.uni-hamburg.de](mailto:fkoeehler@physnet.uni-hamburg.de)

## ABSTRACT

The investigation of the nonequilibrium quantum dynamics of bosonic many-body systems is very challenging due to the excessively growing Hilbert space and poses a major problem for their theoretical description and simulation. We present a novel dynamical pruning approach in the framework of the multiconfiguration time-dependent Hartree method for bosons (MCTDHB) to tackle this issue by dynamically detecting the most relevant number states of the underlying physical system and modifying the many-body Hamiltonian accordingly. We discuss two different number state selection criteria as well as two different ways to modify the Hamiltonian. Our scheme regularly re-evaluates the number state selection in order to dynamically adapt to the time evolution of the system. To benchmark our methodology, we study the nonequilibrium dynamics of bosonic particles confined either in an optical lattice or in a double-well potential. It is shown that our approach reproduces the unpruned MCTDHB results accurately while yielding a significant reduction of the simulation time. The speedup is particularly pronounced in the case of the optical lattice.

Published under license by AIP Publishing. <https://doi.org/10.1063/1.5104344>

## I. INTRODUCTION

Ever since the first realizations of Bose-Einstein condensates (BECs),<sup>1–3</sup> ultracold atomic gases attracted a lot of interest both from the experimental and the theoretical side. Their tunability and almost perfect isolation from the environment render such systems ideal candidates to simulate a variety of quantum many-body systems.<sup>4–6</sup> Due to experimental advancements, ensembles of ultracold atoms with a controlled number of particles<sup>7,8</sup> can be realized in arbitrarily shaped confining potentials<sup>9</sup> such as optical lattices,<sup>10,11</sup> harmonic,<sup>12</sup> or ring traps.<sup>13</sup> By varying the confinement, the crossover from three-dimensional<sup>14,15</sup> to two-dimensional<sup>16,17</sup> to one-dimensional<sup>18,19</sup> traps can be tuned. Feshbach<sup>20,21</sup> and confinement-induced resonances<sup>22–25</sup> offer fine-grained control of the interparticle interaction. Recent studies within the realm of ultracold atoms provide close links to solid-state systems,<sup>26,27</sup> electronic structure of molecules,<sup>28</sup> light-matter interaction,<sup>29</sup> topological

matter,<sup>30,31</sup> and black-hole analogs.<sup>32</sup> The increasing progress of the experimental control of these many-body systems demands appropriate theoretical and numerical methods to describe them and to calculate their properties as well as their dynamical behavior. Exactly solvable models are rare while usually relying on more or less crude approximations or focusing on certain limiting cases.

Let us discuss the state of the art of analytically solvable models and numerical approaches. The time-dependent Schrödinger equation of two bosons in a parabolic and spherically symmetric trapping potential is exactly solvable.<sup>33</sup> However, the applicability of such a small system is very limited. Larger particle numbers can be studied using the Lieb-Liniger model<sup>34,35</sup> for spinless bosons with contact interactions<sup>36</sup> assuming periodic boundary conditions. Yet, this approach is not capable of taking external trapping potentials into account and cannot directly describe the dynamical response of the system. The Tonks-Girardeau<sup>37,38</sup> model on the other hand grants access to the full many-body spectrum



and nonequilibrium solutions by mapping bosons to noninteracting fermions. However, this model is only valid in the limit of infinitely strong interactions and in one spatial dimension. Beyond these limitations of analytical approaches, powerful computational methods are needed to study ensembles of ultracold atoms.

A very useful approach is the Gross-Pitaevskii equation (GPE)<sup>39,40</sup> which represents a nonlinear Schrödinger equation for a bosonic many-body ensemble in the presence of an external trap with contact interparticle interaction in the thermodynamic limit. It assumes the Hartree-Fock approximation<sup>41,42</sup> to the many-body wave function, leading to an effective, mean-field description. The GPE is a partial differential equation which can be solved efficiently using the typical finite element and finite difference methods.<sup>43–49</sup> This mean-field treatment allows for the study of setups containing large particle numbers and enables the description of a multitude of nonlinear wave structures such as dark and bright solitons.<sup>50,51</sup> In some cases, when potential and interaction energy dominate the kinetic energy, the calculation can be further simplified by ignoring the kinetic term of the Schrödinger equation leading to the Thomas-Fermi<sup>52</sup> approximation. In general, however, these mean-field descriptions do not provide an adequate description of the system dynamics as they cannot account for quantum correlations. A prominent example where the GPE fails to capture the correct physical behavior is the bosonic Josephson junction.<sup>53,54</sup> For weakly depleted condensates, Bogoliubov theory<sup>55–57</sup> can be applied. For the investigation of few- to many-body systems with substantial correlations and correlated dynamics, however, *ab initio* beyond-mean-field methods are necessary.

One of the most fundamental of such methods is the exact diagonalization treatment of the many-body Hamiltonian<sup>58–60</sup> which grants access to the spectrum and the eigenstates of the physical system. However, this approach is limited to a small number of particles due to the computational complexity of diagonalization algorithms. Furthermore, the choice of an appropriate basis can prove difficult so that a large number of basis functions may be required, thereby further enlarging the numerical effort. This computational challenge calls for more efficient numerical approaches.

Many computational approaches focus on the investigation of optical lattices as these setups are of major interest in the research of ultracold neutral atoms due to the condensed matter counterparts (crystals). Often the Bose-Hubbard model<sup>10,61</sup> is employed to describe bosonic atoms loaded into the lowest band of a sufficiently deep lattice. In this model, the bosonic field operator is expanded into Wannier states yielding an effective theoretical model, where the kinetic term as well as the trapping potential is reduced to a hopping between lattice sites and the interaction term to an on-site interaction. This model has been studied using a plethora of different methods<sup>62</sup> including density matrix renormalization group (DMRG)<sup>63,64</sup> and Quantum Monte Carlo (QMC).<sup>65,66</sup> However, other approaches are required to describe physical systems and effects beyond the applicability of a Hubbard model, covering, in particular, their out-of-equilibrium dynamics.

The multiconfiguration time-dependent Hartree (MCTDH)<sup>67,68</sup> is such a method and has proven to be a powerful and versatile tool to *ab initio* solve the time-dependent Schrödinger equation

for correlated many-body systems of distinguishable degrees of freedom *ab initio*. MCTDH has been extended to study fermionic ensembles using the multiconfiguration time-dependent Hartree-Fock (MCTDHF) method<sup>69,70</sup> and bosonic systems using the MCTDHB<sup>71,72</sup> rendering the treatment of ultracold atoms possible. Further extensions<sup>73–75</sup> employing a multilayer approach also allow for the treatment of Bose-Bose mixtures and more recently Bose-Fermi and Fermi-Fermi mixtures further increasing the usefulness and applicability of this family of methods. The power of this class of methods stems from the usage of a variationally optimized, time-dependent set of basis functions that allows for a compact representation of the many-body wave function and yields a beyond-mean-field description that takes all correlations into account.

However, like all numerical approaches, MCTDHB faces the problem of an exponentially growing Hilbert space when studying large many-body systems. In particular, when increasing either the number of particles or the size of the single-particle function (SPF) basis used to describe such an atomic ensemble, the number of possible number states or configurations, respectively, grows rapidly rendering the treatment of systems typically with particle numbers larger than 100 (in the superfluid regime) challenging if not computationally prohibitive. To tackle this issue within the family of MCTDH methods, different approaches have been proposed in the literature. For instance, the configuration selection schemes for MCTDH<sup>76–78</sup> or the restricted-active-space (RAS) schemes for MCTDHF<sup>79,80</sup> and MCTDHB<sup>81</sup> perform a static selection of the most relevant Hartree products/Slater determinants for the physical system and exploit this partitioning to reduce the required numerical effort. However, these methods cannot dynamically adapt to the evolution of the system and require *a priori* knowledge such as the choice of an excitation scheme in the case of RAS. Such static truncation schemes of the Hilbert space can impose artificial constraints on the physical system if important many-body states are removed. Therefore, the development of dynamical, self-adapting approaches is required in order to enable a more general treatment of dynamical many-body systems.

Referring to the investigation of distinguishable degrees of freedom, dynamical procedures have been applied successfully within the framework of MCTDH. For example, by pruning the primitive basis/grid<sup>82,83</sup> or the coefficients of the wave function,<sup>83</sup> the runtime of the simulations can be greatly reduced. Unfortunately, however, the pruning of the grid is not very lucrative in calculations with ultracold atoms as these ensembles are usually confined using an external potential so that there rarely exist unoccupied regions of real space. Furthermore, the coefficient based pruning approach presented in Ref. 83 cannot be applied as the proposed neighborhood criterion for the coefficients cannot be easily transferred to the number states of indistinguishable particles. Therefore, the development of new dynamical methods for the treatment of indistinguishable particles is necessary.

In the present work, we develop a general method that automatically detects the important number states of bosonic many-body systems when studying the nonequilibrium dynamics using MCTDHB. This selection procedure dynamically adapts during the time evolution of the system. In Sec. II, we start by briefly reviewing the MCTDHB theory in order to introduce the key concepts of this method and motivate our pruning algorithm. In Sec. III, we show

two different ways to modify the MCTDHB equations of motion (EoMs) in order to reduce the numerical effort. To achieve this, we introduce a pruning threshold and a selection criterion for determining the importance of each number state. In Sec. IV, we present two different criteria for the selection of the number states relying on the overlap with the many-body wave function and the total energy of the system. To showcase the usefulness of our approach, we benchmark it using two different physical scenarios in Sec. V. We focus both on the performance benefits and the accuracy when compared to a regular MCTDHB simulation. Finally, we summarize our findings in Sec. VI and discuss future perspectives of our approach. In Appendix A, we comment on the convergence of our numerical results.

## II. KEY ASPECTS OF THE MULTICONFIGURATION TIME-DEPENDENT HARTREE METHOD FOR BOSONS

The MCTDHB allows us to describe the correlated quantum dynamics of the ensemble of  $N$  interacting bosons. It employs a variationally optimal, time-dependent basis  $\{\varphi_i(t)\}_{i=1}^m$  of  $m$  single-particle functions (SPFs) also called orbitals. Compared to other methods that employ a stationary basis, significantly fewer basis functions are required to achieve the same level of description of correlations. The many-body wave function is expanded as a superposition

$$|\Psi(t)\rangle = \sum_{\mathbf{n} \in \mathcal{V}} C_{\mathbf{n}}(t) |\mathbf{n}; t\rangle \quad (1)$$

of all  $N_{\mathcal{V}} = \binom{N+m-1}{N}$  time-dependent permanents  $\{|\mathbf{n}; t\rangle\}_{\mathbf{n} \in \mathcal{V}}$  that retain the total number of particles  $N$  using time-dependent coefficients  $\{C_{\mathbf{n}}(t)\}_{\mathbf{n} \in \mathcal{V}}$ .

Each vector  $\mathbf{n} = (n_1 \ n_2 \ \dots \ n_m)^T$  resembles one way of distributing  $N$  particles in  $m$  orbitals and is called a configuration. The  $i$ th component  $n_i$  of such a vector specifies the number of particles in the orbital  $\varphi_i(t)$  for the given configuration.  $\mathcal{V} = \{\mathbf{n} \in \mathbb{N}_0^m : \|\mathbf{n}\|_1 = N\}$  is the set of all such configurations that with the total number of particles  $N$ .

The permanents are given by

$$|\mathbf{n}; t\rangle = \left( \prod_{i=1}^m \frac{(a_i^\dagger(t))^{n_i}}{\sqrt{n_i!}} \right) |\mathbf{0}\rangle \quad (2)$$

in terms of the bosonic creation operators  $\{a_i^\dagger(t)\}_{i=1}^m$  with respect to the instantaneous basis.

MCTDHB solves the time-dependent Schrödinger equation  $(i\hbar\partial_t - \hat{H}(t))|\Psi(t)\rangle = 0$  as an initial value problem by propagating an initial wave function  $|\Psi(0)\rangle$  in time according to a, potentially time-dependent, Hamilton operator  $\hat{H}(t)$ . In this work, we limit ourselves to Hamiltonians of the form

$$\hat{H}(t, \{x_i\}) = \sum_{i=1}^N \hat{h}(t, x_i) + \sum_{i < j} \hat{W}(t, x_i, x_j), \quad (3)$$

containing only one-body ( $\hat{h}$ ) and two-body ( $\hat{W}$ ) terms. By employing the Lagrangian,<sup>84</sup> Dirac-Frenkel,<sup>85,86</sup> or McLachlan<sup>87</sup> variational principle, one can derive the corresponding MCTDHB EoMs<sup>71,72,88</sup> which are integrodifferential equations describing the time evolution of the coefficients  $\{C_{\mathbf{n}}(t)\}_{\mathbf{n} \in \mathcal{V}}$  and the SPFs  $\{\varphi_i(t)\}_{i=1}^m$ .

The SPF EoM describes a rotation of the orbitals in such a way that they represent the state of the physical system optimally. For details on this equation, we refer the reader to Ref. 72 as the precise structure is irrelevant for the pruning approach that we describe herein. The time evolution of the time-dependent coefficients  $\{C_{\mathbf{n}}(t)\}_{\mathbf{n} \in \mathcal{V}}$  is governed by

$$i\partial_t C_{\mathbf{n}}(t) = \sum_{\mathbf{m} \in \mathcal{V}} \underbrace{\langle \mathbf{n}; t | \hat{H}(t) | \mathbf{m}; t \rangle}_{H_{\mathbf{nm}}(t)} C_{\mathbf{m}}(t), \quad (4)$$

which is coupled to the EoMs of the orbitals via the configurations  $|\mathbf{n}; t\rangle$ .

## III. PRUNED EQUATIONS OF MOTION

The number of possible configurations  $N_{\mathcal{V}}$  grows rapidly with the number of particles  $N$  and orbitals  $m$ . This scaling behavior renders the treatment of large systems challenging if not infeasible as the number of matrix elements grows quadratically with  $N_{\mathcal{V}}$  causing the integration of Eq. (4) to become very costly and the dominant contribution to the simulation runtime.

From intuition and experience, we know that not all configurations are of equal importance for the corresponding physical systems under consideration. In the present work, we establish measures to automatically detect configurations of lesser importance and leverage this knowledge to reduce the numerical effort of the integration of the coefficient EoMs. Our approach is dynamical and regularly reevaluates the importance of all configurations, in particular, also those that have been deemed negligible previously.

In order to derive our pruning approach, we start by defining a measure  $f : \mathcal{V} \times \mathbb{R} \rightarrow \mathbb{R}$  that determines the importance of each configuration  $\mathbf{n}$  at time  $t$ . We divide the set  $\mathcal{V}$  of all configurations into the subset of unpruned (i.e., active) configurations

$$\mathcal{P}(t) = \{\mathbf{n} : f(\mathbf{n}, t) > \gamma\} \quad (5)$$

and the subset of pruned (i.e., inactive) configurations

$$\mathcal{Q}(t) = \{\mathbf{n} : f(\mathbf{n}, t) \leq \gamma\} \quad (6)$$

by introducing a pruning threshold  $\gamma \in \mathbb{R}$ . Additionally, we introduce the operators

$$\hat{P}(t) = \sum_{\mathbf{m} \in \mathcal{P}(t)} |\mathbf{m}; t\rangle \langle \mathbf{m}; t|, \quad (7)$$

$$\hat{Q}(t) = \sum_{\mathbf{m} \in \mathcal{Q}(t)} |\mathbf{m}; t\rangle \langle \mathbf{m}; t| \quad (8)$$

that project onto the configuration subsets  $\mathcal{P}(t)$  and  $\mathcal{Q}(t)$ . In the following, we drop the explicit notation of the time-dependence of the sets and the projection operators for the sake of readability. The many-body Hamiltonian can be rewritten in terms of  $\hat{P}$  and  $\hat{Q}$  as

$$\begin{aligned} \hat{H} &= \hat{P}\hat{H}\hat{P} + \hat{Q}\hat{H}\hat{P} + \hat{P}\hat{H}\hat{Q} + \hat{Q}\hat{H}\hat{Q} \\ &= \hat{H}\hat{P} + \hat{P}\hat{H}\hat{Q} + \hat{Q}\hat{H}\hat{Q}, \end{aligned} \quad (9)$$

where we exploited the property  $\hat{P} + \hat{Q} = \hat{1}$ .

The idea of the pruning approach is to neglect terms in this representation, thus defining a new, truncated Hamiltonian which replaces the original in Eq. (4). In order to make an adequate choice for the pruning, it is essential to consider the meaning of each term of Eq. (9) within the context of the coefficient EoMs (4), see also Fig. 1. The term  $\hat{Q}\hat{H}\hat{Q}$  mediates between number states belonging to configurations from  $\mathcal{Q}$ , i.e., configurations that we consider negligible. Therefore, the most apparent modification is to neglect this part of the Hamiltonian yielding

$$\hat{H}'_1 = \hat{H}\hat{P} + \hat{P}\hat{H}\hat{Q}. \quad (10)$$

We note that  $\hat{H}'_1$  is Hermitian. When inserting this Hamiltonian into Eq. (4), the resulting modified EoM reads

$$i\partial_t C_n(t) = \sum_{m \in \mathcal{P}(t)} \langle \mathbf{n}; t | \hat{H}(t) | \mathbf{m}; t \rangle C_m(t) + \underbrace{\sum_{m \in \mathcal{Q}(t)} \langle \mathbf{n}; t | \hat{H}(t) | \mathbf{m}; t \rangle C_m(t)}_{\text{if } m \in \mathcal{P}(t)}, \quad (11)$$

where the second term is only present for coefficients associated with configurations from  $\mathcal{P}$ . However, we note that only the right-hand side of the EoMs is modified, while the total number of EoMs remains unchanged such that all coefficients  $\{C_n(t)\}_{n \in \mathcal{V}}$  are propagated in time. This is a key element of our approach as it allows coefficients corresponding to inactive configurations (from the set  $\mathcal{Q}$ ) to evolve such that they could be activated again should they transcend the pruning threshold.

In the present work, we also investigate a second type of pruned Hamiltonian

$$H'_2 = \hat{H}\hat{P} \quad (12)$$

that we obtain by also neglecting the term  $\hat{P}\hat{H}\hat{Q}$  which mediates scattering from the negligible configurations  $\mathcal{Q}$  to the active configurations  $\mathcal{P}$ . However, this operator is non-Hermitian but our numerical results in Sec. V suggest that this weak non-hermiticity may still be acceptable in the sense that the many-body dynamics can still be described to some accuracy (see Sec. V). The corresponding EoM reads

$$i\partial_t C_n(t) = \sum_{m \in \mathcal{P}(t)} \langle \mathbf{n}; t | \hat{H}(t) | \mathbf{m}; t \rangle C_m(t). \quad (13)$$

In the standard MCTDHB algorithm, an initial wave function  $|\Psi(t_0)\rangle$  is propagated from the initial time  $t_0$  to a final time  $t_f$  using some time step  $\Delta t$  at which the wave function is to be computed. The interval  $\Delta t$  is usually divided further due to the usage of an adaptive integrator.<sup>89–91</sup> Algorithm 1 shows how we integrate the pruning approach into this existing procedure. We introduce an additional time scale  $\tau$  that determines when the pruning criterion is to be evaluated. The resulting selection of active configurations is

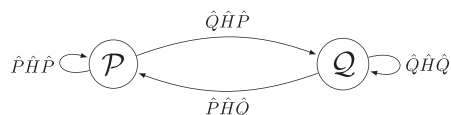


FIG. 1. Illustration of the meaning of the different terms of  $\hat{H}$  with respect to projection operators.

ALGORITHM 1. Propagation procedure for pruned MCTDHB simulations.

```

1: procedure PRUNEDPROPAGATION( $|\Psi(t_0)\rangle, t_0, t_f, \Delta t, \tau, \gamma$ )
2:    $t_{\text{next}} \leftarrow t_0 + \Delta t$ 
3:    $t_{\text{pruning}} \leftarrow t_0 + \tau$ 
4:    $\mathcal{P} \leftarrow \mathcal{V}$ 
5:    $\mathcal{Q} \leftarrow \{\}$ 
6:   while  $t < t_f$  do
7:      $t' \leftarrow \min\{t_{\text{next}}, t_{\text{pruning}}\}$ 
8:      $|\psi(t')\rangle \leftarrow \text{propagate}(t, t', |\psi(t)\rangle, \mathcal{P}, \mathcal{Q})$ 
9:     if  $t' = t_{\text{pruning}}$  then
10:       $\mathcal{P} \leftarrow \{\mathbf{n} : f(\mathbf{n}, t) > \gamma\}$ 
11:       $\mathcal{Q} \leftarrow \{\mathbf{n} : f(\mathbf{n}, t) \leq \gamma\}$ 
12:       $t_{\text{pruning}} \leftarrow t_{\text{pruning}} + \tau$ 
13:    end if
14:    if  $t' = t_{\text{next}}$  then
15:      write  $|\Psi(t)\rangle$ , evaluate observables, etc.
16:       $t_{\text{next}} \leftarrow t_{\text{next}} + \Delta t$ 
17:    end if
18:     $t \leftarrow t'$ 
19:  end while
20: end procedure
    
```

kept constant for the time  $\tau$ . Initially, all configurations are marked as active as can be seen in lines 4 and 5. The initial wave function is then propagated until the target time  $t_f$  is reached (see lines 6–19). Whenever the time  $\tau$  has passed, the pruning criterion is reevaluated and the selection of active configurations is updated (see lines 9–13).

Both the pruning time  $\tau$  and the threshold  $\gamma$  impact the dynamical pruning algorithm. Choosing small values of  $\gamma$  reduces the ratio of configurations that can be disabled on the right-hand side of each EoM [see Eqs. (11) and (13)] and thus the speedup that can be achieved. In the case  $\gamma = 0$ , all configurations are taken into account and the dynamical pruning approach is equivalent to the original MCTDHB. However, choosing  $\gamma$  very large may lead to incorrect results as important number states might be neglected. As the pruning time  $\tau$  determines how often the pruning criterion is evaluated, this parameter has to be chosen appropriately depending on the time scales of the physical system. Small values of  $\tau$  lead to very frequent reevaluations of the pruning criterion which can negate any performance gain due to the decreased number of configurations as the evaluation of the criterion introduces additional computational effort. When using large values for  $\tau$ , the evolution of the physical system might be imprecise. To ensure that the numerical results are accurate enough,  $\tau$  and  $\gamma$  have to be chosen carefully by learning how to handle them via the comparison with converged results, e.g., the original MCTDHB results.

#### IV. PRUNING CRITERIA

In Sec. III, we outlined our pruning approach and introduced the function  $f(\mathbf{n}, t)$  without further specifying it. In the following, we present two different pruning criteria that we use for the applications in Sec. V. We base our choices on the norm of the wave function and the total energy as these quantities are easily accessible and interpretable.

### A. Magnitude criterion

The most obvious way to assess the importance of a configuration is to project the many-body wave function onto the corresponding number state and compute the magnitude of the overlap,

$$f(\mathbf{n}, t) = |\langle \Psi(t) | \mathbf{n}; t \rangle|^2 = |C_{\mathbf{n}}(t)|^2. \quad (14)$$

This criterion, which we refer to as the magnitude criterion (MC) in the following, is intuitive as we can compute a real number  $f(\mathbf{n}, t) \in [0, 1]$  that determines the importance of the configuration  $\mathbf{n}$ . A value of 0 means that the configuration does not contribute at all to the many-body wave function, whereas a value of 1 implies that the wave function is given solely by the corresponding number state.

### B. Energy criterion

In order to investigate the impact of the pruning criterion on the numerical results, we study a second possible choice. For the so-called energy criterion (EC), we determine the contribution of a configuration to the total energy. The energy of a MCTDHB wave function is given by

$$E(t) = E_{\mathcal{V}}(t) = \sum_{\mathbf{n}, m \in \mathcal{V}} C_{\mathbf{n}}^*(t) C_m(t) H_{\mathbf{n}, m}(t) \quad (15)$$

and depends solely on the time-dependent coefficients  $\{C_{\mathbf{n}}(t)\}$ . In order to estimate the energetic contribution of a single, specific configuration  $\mathbf{n}$ , we expand  $E_{\mathcal{V}}(t)$  as a Taylor polynomial of first order with respect to the corresponding coefficient,

$$E_{\mathcal{V}}(t) \approx E_{\mathcal{V} \setminus \{\mathbf{n}\}}(t) + \frac{\partial E_{\mathcal{V}}(t)}{\partial C_{\mathbf{n}}^*(t)} C_{\mathbf{n}}^*(t), \quad (16)$$

where  $E_{\mathcal{V} \setminus \{\mathbf{n}\}}(t)$  is the energy of the system when neglecting the configuration  $\mathbf{n}$ , i.e., setting  $C_{\mathbf{n}}(t)$  to 0. Consequently, an estimate of the absolute, energetic contribution of the configuration  $\mathbf{n}$  is given by

$$E_{\mathbf{n}}(t) = E_{\mathcal{V}}(t) - E_{\mathcal{V} \setminus \{\mathbf{n}\}}(t) = \frac{\partial E_{\mathcal{V}}(t)}{\partial C_{\mathbf{n}}^*(t)} C_{\mathbf{n}}^*(t). \quad (17)$$

We normalize this quantity by dividing the total energy and taking the absolute value

$$f(\mathbf{n}, t) = \Delta E_{\mathbf{n}}(t) = \left| \frac{E_{\mathbf{n}}(t)}{E_{\mathcal{V}}(t)} \right| = \left| \frac{1}{E_{\mathcal{V}}(t)} \frac{\partial E_{\mathcal{V}}(t)}{\partial C_{\mathbf{n}}^*(t)} C_{\mathbf{n}}^*(t) \right| \quad (18)$$

in order to obtain a real number  $f(\mathbf{n}, t) \in [0, 1]$  which can be interpreted as the relative energy contribution.

## V. APPLICATION TO THE QUANTUM DYNAMICS OF TRAPPED ULTRACOLD BOSONIC ENSEMBLES

In the following, we consider a one-dimensional system of  $N$  identical bosons confined in an external potential  $V(x)$ . Note that within the ultracold regime,  $s$ -wave scattering is the dominant interaction process<sup>36,92</sup> such that we consider contact interactions between the particles. The many-body Hamiltonian of such a system is given by

$$\hat{H}(\{x_i\}) = \sum_{i=1}^N \left( -\frac{\hbar}{2m} \frac{\partial^2}{\partial x_i^2} + V(x_i) \right) + \sum_{i < j} g \delta(x_i - x_j). \quad (19)$$

Starting from the ground state of the noninteracting system (i.e.,  $g = 0$ ), we compute the many-body ground state of the interacting ensemble by imaginary time propagation leading to energy relaxation<sup>68,93</sup> or via the improved relaxation algorithm.<sup>94</sup> The resulting initial ground state wave function is then propagated in time with respect to a quenched Hamiltonian which involves an instantaneous change in one of the system parameters.<sup>6,14,95</sup> The propagation of the wave function is performed using the usual, unpruned MCTDHB as well as the pruned variants introduced in Sec. III. To determine the benefits of pruning, we measure the central processing unit (CPU) time of all simulations and also monitor the number of configurations that are pruned at each time step. In order to quantify the amount of deactivated configurations, we define the quantity

$$\beta(t) = \frac{|\mathcal{Q}(t)|}{|\mathcal{V}(t)|} \quad (20)$$

as the ratio between the number of inactive configurations [the cardinality of the set  $\mathcal{Q}(t)$ , see Eq. (6)] and the total number of configurations (the cardinality of the set  $\mathcal{V}$ , see Sec. II). Additionally, we compare different physical quantities between the pruned and unpruned MCTDHB data in order to assess the accuracy of our pruning approach.

MCTDHB provides the full many-body wave function at each time step of the evolution and thus grants access to a plethora of different observables that allow us to analyze and understand the physical system. One of the most general of such quantities is the reduced  $p$ -body density matrix<sup>96</sup>

$$\begin{aligned} \rho_p(x_1, \dots, x_p, x'_1, \dots, x'_p, t) \\ = \frac{N!}{(N-p)!} \int \Psi(x_1, \dots, x_N, t) \\ \times \Psi^*(x'_1, \dots, x'_p, x_{p+1}, \dots, x_N, t) dx_{p+1} \dots dx_N \end{aligned} \quad (21)$$

that can be used to calculate particle densities as well as correlation functions. The reduced one-body density matrix (i.e.,  $p = 1$ ) is of special interest as its diagonal  $\rho_1(x, t) = \rho_1(x, x' = x, t)$  is the one-body density which describes the spatial distribution of particles. The spectral representation of the reduced one-body density matrix

$$\rho_1(x, x', t) = \sum_{\alpha=1}^m \lambda_{\alpha}(t) \phi_{\alpha}(x, t) \phi_{\alpha}^*(x', t) \quad (22)$$

is given by the eigenvectors  $\{\phi_{\alpha}(t)\}$ , the so-called natural orbitals, and the decreasingly ordered eigenvalues  $\lambda_{\alpha}(t) \in [0, 1]$ , the so-called natural populations. The natural populations fulfill  $\sum_{\alpha=1}^m \lambda_{\alpha}(t) = 1$  and determine the degree of interparticle correlations within the ensemble. A system with  $\lambda_1 = 1 \wedge \lambda_{\alpha > 1} = 0$  is called condensed, is accurately described in a mean-field treatment using a single orbital, and does not exhibit interparticle correlations. In order to quantify the impact of the pruning approach on the natural populations, we compute the absolute difference between the natural population  $\lambda_i(t)$  obtained by a regular MCTDHB calculation and the corresponding natural population  $\lambda'_i(t)$  from a pruned simulation,

$$\varepsilon_{\lambda_i}(t) = |\lambda'_i(t) - \lambda_i(t)|. \quad (23)$$

Moreover, we study the reduced two-body density operator which can be used to calculate second order correlation functions and two-particle densities. For the sake of brevity, we only report results on the diagonal  $\rho_2(x, x) = \rho_2(x_1 = x, x_2 = x, x'_1 = x, x'_2 = x, t)$  that can be interpreted as the probability distribution to find two particles at the same position.

Furthermore, the pruning might affect the total energy of the system due to the modifications of the many-body Hamiltonian. In order to quantify any such effects, we introduce the relative deviation

$$\varepsilon_E(t) = \left| \frac{E'(t)}{E(t)} - 1 \right| \quad (24)$$

between the energy  $E'(t)$  of a pruned calculation and  $E(t)$  of a regular MCTDHB calculation.

The MCTDHB algorithm conserves the norm of the wave function, the orthonormality of the SPFs and, if the Hamiltonian is time-independent, the energy. The dynamical pruning might introduce inaccuracies that lead to violations of these properties which we investigate by defining appropriate error quantities. The norm of the wave function should always have the value 1. By computing the absolute difference

$$\xi_{\|\Psi\|^2}(t) = |\langle \Psi(t) | \Psi(t) \rangle^2 - 1| \quad (25)$$

from this target value, we can quantify the violation of the norm conservation at each time  $t$ . In Secs. V A and V B, we study the dynamics after a sudden change of the Hamiltonian at time  $t = 0$ . However, we keep the Hamiltonian  $H(t \geq 0)$  constant such that the energy should be conserved throughout the simulation. In order to measure violations of this conservation law, we compute the relative difference

$$\xi_E(t) = \left| \frac{E(t)}{E(0)} - 1 \right| \quad (26)$$

of the momentary total energy  $E(t)$  with respect to the initial energy  $E(0)$ . During the propagation of a many-body wave function using MCTDHB, the SPF basis should remain orthonormal. To quantify deviations from this property at time  $t$ , we introduce the quantity

$$\xi_{\perp}(t) = \langle \varphi_i(t) | \varphi_j(t) \rangle - \delta_{ij}. \quad (27)$$

However, we do not discuss this property in detail in Secs. V A and V B as we find that it does not seem to be affected by the pruning approach. The value of this quantity is always comparable to the unpruned MCTDHB calculation and is bounded by  $\xi_{\perp}(t) < 10^{-10}$ .

In the following, we discuss two physical scenarios by choosing different potentials and quench procedures to showcase the performance of the pruning approach. To ensure comparability, all numerical simulations were performed on an AMD<sup>®</sup> Ryzen<sup>™</sup> Threadripper<sup>™</sup> 1950X 16-core processor using a single, dedicated core.

### A. Quench dynamics in an optical lattice

We investigate the nonequilibrium dynamics of repulsively interacting bosons trapped in an optical lattice<sup>10</sup> following a sudden change of the interaction strength. This quench procedure is experimentally accessible through Feshbach resonances<sup>20,21</sup> or changes

of the transversal confinement frequency.<sup>23–25</sup> Similar setups have been investigated using MCTDHB in several previous works<sup>97–104</sup> so that this setup serves as an ideal testbed for new methodological advancements.

We parameterize the lattice potential as

$$V(x) = \begin{cases} V_0 \sin^2\left(\frac{\pi p x}{L}\right) & -\frac{L}{2} \leq x \leq \frac{L}{2} \\ \infty & \text{otherwise} \end{cases} \quad (28)$$

with an odd number of wells  $p$ , the barrier height  $V_0$ , and the system size  $L$ . Based on these lattice parameters, we use the recoil energy<sup>105</sup>  $E_R = \hbar^2 \pi^2 p^2 / 2mL^2$  as the natural energy unit of the system and choose a barrier height of  $V_0/E_R = 4$  for the lattice in the following. Starting from the ground state of the system with  $\tilde{g} = p\pi g/LE_R = 0.1$ , we study the dynamics following a quench to  $\tilde{g} = 0.4$  and  $\tilde{g} = 0.8$ . According to the convergence checks that we performed (see Appendix A), it proves sufficient to restrict the SPF basis to  $m = 5$  orbitals.

Figure 2 shows the evolution of the one-body density after the aforementioned quench protocol for the case of  $N = 20$  particles and a quench to  $\tilde{g} = 0.4$  which has been computed using a regular MCTDHB simulation. The quench excites intrawell breathing dynamics which is visible as a periodic expansion and contraction of the atomic cloud around the center of each well. Additionally, over-barrier transport between the wells<sup>97</sup> is induced which can be identified by the finite particle density between the wells. In Fig. 2, we show the propagation up to a final time  $t_f \approx 15 \hbar/E_R$ . In the further analysis, we investigate the different pruning approaches for a varying number of particles and postquench interaction strengths leading to a large number of independent simulations. As the simulation times can become large, especially when treating larger numbers of particles, we simplify the analysis by only studying the dynamics up to a final time  $t_f = 2 \hbar/E_R$  as indicated by the white dotted line in Fig. 2. In order to ensure that our pruning approach also captures the correct long-term behavior of the physical system, we also performed calculations up to a time  $t = 10\hbar/E_R$  for a selection of these simulations, the results of which are not presented for the sake of brevity.

We apply the various pruning methods described in Secs. III and IV to this lattice setup and choose a pruning threshold of

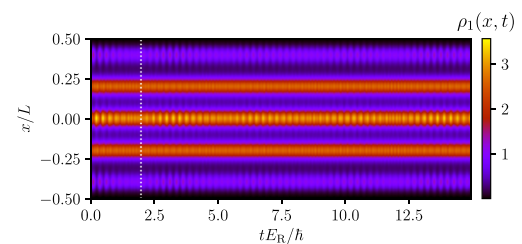
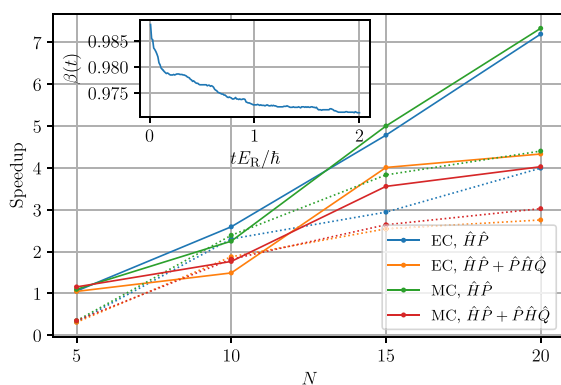


FIG. 2. Time evolution of the one-body density  $\rho_1(x, t)$  for  $N = 20$  bosons in a finite five-well lattice following an interaction quench from  $\tilde{g} = 0.1$  to  $\tilde{g} = 0.4$  according to a regular MCTDHB calculation. The white dotted line indicates the final propagation time  $t_f = 2\hbar/E_R$  that is used for the comparison with the different pruning approaches for different numbers of particles and postquench interaction strengths.

$\gamma = 10^{-8}$  and a pruning time  $\tau = 10^{-2} \hbar/E_R$ . Note that these values of  $\gamma$  and  $\tau$  have been determined by performing simulations for different sets of parameters ( $\gamma$ ,  $\tau$ ). We find that this combination yields both a significant speed-up compared to the unpruned MCTDHB while reproducing the unpruned results accurately up to a certain degree. Figure 3 shows the reduction of the simulation time in comparison with the regular MCTDHB for different numbers of particles. The initial state can be described using only a few configurations such that for small times almost all configurations can be marked as disabled. Over time, this number reduces as can be seen in the inset of Fig. 3. This fact can be explained with scattering from the few initially important configurations to the lesser important ones as mediated by the term  $\hat{Q}\hat{H}\hat{P}$  in Eqs. (10) and (12). However, the number of inactive configurations remains large throughout the simulation such that a significant speedup compared to the regular MCTDHB calculation is achieved. The performance benefit depends on the pruned Hamiltonian that is used as well as the number of particles  $N$  (see Fig. 3). The evaluation of the pruning criterion introduces computational overhead. When propagating wave functions containing only a few configurations, e.g., when studying small particle numbers ( $N \approx 5$ ), only a small speedup can be achieved. However, for larger systems ( $N = 20$ ), a considerably larger speedup by a factor of more than seven can be reached. The EoMs based on the Hamiltonian  $\hat{H}\hat{P}$  yield higher performance gains than the ones based on  $\hat{H}\hat{P} + \hat{P}\hat{H}\hat{Q}$ . This is to be expected as the first variant incorporates less of the original matrix elements while the pruning ratios did not differ substantially. Furthermore, the stronger quench requires a higher number of configurations and thus leads to a smaller speedup.

Moreover, comparing the MCTDHB and the pruned one- and two-body density (see Fig. 4), no difference is noticeable throughout the evolution. Thereby, we can infer that both quantities are



**FIG. 3.** Speedup of the pruned compared to the unpruned simulations for the five-well lattice. The solid lines are affiliated with the weak interaction quench to  $\tilde{g} = 0.4$ , while the dotted lines indicate the strong interaction quench to  $\tilde{g} = 0.8$ . The different colors indicate the number state selection criteria [Eq. (14) or Eq. (18)] and the modified Hamiltonian [Eq. (10) or Eq. (12)] that are used. The inset shows the ratio of the pruned configurations at each time step  $\beta(t)$  [see Eq. (20)] for the case  $N = 20$  using the energy criterion and the Hamiltonian  $\hat{H}\hat{P}$  after a weak interaction quench to  $\tilde{g} = 0.4$ . A pruning threshold of  $\gamma = 10^{-8}$  and a pruning time of  $\tau = 10^{-2} \hbar/E_R$  were employed.

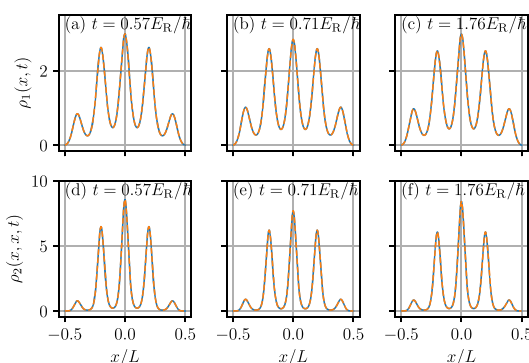


**FIG. 4.** One-body density  $\rho_1(x, t)$  (a)–(c) and diagonal of the reduced two-body density matrix  $\rho_2(x, x, t)$  (d)–(f) at selected time instants (see legends) for  $N = 20$  particles in the five-well lattice following an interaction quench from  $\tilde{g} = 0.1$  to  $\tilde{g} = 0.4$ . The blue solid lines correspond to the regular MCTDHB and the orange dashed lines to a pruned calculation using the energy criterion with the Hamiltonian  $\hat{H}\hat{P} + \hat{P}\hat{H}\hat{Q}$ . However, due to the good agreement of the unpruned and pruned calculation, these lines lie on top of each other. A pruning threshold of  $\gamma = 10^{-8}$  and a pruning time of  $\tau = 10^{-2} \hbar/E_R$  were employed.

reproduced accurately in the pruned simulations. When applying the EC in conjunction with the Hermitian Hamiltonian (10) for  $N = 20$  bosons and a postquench interaction of  $\tilde{g} = 0.4$ , the corresponding, maximal absolute deviation is 0.016 and 0.13 for the one- and two-body density, respectively, over the evolution.

The approximation via the pruning procedure introduces deviations in the energy of the system as well as the natural populations when comparing to the usual MCTDHB. The results for the energetic error  $\varepsilon_E(t)$  [see Eq. (24)] are illustrated in Fig. 5. As it can be seen, we can reproduce the MCTDHB energy up to a precision of the order of  $10^{-6}$ – $10^{-5}$  for the weaker quench to  $\tilde{g} = 0.4$  and of the order of  $10^{-5}$ – $10^{-4}$  for the stronger quench to  $\tilde{g} = 0.8$ . The energetic error increases slightly with the number of particles and is higher for the stronger quench. Among the different pruning approaches, only minor differences are perceivable in this quantity. For instance, the Hermitian operator  $\hat{H}\hat{P} + \hat{P}\hat{H}\hat{Q}$  yields slightly smaller errors. On the other hand, the differences between the energy and the magnitude criterion are negligible. In conjunction with the significant speedup, we consider these deviations from the MCTDHB energy to be acceptable. The inset of Fig. 5 shows the evolution of  $\varepsilon_E(t)$  for  $N = 20$  particles after a quench to  $\tilde{g} = 0.4$  for the energy criterion in conjunction with the Hermitian Hamiltonian. As it can be seen,  $\varepsilon_E(t)$  exhibits a fast growth rate initially, while it increases slowly for  $tE_R/\hbar \gtrsim 1$  and tends to saturate. The long time evolution of  $\varepsilon_E(t)$  is discussed for some case examples in Appendix B.

When reviewing the natural populations during the postquench propagation, we observe that the system cannot be considered a condensed system that could be described in a mean-field manner using only a single orbital as more than one natural orbital is macroscopically occupied. An example for the dynamical behavior of the natural populations is shown in the inset of Fig. 6. The maximal depletion over time, i.e., the maximal deviation of the first natural population from unity, increases with  $N$  and is larger for the stronger quench

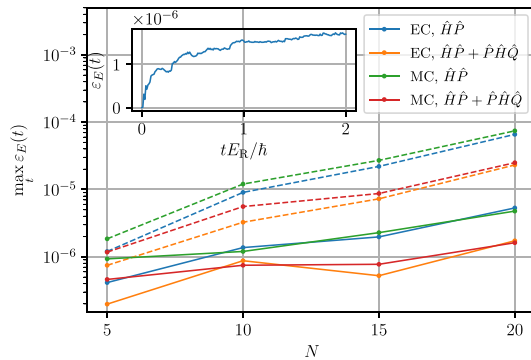


**FIG. 5.** Maximal energetic error [see Eq. (24)] between the unpruned and pruned simulations for the five-well lattice. The solid lines correspond to a quench to  $\tilde{g} = 0.4$  and the dashed lines to  $\tilde{g} = 0.8$ . The inset shows the exemplary evolution of the error over time for  $\tilde{g} = 0.4$  and  $N = 20$  when using the energy criterion and the Hamiltonian  $\hat{H}\hat{P} + \hat{P}\hat{H}\hat{Q}$ . A pruning threshold of  $\gamma = 10^{-8}$  and a pruning time of  $\tau = 10^{-2} \hbar/E_R$  were employed.

to  $\tilde{g} = 0.8$ . For the weak quench to  $\tilde{g} = 0.4$ , we observe a maximal depletion of  $\max_t(1 - \lambda_1(t)) = 0.07$  for  $N = 20$  particles. Similarly, the depletion for a quench to  $\tilde{g} = 0.8$  exhibits a maximum value of  $\max_t(1 - \lambda_1(t)) = 0.16$  for  $N = 20$  particles.

In Fig. 6, we also compare the maximal deviation of the natural populations  $\max_t \varepsilon_{\lambda_i}(t)$  [see Eq. (23)] between the pruned and unpruned simulations over time. We exemplarily present the results for the dominant, first orbital. Over time,  $\varepsilon_{\lambda_1}(t)$  shows an oscillatory behavior around a central value so that we compute the standard deviation of this quantity to quantify these fluctuations (see error bars in Fig. 6). For the natural population error, the pruning criterion has a larger impact than the type of EoM being used.

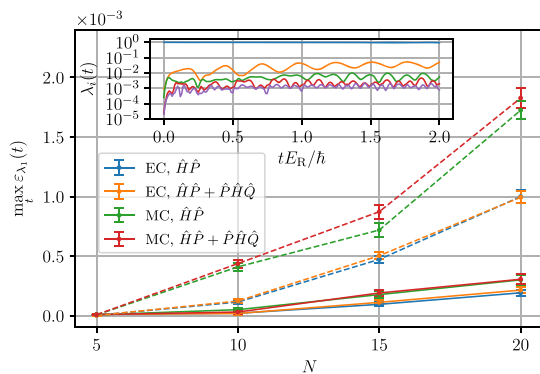


**FIG. 6.** Maximum error of the first natural population as given by Eq. (23) for various numbers of bosons in a five-well lattice. The solid lines illustrate a postquench interaction strength of  $\tilde{g} = 0.4$ , while the dashed lines represent  $\tilde{g} = 0.8$ . The error bars indicate the standard deviation of the error. The inset shows the evolution of all 5 natural populations for the case  $N = 20$  after a weak quench to  $\tilde{g} = 0.4$  and using the regular MCTDHB. A pruning threshold of  $\gamma = 10^{-8}$  and a pruning time of  $\tau = 10^{-2} \hbar/E_R$  were employed.

The energy criterion (blue and orange lines) shows slightly better results than the magnitude criterion (green and red lines) but stays in the same order of magnitude. As the energetic error, the error increases with the system size but stays of the order of  $10^{-4}$  for a postquench interaction of  $\tilde{g} = 0.4$  and of the order of  $10^{-3}$  for  $\tilde{g} = 0.8$ .

The postquench Hamiltonian is time-independent, and therefore the energy should be conserved in addition to the norm of the wave function. Figure 7 shows the maximum violation of these constraints over time. The norm conservation as quantified by  $\xi_{\|\Psi\|^2}(t)$  [see Eq. (25)] shows a drastic difference between the two kinds of EoMs. The non-Hermitian Hamiltonian leads to a deviation that is a few orders of magnitude larger while also still remaining sufficiently small. The violation of the energy conservation  $\xi_E(t)$  [see Eq. (26)] is slightly higher with the non-Hermitian EoMs. Overall however, this error is small and acceptable.

### B. Nonequilibrium dynamics in a double well

Our second physical example system is an ensemble of interacting bosons confined in a double-well that is created from a harmonic trap with an additional Gaussian-shaped barrier at the center, also known as a dimple trap in the literature,<sup>106</sup>

$$V(x) = \frac{1}{2}m\omega x^2 + V_0 \exp\left(-\frac{x^2}{2\sigma^2}\right). \quad (29)$$

Here,  $\sigma$  is the standard deviation of the Gaussian and  $V_0$  is the height of the barrier. We use the harmonic oscillator length  $l_H = \sqrt{m\omega/\hbar}$  as the natural length scale of the system, with  $\omega$  being the angular frequency of the harmonic potential. The energy units are given by  $\hbar\omega$  and the time units by  $1/\omega$ . In order to induce the nonequilibrium dynamics in this setup, we prepare the ground state of the system without a barrier (i.e., for  $V_0 = 0$ ) and then quench the barrier height to  $V_0/\hbar\omega = 4$ . A similar scheme, where the central barrier was continuously ramped up, was investigated in Ref. 71.

We study setups with  $N = 5, 10, 15, 20, 25, 30$  particles using  $m = 10, 9, 7, 6, 5, 5$  orbitals, respectively, and ensure convergence

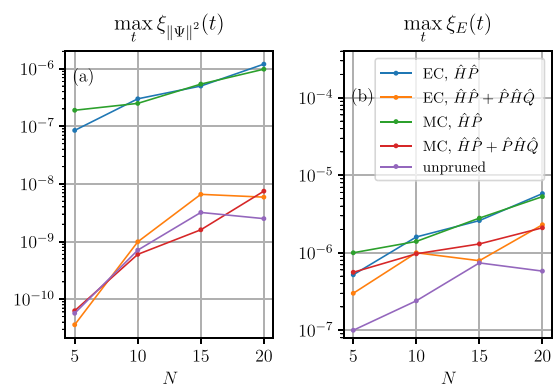


**FIG. 7.** Maximal violation of the conservation of (a) the norm [see Eq. (25)] and (b) the energy [see Eq. (26)] during the propagation of the five-well lattice system for an increasing number of particles  $N$ .

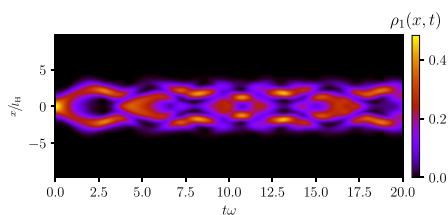


**FIG. 8.** Time evolution of the one-body density  $\rho_1(x, t)$  of  $N = 15$  bosons in a double-well trap after a quench of the central Gaussian barrier to a finite height obtained with a regular MCTDHB calculation.

with respect to  $m$  (see Appendix A). The interaction strength is chosen to be  $g/\hbar\omega_H = 0.1$  and the width of the barrier to be  $\sigma = l_H$ . In order to choose the pruning threshold  $\gamma$  and the pruning time  $\tau$  appropriately, we perform simulations for different values and compared the results to an unpruned MCTDHB simulation. We discuss the convergence procedure for different values of  $\tau$  and  $\gamma$  in detail for the case of  $N = 15$  particles in Appendix C. A pruning threshold of  $\gamma = 10^{-10}$  and a pruning time of  $\tau\omega = 5 \cdot 10^{-2}$  lead to a good agreement with the unpruned MCTDHB simulations.

The evolution of the single-particle density of the system is showcased in Fig. 8. By quenching to a finite height of the central barrier, the initial Gaussian distribution of the bosons is split into two branches veering away from each other with opposite momenta. With the given parameters, the two clouds possess enough energy to overcome the hump after being reflected by the harmonic trap and collide in the trap center  $x = 0$  at a time  $t\omega \approx 4$ . Afterward, these density branches separate again each one moving in one of the wells of the double-well and subsequently collide at  $x = 0$  again. This motion is repeated almost periodically throughout the evolution. Our main focus is the performance of the pruning approach in this scenario, i.e., we do not analyze the overall dynamics in further detail.

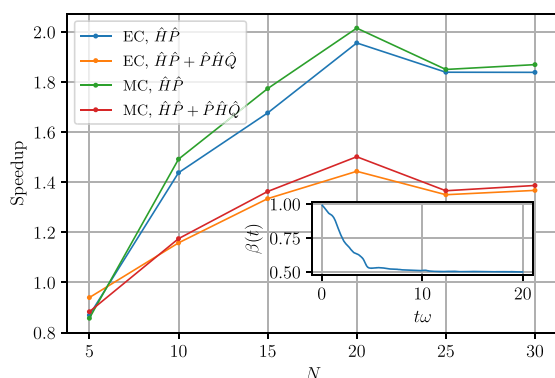


**FIG. 9.** Speedup of the various pruned simulations compared to regular MCTDHB in the double-well setup for varying particle numbers. The inset shows the ratio of inactive configurations  $\beta(t)$  [see (20)] over time for  $N = 15$  particles using the energy criterion and the Hamiltonian  $\hat{H}\hat{P}$ . We used a pruning threshold of  $\gamma = 10^{-10}$  and a pruning time of  $\tau\omega = 5 \cdot 10^{-2}$ .

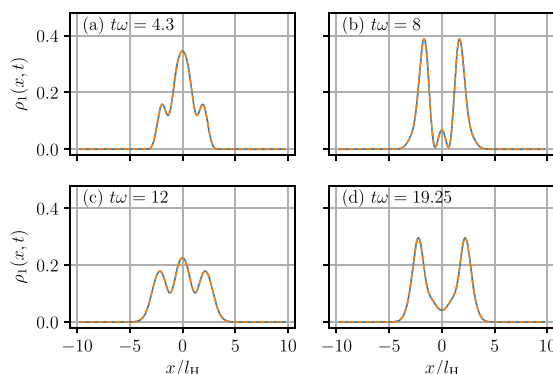


**FIG. 10.** (a)–(d) show the one-body density  $\rho_1(x, t)$  for  $N = 15$  particles in the double-well setup at various time instances (see legends). The blue solid line corresponds to an unpruned simulation and the orange dashed line to a pruned calculation using the energy criterion and the Hamiltonian  $\hat{H}\hat{P} + \hat{P}\hat{H}\hat{Q}$ . However, due to the good agreement between the unpruned and the pruned calculation, these lines lie on top of each other. We used a pruning threshold of  $\gamma = 10^{-10}$  and a pruning time of  $\tau\omega = 5 \cdot 10^{-2}$ .

Figure 9 shows the speedup of the pruned vs the unpruned simulations. In comparison to the lattice system, the benefits of the pruning approach are smaller yielding a speedup between 1.4 and 2 depending on the system size. This can be explained by a smaller pruning ratio as it can be seen in the inset. The ratio of inactive configurations quickly drops from almost 1 to around 0.5 where it saturates, suggesting that a higher amount of configurations is required to describe the physical system accurately.

Even though the pruning approach does not speed up the simulation as much as in the case of an optical lattice, the evolution of

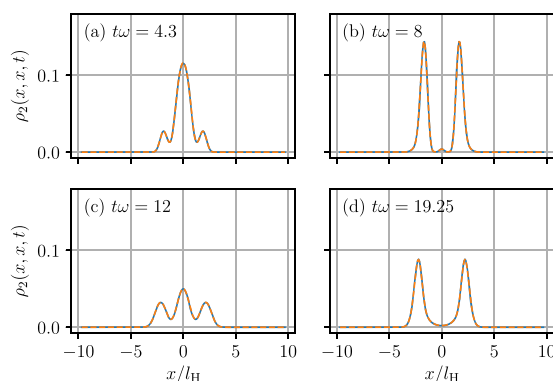


**FIG. 11.** (a)–(d) show the diagonal  $\rho_2(x, x, t)$  of the two-body density matrix at different times  $t$  (see legends) for  $N = 15$  particles in a double-well following the quench of the central Gaussian barrier to a finite height. The solid blue line corresponds to a regular MCTDHB simulation and the orange dashed line to a pruned calculation using the EC and the  $\hat{H}\hat{P} + \hat{P}\hat{H}\hat{Q}$  Hamiltonian. However, due to the good agreement between the unpruned and the pruned calculation, these lines lie on top of each other. We used a pruning threshold of  $\gamma = 10^{-10}$  and a pruning time of  $\tau\omega = 5 \cdot 10^{-2}$ .



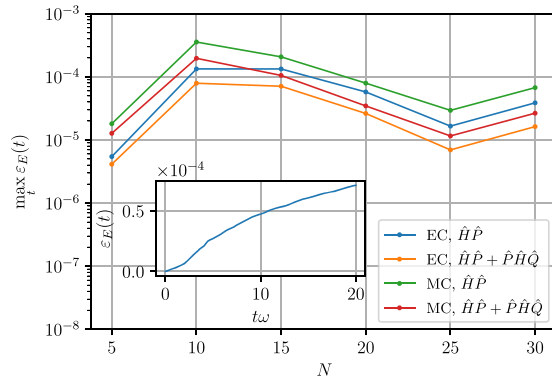


**FIG. 12.** Maximal relative energetic error [see Eq. (24)] between unpruned and pruned simulations for the double-well setup for varying particle numbers  $N$ . The inset shows the evolution of the error over time during a pruned simulation for  $N = 15$  particles using the energy criterion and the  $\hat{H}\hat{P} + \hat{P}\hat{H}\hat{Q}$  Hamiltonian. We used a pruning threshold of  $\gamma = 10^{-10}$  and a pruning time of  $\tau\omega = 5 \cdot 10^{-2}$ .

the system is still reproduced accurately. We show the good agreement of the one-body (see Fig. 10) and the two-body (see Fig. 11) density between a regular MCTDHB and a pruned simulation using the EC in conjunction with the Hermitian Hamiltonian (10). The corresponding maximal, absolute deviation over the evolution time and the whole grid is 0.0013 for the one-body and 0.0012 for the two-body density.

The energetic error  $\varepsilon_E$  [see Eq. (24)] between the pruned and the unpruned MCTDHB calculation is depicted in Fig. 12. In contrast to the lattice system, the difference between the two types of EoMs (11) and (13) is only minor and the error does not increase with the number of particles. Using the pruning approach, the unpruned MCTDHB energy is reproduced up to a relative deviation of the order of  $10^{-4}$ . The inset of Fig. 12 shows that the energetic error

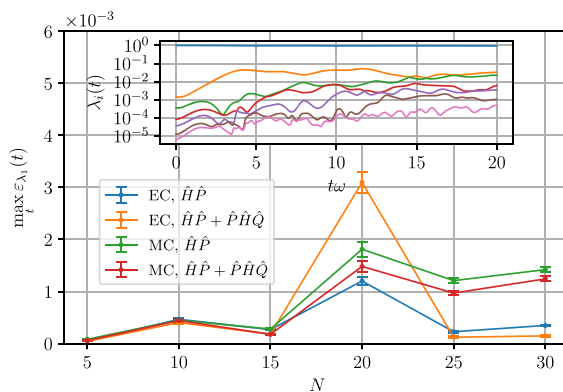


**FIG. 13.** Absolute error of the first natural population [see Eq. (23)] between the pruned and unpruned simulations in the double-well setup. The error bars indicate the standard deviation of this error quantity. The inset shows the evolution of all  $m = 7$  orbitals for the unpruned MCTDHB calculation using  $N = 15$  particles. We used a pruning threshold of  $\gamma = 10^{-10}$  and a pruning time of  $\tau\omega = 5 \cdot 10^{-2}$ .

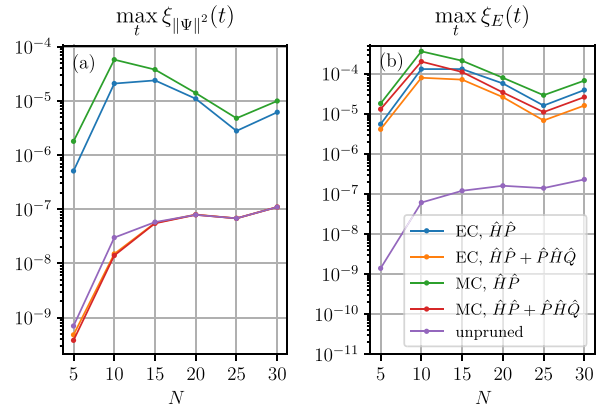


**FIG. 14.** Maximal violation of the conservation of (a) the norm [see Eq. (25)] and (b) the energy [see Eq. (26)] during the propagation after quenching the central Gaussian barrier in the double-well to a finite height. We use a pruning threshold of  $\gamma = 10^{-10}$  and a pruning time of  $\tau\omega = 5 \cdot 10^{-2}$ .

grows in a similar fashion as in the lattice system over the simulated time and that it does saturate within the given time range. In Appendix B, we show exemplarily the long-time evolution of the energetic error for fixed particle number and observe that it grows slowly at longer propagation times.

Again, we also investigate the impact of the pruning on the natural orbitals. The maximal absolute error of the first, dominant natural population  $\max_t \varepsilon_{\lambda_1}(t)$  [see Eq. (23)] is shown in Fig. 13.

We observe that it is at most of the order of  $10^{-3}$  verifying that the first natural population is reproduced accurately. As in the lattice system, the depletion of the system increases with the number of particles. For  $N = 30$  particles, we achieve a maximal depletion of  $\max_t(1 - \lambda_1(t)) = 0.125$  so that the given parameters lead to beyond-mean-field dynamics. The evolution of the natural populations with time is visualized in the inset of Fig. 13.

In Fig. 14(a), we show the violation of the norm conservation  $\xi_{\|\Psi\|^2}(t)$  [see Eq. (25)] for our double-well setup. Similarly to the lattice system, we see a discrepancy between the two types of EoMs with the Hermitian operator  $\hat{H}\hat{P} + \hat{P}\hat{H}\hat{Q}$  yielding comparable results to the unpruned calculations and the non-Hermitian operator  $\hat{H}\hat{P}$  producing errors that are a few orders of magnitude higher. After the quench, the Hamiltonian is time-independent such that the total energy should be conserved. Again, we observe a deviation of this law  $\xi_E(t)$  [see Eq. (26)] that is a couple of orders of magnitude higher than in the unpruned simulation while remaining very small overall.

## VI. CONCLUSIONS AND OUTLOOK

Studying the nonequilibrium quantum dynamics of large many-body systems poses a great challenge for numerical methods due to the excessively growing number of configurations. We have presented an intuitive, novel approach to address this issue in the framework of the multiconfiguration time-dependent Hartree method for bosons (MCTDHB). Our scheme dynamically classifies number states according to their importance for

the physical system under consideration employing pruning criteria that can be controlled using tunable accuracy parameters. We have derived two such criteria based on understandable quantities that can be computed efficiently. Our approach is dynamical and can adapt the number state selection during the evolution of the system to ensure an accurate description. The resulting, time-dependent selection of important configurations can be exploited by modifying the MCTDHB EoMs. Our algorithm cannot overcome the exponential growth of the Hilbert space but can greatly reduce the numerical effort by purposefully neglecting terms of the Hamiltonian.

We have benchmarked our scheme using the quench dynamics of two typical systems from the field of ultracold atoms, namely, an optical lattice and a double-well. The dynamical pruning approach is able to accurately reproduce the results of the unpruned MCTDHB while often reducing the computation time significantly. The speedup was particularly large for the lattice system since a large number of coefficients are of minor importance. The computational gain is much smaller in the double-well setup, suggesting a strong dependence on the physical system under investigation. In this sense, we are hesitant to universally recommend one of the pruning criteria or one of the modified EoMs since all choices lead to an accurate description of the unpruned MCTDHB results. Therefore, it is worthwhile to study all combinations as this situation might change when investigating new, different physical systems. In particular, when choosing one of the modified Hamiltonians, a tradeoff exists between the accuracy and speedup. The Hamiltonian  $\hat{H}\hat{P}$  [see Eq. (12)] takes fewer of the original matrix elements into account which yields a larger speedup while also introducing additional inaccuracies to the simulations. In general, the non-hermiticity could be problematic when studying different physical systems and should be checked carefully. On the other hand, the Hamiltonian  $\hat{H}\hat{P} + \hat{P}\hat{H}\hat{Q}$  leads to a better agreement with the unpruned MCTDHB but offers a smaller speedup as more matrix elements are taken into account. In terms of the pruning criterion, we observe comparable errors introduced by the pruning approach and no difference in the achievable speed-up. In some observables, the energy criterion leads to slightly smaller inaccuracies which are not large enough to lead to a general recommendation especially as this situation might be different when studying other setups.

Based on these results, we can conclude that our scheme captures the important aspects of the physical system correctly while reducing the numerical effort, making it an attractive candidate for future investigations. A promising prospect in doing so is the realization of extrapolation studies. By studying a physical system both with unpruned and pruned MCTDHB up to a certain, feasible size, one can ensure the agreement of both approaches and that the parameters  $\gamma$  and  $\tau$  are chosen appropriately. Afterward, larger system sizes that are not achievable using unpruned MCTDHB could be investigated using the pruning approach while extrapolating the quantities that have been used to compare to the regular MCTDHB for the smaller sizes. Furthermore, the method we presented in this work may be further refined by employing alternative pruning criteria or by modifying the EoMs in a different manner. Another promising direction for further studies is the application of the dynamical pruning scheme to other methods from the family of MCTDH such as the MCTDHF<sup>69,70</sup> for fermionic systems. Due to the strong interest that developed in the

investigation of binary mixtures using the multiconfiguration time-dependent Hartree method for mixtures (ML-MCTDHX)<sup>73–75</sup> in recent years, the implementation of a dynamical pruning scheme for this method could be very helpful in order to reduce the numerical effort of these time-consuming simulations. One possible way is to apply the pruning approach presented in this article on a per-species basis.

#### ACKNOWLEDGMENTS

The authors thank H. R. Larsson for fruitful discussions. F.K. and P.S. gratefully acknowledge funding by the excellence cluster “The Hamburg Centre for Ultrafast Imaging—Structure, Dynamics and Control of Matter at the Atomic Scale” of the Deutsche Forschungsgemeinschaft. S.I.M. and P.S. gratefully acknowledge funding by the Deutsche Forschungsgemeinschaft (DFG) in the framework of SFB 925 (“Light induced dynamics and control of correlated quantum systems”). K.K. acknowledges a scholarship of the Studienstiftung des deutschen Volkes.

#### APPENDIX A: CONVERGENCE OF THE MCTDHB CALCULATIONS

The SPFs used by MCTDHB are variationally optimal; however, the number of these orbitals has to be sufficiently large to ensure the numerical exactness of the method. In order to ensure the convergence with respect to the number of orbitals, we performed calculations with varying number of orbitals. By comparing the results for different basis sizes, we ensure that the employed observables such as the particle densities do not change up to a certain degree when using more orbitals than the numbers we presented in the main text. Additionally, the natural populations are important when discussing the convergence of MCTDHB. In a converged calculation, the natural populations should show a rapidly decreasing hierarchy and orbitals that are neglected should only be weakly occupied.

We use  $m = 5$  orbitals for the investigations of the lattice system in Sec. V A. The least occupied orbital shows a maximal natural population of  $\max_t \lambda_5(t) = \mathcal{O}(10^{-3})$  for all particle numbers and postquench interaction strengths throughout the time evolution. Any orbitals added to the simulation are only weakly occupied. We observe a clear drop in the natural populations as already the next orbital shows an occupation of  $\max_t \lambda_6(t) = \mathcal{O}(10^{-5})$  and further natural populations are even smaller. In general, the occupation of the last orbital increases with the number of particles and is larger for the stronger quench to  $\bar{g} = 0.8$  but only slightly. Overall, we consider  $m = 5$  orbitals to be sufficient due to the clear drop in natural populations and the observation that the evolution of the one- and two-body densities does not change qualitatively. Furthermore, the energy of the final state of the propagation is converged to a precision of at least  $\mathcal{O}(10^{-5})$ .

For the setup with the double-well presented in Sec. V B, we used different numbers of orbitals depending on the number of particles. We ensure that the least occupied orbital that is taken into account is occupied with a natural population of  $\max_t \lambda_m(t) = \mathcal{O}(10^{-4})$ . Further orbitals added do not change the behavior of the system qualitatively, and the corresponding natural populations

decay rapidly. Additionally, the energy of the final state is converged to at least  $\mathcal{O}(10^{-4})$  such that we consider the used number of orbitals to be sufficient.

### APPENDIX B: LONG-TIME EVOLUTION OF THE ENERGY ERROR

In Sec. V A, we employed a final time of  $t_f = 2\hbar/E_R$  when studying the lattice setup. Here, we show the long-time behavior of our pruning approach, i.e., we propagate to a final time of  $t_f = 10\hbar/E_R$  for  $N = 15$  and  $N = 20$  particles in a five-well setup following an interaction quench from  $\tilde{g} = 0.1$  to  $\tilde{g} = 0.4$  and using the energy criterion and both modified Hamiltonians while propagating. Figure 15(a) presents the evolution of the corresponding relative energy error  $\varepsilon_E(t)$  [see Eq. (24)]. The initial wave function at  $t = 0$  is identical for the pruned and unpruned simulations such that initially  $\varepsilon_E(0) = 0$ . In a short initial time range,  $tE_R/\hbar$  not much greater than 0,  $\varepsilon_E(t)$  quickly jumps to a small finite value of the order of  $10^{-6}$  or  $10^{-5}$ . For larger times  $t \gtrsim 4\hbar/E_R$ , however,  $\varepsilon(t)$  grows only slowly with time, almost saturating, i.e., remaining at the same order of magnitude. In this spirit, our pruning approach

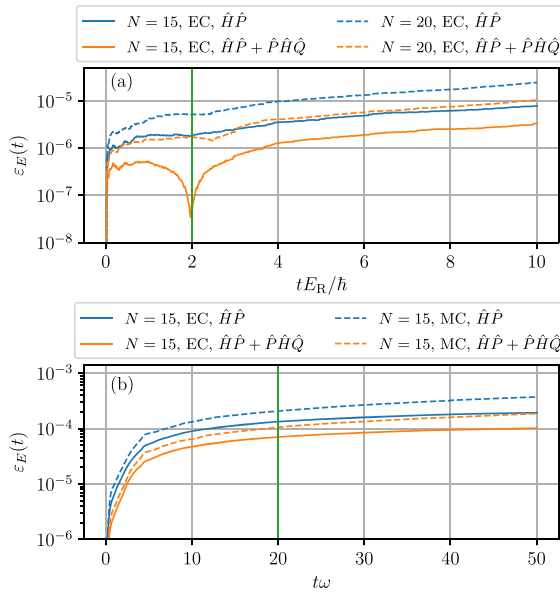


**FIG. 15.** Time evolution of the relative energetic error  $\varepsilon_E(t)$  [see Eq. (24)]. (a) shows  $\varepsilon_E(t)$  for  $N = 15$  and  $N = 20$  particles in a five-well lattice following an interaction quench from  $\tilde{g} = 0.1$  to  $\tilde{g} = 0.4$ . A longer propagation time of  $t_f = 10\hbar/E_R$  compared to Sec. V A is shown (where  $t_f = 2\hbar/E_R = 2$  as indicated by the green line). We use the energy criterion, the Hamiltonian  $\hat{H}\hat{P} + \hat{P}\hat{H}\hat{Q}$ , a pruning threshold of  $\gamma = 10^{-8}$  and a pruning time of  $\tau = 10^{-2}\hbar/E_R$ . (b) illustrates  $\varepsilon_E(t)$  for  $N = 15$  bosons in the double-well setup after quenching the central Gaussian barrier to a finite height of  $V_0 = 4\hbar\omega$ . Compared to the final time of  $t_f\omega = 20$  in Sec. V B (as indicated by the green line), a longer propagation time  $t_f\omega = 50$  was used. We employ both the energy and the magnitude criterion as well as both modified Hamiltonians (see legend) using a pruning threshold of  $\gamma = 10^{-10}$  and a pruning time of  $\tau = 5 \cdot 10^{-2}$ .

is also applicable for the investigation of longer propagation times.

In Sec. V B, we used a final time of  $t_f\omega = 20$  when investigating the double-well setup. Here, we showcase the long-time behavior of our pruning approach for  $N = 15$  particles upon quenching the central Gaussian barrier to a finite height  $V_0 = 4\hbar\omega$  using both pruning criteria and both modified Hamiltonians by propagating to a final time of  $t_f\omega = 50$ . In Fig. 15(b), we show the evolution of the relative energy error  $\varepsilon_E(t)$  [see Eq. (24)]. At  $t\omega = 0$ , the pruned and unpruned simulations coincide, namely,  $\varepsilon_E(0) = 0$ . At small initial times,  $t\omega \lesssim 10$   $\varepsilon_E(t)$  grows significantly due to the inaccuracies introduced by the pruning approach but still acquires small values of the order of  $10^{-4}$  or  $10^{-5}$ . We observe that for large times  $t\omega \gtrsim 10$ ,  $\varepsilon_E(t)$  grows in a slow manner and remains at the same order of magnitude. Consequently, the pruning approach is also suitable to study longer propagation times of this system.

### APPENDIX C: ANALYSIS OF THE PRUNING PARAMETERS

In Secs. V A and V B, we employed fixed values of  $\gamma$  and  $\tau$  that have been determined by comparing pruned simulations with

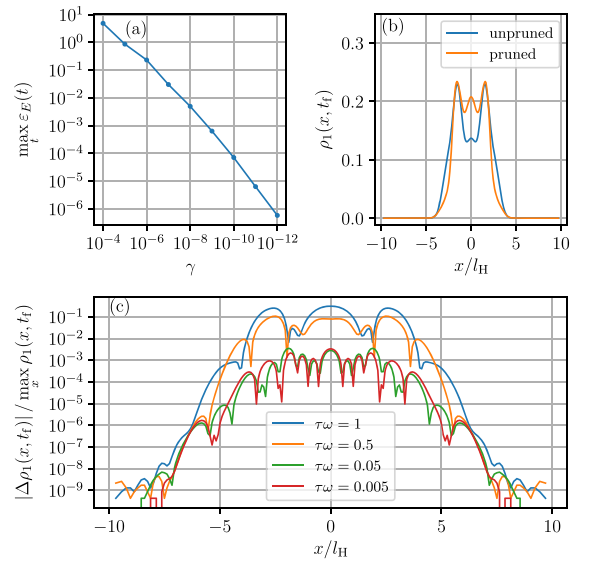


**FIG. 16.** (a) Maximal relative energetic error [see Eq. (24)] for a varying pruning threshold  $\gamma$ . The pruning time is fixed at  $\tau\omega = 5 \cdot 10^{-2}$ . (b) One-body density  $\rho_1(x, t_f)$  after a propagation to a final time of  $t_f\omega = 20$  using an unpruned (blue line) and a pruned (orange line) MCTDHB calculation. The pruning threshold was chosen as  $\gamma = 10^{-10}$  and the pruning time as  $\tau\omega = 1$ . (c) Error in one-body density at the final time  $t_f\omega = 20$  when comparing pruned calculations to an unpruned MCTDHB simulation using varying pruning times  $\tau$ . The quantity shown here is the absolute difference  $|\Delta\rho_1(x, t_f)| = |\rho_1'(x, t_f) - \rho_1(x, t_f)|$  between the density  $\rho_1'(x, t_f)$  of the pruned and the density  $\rho_1(x, t_f)$  of the unpruned simulation normalized to the maximum one-body density. For all three figures, the system consists of  $N = 15$  bosons in a double-well setup (see Sec. V B) following a quench of the central Gaussian barrier to a finite height of  $V_0 = 4\hbar\omega$  for different values of  $\tau$  and  $\gamma$  using the energy criterion and the Hermitian Hamiltonian  $\hat{H}\hat{P} + \hat{P}\hat{H}\hat{Q}$ .

full MCTDHB results. Here, we discuss the impact of these parameters on the accuracy of our pruning approach based on the example of  $N = 15$  particles in the double-well setup from Sec. V B. Figure 16(a) illustrates the maximal relative energetic error  $\max_t \varepsilon_E(t)$  [see Eq. (24)] for a varying pruning threshold  $\gamma$  while keeping the pruning time fixed at a value of  $\tau = 5 \cdot 10^{-2}$ . We expect that the pruned simulations converge toward the unpruned MCTDHB results when decreasing  $\gamma$ . Indeed, according to our numerical results, the maximal energetic error decreases roughly polynomially with  $\gamma$ , i.e.,  $\max_t \varepsilon_E(t) = b\gamma^k$ . The parameters  $k = 0.863 \pm 0.026$  and  $b = (2.5 \pm 1.3) \cdot 10^4$  have been determined using a least-squares fit.


Furthermore, we investigate the impact of the pruning time  $\tau$  in a similar manner by performing pruned simulations for different values of  $\tau$  while keeping the pruning threshold fixed at  $\gamma = 10^{-10}$ . As shown in Fig. 16(b), a large value of  $\tau$  leads to incorrect results, i.e., a discrepancy between the pruning approach and unpruned MCTDHB. In this example, we show how a value of  $\tau\omega = 1$  leads to a different final one-body density compared to the unpruned MCTDHB which manifests itself in a different shape of the outer flanks and, in particular, the central peak of the density. In Fig. 16(c), we show the error in the final one-body density when using various values for  $\tau$  and a fixed pruning threshold of  $\gamma = 10^{-10}$ . We observe that a value of  $\tau\omega = 1$  or  $\tau\omega = 0.5$  leads to a maximal error in the one-body density of the order of  $10^{-1}$  with respect to the maximal density. When employing  $\tau\omega = 0.05$  instead, this error decreases by two orders of magnitude. Smaller values such as  $\tau\omega = 0.005$  lead to an error in the density of the same order of magnitude. Therefore, we use the value of  $\tau\omega = 5 \cdot 10^{-2}$  in Sec. V B since smaller values  $\tau\omega$  do not improve the accuracy of the method while leading to a higher computational effort due to more frequent evaluations of the pruning criterion.

## REFERENCES

- <sup>1</sup>M. H. Anderson, J. R. Ensher, M. R. Matthews, C. E. Wieman, and E. A. Cornell, *Science* **269**, 198 (1995).
- <sup>2</sup>C. C. Bradley, C. A. Sackett, J. J. Tollett, and R. G. Hulet, *Phys. Rev. Lett.* **75**, 1687 (1995).
- <sup>3</sup>K. B. Davis, M. O. Mewes, M. R. Andrews, N. J. van Druten, D. S. Durfee, D. M. Kurn, and W. Ketterle, *Phys. Rev. Lett.* **75**, 3969 (1995).
- <sup>4</sup>I. Bloch, J. Dalibard, and W. Zwerger, *Rev. Mod. Phys.* **80**, 885 (2008).
- <sup>5</sup>I. Bloch, J. Dalibard, and S. Nascimbène, *Nat. Phys.* **8**, 267 (2012).
- <sup>6</sup>A. Polkovnikov, K. Sengupta, A. Silva, and M. Vengalattore, *Rev. Mod. Phys.* **83**, 863 (2011).
- <sup>7</sup>F. Serwane, G. Zürn, T. Lompe, T. B. Ottenstein, A. N. Wenz, and S. Jochim, *Science* **332**, 336 (2011).
- <sup>8</sup>A. M. Kaufman, B. J. Lester, C. M. Reynolds, M. L. Wall, M. Foss-Feig, K. R. A. Hazzard, A. M. Rey, and C. A. Regal, *Science* **345**, 306 (2014).
- <sup>9</sup>K. Henderson, C. Ryu, C. MacCormick, and M. G. Boshier, *New J. Phys.* **11**, 043030 (2009).
- <sup>10</sup>D. Jaksch, C. Bruder, J. I. Cirac, C. W. Gardiner, and P. Zoller, *Phys. Rev. Lett.* **81**, 3108 (1998).
- <sup>11</sup>I. Bloch, *Nat. Phys.* **1**, 23 (2005).
- <sup>12</sup>S. Chu, J. E. Bjorkholm, A. Ashkin, J. P. Gordon, and L. W. Hollberg, *Opt. Lett.* **11**, 73 (1986).
- <sup>13</sup>O. Morizot, Y. Colombe, V. Lorent, H. Perrin, and B. M. Garraway, *Phys. Rev. A* **74**, 023617 (2006).
- <sup>14</sup>M. Greiner, O. Mandel, T. Esslinger, T. W. Hänsch, and I. Bloch, *Nature* **415**, 39 (2002).
- <sup>15</sup>L.-M. Duan, E. Demler, and M. D. Lukin, *Phys. Rev. Lett.* **91**, 090402 (2003).
- <sup>16</sup>O. Zobay and B. M. Garraway, *Phys. Rev. Lett.* **86**, 1195 (2001).
- <sup>17</sup>Y. Colombe, E. Knyazchyan, O. Morizot, B. Mercier, V. Lorent, and H. Perrin, *Europhys. Lett.* **67**, 593 (2004).
- <sup>18</sup>C. Orzel, A. K. Tuchman, M. L. Fenselau, M. Yasuda, and M. A. Kasevich, *Science* **291**, 2386 (2001).
- <sup>19</sup>B. Paredes, A. Widera, V. Murg, O. Mandel, S. Fölling, I. Cirac, G. V. Shlyapnikov, T. W. Hänsch, and I. Bloch, *Nature* **429**, 277 (2004).
- <sup>20</sup>T. Köhler, K. Góral, and P. S. Julienne, *Rev. Mod. Phys.* **78**, 1311 (2006).
- <sup>21</sup>C. Chin, R. Grimm, P. Julienne, and E. Tiesinga, *Rev. Mod. Phys.* **82**, 1225 (2010).
- <sup>22</sup>M. Olshanii, *Phys. Rev. Lett.* **81**, 938 (1998).
- <sup>23</sup>J. I. Kim, V. S. Melezhik, and P. Schmelcher, *Phys. Rev. Lett.* **97**, 193203 (2006).
- <sup>24</sup>P. Giannakeas, F. K. Diakonou, and P. Schmelcher, *Phys. Rev. A* **86**, 042703 (2012).
- <sup>25</sup>P. Giannakeas, V. S. Melezhik, and P. Schmelcher, *Phys. Rev. Lett.* **111**, 183201 (2013).
- <sup>26</sup>B. P. Anderson and M. A. Kasevich, *Science* **282**, 1686 (1998).
- <sup>27</sup>G.-B. Jo, Y.-R. Lee, J.-H. Choi, C. A. Christensen, T. H. Kim, J. H. Thywissen, D. E. Pritchard, and W. Ketterle, *Science* **325**, 1521 (2009).
- <sup>28</sup>D.-S. Lühmann, C. Weitenberg, and K. Sengstock, *Phys. Rev. X* **5**, 031016 (2015).
- <sup>29</sup>S. Sala, J. Förster, and A. Saenz, *Phys. Rev. A* **95**, 011403 (2017).
- <sup>30</sup>G. Jotzu, M. Messer, R. Desbuquois, M. Lebrat, T. Uehlinger, D. Greif, and T. Esslinger, *Nature* **515**, 237 (2014).
- <sup>31</sup>N. Goldman, J. C. Budich, and P. Zoller, *Nat. Phys.* **12**, 639 (2016).
- <sup>32</sup>J. Steinhauser, *Nat. Phys.* **12**, 959 (2016).
- <sup>33</sup>T. Busch, B.-G. Englert, K. Rzazewski, and M. Wilkens, *Found. Phys.* **28**, 549 (1998).
- <sup>34</sup>E. H. Lieb and W. Liniger, *Phys. Rev.* **130**, 1605 (1963).
- <sup>35</sup>E. H. Lieb, *Phys. Rev.* **130**, 1616 (1963).
- <sup>36</sup>C. J. Pethick and H. Smith, *Bose-Einstein Condensation in Dilute Gases*, 2nd ed. (Cambridge University Press, 2008).
- <sup>37</sup>M. Girardeau, *J. Math. Phys.* **1**, 516 (1960).
- <sup>38</sup>V. I. Yukalov and M. D. Girardeau, *Laser Phys. Lett.* **2**, 375 (2005).
- <sup>39</sup>E. P. Gross, *Il Nuovo Cimento* **20**, 454 (1961).
- <sup>40</sup>L. P. Pitaevskii, *Sov. Phys. JETP* **13**, 451 (1961).
- <sup>41</sup>D. R. Hartree, *Math. Proc. Cambridge Philos. Soc.* **24**, 89 (1928).
- <sup>42</sup>V. Fock, *Z. Phys.* **61**, 126 (1930).
- <sup>43</sup>M. M. Cerimele, M. L. Chiofalo, F. Pistella, S. Succi, and M. P. Tosi, *Phys. Rev. E* **62**, 1382 (2000).
- <sup>44</sup>W. Bao, D. Jaksch, and P. A. Markowich, *J. Comput. Phys.* **187**, 318 (2003).
- <sup>45</sup>C. M. Dion and E. Cancès, *Phys. Rev. E* **67**, 046706 (2003).
- <sup>46</sup>P. Muruganandam and S. K. Adhikari, *J. Phys. B: At., Mol. Opt. Phys.* **36**, 2501 (2003).
- <sup>47</sup>P. Muruganandam and S. K. Adhikari, *Comput. Phys. Commun.* **180**, 1888 (2009).
- <sup>48</sup>I. Danaila and P. Kazemi, *SIAM J. Sci. Comput.* **32**, 2447 (2010).
- <sup>49</sup>I. Danaila and F. Hecht, *J. Comput. Phys.* **229**, 6946 (2010).
- <sup>50</sup>S. Burger, K. Bongs, S. Dettmer, W. Ertmer, K. Sengstock, A. Sanpera, G. V. Shlyapnikov, and M. Lewenstein, *Phys. Rev. Lett.* **83**, 5198 (1999).
- <sup>51</sup>U. Al Khawaja, H. T. C. Stoof, R. G. Hulet, K. E. Strecker, and G. B. Partridge, *Phys. Rev. Lett.* **89**, 200404 (2002).
- <sup>52</sup>G. Baym and C. J. Pethick, *Phys. Rev. Lett.* **76**, 6 (1996).
- <sup>53</sup>K. Sakmann, A. I. Streltsov, O. E. Alon, and L. S. Cederbaum, *Phys. Rev. Lett.* **103**, 220601 (2009).
- <sup>54</sup>K. Sakmann, A. I. Streltsov, O. E. Alon, and L. S. Cederbaum, *Phys. Rev. A* **89**, 023602 (2014).
- <sup>55</sup>N. Bogoliubov, *J. Phys.-U.S.S.R.* **11**, 23 (1946).
- <sup>56</sup>T. D. Lee and C. N. Yang, *Phys. Rev.* **105**, 1119 (1957).

- <sup>57</sup>T. D. Lee, K. Huang, and C. N. Yang, *Phys. Rev.* **106**, 1135 (1957).
- <sup>58</sup>B. Damski, H.-U. Everts, A. Honecker, H. Fehrmann, L. Santos, and M. Lewenstein, *Phys. Rev. Lett.* **95**, 060403 (2005).
- <sup>59</sup>J. M. Zhang and R. X. Dong, *Eur. J. Phys.* **31**, 591 (2010).
- <sup>60</sup>H. Hu, B. Ramachandran, H. Pu, and X.-J. Liu, *Phys. Rev. Lett.* **108**, 010402 (2012).
- <sup>61</sup>M. P. A. Fisher, P. B. Weichman, G. Grinstein, and D. S. Fisher, *Phys. Rev. B* **40**, 546 (1989).
- <sup>62</sup>M. Lewenstein, A. Sanpera, V. Ahufinger, B. Damski, A. Sen(De), and U. Sen, *Adv. Phys.* **56**, 243 (2007).
- <sup>63</sup>T. D. Kühner and H. Monien, *Phys. Rev. B* **58**, R14741 (1998).
- <sup>64</sup>S. Rapsch, U. Schollwöck, and W. Zwirger, *Europhys. Lett.* **46**, 559 (1999).
- <sup>65</sup>W. Purwanto and S. Zhang, *Phys. Rev. E* **70**, 056702 (2004).
- <sup>66</sup>S. Wessel, F. Alet, M. Troyer, and G. G. Batrouni, *Phys. Rev. A* **70**, 053615 (2004).
- <sup>67</sup>H.-D. Meyer, U. Manthe, and L. Cederbaum, *Chem. Phys. Lett.* **165**, 73 (1990).
- <sup>68</sup>M. Beck, A. Jäckle, G. Worth, and H.-D. Meyer, *Phys. Rep.* **324**, 1 (2000).
- <sup>69</sup>J. Zanghellini, M. Kitzler, C. Fabian, T. Brabec, and A. Scrinzi, *Laser Phys.* **13**, 1064 (2003).
- <sup>70</sup>J. Caillat, J. Zanghellini, M. Kitzler, O. Koch, W. Kreuzer, and A. Scrinzi, *Phys. Rev. A* **71**, 012712 (2005).
- <sup>71</sup>A. I. Streltsov, O. E. Alon, and L. S. Cederbaum, *Phys. Rev. Lett.* **99**, 030402 (2007).
- <sup>72</sup>O. E. Alon, A. I. Streltsov, and L. S. Cederbaum, *Phys. Rev. A* **77**, 033613 (2008).
- <sup>73</sup>S. Krönke, L. Cao, O. Vendrell, and P. Schmelcher, *New J. Phys.* **15**, 063018 (2013).
- <sup>74</sup>L. Cao, S. Krönke, O. Vendrell, and P. Schmelcher, *J. Chem. Phys.* **139**, 134103 (2013).
- <sup>75</sup>L. Cao, V. Bolsinger, S. I. Mistakidis, G. M. Koutentakis, S. Krönke, J. M. Schurer, and P. Schmelcher, *J. Chem. Phys.* **147**, 044106 (2017).
- <sup>76</sup>G. A. Worth, *J. Chem. Phys.* **112**, 8322 (2000).
- <sup>77</sup>R. Wodraszka and T. Carrington, *J. Chem. Phys.* **145**, 044110 (2016).
- <sup>78</sup>R. Wodraszka and T. Carrington, *J. Chem. Phys.* **146**, 194105 (2017).
- <sup>79</sup>H. Miyagi and L. B. Madsen, *Phys. Rev. A* **87**, 062511 (2013).
- <sup>80</sup>H. Miyagi and L. B. Madsen, *J. Chem. Phys.* **140**, 164309 (2014).
- <sup>81</sup>C. Lévêque and L. B. Madsen, *New J. Phys.* **19**, 043007 (2017).
- <sup>82</sup>H. R. Larsson, B. Hartke, and D. J. Tannor, *J. Chem. Phys.* **145**, 204108 (2016).
- <sup>83</sup>H. R. Larsson and D. J. Tannor, *J. Chem. Phys.* **147**, 044103 (2017).
- <sup>84</sup>J. Broeckhove, L. Lathouwers, E. Kesteloot, and P. Van Leuven, *Chem. Phys. Lett.* **149**, 547 (1988).
- <sup>85</sup>P. A. M. Dirac, *Math. Proc. Cambridge Philos. Soc.* **26**, 376 (1930).
- <sup>86</sup>J. I. Frenkel, *Wave Mechanics* (Clarendon Press, Oxford, 1932), pp. 423–428.
- <sup>87</sup>A. McLachlan, *Mol. Phys.* **8**, 39 (1964).
- <sup>88</sup>O. E. Alon, A. I. Streltsov, and L. S. Cederbaum, *J. Chem. Phys.* **127**, 154103 (2007).
- <sup>89</sup>J. Dormand and P. Prince, *J. Comput. Appl. Math.* **6**, 19 (1980).
- <sup>90</sup>W. H. Press, S. A. Teukolsky, W. T. Vetterling, and B. P. Flannery, *Numerical Recipes 3rd Edition: The Art of Scientific Computing*, 3rd ed. (Cambridge University Press, Cambridge, UK; New York, 2007), pp. 899–954.
- <sup>91</sup>J. Stoer and R. Bulirsch, *Introduction to Numerical Analysis*, Softcover Reprint of Hardcover, 3rd ed. (Springer, New York, NY, 2002), 2002 edition, pp. 465–618.
- <sup>92</sup>L. Pitaevskii and S. Stringari, *Bose-Einstein Condensation*, International Series of Monographs on Physics Vol. 116, 1st ed. (Oxford University Press, Oxford, New York, 2003).
- <sup>93</sup>R. Kosloff and H. Tal-Ezer, *Chem. Phys. Lett.* **127**, 223 (1986).
- <sup>94</sup>H.-D. Meyer and G. A. Worth, *Theor. Chem. Acc.* **109**, 251 (2003).
- <sup>95</sup>M. Greiner, O. Mandel, T. W. Hänsch, and I. Bloch, *Nature* **419**, 51 (2002).
- <sup>96</sup>K. Sakmann, A. I. Streltsov, O. E. Alon, and L. S. Cederbaum, *Phys. Rev. A* **78**, 023615 (2008).
- <sup>97</sup>S. I. Mistakidis, L. Cao, and P. Schmelcher, *J. Phys. B: At., Mol. Opt. Phys.* **47**, 225303 (2014).
- <sup>98</sup>A. U. J. Lode, B. Chakrabarti, and V. K. B. Kota, *Phys. Rev. A* **92**, 033622 (2015).
- <sup>99</sup>S. I. Mistakidis, L. Cao, and P. Schmelcher, *Phys. Rev. A* **91**, 033611 (2015).
- <sup>100</sup>G. M. Koutentakis, S. I. Mistakidis, and P. Schmelcher, *Phys. Rev. A* **95**, 013617 (2017).
- <sup>101</sup>S. I. Mistakidis and P. Schmelcher, *Phys. Rev. A* **95**, 013625 (2017).
- <sup>102</sup>J. Neuhaus-Steinmetz, S. I. Mistakidis, and P. Schmelcher, *Phys. Rev. A* **95**, 053610 (2017).
- <sup>103</sup>S. I. Mistakidis, G. M. Koutentakis, and P. Schmelcher, *Chem. Phys.* **509**, 106 (2018).
- <sup>104</sup>T. Plafmann, S. I. Mistakidis, and P. Schmelcher, *J. Phys. B: At., Mol. Opt. Phys.* **51**, 225001 (2018).
- <sup>105</sup>D. Jaksch and P. Zoller, *Ann. Phys.* **315**, 52 (2005).
- <sup>106</sup>J. Akram and A. Pelster, *Laser Phys.* **26**, 065501 (2016).

## **4.2. Bosonic Quantum Dynamics Following Colliding Potential Wells**

**Bosonic quantum dynamics following colliding potential wells**Fabian Köhler<sup>✉\*</sup>*Center for Optical Quantum Technologies, Department of Physics, University of Hamburg, Luruper Chaussee 149, 22761 Hamburg Germany*Peter Schmelcher<sup>†</sup>*Center for Optical Quantum Technologies, Department of Physics, University of Hamburg, Luruper Chaussee 149, 22761 Hamburg Germany  
and The Hamburg Centre for Ultrafast Imaging, University of Hamburg, Luruper Chaussee 149, 22761 Hamburg, Germany* (Received 2 February 2021; accepted 5 April 2021; published 20 April 2021)

We employ the multiconfiguration time-dependent Hartree method for bosons in order to investigate the correlated nonequilibrium quantum dynamics of two bosons confined in two colliding and uniformly accelerated Gaussian wells. As the wells approach each other an effective, transient double-well structure is formed. This induces a transient and oscillatory over-barrier transport. We monitor both the amplitude of the intrawell dipole mode in the course of the dynamics as well as the final distribution of the particles between the two wells. For fast collisions we observe an emission process which we attribute to two distinct mechanisms. Energy transfer processes lead to an untrapped fraction of bosons and a resonant enhancement of the deconfinement for certain kinematic configurations can be observed. Despite the comparatively weak interaction strengths employed in this work, we identify strong interparticle correlations by analyzing the corresponding von Neumann entropy.

DOI: [10.1103/PhysRevA.103.043326](https://doi.org/10.1103/PhysRevA.103.043326)**I. INTRODUCTION**

Ever since the first realizations of Bose-Einstein condensates [1–3], ultracold quantum gases were the focus of experimental and theoretical research in quantum physics. Their nearly perfect isolation from the environment as well as their excellent tunability render them ideal platforms to simulate a wide variety of quantum many-body systems [4–6] in order to unravel their fundamental physical properties. Experimental advancements in recent years have enabled the study of ensembles of ultracold atoms with a controlled number of particles [7,8] confined in almost arbitrarily shaped external potentials [9] like optical lattices [10,11], harmonic traps [12], and ring traps [13]. By varying the confinement it is possible to realize effectively three-dimensional [14,15], two-dimensional [16,17], and one-dimensional [18,19] systems. Magnetic Feshbach [20,21] and confinement-induced resonances [22–25] provide fine-grained control of the interparticle interaction. Recent studies have employed this versatile toolbox of ultracold atoms to establish links to solid-state systems [26,27], the electronic structure of molecules [28], light-matter interaction [29], topological matter [30,31], and even black-hole analogs [32].

In recent years, optical tweezers have become important instruments to confine and move microscopic objects by exerting small forces via highly focused laser beams. This tool was originally developed to manipulate micrometer-sized particles [33,34] but was later refined to manipulate objects on many different length scales ranging from individual atoms

[35,36] to bacteria and viruses [37]. These advancements sparked strong interest in using optical tweezers for the precise manipulation of ensembles of ultracold neutral atoms [38] including Rydberg atoms [39–41]. A very interesting direction of research is to use multiple optical tweezers to accelerate atomic clouds [42], which allows one to set up optical colliders [43–45]. In these experiments, fundamental properties of quantum scattering processes were observed such as partial wave interference or the loss of particles in resonant collisions. In this light, colliding ultracold atoms could be used to mimic electrons during atom-atom collisions. Since the dynamics of ultracold atoms takes place on much larger timescales, the usually very fast electronic processes could be slowed down [29,46,47], potentially providing in depth insights into the fundamental processes of atom-atom or atom-ion collisions such as projectile ionization [48,49] or charge transfer [50,51].

Another interesting application of ultracold atoms is quantum information processing [52]. In this context, time-dependent colliding trap potentials have been proposed for the realization of two-qubit quantum gates as well as the efficient creation of highly entangled states [53,54], which are two essential features required for a quantum computer.

In the present investigation two bosonic particles are confined in two colliding Gaussian potential wells. We solve this time-dependent problem using the *ab initio* multiconfiguration time-dependent Hartree method for bosons (MCTDHB), which provides an exact description capturing all correlations [55,56]. This allows us to compute the time evolution of the two-body wave function across a wide range of kinematic parameters in contrast to the other theoretical investigations of colliding potentials in the literature [53,54] which relied on employing effective models and were limited to adiabatic

\*fkoehler@physnet.uni-hamburg.de

†pschmelc@physnet.uni-hamburg.de

movements of the traps. We show that during the time evolution of this system an effective time-dependent double-well structure forms that drives an oscillatory over-barrier bosonic transport between the wells. This process terminates when the wells have been separated sufficiently after penetrating each other. During the collision process the displacement of the bosons from the well trajectories induces an intrawell dipole mode and determines the final distribution of the particles between the wells. For fast collisions this setup exhibits deconfinement of the particles, which we can attribute to two different mechanisms. First, for very fast accelerations an increase in kinetic energy leads to a positive total energy of the system towards the end of the time evolution, thereby causing an untrapping of particles. Second, we observe a resonant enhancement of the emission for certain kinematic parameters similar to the ionization processes that take place in atom-atom collisions.

Our work is structured as follows. In Sec. II we introduce the physical setup and describe the computational approach used to solve the time-dependent problem. We proceed by presenting the results for the dynamics of two interacting bosonic particles in Sec. III and discuss suitable observables to unravel the properties of the system. We summarize our findings in Sec. IV and provide an outlook on possible future studies. Finally, we comment on the convergence of our variational multiconfiguration time-dependent Hartree method for bosons (MCTDHB) approach in the Appendix.

## II. PHYSICAL SETUP AND COMPUTATIONAL APPROACH

In the present work we investigate the nonequilibrium quantum dynamics of a closed system of  $N = 2$  interacting bosons. We employ the MCTDHB [55,57,58] to solve the time-dependent many-body Schrödinger equation and gain access to the correlated quantum dynamics of the particles. This approach employs a time-dependent, variationally optimal basis  $\{\phi_i(x, t)\}_{i=1}^M$  of  $M$  single-particle functions (SPFs). The many-body wave function  $|\Psi(t)\rangle$  is then expanded as a superposition

$$|\Psi(t)\rangle = \sum_{\vec{n}|N} C_{\vec{n}}(t) |\vec{n}; t\rangle \quad (1)$$

of all  $\binom{N+M-1}{N}$  time-dependent  $N$ -particle number states  $|\vec{n}; t\rangle$  that can be built from the  $M$  SPFs using time-dependent coefficients  $C_{\vec{n}}(t)$ . Finally, the Lagrangian formulation of the time-dependent variational principle [59,60] yields equations of motion for the SPFs and the coefficients [55,57] are then solved numerically. The MCTDHB provides access to the time evolution of the full many-body wave function, which allows us to compute all relevant characteristics of the underlying system.

We consider  $N = 2$  bosons of mass  $m$  interacting repulsively with a contact interaction of strength of  $g$  [61,62]. The Hamiltonian of the system reads

$$H(\{x_i\}, t) = \sum_{i=1}^N h(x_i, t) + g \sum_{i,j=1}^N \delta(x_i - x_j). \quad (2)$$

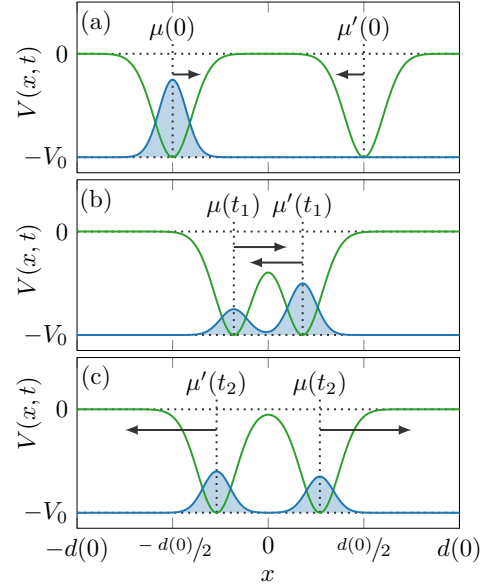


FIG. 1. Sketch of the system at different points in time  $t_0 = 0 < t_1 < t_2$  during the dynamics. The green line indicates the external trapping potential consisting of two Gaussian wells, while the blue line symbolizes the spatial distribution of the particles. (a) The time evolution of the system starts with the interacting ground state in the left well. (b) As the wells accelerate towards each other, a transient time-dependent double-well structure forms. (c) After the wells penetrated each other they separate again, moving in opposite directions.

The one-body Hamiltonian

$$h(x, t) = -\frac{\hbar^2}{2m} \frac{\partial^2}{\partial x^2} + V(x, t) \quad (3)$$

acts on each particle individually and includes both a kinetic term and the external potential  $V(x, t)$ .

In our setup, the external potential

$$V(x, t) = -V_0 \exp\left[-\left(\frac{x - \mu(t)}{\sqrt{2}\sigma}\right)^2\right] - V'_0 \exp\left[-\left(\frac{x - \mu'(t)}{\sqrt{2}\alpha\sigma}\right)^2\right] \quad (4)$$

consists of two Gaussian wells of depths  $V_0$  and  $V'_0$  centered around  $\mu(t)$  and  $\mu'(t)$ , which approach each other in the first phase of the collision process (see Fig. 1). The width of the two Gaussians is characterized by their standard deviations  $\sigma$  and  $\alpha\sigma$ , where  $\alpha$  is a dimensionless asymmetry factor. We drive the nonequilibrium dynamics by a motion of the well centers specified by the expectation values  $\mu(t)$  and  $\mu'(t)$ . Hence, the potential (4) and consequently the Hamiltonians (3) and (2) are time dependent.

The investigation of the physical system can be greatly simplified by employing a suitable unit system. We rescale all positions using the length unit  $l_G = \sqrt{2}\sigma$  and all energies using the energy unit  $E_G = \hbar^2(2m\sigma^2)^{-1}$  in order to obtain a dimensionless formulation and to eliminate both  $\sigma$  and  $m$



as physical parameters from the potential and Hamiltonian. The corresponding time unit  $t_G = 2m\sigma^2\hbar^{-1}$  can be inferred from the Schrödinger equation. For the analysis of the dynamics it is instructive to additionally introduce the unit  $v_G = \hbar(\sqrt{2}m\sigma)^{-1}$  for speeds.

The dynamics of the particles strongly depends on the initial state. A natural choice is to prepare the system in the ground state of the initial many-body Hamiltonian  $H(\{x_i\}, t=0)$  where the particles would be delocalized over the two wells. However, we will use the ground state for  $V'_0 = 0$  which results in all particles being located in the left well centered around  $\mu(0)$  (see Fig. 1). This allows us to track them during the transport processes that occur during the time propagation. This initial state can be computed efficiently using the improved relaxation algorithm [63]. Experimentally, such a state could be prepared with high fidelity by loading two atoms in a single optical microtrap and then slowly ramping on the spatially separated potential wells [7,64,65].

We assume that for  $t = 0$  the potential wells are at rest. The most evident choice for the trajectory of the Gaussian well centers  $\mu(t)$  and  $\mu'(t)$  would be a uniform motion, i.e., by boosting the wells to fixed speeds instantaneously. However, this approach would pump a great deal of energy into the system, thereby causing major excitations which would render the dynamics very “irregular.” Therefore, we choose to accelerate the wells uniformly towards each other using parabolic trajectories

$$\mu(t) = \mu(0) + \frac{1}{2}at^2, \quad (5)$$

$$\mu'(t) = \mu'(0) - \frac{1}{2}at^2 \quad (6)$$

for the well centers. Initially, the wells are located symmetrically around  $x = 0$ , i.e.,  $\mu(0) = -\mu'(0)$  with a separation of  $d(0)$ . The propagation is terminated at the final time

$$t_f = \sqrt{2\frac{d(0)}{a}} \quad (7)$$

when the wells have moved through each other and reached their initial separation again. At this point in time the wells have reached their final speed of  $v_f = at_f = \sqrt{2ad(0)}$ .

### III. DISCUSSION OF THE COLLISIONAL DYNAMICS

In the scope of the present work we limit ourselves to  $N = 2$  particles when investigating the setup described in Sec. II in order to unravel the main signatures of the dynamics of the system. This provides an ideal starting point for future works addressing the case of larger particle numbers. We choose wells of equal width, i.e.,  $\alpha = 1$ , and depth  $V_0 = V'_0 = 20E_G$ , which are deep enough to support ten trapped states of the one-body Hamiltonian (3). Initially, the wells are located at  $\mu(0) = -3.5l_G$  and  $\mu'(0) = 3.5l_G$ , which corresponds to an initial separation of  $d(0) = 7l_G$ . For the interaction strength we choose a value of  $g = 0.5E_Gl_G$ , which is comparable to an interaction strength of  $g_{HO} \approx 0.199$  in harmonic-oscillator units. We find that for this value of  $g$ ,  $M = 6$  SPFs are sufficient for the convergence of our MCTDHB simulations (see Sec. A). We solve the time-dependent problem for varying values of the

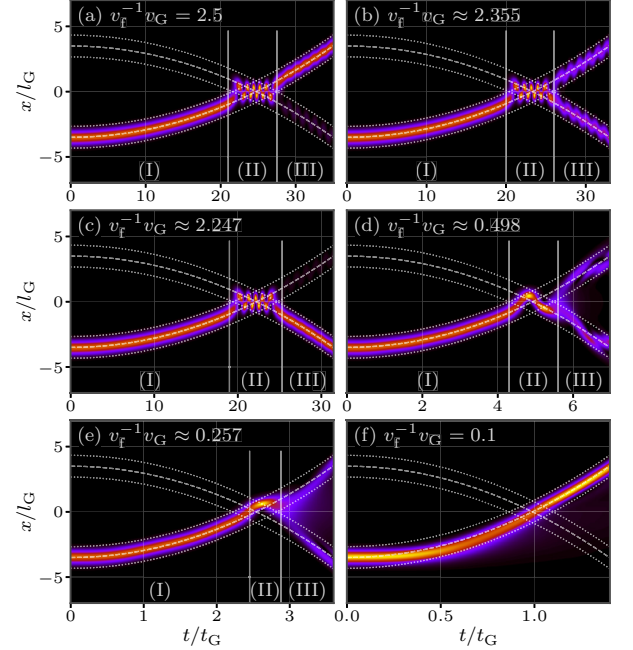


FIG. 2. Time evolution of the one-body density  $\rho^{(1)}(x, t)$  [see Eq. (8)] for different inverse final speeds  $v_f^{-1} \propto a^{-1/2}$ . The dashed white lines indicate the trajectories of the well centers, while the dotted white lines indicate the positions of the FWHM of the Gaussian wells.

acceleration  $a$  chosen such that the corresponding inverse final speeds  $v_f^{-1}$  are equally spaced in the interval  $[0.1v_G^{-1}, 2.5v_G^{-1}]$ . The reason for this choice will become apparent during the analysis since many quantities scale with the inverse speed.

#### A. Time evolution of the one-body density

In order to analyze the dynamics of the system and to guide our further analysis approach, we inspect the one-body density [66,67]

$$\rho^{(1)}(x, t) = N \int |\Psi(x, x_2, \dots, x_N, t)|^2 dx_2, \dots, dx_N, \quad (8)$$

with  $N = 2$  in our case. This quantity provides insight into the temporal evolution of the spatial distribution of the particles since  $\rho^{(1)}(x, t)$  corresponds to the probability density of finding a particle at the position  $x$  at the time  $t$ .

Figures 2(a)–2(f) show the time evolution of  $\rho^{(1)}(x, t)$  for various values of the acceleration which correspond to different inverse final speeds  $v_f^{-1}$ . If the acceleration is not too fast [see Figs. 2(a)–2(e)], we can identify three distinct stages of the dynamics indicated by (I)–(III).

The particles are initially localized in the well centered at  $\mu(0) = -3.5l_G$  and follow its parabolic trajectory  $\mu(t)$  during stage (I) of the dynamics while wells approach each other. No effect of the presence of the second well centered around  $\mu'(t)$  is visible during this phase of the dynamics. During stage (II) the wells are in close proximity and they even penetrate each other. Hence, an effective double-well structure forms (see Fig. 1) that changes its shape over time and we observe a

collective oscillatory particle transport over the central barrier from the left to the right well and vice versa. Towards the end of the propagation, during stage (III), we find several effects depending on the acceleration and hence  $v_f^{-1}$ . In general, the particles are delocalized over both wells with varying ratios. For certain values of  $v_f^{-1}$  however, the bosons are almost completely localized in one of the wells. Additionally, we observe a sloshing motion of the particles within each well. We characterize this motion as a dipole mode [61,62] since the center-of-mass (center of mass (c.m.)) position of the particles oscillates around the center of the wells in which they are confined. This collective excitation is accompanied by a breathing mode which manifests in a periodic widening and contraction of the atomic cloud in each well. However, the breathing is much less pronounced compared to the dipole oscillation such that we refer to the sloshing motion as a dipole mode in the following. Generally, we observe that the one-body density is well contained within one full width at half maximum (FWHM) around the well centers as indicated by the white lines in Fig. 2. However, for fast collisions [see Fig. 2(e)] we notice a faint density halo in the region between the wells, which indicates an untrapped fraction of particles, i.e., a finite probability of detecting a particle in this region. When moving towards even faster accelerations we also observe effects of the inertia of the bosons [see Fig. 2(f)], which seem to move more slowly than the left well and leave the full width at half maximum (FWHM) region before finally catching up with the well towards the end of the dynamics.

### B. Center-of-mass position

In order to analyze the transport of particles, we introduce the c.m. position

$$\langle X \rangle(t) = \frac{1}{N} \sum_{i=1}^N \langle x_i \rangle(t), \quad (9)$$

which measures the average position of the particles. In Figs. 3(a) and 3(b) we show two examples for the time evolution of this quantity. We can clearly make out the three aforementioned phases (I)–(III) of the dynamics. During stage (I) of the time evolution,  $\langle X \rangle(t)$  matches the trajectory of the left well  $\mu(t)$  as the particles simply follow the motion of the potential. In part (II) we observe an oscillation of  $\langle X \rangle(t)$  around 0 which indicates the oscillatory particle transport in the effective double-well structure from the left to the right well and vice versa. During stage (III) we notice that the evolution of  $\langle X \rangle(t)$  strongly depends on the kinematic parameters. For some values of  $v_f^{-1}v_G$ ,  $\langle X \rangle(t)$  closely follows one of the trajectories  $\mu(t)$  and  $\mu'(t)$  and the dipole mode vanishes [see Fig. 3(b)]. In other cases [see Fig. 3(a)]  $\langle X \rangle(t)$  lies in the region between  $\mu(t)$  and  $\mu'(t)$  and the dipole mode is well pronounced. The amplitude of the dipole mode varies depending on  $a$  and is maximal when  $\langle X \rangle(t)$  oscillates close to zero.

As the next step, we quantify the number of transport processes during phase (II) of the dynamics by determining the number of zero crossings  $N_{ZC}^{(II)}$  of the signal  $\langle X \rangle(t)$  for each value of  $v_f^{-1}$  during this stage [see Fig. 3(d)]. Here  $N_{ZC}^{(II)}$  increases monotonically with  $v_f^{-1}$  since the effective double-

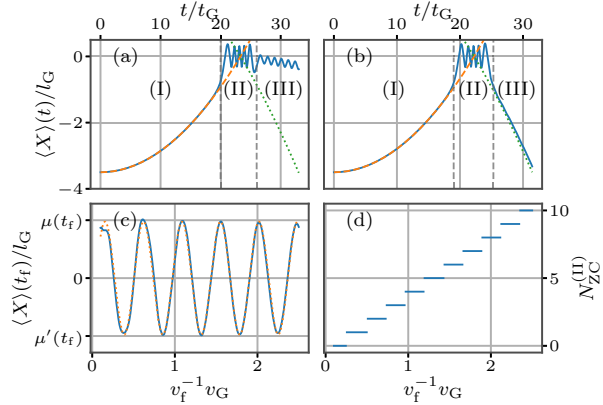


FIG. 3. Time evolution of the c.m. position (blue solid line) as a function of time for (a)  $v_f^{-1}v_G \approx 2.355$  and (b)  $v_f^{-1}v_G \approx 2.247$ . The orange dashed line indicates the trajectory  $\mu(t)$ , while the green dotted line visualizes  $\mu'(t)$ . (c) Expectation value of the c.m. position of the particles in the final state as a function of  $v_f^{-1}$ . The orange dashed line corresponds to a cosine fit of the signal. (d) Number of zero crossings  $N_{ZC}^{(II)}$  of  $\langle X \rangle(t)$  in the region (II) as a function of  $v_f^{-1}$ .

well structure persists for a longer time period and more oscillations can take place. Since the number of zero crossings has to be a non-negative integer,  $N_{ZC}^{(II)}$  is a step function of  $v_f^{-1}$ . We find the step width to be approximately equal for all steps with an average width of  $0.221v_G^{-1}$ .

As mentioned before, the final location of the particles strongly depends on the acceleration  $a$ . Figure 3(c) shows the final c.m. position of the particles  $\langle X \rangle(t_f)$  as a function of  $v_f^{-1}$ , which resembles a cosinelike structure. Using a least-squares fit, we can extract the period  $\Delta v^{-1} = 0.47v_G^{-1}$  and the amplitude  $3.42l_G$  of the signal. From the amplitude of the oscillation, we can deduce that indeed for certain values of  $v_f^{-1}$  the density is almost completely located in one of the wells. A value of  $\langle X \rangle(t_f) = \pm 3.5l_G$  would indicate that the average position of the particles coincides with the final position of one of the well centers. For most values of  $v_f^{-1}$  however, the final center-of-mass position lies somewhere between these extreme cases and indicates that the particles are delocalized across both wells.

A further analysis of the center-of-mass motion shows that the final distribution of the particles as well as the amplitude of the dipole mode depend on the displacement of the c.m. position from the trajectories of the wells at the transition from stage (II) to (III) of the dynamics. If the c.m. position  $\langle X \rangle(t)$  is close to one of the well centers at this transition point, the particles get pinned in that particular well. A small deflection of  $\langle X \rangle(t_f)$  from the well center leads then to small amplitudes of the corresponding dipole mode in this well. For most values of  $v_f^{-1}$  however, the separation of the wells splits the one-body density into two parts and the particles are delocalized across both wells. As emphasized, the displacement of the particles within the wells induces an intrawell dipole mode, the amplitude of which is maximal if  $\langle X \rangle(t)$  is close to 0 at the transition from stage (II) to (III), which corresponds to the maximal deflection of the particles from the well center. In order to distinguish between the intrawell dynamics different

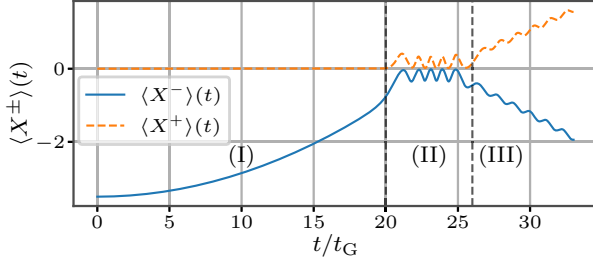


FIG. 4. Time evolution of the truncated c.m. observables  $\langle X^\pm \rangle(t)$  [see Eq. (10)] for  $v_r^{-1}v_G \approx 2.355$ .

wells, we introduce the truncated c.m. observables

$$\langle X^\pm \rangle(t) = \frac{1}{N} \sum_{i=1}^N \langle x_i \Theta(\pm x_i) \rangle(t), \quad (10)$$

which measure the average position of particles on either the positive or the negative side with respect to  $x = 0$ . Figure 4 shows an example for the time evolution of these observables. Here  $\langle X^+ \rangle(t)$  is zero during phase (I) of the dynamics as the particles are initially contained in the left well and follow its trajectory. The periodic transport in the transient double-well potential during phase (II) is clearly visible. During part (III) of the dynamics, the dipole motion of the particles in the initially left [right] well manifests itself in an oscillatory modulation of  $\langle X^+ \rangle(t)$  [ $\langle X^- \rangle(t)$ ]. By analyzing the turning points of these modulations, we determine a phase of  $\frac{\pi}{2}$  between the two oscillations. Furthermore, we notice that the oscillation period of both observables lies in the range  $0.55t_G - 0.6t_G$  and is approximately constant across all values of  $a$ , which is to be expected since the frequency of the dipole mode only depends on the shape of the potential well.

### C. Nature of particle transport

In order to classify the transport process between the left and right wells that takes place in phase (II) of the dynamics, we analyze the two-body wave function  $|\Psi(t)\rangle$  with respect to the time-dependent one-body Hamiltonian  $h(x, t)$  [Eq. (3)]. We consider the instantaneous eigenbasis of  $h(x, t)$  spanned by the time-dependent eigenstates  $\{|\Phi_i(t)\rangle\}$  with the corresponding eigenenergies  $\varepsilon_i(t)$ , i.e.,  $h(x, t)\Phi_i(x, t) = \varepsilon_i(t)\Phi_i(x, t)$ , while assuming an energetic ordering  $\varepsilon_i(t) \leq \varepsilon_{i+1}(t)$  for all times. Figure 5 shows the eigenenergies of the ten energetically lowest eigenstates as a function of the well separation  $d(t) = d(0) - at^2$ . At the initial  $[d(0)]$  and final  $[d(t_f)]$  separations, the external potential is able to support ten trapped eigenstates, i.e., states with negative eigenenergies, which are pairwise degenerate. It should be noted that for positive energies the system exhibits a discrete spectrum of untrapped states instead of a continuous spectrum of extended continuum states since we employ a finite grid for the numerical treatment of the problem which imposes periodic boundary conditions (see the Appendix). However, this does not impact our analysis of the trapped fraction or the occupation of the trapped states. If the wells reach close proximity, an effective double-well structure forms (see Fig. 1), where  $V(x = 0)$  determines the height of the barrier and the

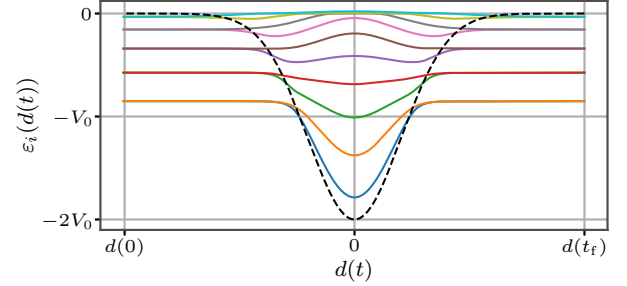


FIG. 5. Spectrum of the one-body Hamiltonian  $h(x, t)$  [Eq. (3)] as a function of the well separation  $d(t)$ . We show the ten energetically lowest eigenenergies (colored solid lines) and the values of the central potential  $V(x = 0)$  (black dashed line).

energetic degeneracies are lifted. In the vicinity of  $d(t) = 0$  the central barrier vanishes and the external potential is a single Gaussian well centered around  $x = 0$  with a depth  $V(x = 0) = -2V_0$ . Here the eigenenergies  $\varepsilon_7(t)$ ,  $\varepsilon_8(t)$ , and  $\varepsilon_9(t)$  cross zero and reach positive values such that the associated eigenstates become untrapped.

We proceed with our analysis by defining the operator

$$P_j(t) = \frac{1}{N} \sum_{i=1}^N |\Phi_j^i(t)\rangle \langle \Phi_j^i(t)|, \quad (11)$$

where  $|\Phi_j^i(t)\rangle \langle \Phi_j^i(t)|$  projects the  $i$ th particle onto the  $j$ th one-body eigenstate  $|\Phi_j(t)\rangle$ . Computing the expectation value of this projector with respect to the many-body wave function yields the probability  $p_j(t) = \langle \Psi(t) | P_j(t) | \Psi(t) \rangle$  of finding a particle in the  $j$ th one-body eigenstate.

In order to unravel the nature of the particle transport so as to answer the question of whether it is a tunneling or over-barrier process, it is instructive to subdivide the set of one-body eigenstates into two categories. First, we introduce the set  $\mathcal{B}_A(t)$  that contains all states that lie below the central barrier, i.e., all states  $|\Phi_i(t)\rangle$  with eigenenergies  $\varepsilon_i(t) < V(x = 0, t)$ . Second,  $\mathcal{B}_B(t)$  captures all remaining trapped states, i.e., all states  $|\Phi_i(t)\rangle$  with eigenenergies  $V(x = 0, t) \leq \varepsilon_i(t) < 0$ . It should be noted that both the eigenenergies and the central potential, and consequently also the sets  $\mathcal{B}_\sigma(t)$ , change over time.

As the next step we construct the operators

$$O_\sigma(t) = \sum_{\substack{j \text{ such that} \\ |\Phi_j(t)\rangle \in \mathcal{B}_\sigma(t)}} P_j(t), \quad \sigma \in \{A, B\}, \quad (12)$$

that project the many-body wave function onto the states in the respective basis sets. The expectation values  $\langle O_\sigma(t) \rangle$  can be understood as the probabilities of a particle to occupy any of the states included in the corresponding basis set  $\mathcal{B}_\sigma(t)$ . Additionally, we define the operator  $O_C(t) = 1 - O_A(t) - O_B(t)$  that projects the wave function onto the orthogonal space of all untrapped eigenstates. Consequently, the expectation value  $\langle O_C(t) \rangle$  correctly captures the occupation of the untrapped continuum which is discretized due to our finite numerical grid.

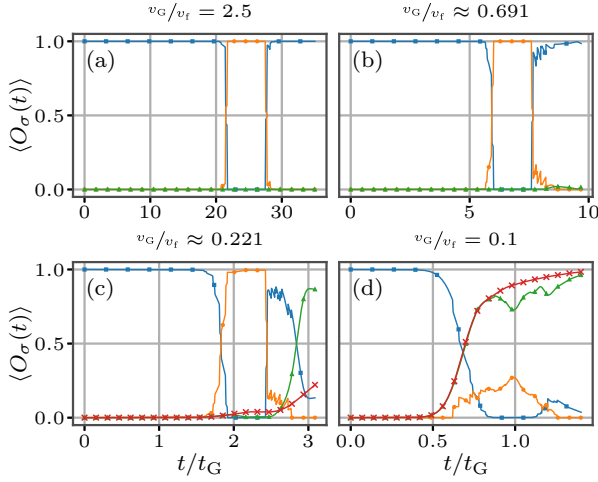


FIG. 6. Time evolution of the projections  $\langle O_A(t) \rangle$  (blue solid line with squares),  $\langle O_B(t) \rangle$  (orange solid line with circles), and  $\langle O_C(t) \rangle$  (green solid line with triangles) for different final speeds  $v_f^{-1}$ . In (c) and (d) we also show the evolution of  $\langle O_C(t) \rangle$  if the initially right well is absent during the propagation ( $V'_0 = 0$ , red solid lines with crosses) in order to highlight the influence of the second well on the deconfinement of the particles (see Sec. III D).

Figure 6 shows examples for the time evolution of these quantities. In the initial state, only under-barrier states are occupied and hence  $\langle O_A(t) \rangle \approx 1$  in the beginning of the time evolution. As the wells start to penetrate each other during part (II) of the dynamics, the occupation of the under-barrier states  $\langle O_A(t) \rangle$  drops to zero while the occupation  $\langle O_B(t) \rangle$  of the trapped over-barrier states rises to approximately one. Consequently, we classify the particle transport that occurs during this stage of the time evolution as an over-barrier process. A deeper analysis shows that the start of transport coincides with the crossing of  $V(x=0, t)$  of the eigenenergies  $\varepsilon_1(t)$  and  $\varepsilon_2(t)$  (see Fig. 5). The corresponding states  $|\Phi_1(t)\rangle$  and  $|\Phi_2(t)\rangle$  are predominantly occupied (see Fig. 7). Consequently, the particle transport occurs when these states lie above the central barrier. Towards the end of the propagation, the over-barrier states become under-barrier states again such that  $\langle O_A(t) \rangle \rightarrow 1$  while  $\langle O_B(t) \rangle \rightarrow 0$  for  $t \rightarrow t_f$ .

For fast collisions [see Figs. 6(c) and 6(d)] untrapped states come into play as can be seen in an increase of  $\langle O_C(t) \rangle$  towards the end of the dynamics. We analyze this phenomenon further in Sec. III D, where we investigate the emission of particles.

#### D. Deconfinement of particles

As the next step in our analysis, we investigate the origin of the faint density halo between the wells that we observe for fast collisions [see Fig. 2(e)], indicating a deconfinement of particles. The increase of  $\langle O_C(t) \rangle > 0$  in Figs. 6(c) and 6(d) shows that indeed untrapped delocalized eigenstates of the one-body Hamiltonian  $h(x, t)$  [see Eq. (3)] come into play. In order to understand how the occupation of the individual eigenstates evolves over time, we analyze the probabilities  $p_j(t) = \langle P_j(t) \rangle$  of finding a particle in a specific one-body

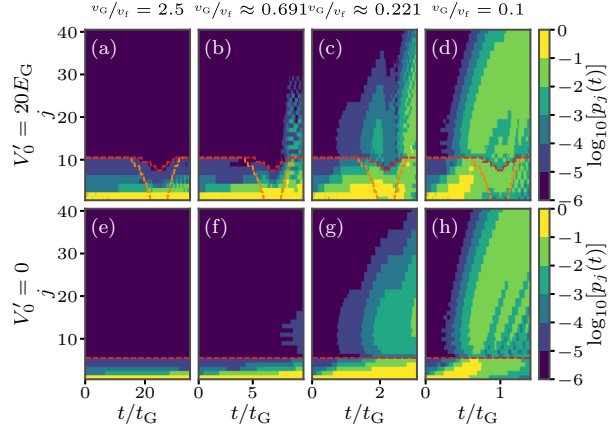


FIG. 7. Time evolution of the occupations  $\log_{10}[p_j(t)]$  of the 40 energetically lowest, instantaneous eigenfunctions of the one-body Hamiltonian (3): (a)–(d) the occupation under the presence of the well centered around  $\mu'(t)$  and (e)–(h) the case  $V'_0 = 0$ . All states below the red dashed line are trapped states, while the states below the orange line are under-barrier states.

eigenstate. Figures 7(a)–7(d) show the time evolution of these quantities for specific values of  $v_f^{-1}$ . For slow collisions [see Fig. 7(a)] we observe that the eigenstates  $|\Phi_1(t)\rangle$  and  $|\Phi_2(t)\rangle$  are predominantly occupied while the other excited trapped states play a minor role and no occupation of the untrapped states takes place. When increasing the acceleration and hence the collision speed, we observe a higher occupation of the excited trapped states and a minor population of several untrapped ones [see Fig. 7(b)]. For the fastest collisions under consideration [see Figs. 7(c) and 7(d)] all 40 depicted eigenstates play a significant role and we even observe an equal population of all eigenstates towards the end of the simulation.

We remark that the occupation of untrapped states occurs at different stages of the dynamics when comparing Figs. 7(b)–7(d). In Fig. 7(b) the population of untrapped states increases abruptly towards the end of the considered dynamics while still remaining small overall  $\langle O_B(t) \rangle \ll 1$  [see Fig. 6(b)]. A similar jump in the occupation of untrapped states towards the end of the dynamics is visible in Fig. 7(c), albeit with a much stronger total occupation of untrapped states  $\langle O_C(t_f) \rangle \approx 0.86 \gg \langle O_A(t_f) \rangle + \langle O_B(t_f) \rangle$ . Here we also observe an additional steady increase in the population of untrapped states that already starts in part (I) of the time evolution. Even though this is a small effect, it still suggests the existence of two distinct mechanisms of the particle deconfinement. For very fast collisions [see Fig. 7(d)] the steady increase of the untrapped population becomes dominant. This enhancement for faster collisions suggests that it is a kinematic effect of the particles which get spilled out of the potential wells due to the fast acceleration.

In order to distinguish between the two effects leading to deconfinement and to unravel their origins, it is instructive to compare the results in Figs. 7(a)–7(d) with simulations where the second, initially empty well is not present, i.e., for  $V'_0 = 0$  [see Figs. 7(e)–7(h)]. The first striking difference is the absence of a sudden jump in the occupation of untrapped states

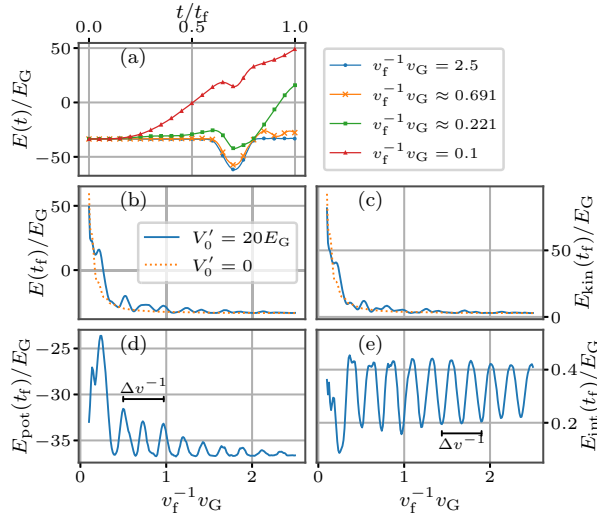


FIG. 8. (a) Time evolution of the total energy of the two bosons during the collision dynamics for various inverse final speeds  $v_f^{-1}$ . Also shown are the (b) total, (c) kinetic, (d) potential, and (e) interaction energies of the final state as a function of  $v_f^{-1}$ . The orange dotted lines in (b) and (c) correspond to computations performed in the absence of the second, initially right, well, i.e.,  $V'_0 = 0$ , thereby highlighting the impact of this well on the total and kinetic energies.

towards the end of the time evolution [compare Figs. 7(b) and 7(c) with Figs. 7(f) and 7(g)]. This contribution to the deconfinement can only be explained due to the presence of the second well. However, the steady increase in the occupation of untrapped one-body states is still present [compare Figs. 7(c) and 7(d) with Figs. 7(g) and 7(h)]. In Fig. 6 these observations become even clearer when comparing the evolution of  $\langle O_C(t) \rangle$  with and without the presence of the initially empty well (see Fig. 6). For very fast collisions [see Fig. 6(d)] the curves match for the biggest part of the dynamics and only deviate slightly towards the end of the time evolution. Consequently, the presence of the second well plays only a minor role concerning the emission of particles. For other parameters however [see Fig. 6(c)], the differences are striking and the occupation of untrapped states is greatly enhanced due to the presence of the second well.

As mentioned before, the emission process during early times of the dynamics is of kinematic origin. We employ the energy of the system as well as its composition to study this phenomenon further. Figure 8(a) shows the total energy  $E(t)$  as a function of  $t$  for various inverse final speeds  $v_f^{-1}$ . Since we prepare the system in the ground state, all energy curves start at the ground state energy  $E(t=0) = E_0 \approx -33.6E_G$ . When focusing on a very slow motion of the wells (see the curve for  $v_f^{-1}v_G = 2.5$ ), the energy remains constant until  $t \approx 0.6t_f$ , where it starts to drop as the particles are now impacted by the second potential well. As the wells separate, the energy increases back to its initial value. The behavior of the total energy changes gradually as we turn towards faster accelerations. First, the dip of the energy becomes less deep and a modulation of the energy becomes visible towards the end of the simulated dynamics. For  $v_f^{-1}v_G \approx 0.221$ , the total energy

exceeds the value zero at the end of the simulations. Consequently, an emission and untrapping of the particles take place for energetic reasons alone. As we increase the acceleration further, the total energy exceeds the value zero earlier during the time evolution, e.g., at  $t \approx 0.5t_f$  for  $v_f^{-1}v_G \approx 0.221$ , and the dip, while the wells are in close proximity, becomes less pronounced. As the next step, we analyze the energy composition of the final state to get an overview of all simulations. Figures 8(b)–8(d) show the total, kinetic, and potential energies of the final state as a function of the final inverse speed  $v_f^{-1}$ . We notice a drastic increase of the kinetic [see Fig. 8(c)] and hence the total energy [see Fig. 8(b)] towards large final speeds, i.e., small  $1/v_f$ . For  $v_f^{-1}v_G < 0.266$  with  $V'_0 = V_0$  as well as for  $v_f^{-1}v_G < 0.170$  with  $V'_0 = 0$  the total energy exceeds zero, indicating that untrapping takes place solely for kinetic energy reasons. The potential energy [see Fig. 8(d)] exhibits equidistant peaks whose height increases towards small values of  $v_f^{-1}$  as the particles become less deeply trapped. As indicated in the figure, the difference between neighboring peaks is equal to half of the period  $\Delta v^{-1} = 0.47v_G$  that we introduced in our discussion of the final c.m. position of the particles. The same characteristics and effects can be seen for the interaction energy [see Fig. 8(e)]. The maxima of the interaction energy coincide with the extrema of  $\langle X \rangle(t_f)$  since the interaction energy is higher when both particles reside in the same well. The potential energy, on the other hand, becomes maximal where  $\langle X \rangle(t_f)$  is zero. In contrast to the potential energy, the interaction energy does not exhibit a strong increase towards small values of  $v_f^{-1}$ . Only a marginal increase in the oscillation amplitude of  $E_{\text{int}}(t_f)$  is visible as the particles become less deeply trapped and are less strongly localized at the well center. Due to the local nature of the interaction term, the value of the interaction energy is mainly determined by the delocalization of the particles across both wells and less by how deeply they are trapped.

So far, our discussion of the particle untrapping has relied on the projection onto one-body eigenstates. We conclude our analysis of this phenomenon using a two-body or in general many-body analysis that relies on projecting the many-body wave function onto number states built from the instantaneous eigenbasis of the one-body Hamiltonian. Let  $\mathcal{N}(t)$  be the time-dependent set of all  $N = 2$  particle number states that can be constructed from all trapped eigenstates of the instantaneous one-body Hamiltonian. We then define the magnitude  $M_B(t) = \sum_{|\vec{n}\rangle \in \mathcal{N}(t)} |\langle \vec{n} | \Psi(t) \rangle|^2$ , which captures the total overlap of the many-body wave function with the number state basis  $\mathcal{N}(t)$ . The maximal possible value of  $M_B(t) = 1$  indicates that the many-body wave function lies completely in the Hilbert space spanned by the basis  $\mathcal{N}(t)$ , while a value of zero would indicate that  $|\Psi(t)\rangle$  is orthogonal to this space. Consequently, the quantity  $M_U(t) = 1 - M_B(t)$  can then be used to quantify the untrapped fraction, i.e., the projection of the many-body function onto the orthogonal space of untrapped eigenstates.

Figures 9(a)–9(d) show the time evolution of  $M_U(t)$  for different values of  $v_f^{-1}$ . For slow to moderately fast collisions [see Figs. 9(a) and 9(b)], no deconfinement of particles is visible in the absence of the second well, i.e., for  $V'_0 = 0$ . As discussed previously, only the kinematic emission of particles takes place when only a single well is present. This process

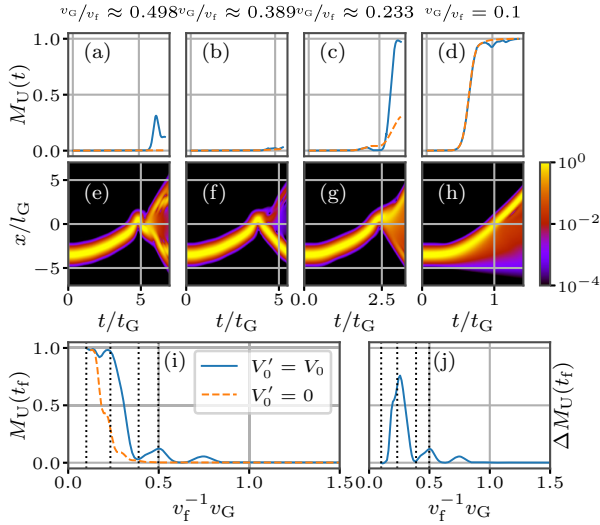


FIG. 9. (a)–(d) Time evolution of the untrapped fraction  $M_U(t)$  for varying  $v_f^{-1}$  (blue solid lines). The orange dashed lines indicate the evolution of  $M_U(t)$  in the absence of the second, initially empty well (i.e.,  $V'_0 = 0$ ), highlighting its importance for the untrapping process for certain values of  $v_f^{-1}$ . (e)–(h) Time evolution of the one-body density  $\log_{10}[\rho^{(1)}(x, t)]$  [see Eq. (8)] for  $V_0 = V'_0$  in a logarithmic representation which increases the visibility of the density halo outside the potential wells in comparison to Fig. 2. (i) Untrapped magnitude  $M_U(t_f)$  of the final state as a function of  $v_f^{-1}$ . The dotted vertical lines indicate the values of  $v_f^{-1}$  that have been used for (a)–(d) and (e)–(h). (j) Untrapped magnitude  $\Delta M_U(t_f)$  due to the presence of the second well (see the main text for details).

is enhanced by the collisional speed and we only observe untrapping for the fastest collisions under consideration [see Figs. 9(c) and 9(d)]. When comparing these results with the simulations with  $V'_0 = V_0$ , the importance of the presence of both wells becomes evident. For certain values of  $v_f^{-1}$  a drastic increase in the untrapped fraction is noticeable that stems from the final stage of the dynamics [see Figs. 9(a) and 9(c)]. At very high speeds however, the kinematic untrapping is the dominant contribution to the emission of particles such that the two curves for  $M_U(t)$  (single- and two-well dynamics) match each other.

The logarithmic representation of the one-body density in Figs. 9(e)–9(h) increases the visibility of the density halo outside of the wells in contrast to the earlier discussion (see Fig. 2). For very fast collisions [see Fig. 9(h)], we notice a density halo on the left side of the initially occupied well due to a fraction of the density getting spilled out of the potential wells due to the inertia of the particles. Furthermore, we observe that in the case of the resonant emission of particles at certain values of  $v_f^{-1}$ , the density halo is located in the space between the two well trajectories [see Figs. 9(e) and 9(g)]. At other values, where almost no deconfinement takes place, this halo is vanishingly small [see Fig. 9(f)]. Figure 9(i) shows the value of  $M_U(t)$  for the final state. In the absence of the second well, i.e., for  $V'_0 = 0$ , the curve of  $M_U(t)$  is flat and close to a value of zero for  $v_f^{-1} v_G \gtrsim 0.39$  since only the kinematic emission of particles can occur which requires high speeds. When

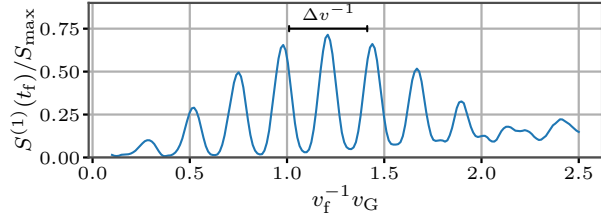


FIG. 10. von Neumann entropy of the final state  $S^{(1)}(t_f)$  normalized by the maximal possible value  $S_{\max}^{(1)}$  as a function of the inverse final speed  $v_f^{-1}$ .

exceeding this threshold for the final speed, the untrapped fraction rapidly grows and reaches the maximal possible value of one. In the presence of the second well ( $V'_0 = V_0$ ),  $M_U(t_f)$  exhibits peaks in the parameter regime  $v_f^{-1} v_G \gtrsim 0.39$  that are not present for  $V'_0 = 0$ . Figure 9(j) shows the difference  $\Delta M_U(t_f)$  between the simulations with  $V'_0 = V_0$  and  $V'_0 = 0$ . This removes all contributions to the untrapping process that exclusively stem from the acceleration and not from the influence of the second well. We are able to identify three distinct peaks at  $0.257v_G^{-1}$ ,  $0.498v_G^{-1}$ , and  $0.751v_G^{-1}$  where the emission of particles is resonantly enhanced. The difference  $\Delta M_U(t_f)$  as a function of  $v_f^{-1}$  is reminiscent of an ionization spectrum.

#### E. Interparticle correlations and entanglement

We now analyze the emergence of correlations and entanglement during the collision dynamics by employing the von Neumann entropy [68], which reads

$$S^{(1)}(t) = -\text{Tr}\{\hat{\rho}^{(1)}(t) \ln[\hat{\rho}^{(1)}(t)]\} = -\sum_{i=1}^M \lambda_i(t) \ln[\lambda_i(t)]. \quad (13)$$

Here  $\hat{\rho}^{(1)}(t)$  refers to the one-body density matrix [66] with eigenvalues  $\lambda_i(t)$ . It should be noted that the natural populations  $\lambda_i(t)$  possess the property  $0 \leq \lambda_i(t) \leq 1$  and fulfill the relation  $\sum_{i=1}^M \lambda_i(t) = 1$ .

A value of  $S^{(1)}(t) = 0$  indicates a mean-field state and implies the absence of any correlations between the two particles. In the same light, a finite value of  $S^{(1)}(t) \neq 0$  corresponds to interparticle correlations and hence a deviation from the mean-field product state. For a maximally entangled state within our simulations using six SPFs, the von Neumann entropy reaches the maximal value of

$$S_{\max}^{(1)} = \ln(M) = \ln(6) \approx 1.79, \quad (14)$$

which is here solely determined by the dimensionality of the one-body Hilbert space  $M = 6$ .

Figure 10 shows the entropy of the final state as a function of the final inverse speed normalized to the maximal possible value. We observe a structure of equidistant peaks of varying height indicating large values of  $S^{(1)}(t_f)$ . The spacing is approximately equal to the period  $\Delta v^{-1} = 0.47v_G^{-1}$  obtained during the c.m. analysis, suggesting a relation to the final location of the particles. This hypothesis can be easily confirmed by analyzing the one-body density and the c.m. observable,

which show that the maxima of the von Neumann entropy correspond to situations where the particles are distributed uniformly over both wells in the final state. Furthermore, we notice that the entropy reaches its largest value of  $S^{(1)}(t_f) \approx 0.715S_{\max}$  for  $v_f^{-1}v_G \approx 1.21$ , indicating a highly entangled state for which the two largest natural populations are almost equal [ $\lambda_1(t_f) \approx 0.517$  and  $\lambda_2(t_f) \approx 0.479$ ]. The minima between the peaks correspond to values of  $v_f^{-1}$  where the particles are localized in one of the wells, i.e., extrema of the c.m. position. Here the first natural population is dominant  $\lambda_1(t_f) \approx 1$ . We notice that the height of the local maxima decreases towards faster collisions and the entropy drops to zero, indicating a mean-field product state. The reason for this behavior is that for  $v_f^{-1} \rightarrow 0$  the first natural population becomes dominant  $\lambda_1 \approx 1$ . When considering slow collisions ( $v_f^{-1}v_G \gtrsim 2$ ), the peak structure of  $S^{(1)}(t_f)$  vanishes but the entropy does not drop to zero. This indicates that still measurable correlations between the two particles exist.

#### IV. CONCLUSION AND OUTLOOK

We have investigated the collisional nonequilibrium quantum dynamics of ultracold bosons confined in two colliding potential wells. We were able to subdivide the dynamics into three distinct stages by identifying the underlying physical processes. Initially, the particles follow the trajectories of the wells closely. When the well separation falls below a certain threshold, a periodic collective particle transport takes place in an effective time-dependent double-well structure. By analyzing the population of single-particle function (SPF) states we were able to classify this transport as an over-barrier process. Using the c.m. position of particles, we have been able to quantify the number of oscillatory transitions that occur during the dynamics. During the separation of the wells in the third part of the time evolution, we noticed a mode motion of the particles within each well. The amplitude of this motion depends on the location of the particles with respect to the well centers at the end of the collision process. We determined a phase of  $\frac{\pi}{2}$  between the dipole modes of both wells while the frequency of this motion is independent of the acceleration. Furthermore, we observed that for certain final speeds the particles are strongly localized in one of the wells while they are generally delocalized. This phenomenon resembles the charge transfer that takes place during atom-atom collisions. Another important feature of our time-dependent setup is the untrapping of particles which we characterized in detail using a SPF, number state, and energetic analysis. We have been able to quantify the untrapped fraction unraveling two different contributions to it. During fast collisions, the kinetic energy grows continuously, which leads to a positive total energy and consequently to a particle untrapping. However, we also observed a resonant untrapping effect for certain kinematic parameters leading to a rapid emission of particles as the wells separate. We have been able to determine the dependence of this second mechanism on the kinematic parameters, which is reminiscent of an ionization spectrum.

Our findings serve as a promising starting point for further studies in different directions. By increasing the interparticle interaction strength one could enhance the amount of correlation that arises during the dynamics and it would be interesting

to explore the corresponding impact on the resonant particle untrapping. A variation of the potential wells, for example, by decreasing the depth or introducing an asymmetry between the two Gaussians could modify the particle transport. In this context, a more detailed study of the correlation and the creation of entanglement, incorporating the spatial and momentum space resolution of correlation functions, might be instructive [69,70]. In the light of atom-atom collisions, a particularly intriguing prospect is to employ different initial states. Employing an initial state that incorporates particles in both wells could lead to an enhancement of the emission due to opposite momenta of the bosons. Furthermore, it would be interesting to investigate the impact of the trajectories of the wells. Finally, the multiconfiguration time-dependent Hartree method for fermions [71,72] allows one to study the nonequilibrium dynamics of fermions in a similar setup. It would be instructive to analyze the role of the particle statistics and how the phenomena described in this work might be modified.

Another exciting route would be the investigation of mixtures of different components, which is of particular interest for ultracold-atom research. Such ensembles can be composed of different elements [73,74], isotopes [75], or hyperfine states [76] and exhibit a plethora of exciting and unique properties such as relative phase evolution [77], composite fermionization [78], nonlinear [79], and collective excitations [80] as well as miscible-immiscible phase transitions [81,82]. Depending on the particle statistics, this allows for the realization of Bose-Bose [83,84], Fermi-Fermi [85,86], and Bose-Fermi mixtures [87–90]. The multilayer multiconfiguration time-dependent Hartree method for mixtures [56] is a powerful numerical approach to treat the correlated nonequilibrium dynamics of such systems which allows one to extend the setup presented in the present work to such mixtures. The role of the interspecies interaction as well as a possible mass imbalance between the constituents are particularly of interest.

#### ACKNOWLEDGMENTS

The authors acknowledge fruitful discussions with K. Keiler. This work was funded by the Deutsche Forschungsgemeinschaft (German Research Foundation) SFB 925 Project No. 170620586.

#### APPENDIX: TECHNICAL ASPECTS AND CONVERGENCE

In the present work we employ the fast Fourier transform (FFT) [91–93] to obtain a spatially discretized representation of the operators and the SPFs. This scheme allows the efficient numerical treatment of large grids consisting of  $n \gtrsim 100$  grid points compared to other approaches relying on discrete variable representations (DVRs) [93]. We use  $n = 675$  grid points that are equally spaced in the interval  $(-7l_G, 7l_G]$ . It should be noted that the FFT scheme implies periodic boundary conditions for the physical system. We repeat the same set of simulations presented in the main text using a sine DVR [93] which incorporates hard-wall boundary conditions. Thereby we are able to confirm that spacing between the potential wells and the edges of the grid is large enough such that no influence of the boundary conditions is visible in the observables discussed in the present work.

The underlying time-dependent variational principle used to derive the MCTDHB equations of motion guarantees that the SPF basis is rotated such that the many-body wave function optimally captures the state of the physical system. However, care has to be taken in order to ensure that the number  $M$  of SPFs is sufficiently large and thereby the numerical convergence of the method is guaranteed [55,93]. We compare the results presented in the main text with simulations that include an additional, seventh SPF and observe that the observables discussed in the main text do not change significantly. The ground state energy exhibits a relative change of the order of  $10^{-5}$  and the energy of the final state of  $10^{-4}$  in the worst case. We observe that the untrapped fraction of the final state  $\Delta M_U(t_f)$  determined changes at most by an absolute value of  $4 \times 10^{-4}$  when including the additional orbital. The

absolute change in the relative entropy  $\frac{S^{(1)}}{S_{\max}^{(1)}}$  of the final state is limited by 0.03. The center-of-mass position of the particles at the end of the time evolution changes at most by 1%.

Additionally, the spectral representation of the one-body density matrix is important to judge the convergence of the approach. The eigenvalues of  $\rho^{(1)}(t)$ , the so-called natural populations, should exhibit a rapidly decreasing hierarchy. This indicates that any natural orbitals (eigenstates of the one-body density matrix) that are neglected due to the truncation of the single-particle Hilbert space play a negligible role. We find that this is the case for all parameters considered in the present work and that the least occupied orbital taken into account shows a population of  $\lambda_6 < 10^{-4}$  for all simulations. Therefore, we consider  $M = 6$  SPFs sufficient to describe the time evolution of the physical system accurately.

- [1] K. B. Davis, M. O. Mewes, M. R. Andrews, N. J. van Druten, D. S. Durfee, D. M. Kurn, and W. Ketterle, *Phys. Rev. Lett.* **75**, 3969 (1995).
- [2] C. C. Bradley, C. A. Sackett, J. J. Tollett, and R. G. Hulet, *Phys. Rev. Lett.* **75**, 1687 (1995).
- [3] M. H. Anderson, J. R. Ensher, M. R. Matthews, C. E. Wieman, and E. A. Cornell, *Science* **269**, 198 (1995).
- [4] I. Bloch, J. Dalibard, and W. Zwerger, *Rev. Mod. Phys.* **80**, 885 (2008).
- [5] A. Polkovnikov, K. Sengupta, A. Silva, and M. Vengalattore, *Rev. Mod. Phys.* **83**, 863 (2011).
- [6] I. Bloch, J. Dalibard, and S. Nascimbène, *Nat. Phys.* **8**, 267 (2012).
- [7] F. Serwane, G. Zürn, T. Lompe, T. B. Ottenstein, A. N. Wenz, and S. Jochim, *Science* **332**, 336 (2011).
- [8] A. M. Kaufman, B. J. Lester, C. M. Reynolds, M. L. Wall, M. Foss-Feig, K. R. A. Hazzard, A. M. Rey, and C. A. Regal, *Science* **345**, 306 (2014).
- [9] K. Henderson, C. Ryu, C. MacCormick, and M. G. Boshier, *New J. Phys.* **11**, 043030 (2009).
- [10] D. Jaksch, C. Bruder, J. I. Cirac, C. W. Gardiner, and P. Zoller, *Phys. Rev. Lett.* **81**, 3108 (1998).
- [11] I. Bloch, *Nat. Phys.* **1**, 23 (2005).
- [12] S. Chu, J. E. Bjorkholm, A. Ashkin, J. P. Gordon, and L. W. Hollberg, *Opt. Lett.* **11**, 73 (1986).
- [13] O. Morizot, Y. Colombe, V. Lorent, H. Perrin, and B. M. Garraway, *Phys. Rev. A* **74**, 023617 (2006).
- [14] M. Greiner, O. Mandel, T. Esslinger, T. W. Hänsch, and I. Bloch, *Nature (London)* **415**, 39 (2002).
- [15] L.-M. Duan, E. Demler, and M. D. Lukin, *Phys. Rev. Lett.* **91**, 090402 (2003).
- [16] O. Zobay and B. M. Garraway, *Phys. Rev. Lett.* **86**, 1195 (2001).
- [17] Y. Colombe, E. Knyazchyan, O. Morizot, B. Mercier, V. Lorent, and H. Perrin, *Europhys. Lett.* **67**, 593 (2004).
- [18] C. Orzel, A. K. Tuchman, M. L. Fenselau, M. Yasuda, and M. A. Kasevich, *Science* **291**, 2386 (2001).
- [19] B. Paredes, A. Widera, V. Murg, O. Mandel, S. Fölling, I. Cirac, G. V. Shlyapnikov, T. W. Hänsch, and I. Bloch, *Nature (London)* **429**, 277 (2004).
- [20] T. Köhler, K. Góral, and P. S. Julienne, *Rev. Mod. Phys.* **78**, 1311 (2006).
- [21] C. Chin, R. Grimm, P. Julienne, and E. Tiesinga, *Rev. Mod. Phys.* **82**, 1225 (2010).
- [22] M. Olshanii, *Phys. Rev. Lett.* **81**, 938 (1998).
- [23] J. I. Kim, V. S. Melezhik, and P. Schmelcher, *Phys. Rev. Lett.* **97**, 193203 (2006).
- [24] P. Giannakeas, F. K. Diakonou, and P. Schmelcher, *Phys. Rev. A* **86**, 042703 (2012).
- [25] P. Giannakeas, V. S. Melezhik, and P. Schmelcher, *Phys. Rev. Lett.* **111**, 183201 (2013).
- [26] B. P. Anderson and M. A. Kasevich, *Science* **282**, 1686 (1998).
- [27] G.-B. Jo, Y.-R. Lee, J.-H. Choi, C. A. Christensen, T. H. Kim, J. H. Thywissen, D. E. Pritchard, and W. Ketterle, *Science* **325**, 1521 (2009).
- [28] D.-S. Lühmann, C. Weitenberg, and K. Sengstock, *Phys. Rev. X* **5**, 031016 (2015).
- [29] S. Sala, J. Förster, and A. Saenz, *Phys. Rev. A* **95**, 011403(R) (2017).
- [30] G. Jotzu, M. Messer, R. Desbuquois, M. Lebrat, T. Uehlinger, D. Greif, and T. Esslinger, *Nature (London)* **515**, 237 (2014).
- [31] N. Goldman, J. C. Budich, and P. Zoller, *Nat. Phys.* **12**, 639 (2016).
- [32] J. Steinhauer, *Nat. Phys.* **12**, 959 (2016).
- [33] A. Ashkin, *Phys. Rev. Lett.* **24**, 156 (1970).
- [34] A. Ashkin, J. M. Dziedzic, J. E. Bjorkholm, and S. Chu, *Opt. Lett.* **11**, 288 (1986).
- [35] A. Gaëtan, Y. Miroshnychenko, T. Wilk, A. Chotia, M. Viteau, D. Comparat, P. Pillet, A. Browaeys, and P. Grangier, *Nat. Phys.* **5**, 115 (2009).
- [36] S. Saska, J. T. Wilson, B. Grinkemeyer, and J. D. Thompson, *Phys. Rev. Lett.* **122**, 143002 (2019).
- [37] A. Ashkin and J. M. Dziedzic, *Science* **235**, 1517 (1987).
- [38] K. O. Roberts, T. McKellar, J. Fekete, A. Rakonjac, A. B. Deb, and N. Kjærgaard, *Opt. Lett.* **39**, 2012 (2014).
- [39] K.-N. Schymik, V. Lienhard, D. Barredo, P. Scholl, H. Williams, A. Browaeys, and T. Lahaye, *Phys. Rev. A* **102**, 063107 (2020).
- [40] P. Scholl, M. Schuler, H. J. Williams, A. A. Eberharter, D. Barredo, K.-N. Schymik, V. Lienhard, L.-P. Henry, T. C. Lang, T. Lahaye, A. M. Läuchli, and A. Browaeys, *arXiv:2012.12268*.
- [41] M. Morgado and S. Whitlock, *arXiv:2011.03031*.



- [42] A. Rakonjac, A. B. Deb, S. Hoinka, D. Hudson, B. J. Sawyer, and N. Kjergaard, *Opt. Lett.* **37**, 1085 (2012).
- [43] N. Kjergaard, A. S. Mellish, and A. C. Wilson, *New J. Phys.* **6**, 146 (2004).
- [44] R. Thomas, M. Chilcott, C. Chisholm, A. B. Deb, M. Horvath, B. J. Sawyer, and Niels Kjergaard, *J. Phys.: Conf. Ser.* **875**, 012007 (2017).
- [45] R. Thomas, M. Chilcott, E. Tiesinga, A. B. Deb, and N. Kjergaard, *Nat. Commun.* **9**, 4895 (2018).
- [46] S. V. Rajagopal, K. M. Fujiwara, R. Senaratne, K. Singh, Z. A. Geiger, and D. M. Weld, *Ann. Phys. (Berlin)* **529**, 1700008 (2017).
- [47] R. Senaratne, S. V. Rajagopal, T. Shimasaki, P. E. Dotti, K. M. Fujiwara, K. Singh, Z. A. Geiger, and D. M. Weld, *Nat. Commun.* **9**, 2065 (2018).
- [48] Y. D. Wang, J. H. McGuire, T. J. M. Zouros, D. H. Lee, J. M. Sanders, and P. Richard, *Nucl. Instrum. Methods Phys. Res. B* **79**, 124 (1993).
- [49] E. C. Montenegro, W. E. Meyerhof, and J. H. McGuire, *Adv. At. Mol. Opt. Phys.* **34**, 249 (1994).
- [50] W. L. Fite, R. F. Stebbings, D. G. Hummer, and R. T. Brackmann, *Phys. Rev.* **119**, 663 (1960).
- [51] R. E. Olson and A. Salop, *Phys. Rev. A* **16**, 531 (1977).
- [52] I. Bloch, *Nature (London)* **453**, 1016 (2008).
- [53] D. Jaksch, H.-J. Briegel, J. I. Cirac, C. W. Gardiner, and P. Zoller, *Phys. Rev. Lett.* **82**, 1975 (1999).
- [54] T. Calarco, E. A. Hinds, D. Jaksch, J. Schmiedmayer, J. I. Cirac, and P. Zoller, *Phys. Rev. A* **61**, 022304 (2000).
- [55] O. E. Alon, A. I. Streltsov, and L. S. Cederbaum, *Phys. Rev. A* **77**, 033613 (2008).
- [56] L. Cao, V. Bolsinger, S. I. Mistakidis, G. M. Koutentakis, S. Krönke, J. M. Schurer, and P. Schmelcher, *J. Chem. Phys.* **147**, 044106 (2017).
- [57] O. E. Alon, A. I. Streltsov, and L. S. Cederbaum, *J. Chem. Phys.* **127**, 154103 (2007).
- [58] A. I. Streltsov, O. E. Alon, and L. S. Cederbaum, *Phys. Rev. Lett.* **99**, 030402 (2007).
- [59] P. Kramer and M. Saraceno, *Geometry of the Time-Dependent Variational Principle in Quantum Mechanics*, Lecture Notes in Physics (Springer, Berlin, 1981), Vol. 140.
- [60] J. Broeckhove, L. Lathouwers, E. Kesteloot, and P. Van Leuven, *Chem. Phys. Lett.* **149**, 547 (1988).
- [61] L. Pitaevskii and S. Stringari, *Bose-Einstein Condensation*, 1st ed., International Series of Monographs on Physics No. 116 (Oxford University Press, Oxford, 2003).
- [62] C. J. Pethick and H. Smith, *Bose-Einstein Condensation in Dilute Gases*, 2nd ed. (Cambridge University Press, Cambridge, 2008).
- [63] H.-D. Meyer and G. A. Worth, *Theor. Chem. Acc.* **109**, 251 (2003).
- [64] B. J. Lester, N. Luick, A. M. Kaufman, C. M. Reynolds, and C. A. Regal, *Phys. Rev. Lett.* **115**, 073003 (2015).
- [65] S. Murmann, A. Bergschneider, V. M. Klinkhamer, G. Zürn, T. Lompe, and S. Jochim, *Phys. Rev. Lett.* **114**, 080402 (2015).
- [66] K. Sakmann, A. I. Streltsov, O. E. Alon, and L. S. Cederbaum, *Phys. Rev. A* **78**, 023615 (2008).
- [67] P. A. M. Dirac, *Math. Proc. Cambridge* **26**, 376 (1930).
- [68] J. von Neumann, *Nachr. Akad. Wiss. Göttingen Math. Phys. Kl.* **1927**, 273 (1927).
- [69] A. Bergschneider, V. M. Klinkhamer, J. H. Becher, R. Klemt, L. Palm, G. Zürn, S. Jochim, and P. M. Preiss, *Nat. Phys.* **15**, 640 (2019).
- [70] J. H. Becher, E. Sindici, R. Klemt, S. Jochim, A. J. Daley, and P. M. Preiss, *Phys. Rev. Lett.* **125**, 180402 (2020).
- [71] J. Zanghellini, M. Kitzler, C. Fabian, T. Brabec, and A. Scrinzi, *Laser Phys.* **13**, 1064 (2003).
- [72] J. Caillat, J. Zanghellini, M. Kitzler, O. Koch, W. Kreuzer, and A. Scrinzi, *Phys. Rev. A* **71**, 012712 (2005).
- [73] G. Ferrari, M. Inguscio, W. Jastrzebski, G. Modugno, G. Roati, and A. Simoni, *Phys. Rev. Lett.* **89**, 053202 (2002).
- [74] D. A. Brue and J. M. Hutson, *Phys. Rev. Lett.* **108**, 043201 (2012).
- [75] N. Poli, R. E. Drullinger, G. Ferrari, J. Léonard, F. Sorrentino, and G. M. Tino, *Phys. Rev. A* **71**, 061403(R) (2005).
- [76] C. J. Myatt, E. A. Burt, R. W. Ghrist, E. A. Cornell, and C. E. Wieman, *Phys. Rev. Lett.* **78**, 586 (1997).
- [77] R. P. Anderson, C. Ticknor, A. I. Sidorov, and B. V. Hall, *Phys. Rev. A* **80**, 023603 (2009).
- [78] M. A. Garcia-March, B. Juliá-Díaz, G. E. Astrakharchik, T. Busch, J. Boronat, and A. Polls, *Phys. Rev. A* **88**, 063604 (2013).
- [79] A. M. Kamchatnov, Y. V. Kartashov, P.-É. Larré, and N. Pavloff, *Phys. Rev. A* **89**, 033618 (2014).
- [80] K. M. Mertes, J. W. Merrill, R. Carretero-González, D. J. Frantzeskakis, P. G. Kevrekidis, and D. S. Hall, *Phys. Rev. Lett.* **99**, 190402 (2007).
- [81] C. Ticknor, *Phys. Rev. A* **88**, 013623 (2013).
- [82] E. Nicklas, W. Muessel, H. Strobel, P. G. Kevrekidis, and M. K. Oberthaler, *Phys. Rev. A* **92**, 053614 (2015).
- [83] G. Modugno, M. Modugno, F. Riboli, G. Roati, and M. Inguscio, *Phys. Rev. Lett.* **89**, 190404 (2002).
- [84] J. Catani, L. De Sarlo, G. Barontini, F. Minardi, and M. Inguscio, *Phys. Rev. A* **77**, 011603(R) (2008).
- [85] E. Wille, F. M. Spiegelhalder, G. Kerner, D. Naik, A. Trenkwalder, G. Hendl, F. Schreck, R. Grimm, T. G. Tiecke, J. T. M. Walraven, S. J. J. M. F. Kokkelmans, E. Tiesinga, and P. S. Julienne, *Phys. Rev. Lett.* **100**, 053201 (2008).
- [86] C. Kohstall, M. Zaccanti, M. Jag, A. Trenkwalder, P. Massignan, G. M. Bruun, F. Schreck, and R. Grimm, *Nature (London)* **485**, 615 (2012).
- [87] F. Schreck, L. Khaykovich, K. L. Corwin, G. Ferrari, T. Bourdel, J. Cubizolles, and C. Salomon, *Phys. Rev. Lett.* **87**, 080403 (2001).
- [88] Z. Hadzibabic, C. A. Stan, K. Dieckmann, S. Gupta, M. W. Zwierlein, A. Görlitz, and W. Ketterle, *Phys. Rev. Lett.* **88**, 160401 (2002).
- [89] C. Ospelkaus, S. Ospelkaus, K. Sengstock, and K. Bongs, *Phys. Rev. Lett.* **96**, 020401 (2006).
- [90] J. Heinze, S. Götze, J. S. Krauser, B. Hundt, N. Fläschner, D.-S. Lühmann, C. Becker, and K. Sengstock, *Phys. Rev. Lett.* **107**, 135303 (2011).
- [91] D. Kosloff and R. Kosloff, *J. Comput. Phys.* **52**, 35 (1983).
- [92] R. Kosloff, *J. Phys. Chem.* **92**, 2087 (1988).
- [93] M. Beck, A. Jäckle, G. Worth, and H.-D. Meyer, *Phys. Rep.* **324**, 1 (2000).

### **4.3. Exploring Disordered Quantum Spin Models with a Multi-Layer Multi-Configurational Approach**

## Exploring disordered quantum spin models with a multilayer multiconfigurational approach

Fabian Köhler<sup>1,\*</sup>, Rick Mukherjee<sup>1,†</sup> and Peter Schmelcher<sup>1,2</sup><sup>1</sup>Center for Optical Quantum Technologies, Department of Physics,  
University of Hamburg, Luruper Chaussee 149, 22761 Hamburg, Germany<sup>2</sup>The Hamburg Centre for Ultrafast Imaging, University of Hamburg, Luruper Chaussee 149, 22761 Hamburg, Germany

(Received 21 December 2022; revised 13 March 2023; accepted 13 April 2023; published 30 May 2023)

Numerical simulations of quantum spin models are crucial for a profound understanding of many-body phenomena in a variety of research areas in physics. An outstanding problem is the availability of methods to tackle systems that violate area laws of entanglement entropy. Such scenarios cover a wide range of compelling physical situations including disordered quantum spin systems among others. In this paper, we employ a numerical technique referred to as multilayer multiconfiguration time-dependent Hartree (ML-MCTDH) to evaluate the ground state of several disordered spin models. ML-MCTDH has previously been used to study problems of high-dimensional quantum dynamics in molecular and ultracold physics but is here applied to study spin systems. We exploit the inherent flexibility of the method to present results in one and two spatial dimensions and treat challenging setups that incorporate long-range interactions as well as disorder. Our results suggest that the hierarchical multilayering inherent to ML-MCTDH allows to tackle a wide range of quantum many-body problems such as spin dynamics of varying dimensionality.

DOI: [10.1103/PhysRevResearch.5.023135](https://doi.org/10.1103/PhysRevResearch.5.023135)

## I. INTRODUCTION

A quantum many-body system satisfies the area law of entanglement if the amount of entanglement between a subsystem and the remainder of the system is proportional to the area of the boundary [1]. Systems that obey the area law typically have constraints such as locality in interaction and underlying symmetries that force their eigenstates to reside on certain submanifolds of the Hilbert space, rendering their numerical simulation efficient. Consequently, several numerical methods that rely on truncating the Hilbert space such as density matrix renormalization group method (DMRG) [2,3], time evolving block decimation (TEBD) [4–6], tensor networks [7,8], and other matrix product states (MPS) based methods have been very successful in simulating quantum matter for a variety of physics [9–13] and chemistry problems [14–20].

However, there are quantum states that exhibit scaling of entanglement proportional to the total system size, in which case the merits of MPS based methods may be questioned. As a matter of fact, quantum systems having strong violation of area law (entanglement grows linearly with the system size) are more common than previously expected [21–27]. Such scenarios are typically described by disordered Hamiltonians

rendering them nontranslationally invariant and inducing a high level of degeneracy in their low-energy spectrum. It is often the case that the experimental realization of many-body quantum systems are far from homogeneous, for example, crystals with dislocations or impurities [28–30], experiments investigating quantum Hall effect [31–33], glassy states of frustrated spin models [34–36], and Anderson localization [37–39]. For such systems, evaluating even the ground state can be challenging with existing methods.

In this paper, we propose an alternative numerical approach that can tackle the simulation of disordered spin systems. The multilayer multiconfiguration time-dependent Hartree (ML-MCTDH) method [40,41] is an extension of the MCTDH method [42–44], which was originally developed to study the multimode high-dimensional wave packet dynamics of complex molecular systems [45–47]. Later extensions allow for the treatment of bosonic [48–52] and fermionic [53–56] ensembles as well as mixtures thereof [57–59]. In an unprecedented approach, we adapt the ML-MCTDH techniques to study the ground-state properties of spin models, in particular spin glass Hamiltonians, which possess random couplings. Our results show that ML-MCTDH characterizes the ground state of disordered spin systems accurately. We demonstrate that this method can handle long-range interactions, scale to large system sizes, as well as work in both one and higher spatial dimensions. The overall flexibility of ML-MCTDH is very promising and might serve as a tool for simulating quantum many-body systems in regimes where conventional methods may falter. Specifically it comprises the perspective of simulating the nonequilibrium quantum dynamics of many-body systems.

This paper is organized as follows. We provide a brief introduction to ML-MCTDH in Sec. II A and discuss the

\*fkoehler@physnet.uni-hamburg.de

†rick.mukherjee@physnet.uni-hamburg.de

Published by the American Physical Society under the terms of the [Creative Commons Attribution 4.0 International](https://creativecommons.org/licenses/by/4.0/) license. Further distribution of this work must maintain attribution to the author(s) and the published article's title, journal citation, and DOI.

different spin models for which we evaluate the ground-state properties in Sec. II B. The two prototypical disordered spin models chosen for this paper include cases of weak and strong violation of area law of entanglement entropy. Additionally, we also include the ubiquitous transverse field Ising model with short-range and long-range interactions for comparison purposes. Our analysis comprises ground-state characteristics such as energy, correlations, and entanglement, which are benchmarked against exact diagonalization [60] and DMRG, all of which are shown in Sec. III. Section IV contains our conclusions and outlook.

## II. THEORETICAL FRAMEWORK

### A. Multilayer multiconfiguration timedependent Hartree method

To set the stage and to be self-contained, we believe it is adequate and instructive to provide a brief introduction to the ML-MCTDH method. One of the main challenges in the numerical treatment of quantum many-body systems is the exponential growth of Hilbert space dimension with system size. In this section, we describe how the ML-MCTDH is able to represent complex many-body wave functions with many degrees of freedom and thus deal with large system sizes. We start by first discussing the original MCTDH method, which already contains the fundamental working principles and extend to ML-MCTDH by adding the notion of a hierarchy of multiple layers.

The traditional and most straightforward approach to wave packet dynamics uses an ansatz given by a linear superposition  $|\Psi(t)\rangle = \sum_J A_J(t) |\Phi_J\rangle$  of time-independent  $|\Phi_J\rangle$  configurations with time-dependent coefficients  $A_J(t)$ . Without loss of generality, we assume a physical scenario with  $N$  degrees of freedom  $x_\kappa$  with  $\kappa = 1, \dots, N$ . Depending on the system under consideration, the degrees of freedom could, for example, be spatial degrees of freedom of particles or bosonic/fermionic occupation numbers. A set of  $n_\kappa$  time-independent (primitive) basis functions  $|\chi_{j_\kappa}^{(\kappa)}(x_\kappa)\rangle$  with  $j_\kappa = 1, \dots, n_\kappa$  is employed for each degree of freedom. The  $|\chi_{j_\kappa}^{(\kappa)}(x_\kappa)\rangle$  are naturally chosen to form an orthonormal basis for each degree of freedom. The configurations  $|\Phi_J\rangle$  are product states with respect to combinations of the primitive basis functions where the multi-index  $J = (j_1, j_2, \dots, j_N)$  runs through all possible combinations such that the full wave function ansatz is given by

$$|\Psi(t)\rangle = \sum_{j_1=1}^{n_1} \cdots \sum_{j_N=1}^{n_N} A_{j_1 \dots j_N}(t) \bigotimes_{\kappa=1}^N |\chi_{j_\kappa}^{(\kappa)}(x_\kappa)\rangle. \quad (1)$$

The time evolution of the many-body wave function  $|\Psi(t)\rangle$  is governed by the Dirac-Frenkel variational principle [61,62],

$$\langle \delta \Psi(t) | (i \partial_t - \hat{H}) | \Psi(t) \rangle = 0. \quad (2)$$

By inserting the wave function ansatz (1) in Eq. (2), one obtains the equation of motion for the expansion coefficients  $A_J(t)$ ,

$$i \dot{A}_J(t) = \sum_L \langle \Phi_J | \hat{H} | \Phi_L \rangle A_L(t), \quad (3)$$

which can be solved numerically using standard time integration methods.

In this traditional wave packet ansatz, the number of configurations and corresponding coefficients  $\prod_{\kappa=1}^N n_\kappa$ , scales exponentially with  $N$ , limiting the applicability of this approach to systems with only few degrees of freedom. In many physical scenarios, it is often the case that using a small set of *time-dependent* basis functions can provide an accurate representation of the many-body wave function thereby allowing to simulate larger systems. Thus, in MCTDH, Eq. (1) is replaced with time-dependent configurations,

$$|\Psi(t)\rangle = \sum_{j_1=1}^{m^{(1;1)}} \cdots \sum_{j_N=1}^{m^{(1;N)}} A_{j_1 \dots j_N}^{(1)}(t) \bigotimes_{\kappa=1}^N |\varphi_{j_\kappa}^{(1;\kappa)}(x_\kappa, t)\rangle, \quad (4)$$

where  $|\varphi_{j_\kappa}^{(1;\kappa)}(x_\kappa, t)\rangle$  denotes the  $j_\kappa$ th time-dependent basis function for the  $\kappa$ th degree of freedom and are referred to as single particle functions (SPFs). The numbers  $m^{(1;\kappa)}$  specify the number of SPFs used for the  $\kappa$ th degree of freedom. The superscript (1) or (1;  $\kappa$ ) for the SPFs, coefficients and SPF numbers indicate that these objects are part of the same, first layer of the wave function ansatz, a notation that will become essential for the multilayer extension below. The SPFs in turn are represented with respect to the time-independent basis of the standard ansatz (1),

$$|\varphi_{j_\kappa}^{(1;\kappa)}(x_\kappa, t)\rangle = \sum_{\ell=1}^{n_\kappa} c_{j_\kappa; \ell}^{(\kappa)}(t) |\chi_\ell^{(\kappa)}(x_\kappa)\rangle. \quad (5)$$

The MCTDH wave function ansatz can be understood as a three-layer approach [see Fig. 1(a)]. The top layer corresponds to the total many-body wave function expanded with respect to the SPFs using time-dependent coefficients. The middle layer refers to the time-dependent SPFs expanded with respect to the time-independent primitive basis functions while the lowest layer contains the primitive basis functions themselves. The time-dependent variational principle (2) yields equations of motion for both the coefficients  $A_{j_1 \dots j_N}^{(1)}(t)$  and the SPFs  $|\varphi_{j_\kappa}^{(1;\kappa)}(x_\kappa, t)\rangle$ , which we omit here for brevity but more details can be found in Ref. [44]. In order to ensure convergence, a sufficient number of SPFs has to be employed such that they span a Hilbert space of adequate size in order to capture the underlying physics correctly. As a matter of fact, it is often the case that the MCTDH wave function ansatz (4) contains a much smaller number of configurations compared to the wave packet ansatz (1), i.e.,  $\prod_{\kappa=1}^N m_\kappa \ll \prod_{\kappa=1}^N n_\kappa$ , leading to a significant reduction of the computational effort. MCTDH was successfully used to study molecular problems with 12–14 degrees of freedom [45–47] and later extended to 15–24 degrees of freedom [63–66] and even 100 degrees of freedom for system-bath problems [67–69] using mode combination [70,71]. However, capturing beyond-mean-field effects requires at least two SPFs for each degree of freedom such that the total number of configurations is at least  $2^N$ , highlighting the exponential scaling with respect to the system size.

In order to treat much larger systems, the ML-MCTDH approach was introduced, which has been highly successful in the treatment of systems with hundreds or even

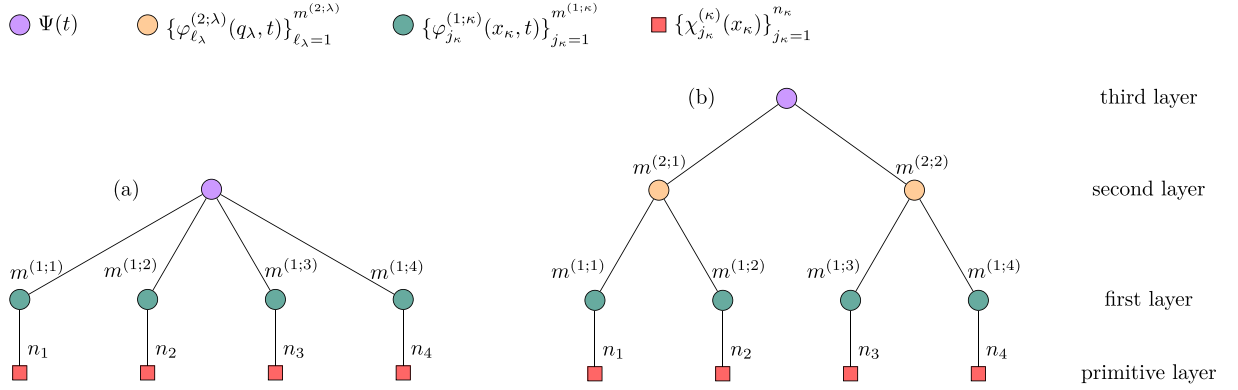


FIG. 1. Diagrammatic representation of a three-layer MCTDH (a) and a four-layer ML-MCTDH (b) ansatz for the many-body wave function  $\Psi(t)$  of a system with  $N = 4$  physical degrees of freedom.

thousands of degrees of freedom [40,72–74] including the study of vibrational as well as electronic dynamical processes in molecules [75,76] or linear rotor chains [77]. The central idea of ML-MCTDH is to group the  $N$  physical degrees of freedom  $x_1, \dots, x_N$  into  $d$  logical coordinates as shown below,

$$\begin{aligned} q_1 &= \{x_1, x_2, \dots, x_{s_1}\} \\ q_2 &= \{x_{s_1+1}, x_{s_1+2}, \dots, x_{s_1+s_2}\} \\ &\vdots \\ q_d &= \{x_{s_1+\dots+s_{d-1}+1}, \dots, x_N\}. \end{aligned} \quad (6)$$

For each logical coordinate  $q_\lambda$  a new set of time-dependent SPFs  $\{|\varphi_{\ell_\lambda}^{(2;\lambda)}(q_\lambda, t)\rangle\}_{\ell_\lambda=1}^{m^{(2;\lambda)}}$  is introduced. In ML-MCTDH, the many-body wave function ansatz Eq. (4) is replaced by expanding it with respect to these new, second layer SPFs

$$|\Psi(t)\rangle = \sum_{\ell_1=1}^{m^{(2;1)}} \cdots \sum_{\ell_d=1}^{m^{(2;d)}} A_{\ell_1, \dots, \ell_d}^{(2)}(t) \bigotimes_{\lambda=1}^d |\varphi_{\ell_\lambda}^{(2;\lambda)}(q_\lambda, t)\rangle. \quad (7)$$

The newly introduced functions  $|\varphi_{\ell_\lambda}^{(2;\lambda)}(q_\lambda, t)\rangle$  are represented with respect to a subset of the original MCTDH SPFs given by Eq. (5) that are associated with the logical coordinate  $q_\lambda$ , i.e.,

$$|\varphi_{\ell_\lambda}^{(2;\lambda)}(q_\lambda, t)\rangle = \sum_{j_\alpha=1}^{m^{(1;\alpha)}} \cdots \sum_{j_\beta=1}^{m^{(1;\beta)}} \left[ A_{\ell_\lambda; j_\alpha, \dots, j_\beta}^{(1;\lambda)}(t) \cdot \bigotimes_{\kappa=\alpha}^{\beta} |\varphi_{j_\kappa}^{(1;\kappa)}(x_\kappa, t)\rangle \right]. \quad (8)$$

Here,  $\alpha = \alpha(\lambda) = 1 + \sum_{i=1}^{\lambda-1} s_i$  and  $\beta = \beta(\lambda) = \sum_{i=1}^{\lambda} s_i$  correspond to the index of the first and last physical coordinate associated with the logical coordinate  $q_\lambda$  respectively. The newly introduced SPFs  $|\varphi_{\ell_\lambda}^{(2;\lambda)}(q_\lambda, t)\rangle$  can be interpreted as a multidimensional wave function that follows an MCTDH ansatz with respect to the original MCTDH SPFs (5). With this interpretation, ML-MCTDH can be viewed as adding another layer to the original MCTDH scheme ending up in a four-layer ansatz for the many-body wave function, which is schematically depicted in Fig. 1(b). In general, more middle layers can be added where each layer introduces a new set

of SPFs that are constructed using an MCTDH ansatz with respect to the layer below in a recursive manner. This allows the tree structure to be adapted and tailored specifically for the physical problem under consideration. It should be noted that the SPFs across all layers are chosen to form orthonormal basis sets and remain orthonormal throughout the time evolution. In summary, ML-MCTDH offers great flexibility regarding the degrees of freedom due to the choice of an appropriate primitive basis according to the physical problem under consideration. When treating the dynamics of particles for example, FFT-based [78,79] schemes or discrete variable representations [80–82] are commonly used to provide a primitive basis for the spatial degrees of freedom. By using fermionic [56] or bosonic [50–52] occupation numbers the treatment of indistinguishable particles is possible as well.

In the present paper, we investigate spin-1/2 systems and consequently employ a two-dimensional primitive basis containing the spin-up and spin-down state for each degree of freedom, i.e.,  $|\chi_1^{(\kappa)}\rangle = |\uparrow\rangle$  and  $|\chi_2^{(\kappa)}\rangle = |\downarrow\rangle$  for all  $\kappa = 1, \dots, N$ . While in general MCTDH and ML-MCTDH are tools to study the dynamics of many-body quantum systems, they also provide access to eigenstates of the underlying Hamiltonian by switching from real to imaginary time propagation. More details can be found in Appendix A.

## B. Spin Models

Three different quantum spin models are investigated in order to study the performance of the ML-MCTDH method. As a starting point and for comparison purposes, it is useful to consider the transverse field Ising model (TFIM) [83,84] as it is one of the most fundamental and well studied models and has been realized in a variety of physical setups including trapped ions [85–88], Rydberg atoms [89–92], and single crystals [93]. The Hamiltonian of the TFIM in 1D is given by

$$H_{\text{TFIM}} = - \sum_{i,j=1}^L J_{ij} \sigma_i^z \sigma_j^z - h_x \sum_{i=1}^L \sigma_i^x - h_z \sum_{i=1}^L \sigma_i^z \quad (9)$$

where  $J_{ij}$  specifies the interaction strength between the  $i$ th and  $j$ th spin while  $h_x$  ( $h_z$ ) determines the strength of a transverse (longitudinal) magnetic field. We consider both

nearest-neighbor interactions (SR-TFIM), i.e.,  $J_{ij} = J\delta_{i+1,j}$ , and long-range interactions that decay as a power law of the distance between the spins, i.e.,  $J_{ij} = J|i-j|^{-\alpha}$  (LR-TFIM). The parameter  $J$  determines the energy scale of the system and the exponent  $\alpha$  controls the range of the interactions. We choose  $J > 0$  such that ferromagnetic order, i.e., the alignment of neighboring spins in the  $z$  direction, is energetically favorable. For the long-range interactions, we choose  $\alpha = 3$ , which is accessible by trapped ions as well as Rydberg atoms.

For the remaining two models in the present paper (see below) we choose disordered systems that violate the area law of entanglement entropy. Numerical methods like DMRG, which are based on matrix product states rely on the area law and may fall short while treating such models. While it has been shown that a homogeneous, gapped 1D spin systems with local interactions like the SR-TFIM obey the area law [1,94], understanding the impact of disorder on the entanglement properties of ground states remains an open and challenging question. It is known that in such nontranslationally invariant scenarios, weak (logarithmic scaling with the system size) [94–96] or even stronger [21–27] violations of the area law can occur. Our first disordered model is a XY spin glass (XYSG) [97–99] given by the Hamiltonian

$$H_{\text{XYSG}} = \sum_{\substack{i,j=1 \\ i < j}}^L \frac{J_{ij}}{|i-j|^\alpha} (\sigma_i^+ \sigma_j^- + \sigma_j^+ \sigma_i^-) \quad (10)$$

with the spin flip operators  $\sigma^\pm = \sigma^x \pm i\sigma^y$ . We choose  $\alpha = 3$  and  $J_{ij}$  from a uniform distribution in  $[-1, 1]$ . This spin glass model exhibits weak violation of the area law [26,27]. The second disordered spin model we analyze is motivated by the strong disorder renormalization group (SDRG) framework [21,100–103] whose ground state is known to exhibit strong area-law violation. The relevant Hamiltonian is

$$H_{\text{SDRG}} = \frac{1}{2} \sum_{i=1}^{L-1} J_i (\sigma_i^x \sigma_{i+1}^x + \sigma_i^y \sigma_{i+1}^y), \quad (11)$$

where the spin couplings are fine-tuned to be  $J_i = J_0 f(|L/2 - i|)$  with  $f(n) = e^{-2n^2}$  [21]. In general, a 1D spin chain with nearest-neighbor interactions like the SR-TFIM (9) can be solved exactly by mapping it to the free fermionic chain via the Jordan-Wigner transformation. Models that incorporate disorder or long-range interactions like Eqs. (10) and (11) cannot be treated this way rendering the development of powerful numerical tools like ML-MCTDH crucial.

*A priori*, it is not clear which tree structure is best suited to treat a given many-body problem with the ML-MCTDH method. In particular, different topologies can lead to vastly different simulation runtimes but yield comparable results as long as proper convergence with respect to the number of SPFs on each layer is ensured. Finding a good tree structure is an iterative process that is guided by monitoring the occupation of the SPFs as well as the physical observables under consideration. As a starting point, it is usually beneficial to couple degrees of freedom at the lowest layers of the tree that are strongly interacting in the underlying Hamiltonian. The goal is to exploit the multilayering aspect of the method as much as possible in order to obtain a very compact representation of the many-body wave function and

thus reduce the computational cost. In Fig. 2 we show the various tree diagrams that are used in the present paper. For the SR-TFIM we employ a binary tree with  $\log_2(L) + 1$  layers, see panel (a). This choice is natural as it couples the neighboring spins on the lowest layers. Since this cannot be achieved for all couplings at the same time, some of these interactions are mediated through the upper layers. The same binary tree topology works for the LR-TFIM as well since the interaction between neighboring spins is still the strongest. However, due to the long-range character of the interactions, more SPFs have to be used on the upper layers in order to capture long-range effects. A binary tree structure also works well for describing the XYSG model where the design of a more optimized tree structure is prohibitive due to the random nature of the couplings. When treating two-dimensional systems more complex tree structures are required [see panel (b)]. In the present example of a  $9 \times 9$  square lattice, we alternate between combining triplets of logical coordinates along the  $x$  and  $y$  direction. We can treat the SDRG model accurately with the tree depicted in panel (c), which is a simple MCTDH ansatz with mode combination that does not rely on any multilayering. This approach combines the strongly interacting central spins into one logical coordinate, which is then coupled to logical coordinates combining the outer spins.

### III. RESULTS AND DISCUSSION

We benchmark the performance of the ML-MCTDH method against exact diagonalization (ED) and DMRG by characterizing the ground state of different spin models using its energy  $E_0$ , correlation functions  $C_{\beta\beta}(i, j)$ , and entanglement entropy  $S_{\text{vN}}$ . The exact diagonalization implementation uses the QuSpin package [104] in conjunction with some routines provided by quimb [105]. The DMRG code is based on the ITensor library [106].

Figure 3(a) shows the ground-state energy per spin for the SR-TFIM as a function of system size  $L$  for a fixed transverse field of  $h_x = J$  for which there is excellent agreement between all three methods. Naturally ED is limited to a few spins, while DMRG and ML-MCTDH can treat much longer chains, exhibiting great scalability with respect to the system size. However, calculating ground states for large systems can be computationally time consuming. In order to accelerate the convergence to the ground state for these large systems, we impose a small longitudinal magnetic field  $h_z = 0.01J$ , which lifts the twofold degeneracy of the ground state. It should be noted that our approach works as well in the absence of a longitudinal field. Figures 3(b) and 3(c) illustrate the convergence of the ground-state energy  $E_{0,\text{M}}$  obtained by ML-MCTDH and DMRG with respect to the ground-state energy  $E_{0,\text{ED}}$  computed with ED. This is quantified by calculating the relative error  $\Delta E = |E_{0,\text{M}}/E_{0,\text{ED}} - 1|$  as a function of time steps for ML-MCTDH in (b) and number of sweeps for DMRG in (c). When compared to ED, both methods achieve excellent accuracy for the SR- and LR-TFIM, but for the disordered XYSG and SDRG systems, it is clear that ML-MCTDH manages to obtain a much higher precision than DMRG.

Figure 3(c) also illustrates that the DMRG ground-state energy converges rapidly and reaches its final value already after

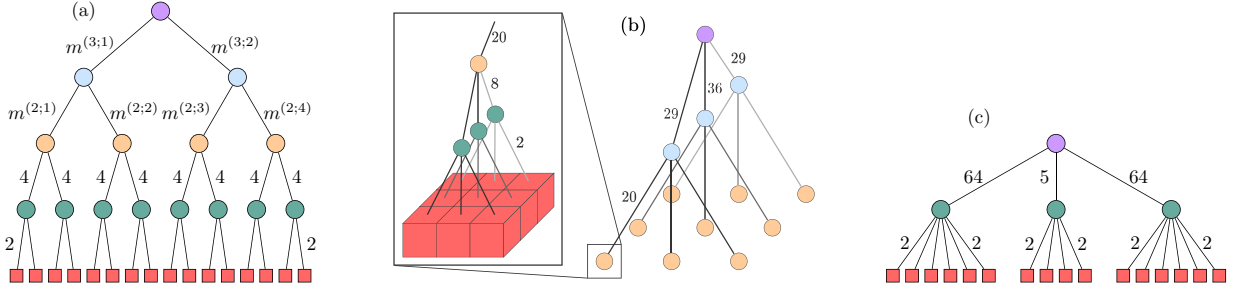


FIG. 2. (a) Tree structure used for the SR-TFIM ( $m^{(3;i)} = 6$  and  $m^{(2;i)} = 12$ ), LR-TFIM ( $m^{(2;i)} = m^{(3;i)} = 16$ ), as well as XY-SG ( $m^{(2;i)} = 16$  and  $m^{(3;i)} = 32$ ) of  $L = 16$  spins in 1D. (b) Tree structure used for the SR-TFIM extended to 2D on a square lattice of  $9 \times 9$  spins. (c) Tree structure used for the SDRG model of  $L = 16$  spins in 1D.

2–4 sweeps. We employ a protocol consisting of nine sweeps and allow the bond dimension of the matrix product states to dynamically grow up to 1000. More details on this scheme can be found in Appendix B. A maximal bond dimension of 14 for the SR-TFIM and 57 for the LR-TFIM of  $L = 16$  spins is sufficient for an accurate description of the ground state across the whole range of transversal fields. The XYSG demands a higher maximal bond dimension of 129 due to its disordered character. The SDRG model requires a surprisingly low final maximal bond dimension of 8. By forcing the DMRG algorithm to use a minimal bond dimension of at least 100 and checking all observables under consideration, we ensured that

our results for the SDRG model are indeed converged and an increase in bond dimension does not improve the results. One of the challenges when studying quantum many-body problems is the ability to capture nontrivial correlations. Here, we use the connected correlation function [107,108], which is defined as

$$C_{\beta\beta}(i, j) = \langle \sigma_i^\beta \sigma_j^\beta \rangle - \langle \sigma_i^\beta \rangle \langle \sigma_j^\beta \rangle, \quad \beta \in \{x, y, z\}, \quad (12)$$

to measure correlations in the system and characterize the magnetic ordering between spins  $i$  and  $j$ . Figure 4 shows results for correlation functions defined in Eq. (12) for different spin models. For the SR-TFIM in 1D and its 2D extension as well as the LR-TFIM we observe excellent agreement between all three methods as seen in panels (a)–(d). The connected correlations in the  $x$  direction denoted by  $C_{xx}(i, j)$  were evaluated for disordered spin models by averaging over 10 disorder realizations and over all unique spin pairings with  $i < j$  corresponding to a given separation  $r = |i - j|$ . The results are shown in panels (e)–(f). In the case of XYSG, DMRG struggles to capture the correlations correctly as the low-energy spectrum exhibits many near-degeneracies, which are not well resolved by the DMRG algorithm such that it usually locks on to one of the first excited states. Although this issue in DMRG can be mitigated by rescaling the Hamiltonian such that the energy splitting is increased this is not practical for larger systems. ML-MCTDH, however, does not have any such issues. When analyzing the correlations for the SDRG model [panel (f)] with respect to one of the center spins  $c = L/2$ , the methods agree with only a minor deviation for the value of  $C(c, c + 3)$  in the case of DMRG. Due to the decay of the coupling constants towards the outer spins, the correlations will also quickly die off with increasing distance from the center spin. Except for the minor deviation in the case of DMRG, all methods agree very well with each other.

In order to determine the entanglement of the ground state, we employ the von Neumann entanglement entropy (VNNE)  $S_{\text{VN}}$  [109] of a subsystem  $A$  with the remainder of the system,

$$S_{\text{VN}} = -\text{Tr}[\rho_A \ln(\rho_A)] \quad (13)$$

where  $\rho_A$  is the reduced density matrix [61] of the subsystem  $A$ . Figure 5 shows the VNNE defined in Eq. (13) for the spin models LR-TFIM in panel (a), XYSG in panel (b), and SDRG in panel (c) as a function of subsystem size  $L_s$ . The subsystem  $A$  was here chosen to consist of the  $L_s$  left-most spins in the chain. In the case of LR-TFIM, we chose the transverse

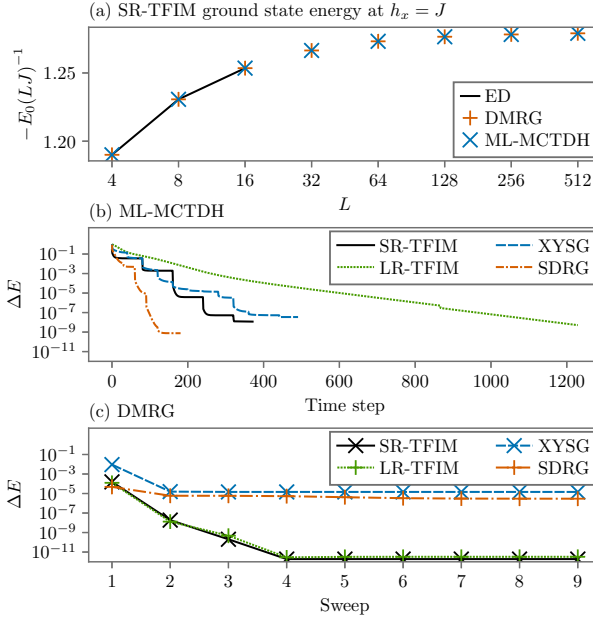


FIG. 3. (a) Ground-state energy per spin of the SR-TFIM in 1D for  $h_x = J$  and  $h_z = 0.01J$  as a function of the system size  $L$ . (b) Relative error of the ML-MCTDH ground-state energy with respect to the ED ground-state energy as a function of imaginary time step for different 1D models of  $L = 16$  spins. (c) Relative error of the DMRG ground-state energy with respect to ED ground-state energy as a function of the sweep index for different 1D models of  $L = 16$  spins.

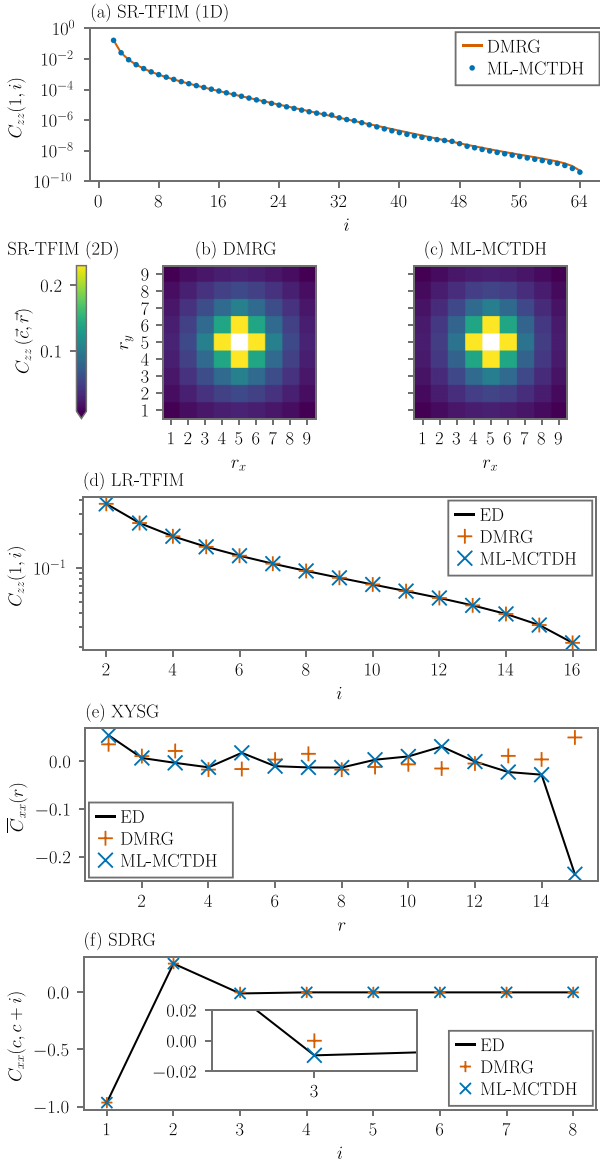


FIG. 4. Connected correlation (12) functions for different models. (a) Correlation of the first spin with the  $i$ th spin in  $z$  direction for the SR-TFIM of  $L = 128$  spins in 1D with  $h_x = 1.5J$  and  $h_z = 0.01J$ . [(b),(c)] Correlation of the central spin with the spin at position  $\vec{r}$  in  $z$  direction for the SR-TFIM extended to 2D on a  $9 \times 9$  square lattice (2D) for  $h_x = 3J$  and  $h_z = 0.01J$ . (d) Correlation in  $z$  direction of the first spin with the  $i$ th spin in the LR-TFIM for  $L = 16$  in 1D with  $h_x = J$  and  $h_z = 0$ . (e) Correlation of the first spin in the XYSG for  $L = 16$  in 1D. We average over 10 disorder realizations as well as all unique spin pairings  $C_{xx}(i, j)$  with  $i < j$  that correspond to a given separation distance  $r = |i - j|$  and show the result as a function of  $r =$ . (f) Correlation in  $x$  direction of one of the central spins  $c = L/2$  with its right-hand side neighbors for the SDRG model with  $L = 16$  in 1D.

field to be  $h_x = 0.5J$  such that the ground state is twofold degenerate due to the global spin-flip symmetry. For a finite system, the ground state is expected to be a superposition

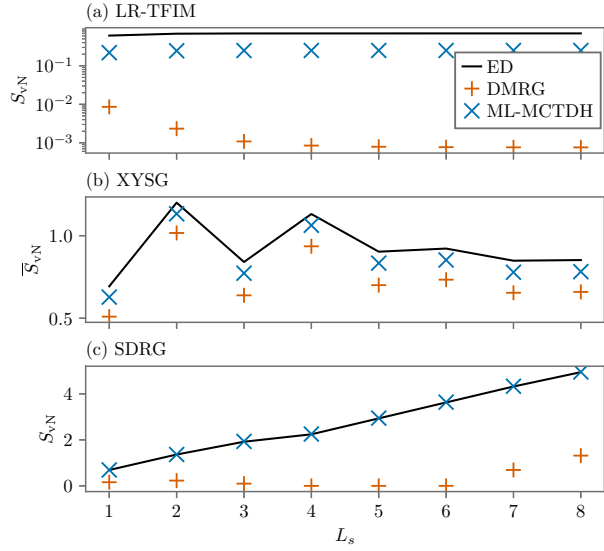


FIG. 5. VNEE (13) for the different models of  $L = 16$  spins in 1D as a function of subsystem size  $L_s$ . Panel (a) shows the result for the LR-TFIM with  $h_x = 0.5J$  and  $h_z = 0$ , Panel (b) for the XYSG, averaged over 10 disorder realizations, and panel (c) for the SDRG model.

state, which possesses non-negligible entanglement. This behavior is correctly captured by ED and ML-MCTDH while DMRG yields a much lower entanglement as it converges to one of the degenerate states. It is important to note that the exact superposition of both degenerate ground states is arbitrary in both ED and ML-MCTDH, which affects the absolute value of  $S_{vN}$  and explains the discrepancy between these two methods. The disordered XYSG model is known to have area-law violation proportional to  $S_{vN} \propto \ln L_s$  which is not visible in Fig. 5(b) due to the small system size and low number of realizations. Here, the discrepancy between the three methods can be attributed to the high amount of degeneracy in the low-energy spectrum. The different algorithms lock on to different states and thus yield different results. In the case of the SDRG model we observe a great agreement between ML-MCTDH and ED. However, DMRG cannot describe the linear growth of entanglement  $S_{vN} \propto L_s$  due to the formation of distant singlet states, which then have to be entangled.

#### IV. CONCLUSIONS AND OUTLOOK

Solving a many-body problem with large system sizes requires sophisticated numerical methods that go beyond exact diagonalization. Quantum Monte Carlo methods [110] rely on the wave function spanning fewer relevant many-body configurations. Other approaches represent the many-body wave function through an efficient compression of the state like with matrix product states, more general tensor networks or in some cases even neural networks [111–113]. Despite the unquestionable success of these methods, they can fail for various reasons like the sign problem in quantum Monte Carlo methods [110], inefficiency of current quantum state compression in high-dimensional systems or due to the area-law violation.



In this paper, we propose an alternative computational method to explore many-body quantum spin models and specifically the case of disordered systems, which are known to violate the area law in entanglement. Focusing on the ground-state properties of prototypical many-body disordered spins models, ML-MCTDH achieves a remarkable accuracy in particular compared to conventional methods. While MCTDH methods are regularly used to solve for complex wave packet dynamics problems, our paper is the first step in adapting these techniques to simulate a larger class of intricate many-body spin models. One of the key advantages of using the multilayer version of MCTDH is its ability to treat large system sizes as well as degrees of freedom with many primitive basis states. The latter aspect can be useful for simulating higher spin degrees of freedom such as  $SU(n)$  physics [114,115] or higher spatial dimensions. In future works, it will be interesting to compare the performance of ML-MCTDH with existing numerical methods applied to higher dimensional spin lattices [9,12,116]. MCTDH algorithms were originally built to study quantum dynamics. Therefore, a natural next step would be to simulate many-body spin dynamics [117] with these methods, which can be achieved very straightforwardly by switching to real time propagation. We are convinced that ML-MCTDH can be a useful tool in this field of active research that includes intriguing topics like thermalization [118,119], quench dynamics [120,121], and optimal control [122,123]. From a more technical point of view, there is also the scope for improving the scheme of building the different layers within ML-MCTDH: One can potentially optimize this process by either using machine learning methods [111–113,124–127] or spawning techniques [128–130] and even combine them with tensor network methods [131]. Thus, ML-MCTDH techniques can prove to be very a powerful alternative theoretical tool in modeling complex many-body (spin) systems.

#### ACKNOWLEDGMENTS

The authors acknowledge fruitful discussions with Henrik R. Larsson and Frank Pollmann. This work is funded by the German Federal Ministry of Education and Research within the funding program “quantum technologies - from basic research to market” under Contract No. 13N16138. This work is supported by the Deutsche Forschungsgemeinschaft (DFG, German Research Foundation), SFB-925, Project No. 170620586.

#### APPENDIX A: COMPUTATION OF EIGENSTATES

Here, we discuss how ML-MCTDH can be applied to determine the many-body ground states of spin models by switching from real time to imaginary time propagation. Solving the time-independent Schrödinger equation by diagonalization of the Hamiltonian matrix [60] is prohibitive for large systems. Instead, eigenstates can be obtained by

propagating an initial trial state according to the time-dependent Schrödinger equation in imaginary time  $\tau = it$  [132]. The evolution of the many-body wave function in the eigenbasis of the Hamiltonian reads  $|\Psi(\tau)\rangle = \sum_n A_n(0)e^{-\tau E_n} |\Psi_n\rangle$ . After a sufficiently long propagation time the ground state becomes the dominant component of the instantaneous many-body wave function as long as its initial contribution  $A_0(0)$  is not zero. This scheme is feasible in the framework in (ML)-MCTDH as well [44] and has been applied for example to compute initial states in photodissociation studies [43,133–135]. Since imaginary time propagation relies on the exponential damping of any contributions from excited states, often long propagation times are required in order to achieve adequate convergence towards the ground state. The improved relaxation algorithm [136–138] employs a hybrid scheme consisting of imaginary time propagation and diagonalization to improve the convergence speed. By applying the time-independent variational principle to the (ML)-MCTDH ansatz, one obtains an eigenvalue equation determining the top layer coefficients  $A_{\ell_1, \dots, \ell_d}^{(T)}(t)$  where  $T$  is the number of layers. The equations determining the SPFs on the lower layers could be solved iteratively, which, however, would result in highly nonlinear equations that are difficult to converge [138], similar to multiconfiguration consistent field theory [139]. Instead, the improved relaxation algorithm alternates between updating the top layer coefficients by solving the eigenvalue equation and imaginary time propagation to adapt the SPFs. By always choosing the  $n$ th eigenvector to obtain a new set of top layer coefficients, the algorithm converges towards the  $n$ th eigenstate of the Hamiltonian. Consequently, improved relaxation provides easy access to excited states, which would otherwise require to first compute and then project out lower lying states. For the diagonalization involved we employ the implicitly restarted Lanczos method [140] via ARPACK [141].

#### APPENDIX B: DMRG PROTOCOL

In the present paper, we chose a sweep protocol of nine sweeps and allow a maximum bond dimension for the matrix product state of up to 1000. We followed a typical procedure of increasing the allowed maximum bond dimension with each sweep while always ensuring enough headroom between this value and the actual maximal bond dimension of the matrix product state. For the first few sweeps we added a small noise term that improves the convergence and decrease its strength with each sweep. Another important parameter is the cutoff that determines the actual bond dimension. We followed best practice and started with a value of  $10^{-6}$  at the beginning of the sweep protocol and decreased it rapidly with each sweep. The last two sweeps were performed with a cutoff of  $10^{-14}$ , which ensures near exact accuracy. We observe that even for a long chain of length  $L = 1024$  in the SR-TFIM, the final maximal bond dimension was only 14, which is expected due to the short-range and homogeneous nature of the model.

[1] M. B. Hastings, An area law for one-dimensional quantum systems, *J. Stat. Mech.* (2007) P08024.

[2] S. R. White, Density Matrix Formulation for Quantum Renormalization Groups, *Phys. Rev. Lett.* **69**, 2863 (1992).

- [3] U. Schollwöck, The density-matrix renormalization group, *Rev. Mod. Phys.* **77**, 259 (2005).
- [4] A. J. Daley, C. Kollath, U. Schollwöck, and G. Vidal, Time-dependent density-matrix renormalization-group using adaptive effective hilbert spaces, *J. Stat. Mech.* (2004) P04005.
- [5] F. Verstraete, J. J. García-Ripoll, and J. I. Cirac, Matrix Product Density Operators: Simulation of Finite-Temperature and Dissipative Systems, *Phys. Rev. Lett.* **93**, 207204 (2004).
- [6] S. R. White and A. E. Feiguin, Real-Time Evolution Using the Density Matrix Renormalization Group, *Phys. Rev. Lett.* **93**, 076401 (2004).
- [7] F. Verstraete, V. Murg, and J. Cirac, Matrix product states, projected entangled pair states, and variational renormalization group methods for quantum spin systems, *Adv. Phys.* **57**, 143 (2008).
- [8] R. Orús, A practical introduction to tensor networks: Matrix product states and projected entangled pair states, *Ann. Phys.* **349**, 117 (2014).
- [9] S. R. White, Spin Gaps in a Frustrated Heisenberg Model for  $\text{CaV}_4\text{O}_9$ , *Phys. Rev. Lett.* **77**, 3633 (1996).
- [10] T. D. Kühner and H. Monien, Phases of the one-dimensional Bose-Hubbard model, *Phys. Rev. B* **58**, R14741(R) (1998).
- [11] M. Tezuka and M. Ueda, Density-Matrix Renormalization Group Study of Trapped Imbalanced Fermi Condensates, *Phys. Rev. Lett.* **100**, 110403 (2008).
- [12] E. Stoudenmire and S. R. White, Studying two-dimensional systems with the density matrix renormalization group, *Annu. Rev. Condens. Matter Phys.* **3**, 111 (2012).
- [13] Y.-C. He, M. P. Zaletel, M. Oshikawa, and F. Pollmann, Signatures of Dirac Cones in a DMRG Study of the Kagome Heisenberg Model, *Phys. Rev. X* **7**, 031020 (2017).
- [14] Ö. Legeza, J. Röder, and B. A. Hess, QC-DMRG study of the ionic-neutral curve crossing of  $\text{LiF}$ , *Mol. Phys.* **101**, 2019 (2003).
- [15] G. Moritz, A. Wolf, and M. Reiher, Relativistic DMRG calculations on the curve crossing of cesium hydride, *J. Chem. Phys.* **123**, 184105 (2005).
- [16] F. Liu, Y. Kurashige, T. Yanai, and K. Morokuma, Multireference ab initio density matrix renormalization group (DMRG)-CASSCF and DMRG-CASPT2 study on the photochromic ring opening of spiropyran, *J. Chem. Theory Comput.* **9**, 4462 (2013).
- [17] S. Wouters, T. Bogaerts, P. Van Der Voort, V. Van Speybroeck, and D. Van Neck, Communication: DMRG-SCF study of the singlet, triplet, and quintet states of Oxo-Mn (Salen), *J. Chem. Phys.* **140**, 241103 (2014).
- [18] S. Wouters, V. Van Speybroeck, and D. Van Neck, DMRG-CASPT2 study of the longitudinal static second hyperpolarizability of all-trans polyenes, *J. Chem. Phys.* **145**, 054120 (2016).
- [19] S. Guo, Z. Li, and G. K.-L. Chan, A perturbative density matrix renormalization group algorithm for large active spaces, *J. Chem. Theory Comput.* **14**, 4063 (2018).
- [20] A. Baiardi and M. Reiher, The density matrix renormalization group in chemistry and molecular physics: recent developments and new challenges, *J. Chem. Phys.* **152**, 040903 (2020).
- [21] G. Vitagliano, A. Riera, and J. I. Latorre, Volume-law scaling for the entanglement entropy in spin-1/2 chains, *New J. Phys.* **12**, 113049 (2010).
- [22] M. Pouranvari and K. Yang, Maximally entangled mode, metal-insulator transition, and violation of entanglement area law in noninteracting fermion ground states, *Phys. Rev. B* **89**, 115104 (2014).
- [23] N. Shiba and T. Takayanagi, Volume law for the entanglement entropy in non-local QFTs, *J. High Energy Phys.* **02** (2014) 033.
- [24] G. Gori, S. Paganelli, A. Sharma, P. Sodano, and A. Trombettoni, Explicit Hamiltonians inducing volume law for entanglement entropy in fermionic lattices, *Phys. Rev. B* **91**, 245138 (2015).
- [25] N. Roy and A. Sharma, Entanglement contour perspective for strong area-law violation in a disordered long-range hopping model, *Phys. Rev. B* **97**, 125116 (2018).
- [26] N. Roy, A. Sharma, and R. Mukherjee, Quantum simulation of long-range XY quantum spin glass with strong area-law violation using trapped ions, *Phys. Rev. A* **99**, 052342 (2019).
- [27] N. Roy, A. Sharma, and R. Mukherjee, Erratum: Quantum simulation of long-range XY quantum spin glass with strong area-law violation using trapped ions [Phys. Rev. A **99**, 052342 (2019)], *Phys. Rev. A* **100**, 059902(E) (2019).
- [28] N. Matsudaira, Ising ferromagnets with random impurities, *J. Phys. Soc. Jpn.* **35**, 1593 (1973).
- [29] M. Oshikawa and I. Affleck, Boundary conformal field theory approach to the critical two-dimensional Ising model with a defect line, *Nucl. Phys. B* **495**, 533 (1997).
- [30] H. Frahm and A. A. Zvyagin, The open spin chain with impurity: An exact solution, *J. Phys.: Condens. Matter* **9**, 9939 (1997).
- [31] D. C. Tsui, H. L. Stormer, and A. C. Gossard, Two-Dimensional Magnetotransport in the Extreme Quantum Limit, *Phys. Rev. Lett.* **48**, 1559 (1982).
- [32] R. B. Laughlin, Anomalous Quantum Hall Effect: An Incompressible Quantum Fluid with Fractionally Charged Excitations, *Phys. Rev. Lett.* **50**, 1395 (1983).
- [33] H. L. Stormer, Nobel lecture: The fractional quantum Hall effect, *Rev. Mod. Phys.* **71**, 875 (1999).
- [34] D. Sherrington and S. Kirkpatrick, Solvable Model of a Spin-Glass, *Phys. Rev. Lett.* **35**, 1792 (1975).
- [35] S. F. Edwards and P. W. Anderson, Theory of spin glasses, *J. Phys. F: Met. Phys.* **5**, 965 (1975).
- [36] K. Binder and A. P. Young, Spin glasses: Experimental facts, theoretical concepts, and open questions, *Rev. Mod. Phys.* **58**, 801 (1986).
- [37] P. W. Anderson, Absence of diffusion in certain random lattices, *Phys. Rev.* **109**, 1492 (1958).
- [38] E. Abrahams, P. W. Anderson, D. C. Licciardello, and T. V. Ramakrishnan, Scaling Theory of Localization: Absence of Quantum Diffusion in Two Dimensions, *Phys. Rev. Lett.* **42**, 673 (1979).
- [39] G. Roati, C. D'Errico, L. Fallani, M. Fattori, C. Fort, M. Zaccanti, G. Modugno, M. Modugno, and M. Inguscio, Anderson localization of a non-interacting Bose-Einstein condensate, *Nature (London)* **453**, 895 (2008).
- [40] H. Wang and M. Thoss, Multilayer formulation of the multi-configuration time-dependent Hartree theory, *J. Chem. Phys.* **119**, 1289 (2003).
- [41] U. Manthe, A multilayer multiconfigurational time-dependent

- Hartree approach for quantum dynamics on general potential energy surfaces, *J. Chem. Phys.* **128**, 164116 (2008).
- [42] H.-D. Meyer, U. Manthe, and L. Cederbaum, The multi-configurational time-dependent Hartree approach, *Chem. Phys. Lett.* **165**, 73 (1990).
- [43] U. Manthe, H.-D. Meyer, and L. S. Cederbaum, Wave-packet dynamics within the multiconfiguration Hartree framework: General aspects and application to NOCl, *J. Chem. Phys.* **97**, 3199 (1992).
- [44] M. Beck, A. Jäckle, G. Worth, and H.-D. Meyer, The multiconfiguration time-dependent Hartree (MCTDH) method: A highly efficient algorithm for propagating wavepackets, *Phys. Rep.* **324**, 1 (2000).
- [45] G. A. Worth, H.-D. Meyer, and L. S. Cederbaum, The effect of a model environment on the S2 absorption spectrum of pyrazine: A wave packet study treating all 24 vibrational modes, *J. Chem. Phys.* **105**, 4412 (1996).
- [46] F. Huarte-Larrañaga and U. Manthe, Vibrational excitation in the transition state: The  $\text{CH}_4 + \text{H} \rightarrow \text{CH}_3 + \text{H}_2$  reaction rate constant in an extended temperature interval, *J. Chem. Phys.* **116**, 2863 (2002).
- [47] T. Wu, H.-J. Werner, and U. Manthe, First-principles theory for the  $\text{H} + \text{CH}_4 \rightarrow \text{H}_2 + \text{CH}_3$  reaction, *Science* **306**, 2227 (2004).
- [48] A. I. Streltsov, O. E. Alon, and L. S. Cederbaum, Role of Excited States in the Splitting of a Trapped Interacting Bose-Einstein Condensate by a Time-Dependent Barrier, *Phys. Rev. Lett.* **99**, 030402 (2007).
- [49] O. E. Alon, A. I. Streltsov, and L. S. Cederbaum, Multi-configurational time-dependent Hartree method for bosons: Many-body dynamics of bosonic systems, *Phys. Rev. A* **77**, 033613 (2008).
- [50] H. Wang and M. Thoss, Numerically exact quantum dynamics for indistinguishable particles: The multilayer multiconfiguration time-dependent Hartree theory in second quantization representation, *J. Chem. Phys.* **131**, 024114 (2009).
- [51] U. Manthe and T. Weiße, On the multi-layer multi-configurational time-dependent Hartree approach for bosons and fermions, *J. Chem. Phys.* **146**, 064117 (2017).
- [52] T. Weiße and U. Manthe, The multi-configurational time-dependent Hartree approach in optimized second quantization: Imaginary time propagation and particle number conservation, *J. Chem. Phys.* **152**, 034101 (2020).
- [53] J. Zanghellini, M. Kitzler, C. Fabian, T. Brabec, and A. Scrinzi, An MCTDHF approach to multielectron dynamics in laser fields, *Laser Phys.* **13**, 1064 (2003).
- [54] J. Zanghellini, M. Kitzler, T. Brabec, and A. Scrinzi, Testing the multi-configuration time-dependent Hartree-Fock method, *J. Phys. B: At. Mol. Opt. Phys.* **37**, 763 (2004).
- [55] J. Caillat, J. Zanghellini, M. Kitzler, O. Koch, W. Kreuzer, and A. Scrinzi, Correlated multielectron systems in strong laser fields: A multiconfiguration time-dependent Hartree-Fock approach, *Phys. Rev. A* **71**, 012712 (2005).
- [56] S. Sasmal and O. Vendrell, Non-adiabatic quantum dynamics without potential energy surfaces based on second-quantized electrons: Application within the framework of the MCTDH method, *J. Chem. Phys.* **153**, 154110 (2020).
- [57] L. Cao, S. Krönke, O. Vendrell, and P. Schmelcher, The multi-layer multi-configuration time-dependent Hartree method for bosons: Theory, implementation, and applications, *J. Chem. Phys.* **139**, 134103 (2013).
- [58] S. Krönke, L. Cao, O. Vendrell, and P. Schmelcher, Non-equilibrium quantum dynamics of ultra-cold atomic mixtures: The multi-layer multi-configuration time-dependent Hartree method for bosons, *New J. Phys.* **15**, 063018 (2013).
- [59] L. Cao, V. Bolsinger, S. I. Mistakidis, G. M. Koutentakis, S. Krönke, J. M. Schurer, and P. Schmelcher, A unified *ab initio* approach to the correlated quantum dynamics of ultracold fermionic and bosonic mixtures, *J. Chem. Phys.* **147**, 044106 (2017).
- [60] H. Q. Lin, Exact diagonalization of quantum-spin models, *Phys. Rev. B* **42**, 6561 (1990).
- [61] P. A. M. Dirac, Note on exchange phenomena in the Thomas atom, *Math. Proc. Camb. Philos. Soc.* **26**, 376 (1930).
- [62] J. Frenkel, *Wave Mechanics - Advanced General Theory* (Oxford University Press, Oxford, 1934), Vol. 1.
- [63] A. Raab, On the Dirac-Frenkel/Mclachlan variational principle, *Chem. Phys. Lett.* **319**, 674 (2000).
- [64] C. Cattarius, G. A. Worth, H.-D. Meyer, and L. S. Cederbaum, All mode dynamics at the conical intersection of an octatomic molecule: multi-configuration time-dependent Hartree (MCTDH) investigation on the butatriene cation, *J. Chem. Phys.* **115**, 2088 (2001).
- [65] O. Vendrell, F. Gatti, D. Lauvergnat, and H.-D. Meyer, Full-dimensional (15-Dimensional) quantum-dynamical simulation of the protonated water dimer. I. Hamiltonian setup and analysis of the ground vibrational state, *J. Chem. Phys.* **127**, 184302 (2007).
- [66] O. Vendrell, F. Gatti, and H.-D. Meyer, Full dimensional (15-Dimensional) quantum-dynamical simulation of the protonated water dimer. II. Infrared spectrum and vibrational dynamics, *J. Chem. Phys.* **127**, 184303 (2007).
- [67] H. Wang, Basis set approach to the quantum dissipative dynamics: Application of the multiconfiguration time-dependent Hartree method to the spin-boson problem, *J. Chem. Phys.* **113**, 9948 (2000).
- [68] H. Wang, M. Thoss, and W. H. Miller, Systematic convergence in the dynamical hybrid approach for complex systems: A numerically exact methodology, *J. Chem. Phys.* **115**, 2979 (2001).
- [69] M. Nest and H.-D. Meyer, Dissipative quantum dynamics of anharmonic oscillators with the multiconfiguration time-dependent Hartree method, *J. Chem. Phys.* **119**, 24 (2003).
- [70] M. Ehara, H.-D. Meyer, and L. S. Cederbaum, Multiconfiguration time-dependent Hartree (MCTDH) study on rotational and diffractive inelastic molecule-surface scattering, *J. Chem. Phys.* **105**, 8865 (1996).
- [71] G. A. Worth, H.-D. Meyer, and L. S. Cederbaum, Relaxation of a system with a conical intersection coupled to a bath: A benchmark 24-dimensional wave packet study treating the environment explicitly, *J. Chem. Phys.* **109**, 3518 (1998).
- [72] H. Wang, D. E. Skinner, and M. Thoss, Calculation of reactive flux correlation functions for systems in a condensed phase environment: A multilayer multiconfiguration time-dependent Hartree approach, *J. Chem. Phys.* **125**, 174502 (2006).
- [73] H. Wang and M. Thoss, Quantum dynamical simulation of electron-transfer reactions in an anharmonic environment, *J. Phys. Chem. A* **111**, 10369 (2007).

- [74] I. Kondov, M. Čížek, C. Benesch, H. Wang, and M. Thoss, Quantum dynamics of photoinduced electron-transfer reactions in dye-semiconductor systems: First-principles description and application to coumarin 343-TiO<sub>2</sub>, *J. Phys. Chem. C* **111**, 11970 (2007).
- [75] T. Westermann, R. Brodbeck, A. B. Rozhenko, W. Schoeller, and U. Manthe, Photodissociation of methyl iodide embedded in a host-guest complex: A full dimensional (189D) quantum dynamics study of CH<sub>3</sub>I@resorc[4]arene, *J. Chem. Phys.* **135**, 184102 (2011).
- [76] J. Schulze and O. Kühn, Explicit correlated exciton-vibrational dynamics of the FMO complex, *J. Phys. Chem. B* **119**, 6211 (2015).
- [77] S. Mainali, F. Gatti, D. Iouchchenko, P.-N. Roy, and H.-D. Meyer, Comparison of the multi-layer multi-configuration time-dependent Hartree (ML-MCTDH) method and the density matrix renormalization group (DMRG) for ground state properties of linear rotor chains, *J. Chem. Phys.* **154**, 174106 (2021).
- [78] D. Kosloff and R. Kosloff, A fourier method solution for the time dependent Schrödinger equation as a tool in molecular dynamics, *J. Comput. Phys.* **52**, 35 (1983).
- [79] R. Kosloff, Time-dependent quantum-mechanical methods for molecular dynamics, *J. Phys. Chem.* **92**, 2087 (1988).
- [80] D. O. Harris, G. G. Engerholm, and W. D. Gwinn, Calculation of matrix elements for one-dimensional quantum-mechanical problems and the application to anharmonic oscillators, *J. Chem. Phys.* **43**, 1515 (1965).
- [81] A. S. Dickinson and P. R. Certain, Calculation of matrix elements for one-dimensional quantum-mechanical problems, *J. Chem. Phys.* **49**, 4209 (1968).
- [82] J. C. Light, I. P. Hamilton, and J. V. Lill, Generalized discrete variable approximation in quantum mechanics, *J. Chem. Phys.* **82**, 1400 (1985).
- [83] P. Pfeuty, The one-dimensional Ising model with a transverse field, *Ann. Phys.* **57**, 79 (1970).
- [84] S. Suzuki, J.-i. Inoue, and B. K. Chakrabarti, *Quantum Ising Phases and Transitions in Transverse Ising Models*, 2nd ed. (Springer, New York, 2012).
- [85] D. Porras and J. I. Cirac, Effective Quantum Spin Systems with Trapped Ions, *Phys. Rev. Lett.* **92**, 207901 (2004).
- [86] K. Kim, M.-S. Chang, R. Islam, S. Korenblit, L.-M. Duan, and C. Monroe, Entanglement and Tunable Spin-Spin Couplings Between Trapped Ions Using Multiple Transverse Modes, *Phys. Rev. Lett.* **103**, 120502 (2009).
- [87] J. W. Britton, B. C. Sawyer, A. C. Keith, C.-C. J. Wang, J. K. Freericks, H. Uys, M. J. Biercuk, and J. J. Bollinger, Engineered two-dimensional Ising interactions in a trapped-ion quantum simulator with hundreds of spins, *Nature (London)* **484**, 489 (2012).
- [88] R. Islam, C. Senko, W. C. Campbell, S. Korenblit, J. Smith, A. Lee, E. E. Edwards, C.-C. J. Wang, J. K. Freericks, and C. Monroe, Emergence and frustration of magnetism with variable-range interactions in a quantum simulator, *Science* **340**, 583 (2013).
- [89] H. Weimer, M. Müller, I. Lesanovsky, P. Zoller, and H. P. Büchler, A Rydberg quantum simulator, *Nat. Phys.* **6**, 382 (2010).
- [90] I. Lesanovsky, Many-Body Spin Interactions and the Ground State of a Dense Rydberg Lattice Gas, *Phys. Rev. Lett.* **106**, 025301 (2011).
- [91] P. Schauß, J. Zeiher, T. Fukuhara, S. Hild, M. Cheneau, T. Macrì, T. Pohl, I. Bloch, and C. Gross, Crystallization in Ising quantum magnets, *Science* **347**, 1455 (2015).
- [92] H. Labuhn, D. Barredo, S. Ravets, S. de Léséleuc, T. Macrì, T. Lahaye, and A. Browaeys, Tunable two-dimensional arrays of single Rydberg atoms for realizing quantum Ising models, *Nature (London)* **534**, 667 (2016).
- [93] R. Coldea, D. A. Tennant, E. M. Wheeler, E. Wawrzynska, D. Prabhakaran, M. Telling, K. Habicht, P. Smeibidl, and K. Kiefer, Quantum criticality in an Ising chain: Experimental evidence for emergent E8 symmetry, *Science* **327**, 177 (2010).
- [94] J. Eisert, M. Cramer, and M. B. Plenio, Colloquium: Area laws for the entanglement entropy, *Rev. Mod. Phys.* **82**, 277 (2010).
- [95] G. Refael and J. E. Moore, Entanglement Entropy of Random Quantum Critical Points in One Dimension, *Phys. Rev. Lett.* **93**, 260602 (2004).
- [96] X. Turkeshi, P. Ruggiero, V. Alba, and P. Calabrese, Entanglement equipartition in critical random spin chains, *Phys. Rev. B* **102**, 014455 (2020).
- [97] H. Albrecht, E. F. Wassermann, F. T. Hedgcock, and P. Monod, Heisenberg, XY, and Ising Spin-Glass Behavior in Hexagonal Metallic Systems, *Phys. Rev. Lett.* **48**, 819 (1982).
- [98] L. De Cesare, K. Lukierska-Walasek, I. Rabuffo, and K. Walasek, Two-spin cluster approach to the infinite-range quantum transverse XY spin-glass model, *Phys. Lett. A* **145**, 291 (1990).
- [99] L. De Cesare, K. Lukierska-Walasek, I. Rabuffo, and K. Walasek, Cavity-fields approach to quantum XY spin-glass models in a transverse field, *Phys. Rev. B* **45**, 1041 (1992).
- [100] A. P. Young and R. B. Stinchcombe, Real-space renormalization group calculations for spin glasses and dilute magnets, *J. Phys. C: Solid State Phys.* **9**, 4419 (1976).
- [101] F. Iglói and C. Monthus, Strong disorder RG approach of random systems, *Phys. Rep.* **412**, 277 (2005).
- [102] F. Iglói, Z. Szatmári, and Y.-C. Lin, Entanglement entropy dynamics of disordered quantum spin chains, *Phys. Rev. B* **85**, 094417 (2012).
- [103] R. Vosk and E. Altman, Dynamical Quantum Phase Transitions in Random Spin Chains, *Phys. Rev. Lett.* **112**, 217204 (2014).
- [104] P. Weinberg and M. Bukov, Quspin: A python package for dynamics and exact diagonalisation of quantum many body systems Part I: Spin chains, *SciPost Phys.* **2**, 003 (2017).
- [105] J. Gray, Quimb: A python package for quantum information and many-body calculations, *J. Open Source Softw.* **3**, 819 (2018).
- [106] M. Fishman, S. White, and E. Stoudenmire, The itensor software library for tensor network calculations, *SciPost Physics Codebases*, 4 (2022).
- [107] G. Parisi, Order Parameter for Spin-Glasses, *Phys. Rev. Lett.* **50**, 1946 (1983).
- [108] F. Verstraete, M. Popp, and J. I. Cirac, Entanglement Versus Correlations in Spin Systems, *Phys. Rev. Lett.* **92**, 027901 (2004).
- [109] J. von Neumann, Thermodynamik quantenmechanischer gesamtheiten, *Nachr. Akad. Wiss. Göttingen Math. Phys. Kl.* **1927**, 273 (1927).

- [110] M. Troyer and U.-J. Wiese, Computational Complexity and Fundamental Limitations to Fermionic Quantum Monte Carlo Simulations, *Phys. Rev. Lett.* **94**, 170201 (2005).
- [111] R. G. Melko, G. Carleo, J. Carrasquilla, and J. I. Cirac, Restricted Boltzmann machines in quantum physics, *Nat. Phys.* **15**, 887 (2019).
- [112] G. Torlai, B. Timar, E. P. L. van Nieuwenburg, H. Levine, A. Omran, A. Keesling, H. Bernien, M. Greiner, V. Vuletić, M. D. Lukin, R. G. Melko, and M. Endres, Integrating Neural Networks with a Quantum Simulator for State Reconstruction, *Phys. Rev. Lett.* **123**, 230504 (2019).
- [113] G. Torlai and R. G. Melko, Machine-learning quantum states in the NISQ Era, *Annu. Rev. Condens. Matter Phys.* **11**, 325 (2020).
- [114] S. R. Manmana, K. R. A. Hazzard, G. Chen, A. E. Feiguin, and A. M. Rey, Su(n) magnetism in chains of ultracold alkaline-earth-metal atoms: Mott transitions and quantum correlations, *Phys. Rev. A* **84**, 043601 (2011).
- [115] P. Nataf and F. Mila, Exact Diagonalization of Heisenberg SU(N) Models, *Phys. Rev. Lett.* **113**, 127204 (2014).
- [116] G. Evenbly and G. Vidal, Tensor network states and geometry, *J. Stat. Phys.* **145**, 891 (2011).
- [117] N. Ng, S. Wenderoth, R. R. Seelam, E. Rabani, H.-D. Meyer, M. Thoss, and M. Kolodrubetz, Localization dynamics in a centrally coupled system, *Phys. Rev. B* **103**, 134201 (2021).
- [118] A. Polkovnikov, K. Sengupta, A. Silva, and M. Vengalattore, Colloquium: Nonequilibrium dynamics of closed interacting quantum systems, *Rev. Mod. Phys.* **83**, 863 (2011).
- [119] C. Gogolin and J. Eisert, Equilibration, thermalisation, and the emergence of statistical mechanics in closed quantum systems, *Rep. Prog. Phys.* **79**, 056001 (2016).
- [120] F. H. L. Essler and M. Fagotti, Quench dynamics and relaxation in isolated integrable quantum spin chains, *J. Stat. Mech.* (2016) 064002.
- [121] E. Guardado-Sanchez, P. T. Brown, D. Mitra, T. Devakul, D. A. Huse, P. Schauß, and W. S. Bakr, Probing the Quench Dynamics of Antiferromagnetic Correlations in a 2D Quantum Ising Spin System, *Phys. Rev. X* **8**, 021069 (2018).
- [122] N. Khaneja, T. Reiss, C. Kehlet, T. Schulte-Herbrüggen, and S. J. Glaser, Optimal control of coupled spin dynamics: Design of NMR pulse sequences by gradient ascent algorithms, *J. Magn. Reson.* **172**, 296 (2005).
- [123] A. Omran, H. Levine, A. Keesling, G. Semeghini, T. T. Wang, S. Ebadi, H. Bernien, A. S. Zibrov, H. Pichler, S. Choi, J. Cui, M. Rossignolo, P. Rembold, S. Montangero, T. Calarco, M. Endres, M. Greiner, V. Vuletic, and M. D. Lukin, Generation and manipulation of Schrödinger cat states in Rydberg atom arrays, *Science* **365**, 570 (2019).
- [124] L. P. Kaelbling, M. L. Littman, and A. W. Moore, Reinforcement learning: A survey, *J. Artif. Intell. Res.* **4**, 237 (1996).
- [125] Y. LeCun, Y. Bengio, and G. Hinton, Deep learning, *Nature* **521**, 436 (2015).
- [126] I. Goodfellow, Y. Bengio, and A. Courville, *Deep Learning* (MIT Press, Cambridge, MA, 2016).
- [127] R. S. Sutton and A. G. Barto, *Reinforcement Learning, Second Edition: An Introduction* (MIT Press, Cambridge, MA, 2018).
- [128] D. Mendive-Tapia and H.-D. Meyer, Regularizing the Mctdh equations of motion through an optimal choice on-the-fly (i.e., Spawning) of unoccupied single-particle functions, *J. Chem. Phys.* **153**, 234114 (2020).
- [129] R. Martinazzo and I. Burghardt, Comment on “Regularizing the MCTDH equations of motion through an optimal choice on-the-fly (i.e., spawning) of unoccupied single-particle functions” [D. Mendive-Tapia, H.-D. Meyer, *J. Chem. Phys.* **153**, 234114 (2020)], [arXiv:2102.12117](https://arxiv.org/abs/2102.12117).
- [130] R. Martinazzo and I. Burghardt, Local-in-Time Error in Variational Quantum Dynamics, *Phys. Rev. Lett.* **124**, 150601 (2020).
- [131] H. R. Larsson, Computing vibrational eigenstates with tree tensor network states (TTNS), *J. Chem. Phys.* **151**, 204102 (2019).
- [132] R. Kosloff and H. Tal-Ezer, A direct relaxation method for calculating eigenfunctions and eigenvalues of the Schrödinger equation on a grid, *Chem. Phys. Lett.* **127**, 223 (1986).
- [133] U. Manthe, H.-D. Meyer, and L. S. Cederbaum, Multi-configurational time-dependent Hartree study of complex dynamics: Photodissociation of NO<sub>2</sub>, *J. Chem. Phys.* **97**, 9062 (1992).
- [134] U. Manthe and A. D. Hammerich, Wavepacket dynamics in five dimensions. Photodissociation of Methyl Iodide, *Chem. Phys. Lett.* **211**, 7 (1993).
- [135] A. D. Hammerich, U. Manthe, R. Kosloff, H.-D. Meyer, and L. S. Cederbaum, Time-dependent photodissociation of methyl iodide with five active modes, *J. Chem. Phys.* **101**, 5623 (1994).
- [136] H.-D. Meyer and G. A. Worth, Quantum molecular dynamics: propagating wavepackets and density operators using the multiconfiguration time-dependent Hartree method, *Theor. Chem. Acc.* **109**, 251 (2003).
- [137] H. Wang, Iterative calculation of energy eigenstates employing the multilayer multiconfiguration time-dependent Hartree theory, *J. Phys. Chem. A* **118**, 9253 (2014).
- [138] H. Wang, Multilayer multiconfiguration time-dependent Hartree theory, *J. Phys. Chem. A* **119**, 7951 (2015).
- [139] J. Hinze, The multi-configuration self-consistent-field method, *J. Chem. Phys.* **59**, 6424 (1973).
- [140] D. Calvetti, L. Reichel, and D. C. Sorensen, An implicitly restarted lanczos method for large symmetric eigenvalue problems, *Electron. T. Numer. Ana.* **2**, 21 (1994).
- [141] R. Lehoucq, D. Sorensen, and C. Yang, *ARPACK Users' Guide*, Software, Environments and Tools (Society for Industrial and Applied Mathematics, Philadelphia, 1998).



## Conclusion & Outlook

THE present cumulative dissertation demonstrates that **ML-MCTDH** methods are powerful tools for the description of quantum many-body systems and useful for the numerical treatment of various models encountered in the field of ultracold atom physics. This chapter summarizes the main findings and provides an outlook on future methodological refinements (Section 5.1), improvements of the software implementation (Section 5.2) as well as promising subsequent physical applications (Section 5.3).

### 5.1. Methodological Perspectives

Ref. [FK1], proposes a pruning approach for **MCTDHB** that dynamically adapts its selection of the most relevant number states used for the description of the physical system. The scheme is benchmarked using two different but typical dynamical scenarios when studying the nonequilibrium dynamics of ultracold atoms. The dynamical pruning method is found to capture the dynamics accurately for proper choices of its parameters which is showcased by a variety of observables. While these findings highlight that there is still room for algorithmic refinement within the **MCTDHB** method, it should also be noted that the gain in numerical efficiency varied drastically between the two physical setups. In the case of an interaction quench of bosons trapped in an optical lattice, the simulation time can be reduced sevenfold while in the case of a harmonic trap quenched to a double-well potential yields a speed-up of up to a factor of two. Consequently, it is instructive to further explore the efficiency of the pruning approach across a wider range of dynamical scenarios in future research and gain insight into the facets that determine its performance. In addition, the **MCTDHB** method offers the freedom of choosing an arbitrary, Hermitian constraint operator that lifts the ambiguity of the wave function ansatz (see Sections 2.3.2 and 2.7.3) and which is linked to the transformation between equivalent representations of the same wave function. Hence, it is natural to ask whether this flexibility can lead to a representation that is more favorable for the dynamical pruning scheme. For this purpose the natural orbital gauge (see Appendix B) and a diagonalization gauge (see Appendix C) have been derived and implemented. However, both choices only impact the results marginally and do not increase the sparsity of the coefficient vector with respect to the pruning criteria leaving the performance of the scheme unaffected. Still, future investigations could find a choice of the constraint operator that improves the efficiency of the dynamical pruning approach. Other directions for future research include the application of this scheme to imaginary time propagation (see Section 2.8), multiple indistinguishable species in the context of **ML-MCTDHX** or the development of more sophisticated pruning criteria that potentially involve machine learning techniques [806–808] to select the most relevant

configurations.

The **EOMs** governing the time-evolution of the **SPFs** in the **ML-MCTDH** family of methods (see Eqs. (2.24), (2.56) and (A.8)) all include the inverse of the one-body density matrix. If the wave function ansatz contains unoccupied orbitals, the one-body density matrix is singular and the **EOMs** are ill-defined. For decades, implementations have relied on regularizing the one-body density [420, 522] as shown in Eq. (2.30) to circumnavigate this issue. The error introduced by this small modification is usually negligible and **ML-MCTDH** methods have been successfully applied to a wide range of problems reaching excellent accuracy. However, mathematical analyses of the **MCTDH** method [809] as well as isolated reports of scenarios where the regularization can lead to unphysical results [547, 810–813] raised concerns regarding the exactness of the method. Consequently, the development of novel regularization techniques has been the subject of recent methodological research. It has been shown that it can be advantageous to move the regularization from the one-body density matrix to the coefficient tensor [547, 812, 813]. Since the singularity arises from the presence of unoccupied **SPFs**, schemes have been proposed to choose them in an optimized fashion [810] or to start only with occupied orbitals and dynamically spawn new ones as they are needed for the description of the system [814–816].

In a 2015 paper, Lubich [817] proposed a novel projector-splitting integration scheme for **MCTDH**<sup>1</sup>. This approach does not require the evaluation of the inverse one-body density matrix and instead alternates between computing orthogonal matrix decompositions and solving linear differential equations. The projector-splitting approach was first tested in Ref. [819], but as the authors point out, the merits of this scheme have to be further analyzed in the future. In particular, they hint that **ML-MCTDH** wave functions are often more sensitive towards singularities in the one-body densities than simple **MCTDH** wave functions. Consequently, extensions of the projector-splitting integration scheme to **ML-MCTDH** have been developed very recently [548, 820, 821]. Since, all the aforementioned strategies to tackle the regularization issue have been developed in the context of distinguishable **DOFs** for **MCTDH** and **ML-MCTDH**, a natural question for future research is whether these regularization techniques can be transferred to **MCTDHB**, **MCTDHF** and **ML-MCTDHX**.

Both **MCTDH** and its multilayer extension rely on tensor decompositions of the full coefficient tensor which closely relates them to the field of tensor network states (see Section 2.5). Recent years have seen a surge in the transfer of ideas from the tensor network community to the family of **ML-MCTDH** methods. Larsson demonstrated how a **DMRG**-like algorithm can be applied to the tree tensor network states that underlie the construction of the **ML-MCTDH**. This approach allows the efficient computation of many excited states, thus complementing **ML-MCTDH** which is usually limited to the first few excited states and far less efficient as it relies on rather slow on imaginary time propagation (see Section 2.8). It would be instructive to further compare the two approaches regarding their performance and accuracy as well as the compactness of the resulting wave function as **ML-MCTDH** might potentially yield a smaller, optimized basis. Furthermore, many approaches for the time evolution of **MPS** have been developed including time-evolving block decimation [584–586, 736], **TDVP** based schemes [591–595] or **MPS-MCTDH** [596]. Some of these algorithms have already been shown to be transferrable to the propagation of tree tensor network states [597, 598]. Hence, it will

---

<sup>1</sup>Ref. [818] provides an alternative formulation of the projector-splitting integration scheme that is closer to the usual chemical physics notation of **MCTDH** and highlights some key features of this approach.



be very illuminating to compare the performance of [ML-MCTDH](#) and tensor network methods when it comes to the dynamics of quantum many-body systems. Hopefully, the future will see a further cross-fertilization between the [ML-MCTDH](#) and tensor network communities leading to advancements in both fields, yielding to more refined and powerful numerical methods.

One particular challenge when applying the [ML-MCTDH](#) is the design of the wave function tree structure and ensuring the convergence with respect to the number of [SPFs](#) at each node. There might be opportunities to devise algorithms that help in the construction of the ansatz, e.g., by using machine learning techniques [806–808]. Furthermore, it might be instructive to develop a deeper understanding of the mathematical properties and limitations when it comes to the description of many-body systems using tree tensor network states. Ref. [FK3] shows an example where [ML-MCTDH](#) describes a system exhibiting strong area law violation accurately, a more exhaustive and rigorous study might be a fruitful perspective for future research. Especially, geometries with more than one spatial dimension quickly become challenging for numerical methods. So far, most studies involving tree tensor network states have been mostly limited to ordered systems in two spatial dimensions involving very localized interactions [FK3, 561].

## 5.2. Implementational Improvements

The robustness of the [ML-MCTDHX](#) code has been greatly improved by replacing custom routines with well-tested and optimized libraries. The stability and performance of the improved relaxation algorithm (see Section 2.8.2) has been significantly enhanced by swapping out an error-prone Lanczos code with a well-tested, implicitly restarted Lanczos implementation [366] provided by the ARPACK library [703]. The FFTW package contains state of the art [FFT](#) codes and is now used for the [FFT](#) representation outlined in Section 2.6.3 also enhancing the robustness and efficiency of the implementation. The current version of the framework only makes use of a single CPU core at a time such that parallelization of the program holds potential for further performance improvements. In the context of a single bosonic species, i.e., [MCTDHB](#), the performance characteristics of the implementation can differ drastically depending on the system under consideration. For the purpose of systems that require many orbitals and also contain a reasonable number of particles, the most time-consuming part of the program is the computation of the reduced density matrices. Unfortunately, a shared-memory parallelization over the involved number state loops using OpenMP has been found to be inefficient, mostly yielding only small speedups. When considering bosons in more than one spatial dimension, a major bottleneck for the performance is the large number of terms introduced by computing a sum-of-product form of the Gaussian model potential (see Section 2.7.2) using the POTFIT algorithm. In principle, all these terms could be applied to the wave function in parallel as they are independent of each other. Again, shared-memory parallelization has been explored to accelerate these otherwise very time-consuming multidimensional calculations. However, in the current implementation this leads to a performance bottleneck due to inefficient memory access patterns that fully saturate the available memory bandwidth, sometimes even resulting in a slowdown of the program. Additionally, the historical growth of the codebase led to a non-ideal structure of the code, that often makes it hard to maintain, difficult to implement new features, explore novel methodological ideas or improve the overall efficiency of the program. Due to the aforementioned issues, the group is currently undertaking a com-

plete rewrite of the codebase in collaboration with the group of Prof. Dr. O. Vendrell at Heidelberg University. By switching from Fortran to Python, the new codebase will be much more flexible and approachable for new developers. The vast ecosystem of numerical software available for Python allows leveraging very efficient libraries, including machine learning frameworks such as PyTorch [822, 823] and TensorFlow [824, 825] which provide efficient implementations of tensor operations and support GPUs. Further ideas include the investigation of different numerical integrators for ordinary differential equations and the addition of the CMF integration schemes [420, 522, 529] (see Section 2.3.3) as alternatives to the available variable mean-field (VMF) approach. A common task when studying many-body systems with ML-MCTDHX is the computation of eigenstates of the Hamiltonian using the relaxation procedures described in Section 2.8 which rely on propagation in imaginary time. The current version of the software package employs real-valued arithmetic for the propagation of the wave function in all cases. For real-valued Hamiltonians and initial states, the propagation in imaginary time could be implemented using only real-valued arithmetic which would cut the number of arithmetic operations in half, thus drastically reducing the computational effort. Such a flexible implementation could be easily achieved in the new Python package. Even more computing time might be saved by performing the first part of the imaginary time propagation in single-precision floating arithmetic to come close to the desired state and then switch to double-precision in order to refine the result.

### 5.3. Future Applications

Ref. [FK2] investigates the dynamics of a single bosonic species trapped in two colliding potential wells unraveling the fundamental processes such as particle untrapping, the transport mechanism and the build-up of entanglement. This study highlights that even when considering a few-particle problem of a single atomic species, fascinating dynamical scenarios can be realized. As a next step the ML-MCTDHX method can be employed to simulate the collision of two different atomic species and to analyze the build-up of interparticle correlations. In Ref. [682] the authors consider a similar setup of an impurity confined in a moving harmonic trap with a bosonic bath subject to an external double-well potential. They study the impact of the interspecies interactions on the damped oscillatory motion of the impurity within the bath and the build-up of entanglement between the species. Another promising direction, would be to consider the collision of a single atomic species confined in a moving projectile well with a lattice of stationary wells. This could be achieved using a more complex time-dependent potential of the form

$$V(x, t) = \underbrace{-V_0^{(0)} \exp \left[ -\left( \frac{x - \mu^{(0)}(t)}{\sqrt{2}\alpha^{(0)}\sigma} \right)^2 \right]}_{\text{projectile}} - \underbrace{\sum_{i=1}^N V_0^{(i)} \exp \left[ -\left( \frac{x - \mu^{(i)}}{\sqrt{2}\alpha^{(i)}\sigma} \right)^2 \right]}_{\text{stationary lattice}} \quad (5.1)$$

which is sketched in Fig. 5.1. Such a setup could be viewed as a simplistic model for the collision of an incident atom with a linear molecule or serve as platform to study schemes of loading particles confined in a moving optical tweezer into an optical lattice.

Ref. [FK3] demonstrates the applicability of the ML-MCTDH method to quantum spin models by exploring the ground states of various different setups. The approach is first benchmarked in the context of homogeneous systems and then applied to study

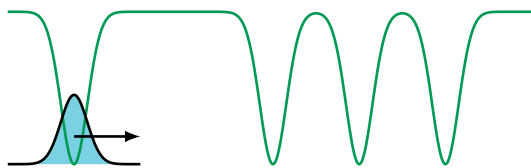


Figure 5.1.: Collision between a moving projectile well loaded with ultracold bosons and a lattice of multiple stationary wells.

intricate disordered models that are notoriously hard to tackle due to the high amount of degeneracy in the low energy spectrum. For all scenarios considered, [ML-MCTDH](#) captures the relevant characteristics of the ground state such as its energy, correlations, and entanglement entropy accurately, rendering it a powerful alternative to established methods in this domain of physics such as exact diagonalization or [MPS](#) based approaches. One particularly striking finding of this work is that the method is able to reproduce the strong area law violation that is present in one of the models and which is beyond the reach of the [DMRG](#). This observation may serve as a starting point for further research in order to explore other challenging models that exhibit strong area law violations due to disorder. A natural next step is to switch from imaginary to real time propagation and to investigate the dynamics of spin models. So far the many-body localization dynamics of a spin- $1/2$  chain coupled to a central qudit has been studied with the [ML-MCTDH](#) method [826]. Interesting further applications in this context are optimal control problems [349, 350] and the simulation nonequilibrium dynamics such as quenches [827, 828] and thermalization processes [102, 348]. The spin basis presented in Section 2.6.4 can be easily extended to higher total spins, such as spin-1, spin- $3/2$ , etc., only requiring a suitable matrix representation of the involved spin operators. [ML-MCTDH](#) could then be used to explore the fascinating field of  $SU(n)$  models [829–833] which play an important role in many areas of physics such as quantum chromodynamics [242, 243, 834] or atomic physics [835–837].

As mentioned in Section 2.7.5, the Jordan-Wigner transformation [666] allows mapping fermionic lattice models onto spin models which could then be treated using [ML-MCTDH](#). Since the fermion sign problem poses a major obstacle for methods like quantum Monte Carlo [382], it would be illuminating to explore the performance of [ML-MCTDH](#) in this situation. By implementing the [SQR](#) of [ML-MCTDH](#), the software package has been enriched by a useful alternative to [MCTDHB](#) when simulating bosonic systems that is particularly well suited for lattice models. So far the application of this feature within the group was mainly focused on Bose-Hubbard models [38, 96], but currently the applicability to more exotic systems is being investigated. An example for such a setup is the bosonic formulation of the anyonic Hubbard model [665, 838–842] which contains an occupation dependent, Peierls-like phase [843, 844] in the hopping term,

$$\sum_i (\hat{b}_i^\dagger e^{i\theta \hat{n}_i} \hat{b}_{i+1} + \text{H.c.}) , \quad (5.2)$$

where the angle  $\theta$  determines the statistics of the particles<sup>2</sup>. The experimental realization of this model with arbitrary statistical phases was achieved very recently by inducing

<sup>2</sup>For  $\theta = 0$  the original Bose-Hubbard model is recovered, while  $\theta = \pi$  results in pseudofermions. For arbitrary angles of  $\theta$  the Peierls phase breaks the spatial inversion and the time reversal symmetry [665].

artificial gauge fields via periodic shaking of a one-dimensional optical lattice, i.e., by Floquet engineering [845].

## Bibliography

- [1] Bose. “Plancks Gesetz und Lichtquantenhypothese”. In: *Z. Phys.* 26.1 (Dec. 1, 1924), pp. 178–181. ISSN: 0044-3328. DOI: [10.1007/BF01327326](https://doi.org/10.1007/BF01327326).
- [2] M. Planck and M. Masius. *The Theory of Heat Radiation*. In collab. with University of California Libraries. Philadelphia, P. Blakiston’s Son & Co, 1914. 256 pp. URL: <http://archive.org/details/theoryofheatradi00planrich>.
- [3] A. Einstein. “Quantentheorie Des Einatomigen Idealen Gases”. In: *Albert Einstein: Akademie-Vorträge*. John Wiley & Sons, Ltd, 2005, pp. 237–244. ISBN: 978-3-527-60895-9. DOI: [10.1002/3527608958.ch27](https://doi.org/10.1002/3527608958.ch27).
- [4] A. Einstein. “Quantentheorie Des Einatomigen Idealen Gases. Zweite Abhandlung”. In: *Albert Einstein: Akademie-Vorträge*. John Wiley & Sons, Ltd, 2005, pp. 245–257. ISBN: 978-3-527-60895-9. DOI: [10.1002/3527608958.ch28](https://doi.org/10.1002/3527608958.ch28).
- [5] F. London. “The  $\lambda$ -Phenomenon of Liquid Helium and the Bose-Einstein Degeneracy”. In: *Nature* 141.3571 (3571 Apr. 1938), pp. 643–644. ISSN: 1476-4687. DOI: [10.1038/141643a0](https://doi.org/10.1038/141643a0).
- [6] J. Bardeen, L. N. Cooper, and J. R. Schrieffer. “Microscopic Theory of Superconductivity”. In: *Phys. Rev.* 106.1 (Apr. 1, 1957), pp. 162–164. DOI: [10.1103/PhysRev.106.162](https://doi.org/10.1103/PhysRev.106.162).
- [7] J. Bardeen, L. N. Cooper, and J. R. Schrieffer. “Theory of Superconductivity”. In: *Phys. Rev.* 108.5 (Dec. 1, 1957), pp. 1175–1204. DOI: [10.1103/PhysRev.108.1175](https://doi.org/10.1103/PhysRev.108.1175).
- [8] K. B. Davis et al. “Bose-Einstein Condensation in a Gas of Sodium Atoms”. In: *Phys. Rev. Lett.* 75.22 (Nov. 27, 1995), pp. 3969–3973. DOI: [10/drjzvd](https://doi.org/10/drjzvd).
- [9] M. H. Anderson et al. “Observation of Bose-Einstein Condensation in a Dilute Atomic Vapor”. In: *Science* 269.5221 (July 14, 1995), pp. 198–201. ISSN: 0036-8075, 1095-9203. DOI: [10/cr87gf](https://doi.org/10/cr87gf).
- [10] J. Klaers et al. “Bose-Einstein Condensation of Photons in an Optical Microcavity”. In: *Nature* 468.7323 (7323 Nov. 2010), pp. 545–548. ISSN: 1476-4687. DOI: [10.1038/nature09567](https://doi.org/10.1038/nature09567).
- [11] H. Deng et al. “Condensation of Semiconductor Microcavity Exciton Polaritons”. In: *Science* 298.5591 (Oct. 4, 2002), pp. 199–202. DOI: [10.1126/science.1074464](https://doi.org/10.1126/science.1074464).
- [12] J. Kasprzak et al. “Bose-Einstein Condensation of Exciton Polaritons”. In: *Nature* 443.7110 (7110 Sept. 2006), pp. 409–414. ISSN: 1476-4687. DOI: [10.1038/nature05131](https://doi.org/10.1038/nature05131).
- [13] R. Balili et al. “Bose-Einstein Condensation of Microcavity Polaritons in a Trap”. In: *Science* 316.5827 (May 18, 2007), pp. 1007–1010. DOI: [10.1126/science.1140990](https://doi.org/10.1126/science.1140990).
- [14] S. O. Demokritov et al. “Bose-Einstein Condensation of Quasi-Equilibrium Magnons at Room Temperature under Pumping”. In: *Nature* 443.7110 (7110 Sept. 2006), pp. 430–433. ISSN: 1476-4687. DOI: [10.1038/nature05117](https://doi.org/10.1038/nature05117).

- [15] H. F. Hess. “Evaporative Cooling of Magnetically Trapped and Compressed Spin-Polarized Hydrogen”. In: *Phys. Rev. B* 34.5 (Sept. 1, 1986), pp. 3476–3479. doi: [10.1103/PhysRevB.34.3476](https://doi.org/10.1103/PhysRevB.34.3476).
- [16] N. Masuhara et al. “Evaporative Cooling of Spin-Polarized Atomic Hydrogen”. In: *Phys. Rev. Lett.* 61.8 (Aug. 22, 1988), pp. 935–938. doi: [10.1103/PhysRevLett.61.935](https://doi.org/10.1103/PhysRevLett.61.935).
- [17] K. B. Davis et al. “Evaporative Cooling of Sodium Atoms”. In: *Phys. Rev. Lett.* 74.26 (June 26, 1995), pp. 5202–5205. doi: [10.1103/PhysRevLett.74.5202](https://doi.org/10.1103/PhysRevLett.74.5202).
- [18] L. V. Hau et al. “Light Speed Reduction to 17 Metres per Second in an Ultracold Atomic Gas”. In: *Nature* 397.6720 (6720 Feb. 1999), pp. 594–598. issn: 1476-4687. doi: [10.1038/17561](https://doi.org/10.1038/17561).
- [19] T. W. Hänsch and A. L. Schawlow. “Cooling of Gases by Laser Radiation”. In: *Optics Communications* 13.1 (Jan. 1, 1975), pp. 68–69. issn: 0030-4018. doi: [10.1016/0030-4018\(75\)90159-5](https://doi.org/10.1016/0030-4018(75)90159-5).
- [20] D. J. Wineland, R. E. Drullinger, and F. L. Walls. “Radiation-Pressure Cooling of Bound Resonant Absorbers”. In: *Phys. Rev. Lett.* 40.25 (June 19, 1978), pp. 1639–1642. doi: [10.1103/PhysRevLett.40.1639](https://doi.org/10.1103/PhysRevLett.40.1639).
- [21] J. Dalibard and C. Cohen-Tannoudji. “Laser Cooling below the Doppler Limit by Polarization Gradients: Simple Theoretical Models”. In: *J. Opt. Soc. Am. B* 6.11 (Nov. 1, 1989), pp. 2023–2045. issn: 1520-8540. doi: [10.1364/JOSAB.6.002023](https://doi.org/10.1364/JOSAB.6.002023).
- [22] M. Kasevich and S. Chu. “Laser Cooling below a Photon Recoil with Three-Level Atoms”. In: *Phys. Rev. Lett.* 69.12 (Sept. 21, 1992), pp. 1741–1744. doi: [10.1103/PhysRevLett.69.1741](https://doi.org/10.1103/PhysRevLett.69.1741).
- [23] A. J. Kerman et al. “Beyond Optical Molasses: 3D Raman Sideband Cooling of Atomic Cesium to High Phase-Space Density”. In: *Phys. Rev. Lett.* 84.3 (Jan. 17, 2000), pp. 439–442. doi: [10.1103/PhysRevLett.84.439](https://doi.org/10.1103/PhysRevLett.84.439).
- [24] D. E. Pritchard. “Cooling Neutral Atoms in a Magnetic Trap for Precision Spectroscopy”. In: *Phys. Rev. Lett.* 51 (Oct. 1, 1983), pp. 1336–1339. issn: 0031-9007. doi: [10.1103/PhysRevLett.51.1336](https://doi.org/10.1103/PhysRevLett.51.1336).
- [25] A. M. Steane, M. Chowdhury, and C. J. Foot. “Radiation Force in the Magneto-Optical Trap”. In: *J. Opt. Soc. Am. B* 9.12 (Dec. 1, 1992), pp. 2142–2158. issn: 1520-8540. doi: [10.1364/JOSAB.9.002142](https://doi.org/10.1364/JOSAB.9.002142).
- [26] P. Kohns et al. “On-Line Measurement of Sub-Doppler Temperatures in a Rb Magneto-optical Trap-by-Trap Centre Oscillations”. In: *Europhys. Lett.* 22.7 (June 1993), p. 517. issn: 0295-5075. doi: [10.1209/0295-5075/22/7/007](https://doi.org/10.1209/0295-5075/22/7/007).
- [27] M. Drewsen et al. “Investigation of Sub-Doppler Cooling Effects in a Cesium Magneto-Optical Trap”. In: *Appl. Phys. B* 59.3 (Sept. 1, 1994), pp. 283–298. issn: 1432-0649. doi: [10.1007/BF01081396](https://doi.org/10.1007/BF01081396).
- [28] C. D. Wallace et al. “Measurements of Temperature and Spring Constant in a Magneto-Optical Trap”. In: *J. Opt. Soc. Am. B* 11.5 (May 1, 1994), pp. 703–711. issn: 1520-8540. doi: [10.1364/JOSAB.11.000703](https://doi.org/10.1364/JOSAB.11.000703).
- [29] C. G. Townsend et al. “Phase-Space Density in the Magneto-Optical Trap”. In: *Phys. Rev. A* 52.2 (Aug. 1, 1995), pp. 1423–1440. doi: [10.1103/PhysRevA.52.1423](https://doi.org/10.1103/PhysRevA.52.1423).

- 
- [30] K. Dieckmann et al. "Two-Dimensional Magneto-Optical Trap as a Source of Slow Atoms". In: *Phys. Rev. A* 58.5 (Nov. 1, 1998), pp. 3891–3895. doi: [10.1103/PhysRevA.58.3891](https://doi.org/10.1103/PhysRevA.58.3891).
- [31] S. Chu. "Nobel Lecture: The Manipulation of Neutral Particles". In: *Rev. Mod. Phys.* 70.3 (July 1, 1998), pp. 685–706. doi: [10.1103/RevModPhys.70.685](https://doi.org/10.1103/RevModPhys.70.685).
- [32] C. N. Cohen-Tannoudji. "Nobel Lecture: Manipulating Atoms with Photons". In: *Rev. Mod. Phys.* 70.3 (July 1, 1998), pp. 707–719. doi: [10.1103/RevModPhys.70.707](https://doi.org/10.1103/RevModPhys.70.707).
- [33] W. D. Phillips. "Nobel Lecture: Laser Cooling and Trapping of Neutral Atoms". In: *Rev. Mod. Phys.* 70.3 (July 1, 1998), pp. 721–741. doi: [10.1103/RevModPhys.70.721](https://doi.org/10.1103/RevModPhys.70.721).
- [34] F. Serwane et al. "Deterministic Preparation of a Tunable Few-Fermion System". In: *Science* 332.6027 (Apr. 15, 2011), pp. 336–338. issn: 0036-8075, 1095-9203. doi: [10/dm6f9v](https://doi.org/10/dm6f9v).
- [35] A. N. Wenz et al. "From Few to Many: Observing the Formation of a Fermi Sea One Atom at a Time". In: *Science* 342.6157 (Oct. 25, 2013), pp. 457–460. doi: [10.1126/science.1240516](https://doi.org/10.1126/science.1240516).
- [36] A. M. Kaufman et al. "Two-Particle Quantum Interference in Tunnel-Coupled Optical Tweezers". In: *Science* 345.6194 (July 18, 2014), pp. 306–309. issn: 0036-8075, 1095-9203. doi: [10/f6brb6](https://doi.org/10/f6brb6).
- [37] K. Henderson et al. "Experimental Demonstration of Painting Arbitrary and Dynamic Potentials for Bose–Einstein Condensates". In: *New J. Phys.* 11.4 (Apr. 2009), p. 043030. issn: 1367-2630. doi: [10/cqb5nz](https://doi.org/10/cqb5nz).
- [38] D. Jaksch et al. "Cold Bosonic Atoms in Optical Lattices". In: *Phys. Rev. Lett.* 81.15 (Oct. 12, 1998), pp. 3108–3111. doi: [10/dn97pr](https://doi.org/10/dn97pr).
- [39] R. Grimm, M. Weidemüller, and Y. B. Ovchinnikov. "Optical Dipole Traps for Neutral Atoms". In: *Advances In Atomic, Molecular, and Optical Physics*. Ed. by B. Bederson and H. Walther. Vol. 42. Academic Press, Jan. 1, 2000, pp. 95–170. doi: [10.1016/S1049-250X\(08\)60186-X](https://doi.org/10.1016/S1049-250X(08)60186-X).
- [40] I. Bloch. "Ultracold Quantum Gases in Optical Lattices". In: *Nat. Phys.* 1.1 (Oct. 2005), pp. 23–30. issn: 1745-2473. doi: [10/bcxr5q](https://doi.org/10/bcxr5q).
- [41] M. Greiner and S. Fölling. "Optical Lattices". In: *Nature* 453.7196 (7196 June 2008), pp. 736–738. issn: 1476-4687. doi: [10.1038/453736a](https://doi.org/10.1038/453736a).
- [42] S. Chu et al. "Proposal for Optically Cooling Atoms to Temperatures of the Order of  $10^{-6}$  K". In: *Opt. Lett.* 11.2 (Feb. 1, 1986), pp. 73–75. issn: 1539-4794. doi: [10/d7v9qf](https://doi.org/10/d7v9qf).
- [43] O. Morizot et al. "Ring Trap for Ultracold Atoms". In: *Phys. Rev. A* 74.2 (Aug. 23, 2006), p. 023617. doi: [10/cctm74](https://doi.org/10/cctm74).
- [44] A. Görlitz et al. "Realization of Bose-Einstein Condensates in Lower Dimensions". In: *Phys. Rev. Lett.* 87.13 (Sept. 4, 2001), p. 130402. doi: [10.1103/PhysRevLett.87.130402](https://doi.org/10.1103/PhysRevLett.87.130402).
- [45] C. Orzel et al. "Squeezed States in a Bose-Einstein Condensate". In: *Science* 291.5512 (Mar. 23, 2001), pp. 2386–2389. issn: 0036-8075, 1095-9203. doi: [10/dckkdf](https://doi.org/10/dckkdf).
-

- [46] B. Paredes et al. “Tonks–Girardeau Gas of Ultracold Atoms in an Optical Lattice”. In: *Nature* 429.6989 (6989 May 2004), pp. 277–281. ISSN: 1476-4687. DOI: [10/dmc99q](https://doi.org/10/dmc99q).
- [47] T. Kinoshita, T. Wenger, and D. S. Weiss. “A Quantum Newton’s Cradle”. In: *Nature* 440.7086 (Apr. 13, 2006), pp. 900–903. ISSN: 0028-0836. DOI: [10/b8sk6z](https://doi.org/10/b8sk6z).
- [48] O. Zobay and B. M. Garraway. “Two-Dimensional Atom Trapping in Field-Induced Adiabatic Potentials”. In: *Phys. Rev. Lett.* 86.7 (Feb. 12, 2001), pp. 1195–1198. DOI: [10/cwwdxf](https://doi.org/10/cwwdxf).
- [49] Y. Colombe et al. “Ultracold Atoms Confined in RF-Induced Two-Dimensional Trapping Potentials”. In: *Europhys. Lett.* 67.4 (Aug. 2004), p. 593. ISSN: 0295-5075. DOI: [10/btbhrn](https://doi.org/10/btbhrn).
- [50] M. Greiner et al. “Quantum Phase Transition from a Superfluid to a Mott Insulator in a Gas of Ultracold Atoms”. In: *Nature* 415.6867 (Jan. 2002), pp. 39–44. ISSN: 1476-4687. DOI: [10/dr59dj](https://doi.org/10/dr59dj).
- [51] L.-M. Duan, E. Demler, and M. D. Lukin. “Controlling Spin Exchange Interactions of Ultracold Atoms in Optical Lattices”. In: *Phys. Rev. Lett.* 91.9 (Aug. 26, 2003), p. 090402. DOI: [10/d8v5pz](https://doi.org/10/d8v5pz).
- [52] N. Kjærgaard, A. S. Mellish, and A. C. Wilson. “Differential Scattering Measurements from a Collider for Ultracold Atoms”. In: *New J. Phys.* 6 (Oct. 2004), pp. 146–146. ISSN: 1367-2630. DOI: [10/dxbwtg](https://doi.org/10/dxbwtg).
- [53] A. Rakonjac et al. “Laser Based Accelerator for Ultracold Atoms”. In: *Opt. Lett.* 37.6 (Mar. 15, 2012), pp. 1085–1087. ISSN: 1539-4794. DOI: [10/gffmkw](https://doi.org/10/gffmkw).
- [54] K. O. Roberts et al. “Steerable Optical Tweezers for Ultracold Atom Studies”. In: *Opt. Lett.* 39.7 (Apr. 1, 2014), pp. 2012–2015. ISSN: 1539-4794. DOI: [10/gffmkz](https://doi.org/10/gffmkz).
- [55] R. Thomas et al. “Quantum Scattering in an Optical Collider for Ultracold Atoms”. In: *J. Phys.: Conf. Ser.* 875.2 (2017), p. 012007. ISSN: 1742-6596. DOI: [10/gddj86](https://doi.org/10/gddj86).
- [56] R. Thomas et al. “Observation of Bound State Self-Interaction in a Nano-eV Atom Collider”. In: *Nat. Commun.* 9.1 (Nov. 20, 2018), p. 4895. ISSN: 2041-1723. DOI: [10/gftc9n](https://doi.org/10/gftc9n).
- [57] N. Schlosser et al. “Sub-Poissonian Loading of Single Atoms in a Microscopic Dipole Trap”. In: *Nature* 411.6841 (6841 June 2001), pp. 1024–1027. ISSN: 1476-4687. DOI: [10.1038/35082512](https://doi.org/10.1038/35082512).
- [58] M. A. Norcia, A. W. Young, and A. M. Kaufman. “Microscopic Control and Detection of Ultracold Strontium in Optical-Tweezer Arrays”. In: *Phys. Rev. X* 8.4 (Dec. 28, 2018), p. 041054. DOI: [10.1103/PhysRevX.8.041054](https://doi.org/10.1103/PhysRevX.8.041054).
- [59] A. M. Kaufman and K.-K. Ni. “Quantum Science with Optical Tweezer Arrays of Ultracold Atoms and Molecules”. In: *Nat. Phys.* 17.12 (12 Dec. 2021), pp. 1324–1333. ISSN: 1745-2481. DOI: [10.1038/s41567-021-01357-2](https://doi.org/10.1038/s41567-021-01357-2).
- [60] W. S. Bakr et al. “A Quantum Gas Microscope for Detecting Single Atoms in a Hubbard-regime Optical Lattice”. In: *Nature* 462.7269 (7269 Nov. 2009), pp. 74–77. ISSN: 1476-4687. DOI: [10.1038/nature08482](https://doi.org/10.1038/nature08482).
- [61] J. F. Sherson et al. “Single-Atom-Resolved Fluorescence Imaging of an Atomic Mott Insulator”. In: *Nature* 467.7311 (7311 Sept. 2010), pp. 68–72. ISSN: 1476-4687. DOI: [10.1038/nature09378](https://doi.org/10.1038/nature09378).



- 
- [62] L. W. Cheuk et al. “Quantum-Gas Microscope for Fermionic Atoms”. In: *Phys. Rev. Lett.* 114.19 (May 13, 2015), p. 193001. doi: [10.1103/PhysRevLett.114.193001](https://doi.org/10.1103/PhysRevLett.114.193001).
- [63] G. J. A. Edge et al. “Imaging and Addressing of Individual Fermionic Atoms in an Optical Lattice”. In: *Phys. Rev. A* 92.6 (Dec. 8, 2015), p. 063406. doi: [10.1103/PhysRevA.92.063406](https://doi.org/10.1103/PhysRevA.92.063406).
- [64] E. Haller et al. “Single-Atom Imaging of Fermions in a Quantum-Gas Microscope”. In: *Nat. Phys.* 11.9 (9 Sept. 2015), pp. 738–742. issn: 1745-2481. doi: [10.1038/nphys3403](https://doi.org/10.1038/nphys3403).
- [65] M. F. Parsons et al. “Site-Resolved Imaging of Fermionic  ${}^6\text{Li}$  in an Optical Lattice”. In: *Phys. Rev. Lett.* 114.21 (May 28, 2015), p. 213002. doi: [10.1103/PhysRevLett.114.213002](https://doi.org/10.1103/PhysRevLett.114.213002).
- [66] M. Pyzh et al. “Quantum Point Spread Function for Imaging Trapped Few-Body Systems with a Quantum Gas Microscope”. In: *New J. Phys.* 21.5 (May 2019), p. 053013. issn: 1367-2630. doi: [10.1088/1367-2630/ab1ae7](https://doi.org/10.1088/1367-2630/ab1ae7).
- [67] M. Endres et al. “Observation of Correlated Particle-Hole Pairs and String Order in Low-Dimensional Mott Insulators”. In: *Science* 334.6053 (Oct. 14, 2011), pp. 200–203. doi: [10.1126/science.1209284](https://doi.org/10.1126/science.1209284).
- [68] R. Islam et al. “Measuring Entanglement Entropy in a Quantum Many-Body System”. In: *Nature* 528.7580 (7580 Dec. 2015), pp. 77–83. issn: 1476-4687. doi: [10.1038/nature15750](https://doi.org/10.1038/nature15750).
- [69] A. Mazurenko et al. “A Cold-Atom Fermi–Hubbard Antiferromagnet”. In: *Nature* 545.7655 (7655 May 2017), pp. 462–466. issn: 1476-4687. doi: [10.1038/nature22362](https://doi.org/10.1038/nature22362).
- [70] H. Ott. “Single Atom Detection in Ultracold Quantum Gases: A Review of Current Progress”. In: *Rep. Prog. Phys.* 79.5 (Apr. 2016), p. 054401. issn: 0034-4885. doi: [10.1088/0034-4885/79/5/054401](https://doi.org/10.1088/0034-4885/79/5/054401).
- [71] C. Gross and W. S. Bakr. “Quantum Gas Microscopy for Single Atom and Spin Detection”. In: *Nat. Phys.* 17.12 (12 Dec. 2021), pp. 1316–1323. issn: 1745-2481. doi: [10.1038/s41567-021-01370-5](https://doi.org/10.1038/s41567-021-01370-5).
- [72] T. Köhler, K. Góral, and P. S. Julienne. “Production of Cold Molecules Via Magnetically Tunable Feshbach Resonances”. In: *Rev. Mod. Phys.* 78.4 (Dec. 1, 2006), pp. 1311–1361. doi: [10/br8tdz](https://doi.org/10/br8tdz).
- [73] C. Chin et al. “Feshbach Resonances in Ultracold Gases”. In: *Rev. Mod. Phys.* 82.2 (Apr. 29, 2010), pp. 1225–1286. doi: [10/fmvjms](https://doi.org/10/fmvjms).
- [74] M. Olshanii. “Atomic Scattering in the Presence of an External Confinement and a Gas of Impenetrable Bosons”. In: *Phys. Rev. Lett.* 81.5 (Aug. 3, 1998), pp. 938–941. doi: [10/bw6g5w](https://doi.org/10/bw6g5w).
- [75] J. I. Kim, V. S. Melezhik, and P. Schmelcher. “Suppression of Quantum Scattering in Strongly Confined Systems”. In: *Phys. Rev. Lett.* 97.19 (Nov. 10, 2006), p. 193203. doi: [10/cnbr67](https://doi.org/10/cnbr67).
- [76] P. Giannakeas, F. K. Diakonou, and P. Schmelcher. “Coupled  $l$ -Wave Confinement-Induced Resonances in Cylindrically Symmetric Waveguides”. In: *Phys. Rev. A* 86.4 (Oct. 8, 2012), p. 042703. doi: [10/gft2j8](https://doi.org/10/gft2j8).
-

- [77] P. Giannakeas, V. S. Melezhik, and P. Schmelcher. “Dipolar Confinement-Induced Resonances of Ultracold Gases in Waveguides”. In: *Phys. Rev. Lett.* 111.18 (Oct. 28, 2013), p. 183201. doi: [10/f5k2zs](https://doi.org/10/f5k2zs).
- [78] C. J. Pethick and H. Smith. *Bose–Einstein Condensation in Dilute Gases*. 2nd ed. Cambridge University Press, Sept. 2008. 584 pp. ISBN: 978-0-521-84651-6.
- [79] S. Burger et al. “Dark Solitons in Bose-Einstein Condensates”. In: *Phys. Rev. Lett.* 83.25 (Dec. 20, 1999), pp. 5198–5201. doi: [10/b852dg](https://doi.org/10/b852dg).
- [80] J. Denschlag et al. “Generating Solitons by Phase Engineering of a Bose-Einstein Condensate”. In: *Science* 287.5450 (Jan. 7, 2000), pp. 97–101. doi: [10.1126/science.287.5450.97](https://doi.org/10.1126/science.287.5450.97).
- [81] P. G. Kevrekidis, D. J. Frantzeskakis, and R. Carretero-González. *Emergent Non-linear Phenomena in Bose-Einstein Condensates: Theory and Experiment*. Vol. 45. Springer, 2008.
- [82] D. J. Frantzeskakis. “Dark Solitons in Atomic Bose–Einstein Condensates: From Theory to Experiments”. In: *J. Phys. A: Math. Theor.* 43.21 (May 2010), p. 213001. ISSN: 1751-8121. doi: [10.1088/1751-8113/43/21/213001](https://doi.org/10.1088/1751-8113/43/21/213001).
- [83] A. L. Fetter. “Rotating Trapped Bose-Einstein Condensates”. In: *Rev. Mod. Phys.* 81.2 (May 18, 2009), pp. 647–691. doi: [10.1103/RevModPhys.81.647](https://doi.org/10.1103/RevModPhys.81.647).
- [84] T.-L. Ho and M. Ma. “Quasi 1 and 2d Dilute Bose Gas in Magnetic Traps: Existence of Off-Diagonal Order and Anomalous Quantum Fluctuations”. In: *J. Low. Temp. Phys.* 115.1 (Apr. 1, 1999), pp. 61–70. ISSN: 1573-7357. doi: [10.1023/A:1021894713105](https://doi.org/10.1023/A:1021894713105).
- [85] C. Menotti and S. Stringari. “Collective Oscillations of a One-Dimensional Trapped Bose-Einstein Gas”. In: *Phys. Rev. A* 66.4 (Oct. 21, 2002), p. 043610. doi: [10.1103/PhysRevA.66.043610](https://doi.org/10.1103/PhysRevA.66.043610).
- [86] H. Moritz et al. “Exciting Collective Oscillations in a Trapped 1D Gas”. In: *Phys. Rev. Lett.* 91.25 (Dec. 18, 2003), p. 250402. doi: [10.1103/PhysRevLett.91.250402](https://doi.org/10.1103/PhysRevLett.91.250402).
- [87] P. Pedri and L. Santos. “Three-Dimensional Quasi-Tonks Gas in a Harmonic Trap”. In: *Phys. Rev. Lett.* 91.11 (Sept. 9, 2003), p. 110401. doi: [10.1103/PhysRevLett.91.110401](https://doi.org/10.1103/PhysRevLett.91.110401).
- [88] S. Zöllner, H.-D. Meyer, and P. Schmelcher. “Tunneling Dynamics of a Few Bosons in a Double Well”. In: *Phys. Rev. A* 78.1 (July 2008), p. 013621. doi: [10/d3h88f](https://doi.org/10/d3h88f).
- [89] S. Zöllner, H.-D. Meyer, and P. Schmelcher. “Few-Boson Dynamics in Double Wells: From Single-Atom to Correlated Pair Tunneling”. In: *Phys. Rev. Lett.* 100.4 (Jan. 2008), p. 040401. doi: [10/ftbmh8](https://doi.org/10/ftbmh8).
- [90] B. Chatterjee et al. “Few-Boson Tunneling in a Double Well with Spatially Modulated Interaction”. In: *Phys. Rev. A* 82.4 (Oct. 22, 2010), p. 043619. doi: [10.1103/PhysRevA.82.043619](https://doi.org/10.1103/PhysRevA.82.043619).
- [91] G. J. Milburn et al. “Quantum Dynamics of an Atomic Bose-Einstein Condensate in a Double-Well Potential”. In: *Phys. Rev. A* 55.6 (June 1, 1997), pp. 4318–4324. doi: [10.1103/PhysRevA.55.4318](https://doi.org/10.1103/PhysRevA.55.4318).

- 
- [92] M. Holthaus. “Towards Coherent Control of a Bose-Einstein Condensate in a Double Well”. In: *Phys. Rev. A* 64.1 (June 6, 2001), p. 011601. doi: [10.1103/PhysRevA.64.011601](https://doi.org/10.1103/PhysRevA.64.011601).
- [93] K. Sakmann et al. “Exact Quantum Dynamics of a Bosonic Josephson Junction”. In: *Phys. Rev. Lett.* 103.22 (Nov. 23, 2009), p. 220601. doi: [10/ch9m3g](https://doi.org/10/ch9m3g).
- [94] M. Albiez et al. “Direct Observation of Tunneling and Nonlinear Self-Trapping in a Single Bosonic Josephson Junction”. In: *Phys. Rev. Lett.* 95.1 (June 27, 2005), p. 010402. doi: [10.1103/PhysRevLett.95.010402](https://doi.org/10.1103/PhysRevLett.95.010402).
- [95] B. D. Josephson. “Possible New Effects in Superconductive Tunnelling”. In: *Phys. Lett.* 1.7 (July 1, 1962), pp. 251–253. issn: 0031-9163. doi: [10.1016/0031-9163\(62\)91369-0](https://doi.org/10.1016/0031-9163(62)91369-0).
- [96] M. P. A. Fisher et al. “Boson Localization and the Superfluid-Insulator Transition”. In: *Phys. Rev. B* 40.1 (July 1, 1989), pp. 546–570. doi: [10/fqqpbs](https://doi.org/10/fqqpbs).
- [97] M. Ölschläger, G. Wirth, and A. Hemmerich. “Unconventional Superfluid Order in the F Band of a Bipartite Optical Square Lattice”. In: *Phys. Rev. Lett.* 106.1 (Jan. 6, 2011), p. 015302. doi: [10.1103/PhysRevLett.106.015302](https://doi.org/10.1103/PhysRevLett.106.015302).
- [98] G. Wirth, M. Ölschläger, and A. Hemmerich. “Evidence for Orbital Superfluidity in the P-band of a Bipartite Optical Square Lattice”. In: *Nat. Phys.* 7.2 (2 Feb. 2011), pp. 147–153. issn: 1745-2481. doi: [10.1038/nphys1857](https://doi.org/10.1038/nphys1857).
- [99] P. Soltan-Panahi et al. “Quantum Phase Transition to Unconventional Multi-Orbital Superfluidity in Optical Lattices”. In: *Nat. Phys.* 8.1 (1 Jan. 2012), pp. 71–75. issn: 1745-2481. doi: [10.1038/nphys2128](https://doi.org/10.1038/nphys2128).
- [100] S. Hofferberth et al. “Non-Equilibrium Coherence Dynamics in One-Dimensional Bose Gases”. In: *Nature* 449.7160 (7160 Sept. 2007), pp. 324–327. issn: 1476-4687. doi: [10.1038/nature06149](https://doi.org/10.1038/nature06149).
- [101] M. Rigol, V. Dunjko, and M. Olshanii. “Thermalization and Its Mechanism for Generic Isolated Quantum Systems”. In: *Nature* 452.7189 (Apr. 17, 2008), pp. 854–858. issn: 0028-0836. doi: [10/fw9n2q](https://doi.org/10/fw9n2q).
- [102] A. Polkovnikov et al. “Colloquium: Nonequilibrium Dynamics of Closed Interacting Quantum Systems”. In: *Rev. Mod. Phys.* 83.3 (Aug. 2011), pp. 863–883. doi: [10/cf8tkp](https://doi.org/10/cf8tkp).
- [103] M. Gring et al. “Relaxation and Prethermalization in an Isolated Quantum System”. In: *Science* 337.6100 (Sept. 14, 2012), pp. 1318–1322. doi: [10.1126/science.1224953](https://doi.org/10.1126/science.1224953).
- [104] J. P. Ronzheimer et al. “Expansion Dynamics of Interacting Bosons in Homogeneous Lattices in One and Two Dimensions”. In: *Phys. Rev. Lett.* 110.20 (May 2013), p. 205301. doi: [10/gddj2g](https://doi.org/10/gddj2g).
- [105] J. P. Ronzheimer. “Non-equilibrium dynamics of ultracold atoms in optical lattices”. PhD thesis. Ludwig-Maximilians-Universität München, Jan. 30, 2014. url: <https://edoc.ub.uni-muenchen.de/16814/>.
- [106] H. Ott et al. “Collisionally Induced Transport in Periodic Potentials”. In: *Phys. Rev. Lett.* 92.16 (Apr. 20, 2004), p. 160601. doi: [10.1103/PhysRevLett.92.160601](https://doi.org/10.1103/PhysRevLett.92.160601).
-

- [107] C. D. Fertig et al. “Strongly Inhibited Transport of a Degenerate 1D Bose Gas in a Lattice”. In: *Phys. Rev. Lett.* 94.12 (Apr. 1, 2005), p. 120403. doi: [10.1103/PhysRevLett.94.120403](https://doi.org/10.1103/PhysRevLett.94.120403).
- [108] N. Strohmaier et al. “Interaction-Controlled Transport of an Ultracold Fermi Gas”. In: *Phys. Rev. Lett.* 99.22 (Nov. 2007), p. 220601. doi: [10/dd8t7r](https://doi.org/10/dd8t7r).
- [109] U. Schneider et al. “Fermionic Transport and Out-of-Equilibrium Dynamics in a Homogeneous Hubbard Model with Ultracold Atoms”. In: *Nat Phys* 8.3 (Mar. 2012), pp. 213–218. issn: 1745-2473. doi: [10/fxh57q](https://doi.org/10/fxh57q).
- [110] L. Tonks. “The Complete Equation of State of One, Two and Three-Dimensional Gases of Hard Elastic Spheres”. In: *Phys. Rev.* 50.10 (Nov. 15, 1936), pp. 955–963. doi: [10.1103/PhysRev.50.955](https://doi.org/10.1103/PhysRev.50.955).
- [111] M. Girardeau. “Relationship between Systems of Impenetrable Bosons and Fermions in One Dimension”. In: *J. Math. Phys.* 1.6 (Nov. 1, 1960), pp. 516–523. issn: 0022-2488. doi: [10/c3tgzx](https://doi.org/10/c3tgzx).
- [112] T. Kinoshita, T. Wenger, and D. S. Weiss. “Observation of a One-Dimensional Tonks-Girardeau Gas”. In: *Science* 305.5687 (Aug. 20, 2004), pp. 1125–1128. issn: 0036-8075, 1095-9203. doi: [10.1126/science.1100700](https://doi.org/10.1126/science.1100700).
- [113] Z.-H. Luo et al. “A New Form of Liquid Matter: Quantum Droplets”. In: *Front. Phys.* 16.3 (Dec. 2, 2020), p. 32201. issn: 2095-0470. doi: [10.1007/s11467-020-1020-2](https://doi.org/10.1007/s11467-020-1020-2).
- [114] I. Ferrier-Barbut et al. “Observation of Quantum Droplets in a Strongly Dipolar Bose Gas”. In: *Phys. Rev. Lett.* 116.21 (May 23, 2016), p. 215301. doi: [10.1103/PhysRevLett.116.215301](https://doi.org/10.1103/PhysRevLett.116.215301).
- [115] I. Ferrier-Barbut et al. “Liquid Quantum Droplets of Ultracold Magnetic Atoms”. In: *J. Phys. B: At. Mol. Opt. Phys.* 49.21 (Oct. 2016), p. 214004. issn: 0953-4075. doi: [10.1088/0953-4075/49/21/214004](https://doi.org/10.1088/0953-4075/49/21/214004).
- [116] H. Kadau et al. “Observing the Rosensweig Instability of a Quantum Ferrofluid”. In: *Nature* 530.7589 (7589 Feb. 2016), pp. 194–197. issn: 1476-4687. doi: [10.1038/nature16485](https://doi.org/10.1038/nature16485).
- [117] M. Schmitt et al. “Self-Bound Droplets of a Dilute Magnetic Quantum Liquid”. In: *Nature* 539.7628 (Nov. 2016), pp. 259–262. issn: 1476-4687. doi: [10/f9bth7](https://doi.org/10/f9bth7).
- [118] I. Ferrier-Barbut et al. “Scissors Mode of Dipolar Quantum Droplets of Dysprosium Atoms”. In: *Phys. Rev. Lett.* 120.16 (Apr. 18, 2018), p. 160402. doi: [10.1103/PhysRevLett.120.160402](https://doi.org/10.1103/PhysRevLett.120.160402).
- [119] I. Ferrier-Barbut et al. “Onset of a Modulational Instability in Trapped Dipolar Bose-Einstein Condensates”. In: *Phys. Rev. A* 97.1 (Jan. 25, 2018), p. 011604. doi: [10.1103/PhysRevA.97.011604](https://doi.org/10.1103/PhysRevA.97.011604).
- [120] F. Böttcher et al. “Dilute Dipolar Quantum Droplets beyond the Extended Gross-Pitaevskii Equation”. In: *Phys. Rev. Res.* 1.3 (Nov. 8, 2019), p. 033088. doi: [10.1103/PhysRevResearch.1.033088](https://doi.org/10.1103/PhysRevResearch.1.033088).
- [121] L. Chomaz et al. “Quantum-Fluctuation-Driven Crossover from a Dilute Bose-Einstein Condensate to a Macrodroplet in a Dipolar Quantum Fluid”. In: *Phys. Rev. X* 6.4 (Nov. 22, 2016), p. 041039. doi: [10.1103/PhysRevX.6.041039](https://doi.org/10.1103/PhysRevX.6.041039).

- 
- [122] T. D. Lee, K. Huang, and C. N. Yang. “Eigenvalues and Eigenfunctions of a Bose System of Hard Spheres and Its Low-Temperature Properties”. In: *Phys. Rev.* 106.6 (June 15, 1957), pp. 1135–1145. doi: [10/bkrhf8](https://doi.org/10/bkrhf8).
- [123] F. Böttcher et al. “Transient Supersolid Properties in an Array of Dipolar Quantum Droplets”. In: *Phys. Rev. X* 9.1 (Mar. 22, 2019), p. 011051. doi: [10.1103/PhysRevX.9.011051](https://doi.org/10.1103/PhysRevX.9.011051).
- [124] L. Chomaz et al. “Long-Lived and Transient Supersolid Behaviors in Dipolar Quantum Gases”. In: *Phys. Rev. X* 9.2 (Apr. 19, 2019), p. 021012. doi: [10.1103/PhysRevX.9.021012](https://doi.org/10.1103/PhysRevX.9.021012).
- [125] L. Tanzi et al. “Observation of a Dipolar Quantum Gas with Metastable Supersolid Properties”. In: *Phys. Rev. Lett.* 122.13 (Apr. 3, 2019), p. 130405. doi: [10.1103/PhysRevLett.122.130405](https://doi.org/10.1103/PhysRevLett.122.130405).
- [126] G. V. Chester. “Speculations on Bose-Einstein Condensation and Quantum Crystals”. In: *Phys. Rev. A* 2.1 (July 1, 1970), pp. 256–258. doi: [10.1103/PhysRevA.2.256](https://doi.org/10.1103/PhysRevA.2.256).
- [127] A. J. Leggett. “Can a Solid Be “Superfluid”?” In: *Phys. Rev. Lett.* 25.22 (Nov. 30, 1970), pp. 1543–1546. doi: [10.1103/PhysRevLett.25.1543](https://doi.org/10.1103/PhysRevLett.25.1543).
- [128] S. Balibar. “The Enigma of Supersolidity”. In: *Nature* 464.7286 (7286 Mar. 2010), pp. 176–182. ISSN: 1476-4687. doi: [10.1038/nature08913](https://doi.org/10.1038/nature08913).
- [129] E. Kim and M. H. W. Chan. “Probable Observation of a Supersolid Helium Phase”. In: *Nature* 427.6971 (6971 Jan. 2004), pp. 225–227. ISSN: 1476-4687. doi: [10.1038/nature02220](https://doi.org/10.1038/nature02220).
- [130] J. Day and J. Beamish. “Low-Temperature Shear Modulus Changes in Solid 4He and Connection to Supersolidity”. In: *Nature* 450.7171 (7171 Dec. 2007), pp. 853–856. ISSN: 1476-4687. doi: [10.1038/nature06383](https://doi.org/10.1038/nature06383).
- [131] D. Y. Kim and M. H. W. Chan. “Absence of Supersolidity in Solid Helium in Porous Vycor Glass”. In: *Phys. Rev. Lett.* 109.15 (Oct. 8, 2012), p. 155301. doi: [10.1103/PhysRevLett.109.155301](https://doi.org/10.1103/PhysRevLett.109.155301).
- [132] E. Braaten and H. -. Hammer. “Universality in Few-Body Systems with Large Scattering Length”. In: *Phys. Rep.* 428.5 (June 1, 2006), pp. 259–390. ISSN: 0370-1573. doi: [10.1016/j.physrep.2006.03.001](https://doi.org/10.1016/j.physrep.2006.03.001).
- [133] X.-J. Liu, H. Hu, and P. D. Drummond. “Virial Expansion for a Strongly Correlated Fermi Gas”. In: *Phys. Rev. Lett.* 102.16 (Apr. 22, 2009), p. 160401. doi: [10.1103/PhysRevLett.102.160401](https://doi.org/10.1103/PhysRevLett.102.160401).
- [134] I. Brouzos and P. Schmelcher. “Construction of Analytical Many-Body Wave Functions for Correlated Bosons in a Harmonic Trap”. In: *Phys. Rev. Lett.* 108.4 (Jan. 24, 2012), p. 045301. doi: [10.1103/PhysRevLett.108.045301](https://doi.org/10.1103/PhysRevLett.108.045301).
- [135] I. Brouzos and P. Schmelcher. “Controlled Excitation and Resonant Acceleration of Ultracold Few-Boson Systems by Driven Interactions in a Harmonic Trap”. In: *Phys. Rev. A* 85.3 (Mar. 26, 2012), p. 033635. doi: [10.1103/PhysRevA.85.033635](https://doi.org/10.1103/PhysRevA.85.033635).
- [136] C. H. Greene, P. Giannakeas, and J. Pérez-Ríos. “Universal Few-Body Physics and Cluster Formation”. In: *Rev. Mod. Phys.* 89.3 (Aug. 28, 2017), p. 035006. doi: [10.1103/RevModPhys.89.035006](https://doi.org/10.1103/RevModPhys.89.035006).
-

- [137] D. Blume. “Few-Body Physics with Ultracold Atomic and Molecular Systems in Traps”. In: *Rep. Prog. Phys.* 75.4 (Mar. 2012), p. 046401. ISSN: 0034-4885. DOI: [10.1088/0034-4885/75/4/046401](https://doi.org/10.1088/0034-4885/75/4/046401).
- [138] P. Naidon and S. Endo. “Efimov Physics: A Review”. In: *Rep. Prog. Phys.* 80.5 (Mar. 2017), p. 056001. ISSN: 0034-4885. DOI: [10.1088/1361-6633/aa50e8](https://doi.org/10.1088/1361-6633/aa50e8).
- [139] V. N. Efimov. “Weakly Bound States of Three Resonantly Interacting Particles.” In: *Yadern. Fiz.* (Nov. 1970), pp. 1080–1091. URL: <https://www.osti.gov/biblio/4068792>.
- [140] V. N. Efimov. “Energy Levels Arising from Resonant Two-Body Forces in a Three-Body System”. In: *Phys. Lett. B* 33.8 (Dec. 21, 1970), pp. 563–564. ISSN: 0370-2693. DOI: [10.1016/0370-2693\(70\)90349-7](https://doi.org/10.1016/0370-2693(70)90349-7).
- [141] T. Kraemer et al. “Evidence for Efimov Quantum States in an Ultracold Gas of Caesium Atoms”. In: *Nature* 440.7082 (7082 Mar. 2006), pp. 315–318. ISSN: 1476-4687. DOI: [10.1038/nature04626](https://doi.org/10.1038/nature04626).
- [142] S. Knoop et al. “Observation of an Efimov-like Trimer Resonance in Ultracold Atom–Dimer Scattering”. In: *Nature Phys* 5.3 (3 Mar. 2009), pp. 227–230. ISSN: 1745-2481. DOI: [10.1038/nphys1203](https://doi.org/10.1038/nphys1203).
- [143] M. Zaccanti et al. “Observation of an Efimov Spectrum in an Atomic System”. In: *Nat. Phys.* 5.8 (8 Aug. 2009), pp. 586–591. ISSN: 1745-2481. DOI: [10.1038/nphys1334](https://doi.org/10.1038/nphys1334).
- [144] S. E. Pollack, D. Dries, and R. G. Hulet. “Universality in Three- and Four-Body Bound States of Ultracold Atoms”. In: *Science* 326.5960 (Dec. 18, 2009), pp. 1683–1685. DOI: [10.1126/science.1182840](https://doi.org/10.1126/science.1182840).
- [145] M. S. Santos et al. “Simultaneous Trapping of Two Different Atomic Species in a Vapor-Cell Magneto-Optical Trap”. In: *Phys. Rev. A* 52.6 (Dec. 1, 1995), R4340–R4343. DOI: [10.1103/PhysRevA.52.R4340](https://doi.org/10.1103/PhysRevA.52.R4340).
- [146] G. D. Telles et al. “Inelastic Cold Collisions of a Na/Rb Mixture in a Magneto-Optical Trap”. In: *Phys. Rev. A* 59.1 (Jan. 1, 1999), R23–R26. DOI: [10.1103/PhysRevA.59.R23](https://doi.org/10.1103/PhysRevA.59.R23).
- [147] L. G. Marcassa et al. “Collisional Losses in a K-Rb Cold Mixture”. In: *Phys. Rev. A* 63.1 (Dec. 13, 2000), p. 013413. DOI: [10.1103/PhysRevA.63.013413](https://doi.org/10.1103/PhysRevA.63.013413).
- [148] G. Ferrari et al. “Collisional Properties of Ultracold K-Rb Mixtures”. In: *Phys. Rev. Lett.* 89.5 (July 15, 2002), p. 053202. DOI: [10/bshxv2](https://doi.org/10/bshxv2).
- [149] D. A. Brue and J. M. Hutson. “Magnetically Tunable Feshbach Resonances in Ultracold Li-Yb Mixtures”. In: *Phys. Rev. Lett.* 108.4 (Jan. 25, 2012), p. 043201. DOI: [10/fz334j](https://doi.org/10/fz334j).
- [150] B. Pasquiou et al. “Quantum Degenerate Mixtures of Strontium and Rubidium Atoms”. In: *Phys. Rev. A* 88.2 (Aug. 1, 2013), p. 023601. DOI: [10.1103/PhysRevA.88.023601](https://doi.org/10.1103/PhysRevA.88.023601).
- [151] W. Süptitz et al. “Simultaneous Cooling and Trapping of  $^{85}\text{Rb}$  and  $^{87}\text{Rb}$  in a Magneto-Optical Trap”. In: *Opt. Lett.* 19.19 (Oct. 1, 1994), pp. 1571–1573. ISSN: 1539-4794. DOI: [10.1364/OL.19.001571](https://doi.org/10.1364/OL.19.001571).

- 
- [152] M.-O. Mewes et al. “Simultaneous Magneto-Optical Trapping of Two Lithium Isotopes”. In: *Phys. Rev. A* 61.1 (Dec. 8, 1999), p. 011403. doi: [10.1103/PhysRevA.61.011403](https://doi.org/10.1103/PhysRevA.61.011403).
- [153] N. Poli et al. “Cooling and Trapping of Ultracold Strontium Isotopic Mixtures”. In: *Phys. Rev. A* 71.6 (June 13, 2005), 061403(R). doi: [10/bbkfrq](https://doi.org/10/bbkfrq).
- [154] G. Ferrari et al. “Cooling of Sr to High Phase-Space Density by Laser and Sympathetic Cooling in Isotopic Mixtures”. In: *Phys. Rev. A* 73.2 (Feb. 10, 2006), p. 023408. doi: [10.1103/PhysRevA.73.023408](https://doi.org/10.1103/PhysRevA.73.023408).
- [155] T. Fukuhara et al. “All-Optical Formation of Quantum Degenerate Mixtures”. In: *Phys. Rev. A* 79.2 (Feb. 3, 2009), p. 021601. doi: [10.1103/PhysRevA.79.021601](https://doi.org/10.1103/PhysRevA.79.021601).
- [156] P. G. Mickelson et al. “Bose-Einstein Condensation of  $^{88}\text{Sr}$  through Sympathetic Cooling with  $^{87}\text{Sr}$ ”. In: *Phys. Rev. A* 81.5 (May 5, 2010), p. 051601. doi: [10.1103/PhysRevA.81.051601](https://doi.org/10.1103/PhysRevA.81.051601).
- [157] C. J. Myatt et al. “Production of Two Overlapping Bose-Einstein Condensates by Sympathetic Cooling”. In: *Phys. Rev. Lett.* 78.4 (Jan. 27, 1997), pp. 586–589. doi: [10/bbsh46](https://doi.org/10/bbsh46).
- [158] D. S. Hall et al. “Dynamics of Component Separation in a Binary Mixture of Bose-Einstein Condensates”. In: *Phys. Rev. Lett.* 81.8 (Aug. 24, 1998), pp. 1539–1542. doi: [10.1103/PhysRevLett.81.1539](https://doi.org/10.1103/PhysRevLett.81.1539).
- [159] P. Maddaloni et al. “Collective Oscillations of Two Colliding Bose-Einstein Condensates”. In: *Phys. Rev. Lett.* 85.12 (Sept. 18, 2000), pp. 2413–2417. doi: [10.1103/PhysRevLett.85.2413](https://doi.org/10.1103/PhysRevLett.85.2413).
- [160] K. M. Mertes et al. “Nonequilibrium Dynamics and Superfluid Ring Excitations in Binary Bose-Einstein Condensates”. In: *Phys. Rev. Lett.* 99.19 (Nov. 5, 2007), p. 190402. doi: [10/bsqqvj](https://doi.org/10/bsqqvj).
- [161] C. Becker et al. “Oscillations and Interactions of Dark and Dark-Bright Solitons in Bose-Einstein Condensates”. In: *Nature Phys* 4.6 (6 June 2008), pp. 496–501. ISSN: 1745-2481. doi: [10.1038/nphys962](https://doi.org/10.1038/nphys962).
- [162] C. Hamner et al. “Generation of Dark-Bright Soliton Trains in Superfluid-Superfluid Counterflow”. In: *Phys. Rev. Lett.* 106.6 (Feb. 11, 2011), p. 065302. doi: [10.1103/PhysRevLett.106.065302](https://doi.org/10.1103/PhysRevLett.106.065302).
- [163] E. Nicklas et al. “Observation of Scaling in the Dynamics of a Strongly Quenched Quantum Gas”. In: *Phys. Rev. Lett.* 115.24 (Dec. 11, 2015), p. 245301. doi: [10.1103/PhysRevLett.115.245301](https://doi.org/10.1103/PhysRevLett.115.245301).
- [164] C. R. Cabrera et al. “Quantum Liquid Droplets in a Mixture of Bose-Einstein Condensates”. In: *Science* 359.6373 (Jan. 19, 2018), pp. 301–304. doi: [10.1126/science.aao5686](https://doi.org/10.1126/science.aao5686).
- [165] G. Semeghini et al. “Self-Bound Quantum Droplets of Atomic Mixtures in Free Space”. In: *Phys. Rev. Lett.* 120.23 (June 7, 2018), p. 235301. doi: [10.1103/PhysRevLett.120.235301](https://doi.org/10.1103/PhysRevLett.120.235301).
- [166] G. Modugno et al. “Two Atomic Species Superfluid”. In: *Phys. Rev. Lett.* 89.19 (Oct. 21, 2002), p. 190404. doi: [10/fpkqc8](https://doi.org/10/fpkqc8).
- [167] J. Catani et al. “Degenerate Bose-Bose Mixture in a Three-Dimensional Optical Lattice”. In: *Phys. Rev. A* 77.1 (Jan. 24, 2008), 011603(R). doi: [10/c9k73v](https://doi.org/10/c9k73v).
-

- [168] E. Wille et al. "Exploring an Ultracold Fermi-Fermi Mixture: Interspecies Feshbach Resonances and Scattering Properties of  ${}^6\text{Li}$  and  ${}^{40}\text{K}$ ". In: *Phys. Rev. Lett.* 100.5 (Feb. 5, 2008), p. 053201. doi: [10/dgvhxd](https://doi.org/10/dgvhxd).
- [169] C. Kohstall et al. "Metastability and Coherence of Repulsive Polarons in a Strongly Interacting Fermi Mixture". In: *Nature* 485.7400 (7400 May 2012), pp. 615–618. ISSN: 1476-4687. doi: [10.1038/nature11065](https://doi.org/10.1038/nature11065).
- [170] F. Schreck et al. "Quasipure Bose-Einstein Condensate Immersed in a Fermi Sea". In: *Phys. Rev. Lett.* 87.8 (Aug. 7, 2001), p. 080403. doi: [10/d6n4tm](https://doi.org/10/d6n4tm).
- [171] Z. Hadzibabic et al. "Two-Species Mixture of Quantum Degenerate Bose and Fermi Gases". In: *Phys. Rev. Lett.* 88.16 (Apr. 4, 2002), p. 160401. doi: [10/bxf3dj](https://doi.org/10/bxf3dj).
- [172] C. Ospelkaus et al. "Interaction-Driven Dynamics of  ${}^{40}\text{K}$ - ${}^{87}\text{Rb}$  Fermion-Boson Gas Mixtures in the Large-Particle-Number Limit". In: *Phys. Rev. Lett.* 96.2 (Jan. 18, 2006), p. 020401. doi: [10/d74cv4](https://doi.org/10/d74cv4).
- [173] J. Heinze et al. "Multiband Spectroscopy of Ultracold Fermions: Observation of Reduced Tunneling in Attractive Bose-Fermi Mixtures". In: *Phys. Rev. Lett.* 107.13 (Sept. 23, 2011), p. 135303. doi: [10/fn8tzc](https://doi.org/10/fn8tzc).
- [174] H. Pu and N. P. Bigelow. "Collective Excitations, Metastability, and Nonlinear Response of a Trapped Two-Species Bose-Einstein Condensate". In: *Phys. Rev. Lett.* 80.6 (Feb. 9, 1998), pp. 1134–1137. doi: [10.1103/PhysRevLett.80.1134](https://doi.org/10.1103/PhysRevLett.80.1134).
- [175] J. S. Krauser et al. "Investigation of Feshbach Resonances in Ultracold  ${}^{40}\text{K}$  Spin Mixtures". In: *Phys. Rev. A* 95.4 (Apr. 3, 2017), p. 042701. doi: [10.1103/PhysRevA.95.042701](https://doi.org/10.1103/PhysRevA.95.042701).
- [176] A. M. Kamchatnov et al. "Nonlinear Polarization Waves in a Two-Component Bose-Einstein Condensate". In: *Phys. Rev. A* 89.3 (Mar. 13, 2014), p. 033618. doi: [10/ghhfdp](https://doi.org/10/ghhfdp).
- [177] M. A. García-March et al. "Quantum Correlations and Spatial Localization in One-Dimensional Ultracold Bosonic Mixtures". In: *New J. Phys.* 16.10 (Oct. 2014), p. 103004. ISSN: 1367-2630. doi: [10.1088/1367-2630/16/10/103004](https://doi.org/10.1088/1367-2630/16/10/103004).
- [178] S. Zöllner, H.-D. Meyer, and P. Schmelcher. "Composite Fermionization of One-Dimensional Bose-Bose Mixtures". In: *Phys. Rev. A* 78.1 (July 22, 2008), p. 013629. doi: [10.1103/PhysRevA.78.013629](https://doi.org/10.1103/PhysRevA.78.013629).
- [179] Y. J. Hao and S. Chen. "Ground-State Properties of Interacting Two-Component Bose Gases in a One-Dimensional Harmonic Trap". In: *Eur. Phys. J. D* 51.2 (Feb. 1, 2009), pp. 261–266. ISSN: 1434-6079. doi: [10.1140/epjd/e2008-00266-0](https://doi.org/10.1140/epjd/e2008-00266-0).
- [180] M. A. Garcia-March et al. "Sharp Crossover from Composite Fermionization to Phase Separation in Microscopic Mixtures of Ultracold Bosons". In: *Phys. Rev. A* 88.6 (Dec. 3, 2013), p. 063604. doi: [10/ghhfdh](https://doi.org/10/ghhfdh).
- [181] M. D. Girardeau and A. Minguzzi. "Soluble Models of Strongly Interacting Ultracold Gas Mixtures in Tight Waveguides". In: *Phys. Rev. Lett.* 99.23 (Dec. 5, 2007), p. 230402. doi: [10.1103/PhysRevLett.99.230402](https://doi.org/10.1103/PhysRevLett.99.230402).
- [182] F. Deuretzbacher et al. "Exact Solution of Strongly Interacting Quasi-One-Dimensional Spinor Bose Gases". In: *Phys. Rev. Lett.* 100.16 (Apr. 23, 2008), p. 160405. doi: [10.1103/PhysRevLett.100.160405](https://doi.org/10.1103/PhysRevLett.100.160405).



- 
- [183] B. Fang et al. “Exact Solution for the Degenerate Ground-State Manifold of a Strongly Interacting One-Dimensional Bose-Fermi Mixture”. In: *Phys. Rev. A* 84.2 (Aug. 17, 2011), p. 023626. doi: [10.1103/PhysRevA.84.023626](https://doi.org/10.1103/PhysRevA.84.023626).
- [184] G. Modugno et al. “Bose-Einstein Condensation of Potassium Atoms by Sympathetic Cooling”. In: *Science* 294.5545 (Nov. 9, 2001), pp. 1320–1322. doi: [10.1126/science.1066687](https://doi.org/10.1126/science.1066687).
- [185] S. B. Papp, J. M. Pino, and C. E. Wieman. “Tunable Miscibility in a Dual-Species Bose-Einstein Condensate”. In: *Phys. Rev. Lett.* 101.4 (July 24, 2008), p. 040402. doi: [10.1103/PhysRevLett.101.040402](https://doi.org/10.1103/PhysRevLett.101.040402).
- [186] S. Tojo et al. “Controlling Phase Separation of Binary Bose-Einstein Condensates via Mixed-Spin-Channel Feshbach Resonance”. In: *Phys. Rev. A* 82.3 (Sept. 14, 2010), p. 033609. doi: [10.1103/PhysRevA.82.033609](https://doi.org/10.1103/PhysRevA.82.033609).
- [187] L. Wen et al. “Controlling Phase Separation of a Two-Component Bose-Einstein Condensate by Confinement”. In: *Phys. Rev. A* 85.4 (Apr. 5, 2012), p. 043602. doi: [10.1103/PhysRevA.85.043602](https://doi.org/10.1103/PhysRevA.85.043602).
- [188] C. Ticknor. “Excitations of a Trapped Two-Component Bose-Einstein Condensate”. In: *Phys. Rev. A* 88.1 (July 15, 2013), p. 013623. doi: [10/gghfdq](https://doi.org/10/gghfdq).
- [189] E. Nicklas et al. “Nonlinear Dressed States at the Miscibility-Immiscibility Threshold”. In: *Phys. Rev. A* 92.5 (Nov. 17, 2015), p. 053614. doi: [10/gghfdr](https://doi.org/10/gghfdr).
- [190] F. Wang et al. “A Double Species  $^{23}\text{Na}$  and  $^{87}\text{Rb}$  Bose-Einstein Condensate with Tunable Miscibility via an Interspecies Feshbach Resonance”. In: *J. Phys. B: At. Mol. Opt. Phys.* 49.1 (Nov. 2015), p. 015302. issn: 0953-4075. doi: [10.1088/0953-4075/49/1/015302](https://doi.org/10.1088/0953-4075/49/1/015302).
- [191] K. Kasamatsu and M. Tsubota. “Multiple Domain Formation Induced by Modulation Instability in Two-Component Bose-Einstein Condensates”. In: *Phys. Rev. Lett.* 93.10 (Sept. 2, 2004), p. 100402. doi: [10.1103/PhysRevLett.93.100402](https://doi.org/10.1103/PhysRevLett.93.100402).
- [192] S. Ronen et al. “Dynamical Pattern Formation during Growth of a Dual-Species Bose-Einstein Condensate”. In: *Phys. Rev. A* 78.5 (Nov. 7, 2008), p. 053613. doi: [10.1103/PhysRevA.78.053613](https://doi.org/10.1103/PhysRevA.78.053613).
- [193] J. Hofmann, S. S. Natu, and S. Das Sarma. “Coarsening Dynamics of Binary Bose Condensates”. In: *Phys. Rev. Lett.* 113.9 (Aug. 27, 2014), p. 095702. doi: [10.1103/PhysRevLett.113.095702](https://doi.org/10.1103/PhysRevLett.113.095702).
- [194] P. Mason and A. Aftalion. “Classification of the Ground States and Topological Defects in a Rotating Two-Component Bose-Einstein Condensate”. In: *Phys. Rev. A* 84.3 (Sept. 12, 2011), p. 033611. doi: [10.1103/PhysRevA.84.033611](https://doi.org/10.1103/PhysRevA.84.033611).
- [195] G. Delannoy et al. “Understanding the Production of Dual Bose-Einstein Condensation with Sympathetic Cooling”. In: *Phys. Rev. A* 63.5 (Apr. 9, 2001), p. 051602. doi: [10.1103/PhysRevA.63.051602](https://doi.org/10.1103/PhysRevA.63.051602).
- [196] M. Mudrich et al. “Sympathetic Cooling with Two Atomic Species in an Optical Trap”. In: *Phys. Rev. Lett.* 88.25 (June 7, 2002), p. 253001. doi: [10.1103/PhysRevLett.88.253001](https://doi.org/10.1103/PhysRevLett.88.253001).
- [197] K.-K. Ni et al. “A High Phase-Space-Density Gas of Polar Molecules”. In: *Science* 322.5899 (Oct. 10, 2008), pp. 231–235. doi: [10.1126/science.1163861](https://doi.org/10.1126/science.1163861).
-

- [198] P. K. Molony et al. "Creation of Ultracold  $^{87}\text{Rb}^{133}\text{Cs}$  Molecules in the Rovibrational Ground State". In: *Phys. Rev. Lett.* 113.25 (Dec. 17, 2014), p. 255301. doi: [10.1103/PhysRevLett.113.255301](https://doi.org/10.1103/PhysRevLett.113.255301).
- [199] T. Takekoshi et al. "Ultracold Dense Samples of Dipolar RbCs Molecules in the Rovibrational and Hyperfine Ground State". In: *Phys. Rev. Lett.* 113.20 (Nov. 12, 2014), p. 205301. doi: [10.1103/PhysRevLett.113.205301](https://doi.org/10.1103/PhysRevLett.113.205301).
- [200] J. T. Devreese and A. S. Alexandrov. "Fröhlich Polaron and Bipolaron: Recent Developments". In: *Rep. Prog. Phys.* 72.6 (May 2009), p. 066501. issn: 0034-4885. doi: [10.1088/0034-4885/72/6/066501](https://doi.org/10.1088/0034-4885/72/6/066501).
- [201] A. S. Alexandrov and J. T. Devreese. *Advances in Polaron Physics*. Vol. 159. Springer, 2010.
- [202] M. Koschorreck et al. "Attractive and Repulsive Fermi Polarons in Two Dimensions". In: *Nature* 485.7400 (7400 May 2012), pp. 619–622. issn: 1476-4687. doi: [10.1038/nature11151](https://doi.org/10.1038/nature11151).
- [203] P. Massignan, M. Zaccanti, and G. M. Bruun. "Polarons, Dressed Molecules and Itinerant Ferromagnetism in Ultracold Fermi Gases". In: *Rep. Prog. Phys.* 77.3 (Feb. 2014), p. 034401. issn: 0034-4885. doi: [10.1088/0034-4885/77/3/034401](https://doi.org/10.1088/0034-4885/77/3/034401).
- [204] F. Grusdt and E. Demler. "New Theoretical Approaches to Bose Polarons". In: *Quantum Matter at Ultralow Temperatures*. IOS Press, 2016, pp. 325–411. doi: [10.3254/978-1-61499-694-1-325](https://doi.org/10.3254/978-1-61499-694-1-325).
- [205] F. Grusdt, G. E. Astrakharchik, and E. Demler. "Bose Polarons in Ultracold Atoms in One Dimension: Beyond the Fröhlich Paradigm". In: *New J. Phys.* 19.10 (Oct. 2017), p. 103035. issn: 1367-2630. doi: [10.1088/1367-2630/aa8a2e](https://doi.org/10.1088/1367-2630/aa8a2e).
- [206] F. Scazza et al. "Repulsive Fermi Polarons in a Resonant Mixture of Ultracold  $^6\text{Li}$  Atoms". In: *Phys. Rev. Lett.* 118.8 (Feb. 21, 2017), p. 083602. doi: [10.1103/PhysRevLett.118.083602](https://doi.org/10.1103/PhysRevLett.118.083602).
- [207] R. Schmidt et al. "Universal Many-Body Response of Heavy Impurities Coupled to a Fermi Sea: A Review of Recent Progress". In: *Rep. Prog. Phys.* 81.2 (Jan. 2018), p. 024401. issn: 0034-4885. doi: [10.1088/1361-6633/aa9593](https://doi.org/10.1088/1361-6633/aa9593).
- [208] K. Keiler, S. I. Mistakidis, and P. Schmelcher. "Polarons and Their Induced Interactions in Highly Imbalanced Triple Mixtures". In: *Phys. Rev. A* 104.3 (Sept. 7, 2021), p. L031301. doi: [10.1103/PhysRevA.104.L031301](https://doi.org/10.1103/PhysRevA.104.L031301).
- [209] T. Kasuya, A. Yanase, and T. Takeda. "Stability Condition for the Paramagnetic Polaron in a Magnetic Semiconductor". In: *Solid State Commun.* 8.19 (Oct. 1, 1970), pp. 1543–1546. issn: 0038-1098. doi: [10.1016/0038-1098\(70\)90604-6](https://doi.org/10.1016/0038-1098(70)90604-6).
- [210] A. Kaminski and S. Das Sarma. "Polaron Percolation in Diluted Magnetic Semiconductors". In: *Phys. Rev. Lett.* 88.24 (May 31, 2002), p. 247202. doi: [10.1103/PhysRevLett.88.247202](https://doi.org/10.1103/PhysRevLett.88.247202).
- [211] M. E. Gershenson, V. Podzorov, and A. F. Morpurgo. "Colloquium: Electronic Transport in Single-Crystal Organic Transistors". In: *Rev. Mod. Phys.* 78.3 (Sept. 29, 2006), pp. 973–989. doi: [10.1103/RevModPhys.78.973](https://doi.org/10.1103/RevModPhys.78.973).
- [212] C. Deibel, A. Wagenpfahl, and V. Dyakonov. "Origin of Reduced Polaron Recombination in Organic Semiconductor Devices". In: *Phys. Rev. B* 80.7 (Aug. 7, 2009), p. 075203. doi: [10.1103/PhysRevB.80.075203](https://doi.org/10.1103/PhysRevB.80.075203).

- 
- [213] A. S. Alexandrov and A. B. Krebs. "Polarons in High-Temperature Superconductors". In: *Sov. Phys. Uspekhi* 35.5 (May 31, 1992), p. 345. ISSN: 0038-5670. DOI: [10.1070/PU1992v035n05ABEH002235](https://doi.org/10.1070/PU1992v035n05ABEH002235).
- [214] E. K. H. Salje, A. S. Alexandrov, and W. Y. Liang. *Polarons and Bipolarons in High-Tc Superconductors and Related Materials*. July 1, 2005. ISBN: 978-0-511-59981-1. URL: <https://doi.org/10.1017/CB09780511599811>.
- [215] A. S. Alexandrov. *Polarons in Advanced Materials*. Springer Science & Business Media, Jan. 11, 2008. 678 pp. ISBN: 978-1-4020-6348-0.
- [216] S. T. Ruggiero. *Superconducting Devices*. Elsevier, July 10, 2013. 411 pp. ISBN: 978-0-323-15164-1.
- [217] G. Barontini et al. "Observation of Heteronuclear Atomic Efimov Resonances". In: *Phys. Rev. Lett.* 103.4 (July 20, 2009), p. 043201. DOI: [10.1103/PhysRevLett.103.043201](https://doi.org/10.1103/PhysRevLett.103.043201).
- [218] R. Pires et al. "Observation of Efimov Resonances in a Mixture with Extreme Mass Imbalance". In: *Phys. Rev. Lett.* 112.25 (June 25, 2014), p. 250404. DOI: [10.1103/PhysRevLett.112.250404](https://doi.org/10.1103/PhysRevLett.112.250404).
- [219] S.-K. Tung et al. "Geometric Scaling of Efimov States in a  ${}^6\text{Li}$ - ${}^{133}\text{Cs}$  Mixture". In: *Phys. Rev. Lett.* 113.24 (Dec. 9, 2014), p. 240402. DOI: [10.1103/PhysRevLett.113.240402](https://doi.org/10.1103/PhysRevLett.113.240402).
- [220] X. W. Guan et al. "Magnetic Phase Transitions in One-Dimensional Strongly Attractive Three-Component Ultracold Fermions". In: *Phys. Rev. Lett.* 100.20 (May 19, 2008), p. 200401. DOI: [10.1103/PhysRevLett.100.200401](https://doi.org/10.1103/PhysRevLett.100.200401).
- [221] T. B. Ottenstein et al. "Collisional Stability of a Three-Component Degenerate Fermi Gas". In: *Phys. Rev. Lett.* 101.20 (Nov. 14, 2008), p. 203202. DOI: [10.1103/PhysRevLett.101.203202](https://doi.org/10.1103/PhysRevLett.101.203202).
- [222] T. Ozawa and G. Baym. "Population Imbalance and Pairing in the BCS-BEC Crossover of Three-Component Ultracold Fermions". In: *Phys. Rev. A* 82.6 (Dec. 14, 2010), p. 063615. DOI: [10.1103/PhysRevA.82.063615](https://doi.org/10.1103/PhysRevA.82.063615).
- [223] A. Sotnikov and W. Hofstetter. "Magnetic Ordering of Three-Component Ultracold Fermionic Mixtures in Optical Lattices". In: *Phys. Rev. A* 89.6 (June 2, 2014), p. 063601. DOI: [10.1103/PhysRevA.89.063601](https://doi.org/10.1103/PhysRevA.89.063601).
- [224] I. Bloch, J. Dalibard, and S. Nascimbène. "Quantum Simulations with Ultracold Quantum Gases". In: *Nat. Phys.* 8.4 (Apr. 2012), pp. 267–276. ISSN: 1745-2481. DOI: [10/gcsjdc](https://doi.org/10/gcsjdc).
- [225] M. Lewenstein, A. Sanpera, and V. Ahufinger. *Ultracold Atoms in Optical Lattices: Simulating Quantum Many-Body Systems*. OUP Oxford, Mar. 8, 2012. 494 pp. ISBN: 978-0-19-162743-9.
- [226] C. Gross and I. Bloch. "Quantum Simulations with Ultracold Atoms in Optical Lattices". In: *Science* 357.6355 (Sept. 8, 2017), pp. 995–1001. DOI: [10.1126/science.aal3837](https://doi.org/10.1126/science.aal3837).
- [227] B. P. Anderson and M. A. Kasevich. "Macroscopic Quantum Interference from Atomic Tunnel Arrays". In: *Science* 282.5394 (Nov. 27, 1998), pp. 1686–1689. ISSN: 0036-8075, 1095-9203. DOI: [10/cvdhzt](https://doi.org/10/cvdhzt).
-

- [228] M. Lewenstein et al. “Ultracold Atomic Gases in Optical Lattices: Mimicking Condensed Matter Physics and Beyond”. In: *Adv. Phys.* 56.2 (Mar. 1, 2007), pp. 243–379. ISSN: 0001-8732. DOI: [10/bwdppg](https://doi.org/10/bwdppg).
- [229] I. Bloch, J. Dalibard, and W. Zwerger. “Many-Body Physics with Ultracold Gases”. In: *Rev. Mod. Phys.* 80.3 (July 2008), pp. 885–964. DOI: [10/d32c2r](https://doi.org/10/d32c2r).
- [230] G.-B. Jo et al. “Itinerant Ferromagnetism in a Fermi Gas of Ultracold Atoms”. In: *Science* 325.5947 (Sept. 18, 2009), pp. 1521–1524. ISSN: 0036-8075, 1095-9203. DOI: [10/bssjzn](https://doi.org/10/bssjzn).
- [231] J. Simon et al. “Quantum Simulation of Antiferromagnetic Spin Chains in an Optical Lattice”. In: *Nature* 472.7343 (2011), pp. 307–312.
- [232] G. Jotzu et al. “Experimental Realization of the Topological Haldane Model with Ultracold Fermions”. In: *Nature* 515.7526 (Nov. 2014), pp. 237–240. ISSN: 1476-4687. DOI: [10/f6p4rn](https://doi.org/10/f6p4rn).
- [233] N. Goldman, J. C. Budich, and P. Zoller. “Topological Quantum Matter with Ultracold Gases in Optical Lattices”. In: *Nat. Phys.* 12.7 (July 2016), pp. 639–645. ISSN: 1745-2481. DOI: [10/f8tsdw](https://doi.org/10/f8tsdw).
- [234] U. Schneider et al. “Metallic and Insulating Phases of Repulsively Interacting Fermions in a 3D Optical Lattice”. In: *Science* 322.5907 (Dec. 5, 2008), p. 1520. DOI: [10/c677d3](https://doi.org/10/c677d3).
- [235] D.-S. Lühmann, C. Weitenberg, and K. Sengstock. “Emulating Molecular Orbitals and Electronic Dynamics with Ultracold Atoms”. In: *Phys. Rev. X* 5.3 (Aug. 17, 2015), p. 031016. DOI: [10/gddjsp](https://doi.org/10/gddjsp).
- [236] S. Arlinghaus and M. Holthaus. “Driven Optical Lattices as Strong-Field Simulators”. In: *Phys. Rev. A* 81.6 (June 8, 2010), p. 063612. DOI: [10.1103/PhysRevA.81.063612](https://doi.org/10.1103/PhysRevA.81.063612).
- [237] S. V. Rajagopal et al. “Quantum Emulation of Extreme Non-Equilibrium Phenomena with Trapped Atoms”. In: *Ann. Phys.* 529.8 (2017), p. 1700008. ISSN: 1521-3889. DOI: [10/ghgth3](https://doi.org/10/ghgth3).
- [238] S. Sala, J. Förster, and A. Saenz. “Ultracold-Atom Quantum Simulator for Attosecond Science”. In: *Phys. Rev. A* 95.1 (Jan. 25, 2017), 011403(R). DOI: [10/gffmk3](https://doi.org/10/gffmk3).
- [239] R. Gerritsma et al. “Quantum Simulation of the Dirac Equation”. In: *Nature* 463.7277 (7277 Jan. 2010), pp. 68–71. ISSN: 1476-4687. DOI: [10.1038/nature08688](https://doi.org/10.1038/nature08688).
- [240] D. W. Zhang, Z. D. Wang, and S. L. Zhu. “Relativistic Quantum Effects of Dirac Particles Simulated by Ultracold Atoms”. In: *Front. Phys.* 7.1 (Feb. 1, 2012), pp. 31–53. ISSN: 2095-0470. DOI: [10.1007/s11467-011-0223-y](https://doi.org/10.1007/s11467-011-0223-y).
- [241] V. Kasper et al. “Schwinger Pair Production with Ultracold Atoms”. In: *Phys. Lett. B* 760 (Sept. 10, 2016), pp. 742–746. ISSN: 0370-2693. DOI: [10.1016/j.physletb.2016.07.036](https://doi.org/10.1016/j.physletb.2016.07.036).
- [242] Á. Rapp et al. “Color Superfluidity and “Baryon” Formation in Ultracold Fermions”. In: *Phys. Rev. Lett.* 98.16 (Apr. 18, 2007), p. 160405. DOI: [10.1103/PhysRevLett.98.160405](https://doi.org/10.1103/PhysRevLett.98.160405).
- [243] E. Zohar, J. I. Cirac, and B. Reznik. “Quantum Simulations of Lattice Gauge Theories Using Ultracold Atoms in Optical Lattices”. In: *Rep. Prog. Phys.* 79.1 (Dec. 2015), p. 014401. ISSN: 0034-4885. DOI: [10.1088/0034-4885/79/1/014401](https://doi.org/10.1088/0034-4885/79/1/014401).

- 
- [244] A. Gezerlis and J. Carlson. “Strongly Paired Fermions: Cold Atoms and Neutron Matter”. In: *Phys. Rev. C* 77.3 (Mar. 12, 2008), p. 032801. doi: [10.1103/PhysRevC.77.032801](https://doi.org/10.1103/PhysRevC.77.032801).
- [245] P. van Wyk et al. “Superfluid Fermi Atomic Gas as a Quantum Simulator for the Study of the Neutron-Star Equation of State in the Low-Density Region”. In: *Phys. Rev. A* 97.1 (Jan. 3, 2018), p. 013601. doi: [10.1103/PhysRevA.97.013601](https://doi.org/10.1103/PhysRevA.97.013601).
- [246] L. J. Garay et al. “Sonic Analog of Gravitational Black Holes in Bose-Einstein Condensates”. In: *Phys. Rev. Lett.* 85.22 (Nov. 27, 2000), pp. 4643–4647. doi: [10.1103/PhysRevLett.85.4643](https://doi.org/10.1103/PhysRevLett.85.4643).
- [247] J. Steinhauer. “Observation of Quantum Hawking Radiation and Its Entanglement in an Analogue Black Hole”. In: *Nat. Phys.* 12.10 (Oct. 2016), pp. 959–965. issn: 1745-2481. doi: [10/bn7r](https://doi.org/10/bn7r).
- [248] L. Amico et al. “Roadmap on Atomtronics: State of the Art and Perspective”. In: *AVS Quant. Sci.* 3.3 (Aug. 25, 2021), p. 039201. issn: 2639-0213. doi: [10.1116/5.0026178](https://doi.org/10.1116/5.0026178).
- [249] L. Amico et al. “Colloquium: Atomtronic Circuits: From Many-Body Physics to Quantum Technologies”. In: *Rev. Mod. Phys.* 94.4 (Nov. 18, 2022), p. 041001. doi: [10.1103/RevModPhys.94.041001](https://doi.org/10.1103/RevModPhys.94.041001).
- [250] N. R. Cooper, J. Dalibard, and I. B. Spielman. “Topological Bands for Ultracold Atoms”. In: *Rev. Mod. Phys.* 91.1 (Mar. 25, 2019), p. 015005. doi: [10.1103/RevModPhys.91.015005](https://doi.org/10.1103/RevModPhys.91.015005).
- [251] J. Ruostekoski, G. V. Dunne, and J. Javanainen. “Particle Number Fractionalization of an Atomic Fermi-Dirac Gas in an Optical Lattice”. In: *Phys. Rev. Lett.* 88.18 (Apr. 17, 2002), p. 180401. doi: [10.1103/PhysRevLett.88.180401](https://doi.org/10.1103/PhysRevLett.88.180401).
- [252] D. Jaksch and P. Zoller. “Creation of Effective Magnetic Fields in Optical Lattices: The Hofstadter Butterfly for Cold Neutral Atoms”. In: *New J. Phys.* 5.1 (May 2003), p. 56. issn: 1367-2630. doi: [10.1088/1367-2630/5/1/356](https://doi.org/10.1088/1367-2630/5/1/356).
- [253] F. Gerbier and J. Dalibard. “Gauge Fields for Ultracold Atoms in Optical Superlattices”. In: *New J. Phys.* 12.3 (Mar. 2010), p. 033007. issn: 1367-2630. doi: [10.1088/1367-2630/12/3/033007](https://doi.org/10.1088/1367-2630/12/3/033007).
- [254] N. Goldman et al. “Realistic Time-Reversal Invariant Topological Insulators with Neutral Atoms”. In: *Phys. Rev. Lett.* 105.25 (Dec. 16, 2010), p. 255302. doi: [10.1103/PhysRevLett.105.255302](https://doi.org/10.1103/PhysRevLett.105.255302).
- [255] X.-J. Liu, K. T. Law, and T. K. Ng. “Realization of 2D Spin-Orbit Interaction and Exotic Topological Orders in Cold Atoms”. In: *Phys. Rev. Lett.* 112.8 (Feb. 24, 2014), p. 086401. doi: [10.1103/PhysRevLett.112.086401](https://doi.org/10.1103/PhysRevLett.112.086401).
- [256] T. Dubček et al. “Weyl Points in Three-Dimensional Optical Lattices: Synthetic Magnetic Monopoles in Momentum Space”. In: *Phys. Rev. Lett.* 114.22 (June 3, 2015), p. 225301. doi: [10.1103/PhysRevLett.114.225301](https://doi.org/10.1103/PhysRevLett.114.225301).
- [257] Z. Wu et al. “Realization of Two-Dimensional Spin-Orbit Coupling for Bose-Einstein Condensates”. In: *Science* 354.6308 (Oct. 7, 2016), pp. 83–88. doi: [10.1126/science.aaf6689](https://doi.org/10.1126/science.aaf6689).
-

- [258] A. Dauphin, M. Müller, and M. A. Martin-Delgado. “Rydberg-Atom Quantum Simulation and Chern-number Characterization of a Topological Mott Insulator”. In: *Phys. Rev. A* 86.5 (Nov. 20, 2012), p. 053618. doi: [10.1103/PhysRevA.86.053618](https://doi.org/10.1103/PhysRevA.86.053618).
- [259] K. Sun et al. “Topological Semimetal in a Fermionic Optical Lattice”. In: *Nat. Phys.* 8.1 (1 Jan. 2012), pp. 67–70. issn: 1745-2481. doi: [10.1038/nphys2134](https://doi.org/10.1038/nphys2134).
- [260] N. Y. Yao et al. “Topological Flat Bands from Dipolar Spin Systems”. In: *Phys. Rev. Lett.* 109.26 (Dec. 26, 2012), p. 266804. doi: [10.1103/PhysRevLett.109.266804](https://doi.org/10.1103/PhysRevLett.109.266804).
- [261] A. Celi et al. “Synthetic Gauge Fields in Synthetic Dimensions”. In: *Phys. Rev. Lett.* 112.4 (Jan. 28, 2014), p. 043001. doi: [10.1103/PhysRevLett.112.043001](https://doi.org/10.1103/PhysRevLett.112.043001).
- [262] M. Mancini et al. “Observation of Chiral Edge States with Neutral Fermions in Synthetic Hall Ribbons”. In: *Science* 349.6255 (Sept. 25, 2015), pp. 1510–1513. doi: [10.1126/science.aaa8736](https://doi.org/10.1126/science.aaa8736).
- [263] B. K. Stuhl et al. “Visualizing Edge States with an Atomic Bose Gas in the Quantum Hall Regime”. In: *Science* 349.6255 (Sept. 25, 2015), pp. 1514–1518. doi: [10.1126/science.aaa8515](https://doi.org/10.1126/science.aaa8515).
- [264] H. M. Price et al. “Four-Dimensional Quantum Hall Effect with Ultracold Atoms”. In: *Phys. Rev. Lett.* 115.19 (Nov. 3, 2015), p. 195303. doi: [10.1103/PhysRevLett.115.195303](https://doi.org/10.1103/PhysRevLett.115.195303).
- [265] T. Oka and H. Aoki. “Photovoltaic Hall Effect in Graphene”. In: *Phys. Rev. B* 79.8 (Feb. 23, 2009), p. 081406. doi: [10.1103/PhysRevB.79.081406](https://doi.org/10.1103/PhysRevB.79.081406).
- [266] T. Kitagawa et al. “Topological Characterization of Periodically Driven Quantum Systems”. In: *Phys. Rev. B* 82.23 (Dec. 10, 2010), p. 235114. doi: [10.1103/PhysRevB.82.235114](https://doi.org/10.1103/PhysRevB.82.235114).
- [267] N. H. Lindner, G. Refael, and V. Galitski. “Floquet Topological Insulator in Semiconductor Quantum Wells”. In: *Nat. Phys.* 7.6 (6 June 2011), pp. 490–495. issn: 1745-2481. doi: [10.1038/nphys1926](https://doi.org/10.1038/nphys1926).
- [268] J. Struck et al. “Engineering Ising-XY Spin-Models in a Triangular Lattice Using Tunable Artificial Gauge Fields”. In: *Nat. Phys.* 9.11 (11 Nov. 2013), pp. 738–743. issn: 1745-2481. doi: [10.1038/nphys2750](https://doi.org/10.1038/nphys2750).
- [269] W. Zheng and H. Zhai. “Floquet Topological States in Shaking Optical Lattices”. In: *Phys. Rev. A* 89.6 (June 27, 2014), p. 061603. doi: [10.1103/PhysRevA.89.061603](https://doi.org/10.1103/PhysRevA.89.061603).
- [270] H. M. Price, T. Ozawa, and N. Goldman. “Synthetic Dimensions for Cold Atoms from Shaking a Harmonic Trap”. In: *Phys. Rev. A* 95.2 (Feb. 9, 2017), p. 023607. doi: [10.1103/PhysRevA.95.023607](https://doi.org/10.1103/PhysRevA.95.023607).
- [271] L. Pezzè et al. “Quantum Metrology with Nonclassical States of Atomic Ensembles”. In: *Rev. Mod. Phys.* 90.3 (Sept. 5, 2018), p. 035005. doi: [10.1103/RevModPhys.90.035005](https://doi.org/10.1103/RevModPhys.90.035005).
- [272] C. Freier et al. “Mobile Quantum Gravity Sensor with Unprecedented Stability”. In: *J. Phys.: Conf. Ser.* 723.1 (June 2016), p. 012050. issn: 1742-6596. doi: [10.1088/1742-6596/723/1/012050](https://doi.org/10.1088/1742-6596/723/1/012050).

- 
- [273] V. Ménoret et al. “Gravity Measurements below  $10^{-9}$ g with a Transportable Absolute Quantum Gravimeter”. In: *Sci. Rep.* 8.1 (1 Aug. 17, 2018), p. 12300. issn: 2045-2322. doi: [10.1038/s41598-018-30608-1](https://doi.org/10.1038/s41598-018-30608-1).
- [274] K. W. Murch et al. “Observation of Quantum-Measurement Backaction with an Ultracold Atomic Gas”. In: *Nat. Phys.* 4.7 (7 July 2008), pp. 561–564. issn: 1745-2481. doi: [10.1038/nphys965](https://doi.org/10.1038/nphys965).
- [275] J. J. Cooper, D. W. Hallwood, and J. A. Dunningham. “Entanglement-Enhanced Atomic Gyroscope”. In: *Phys. Rev. A* 81.4 (Apr. 22, 2010), p. 043624. doi: [10.1103/PhysRevA.81.043624](https://doi.org/10.1103/PhysRevA.81.043624).
- [276] D. Budker and M. Romalis. “Optical Magnetometry”. In: *Nat. Phys.* 3.4 (4 Apr. 2007), pp. 227–234. issn: 1745-2481. doi: [10.1038/nphys566](https://doi.org/10.1038/nphys566).
- [277] H. Fan et al. “Atom Based RF Electric Field Sensing”. In: *J. Phys. B: At. Mol. Opt. Phys.* 48.20 (Sept. 2015), p. 202001. issn: 0953-4075. doi: [10.1088/0953-4075/48/20/202001](https://doi.org/10.1088/0953-4075/48/20/202001).
- [278] C. W. Oates, E. A. Curtis, and L. Hollberg. “Improved Short-Term Stability of Optical Frequency Standards: Approaching 1 Hz in 1 s with the Ca Standard at 657 Nm”. In: *Opt. Lett.* 25.21 (Nov. 1, 2000), pp. 1603–1605. issn: 1539-4794. doi: [10.1364/OL.25.001603](https://doi.org/10.1364/OL.25.001603).
- [279] G. Wilpers et al. “Optical Clock with Ultracold Neutral Atoms”. In: *Phys. Rev. Lett.* 89.23 (Nov. 15, 2002), p. 230801. doi: [10.1103/PhysRevLett.89.230801](https://doi.org/10.1103/PhysRevLett.89.230801).
- [280] M. Takamoto et al. “An Optical Lattice Clock”. In: *Nature* 435.7040 (7040 May 2005), pp. 321–324. issn: 1476-4687. doi: [10.1038/nature03541](https://doi.org/10.1038/nature03541).
- [281] I. Bloch. “Quantum Coherence and Entanglement with Ultracold Atoms in Optical Lattices”. In: *Nature* 453.7198 (7198 June 2008), pp. 1016–1022. issn: 1476-4687. doi: [10.1038/nature07126](https://doi.org/10.1038/nature07126).
- [282] T. Gallagher. “Rydberg Atoms”. In: *Springer Handbook of Atomic, Molecular, and Optical Physics*. Ed. by G. Drake. Springer Handbooks. New York, NY: Springer, 2006, pp. 235–245. isbn: 978-0-387-26308-3. doi: [10.1007/978-0-387-26308-3\\_14](https://doi.org/10.1007/978-0-387-26308-3_14).
- [283] F. B. Dunning et al. “Engineering Atomic Rydberg States with Pulsed Electric Fields”. In: *J. Phys. B: At. Mol. Opt. Phys.* 42.2 (Jan. 2009), p. 022001. issn: 0953-4075. doi: [10.1088/0953-4075/42/2/022001](https://doi.org/10.1088/0953-4075/42/2/022001).
- [284] S. V. Stepkin et al. “Radio Recombination Lines from the Largest Bound Atoms in Space”. In: *Mon. Not. R. Astron. Soc.* 374.3 (Jan. 21, 2007), pp. 852–856. issn: 0035-8711. doi: [10.1111/j.1365-2966.2006.11190.x](https://doi.org/10.1111/j.1365-2966.2006.11190.x).
- [285] A. Browaeys and T. Lahaye. “Many-Body Physics with Individually Controlled Rydberg Atoms”. In: *Nat. Phys.* 16.2 (2 Feb. 2020), pp. 132–142. issn: 1745-2481. doi: [10.1038/s41567-019-0733-z](https://doi.org/10.1038/s41567-019-0733-z).
- [286] E. Amaldi and E. Segrè. “Effect of Pressure on High Terms of Alkaline Spectra”. In: *Nature* 133.3352 (3352 Jan. 1934), pp. 141–141. issn: 1476-4687. doi: [10.1038/133141a0](https://doi.org/10.1038/133141a0).
- [287] E. Amaldi and E. Segrè. “Effetto della Pressione Sui Termini Elevati Degli Alcalini”. In: *Nuovo Cimento* 11.3 (Mar. 1, 1934), pp. 145–156. issn: 1827-6121. doi: [10.1007/BF02959828](https://doi.org/10.1007/BF02959828).
-

- [288] M. Gross et al. "Maser Oscillation and Microwave Superradiance in Small Systems of Rydberg Atoms". In: *Phys. Rev. Lett.* 43.5 (July 30, 1979), pp. 343–346. doi: [10.1103/PhysRevLett.43.343](https://doi.org/10.1103/PhysRevLett.43.343).
- [289] P. Goy et al. "Observation of Cavity-Enhanced Single-Atom Spontaneous Emission". In: *Phys. Rev. Lett.* 50.24 (June 13, 1983), pp. 1903–1906. doi: [10.1103/PhysRevLett.50.1903](https://doi.org/10.1103/PhysRevLett.50.1903).
- [290] M. Hugon et al. "Collisional Properties of Highly Excited Rubidium Atoms". In: *J. Phys. B: Atom. Mol. Phys.* 12.16 (Aug. 1979), p. 2707. issn: 0022-3700. doi: [10.1088/0022-3700/12/16/017](https://doi.org/10.1088/0022-3700/12/16/017).
- [291] A. N. Klucharev, A. V. Lazarenko, and V. Vujnovic. "The Ionisation Rate Coefficients of Radiatively Excited Rubidium Atoms  $\text{Rb}(n^2\text{P}) + \text{Rb}(5^2\text{S})$ ". In: *J. Phys. B: Atom. Mol. Phys.* 13.6 (Mar. 1980), p. 1143. issn: 0022-3700. doi: [10.1088/0022-3700/13/6/019](https://doi.org/10.1088/0022-3700/13/6/019).
- [292] M. Cheret et al. "Penning and Associative Ionisation of Highly Excited Rubidium Atoms". In: *J. Phys. B: Atom. Mol. Phys.* 15.19 (Oct. 1982), p. 3463. issn: 0022-3700. doi: [10.1088/0022-3700/15/19/015](https://doi.org/10.1088/0022-3700/15/19/015).
- [293] L. Barbier and M. Cheret. "Experimental Study of Penning and Hornbeck-Molnar Ionisation of Rubidium Atoms Excited in a High s or d Level ( $5d \leq n_l \leq 11s$ )". In: *J. Phys. B: Atom. Mol. Phys.* 20.6 (Mar. 1987), p. 1229. issn: 0022-3700. doi: [10.1088/0022-3700/20/6/011](https://doi.org/10.1088/0022-3700/20/6/011).
- [294] I. L. Beigman and V. S. Lebedev. "Collision Theory of Rydberg Atoms with Neutral and Charged Particles". In: *Phys. Rep.* 250.3 (Jan. 1, 1995), pp. 95–328. issn: 0370-1573. doi: [10.1016/0370-1573\(95\)00074-Q](https://doi.org/10.1016/0370-1573(95)00074-Q).
- [295] S. Haroche. "Nobel Lecture: Controlling Photons in a Box and Exploring the Quantum to Classical Boundary". In: *Rev. Mod. Phys.* 85.3 (July 12, 2013), pp. 1083–1102. doi: [10.1103/RevModPhys.85.1083](https://doi.org/10.1103/RevModPhys.85.1083).
- [296] D. Jaksch et al. "Fast Quantum Gates for Neutral Atoms". In: *Phys. Rev. Lett.* 85.10 (Sept. 4, 2000), pp. 2208–2211. doi: [10.1103/PhysRevLett.85.2208](https://doi.org/10.1103/PhysRevLett.85.2208).
- [297] M. D. Lukin et al. "Dipole Blockade and Quantum Information Processing in Mesoscopic Atomic Ensembles". In: *Phys. Rev. Lett.* 87.3 (June 26, 2001), p. 037901. doi: [10.1103/PhysRevLett.87.037901](https://doi.org/10.1103/PhysRevLett.87.037901).
- [298] K. Singer et al. "Suppression of Excitation and Spectral Broadening Induced by Interactions in a Cold Gas of Rydberg Atoms". In: *Phys. Rev. Lett.* 93.16 (Oct. 13, 2004), p. 163001. doi: [10.1103/PhysRevLett.93.163001](https://doi.org/10.1103/PhysRevLett.93.163001).
- [299] D. Tong et al. "Local Blockade of Rydberg Excitation in an Ultracold Gas". In: *Phys. Rev. Lett.* 93.6 (Aug. 3, 2004), p. 063001. doi: [10.1103/PhysRevLett.93.063001](https://doi.org/10.1103/PhysRevLett.93.063001).
- [300] T. C. Liebisch et al. "Atom Counting Statistics in Ensembles of Interacting Rydberg Atoms". In: *Phys. Rev. Lett.* 95.25 (Dec. 13, 2005), p. 253002. doi: [10.1103/PhysRevLett.95.253002](https://doi.org/10.1103/PhysRevLett.95.253002).
- [301] E. Urban et al. "Observation of Rydberg Blockade between Two Atoms". In: *Nat. Phys.* 5.2 (2 Feb. 2009), pp. 110–114. issn: 1745-2481. doi: [10.1038/nphys1178](https://doi.org/10.1038/nphys1178).
- [302] P. Schauß et al. "Observation of Spatially Ordered Structures in a Two-Dimensional Rydberg Gas". In: *Nature* 491.7422 (7422 Nov. 2012), pp. 87–91. issn: 1476-4687. doi: [10.1038/nature11596](https://doi.org/10.1038/nature11596).



- 
- [303] L. Santos et al. “Bose-Einstein Condensation in Trapped Dipolar Gases”. In: *Phys. Rev. Lett.* 85.9 (Aug. 28, 2000), pp. 1791–1794. doi: [10.1103/PhysRevLett.85.1791](https://doi.org/10.1103/PhysRevLett.85.1791).
- [304] J. Honer et al. “Collective Many-Body Interaction in Rydberg Dressed Atoms”. In: *Phys. Rev. Lett.* 105.16 (Oct. 15, 2010), p. 160404. doi: [10.1103/PhysRevLett.105.160404](https://doi.org/10.1103/PhysRevLett.105.160404).
- [305] T. Wilk et al. “Entanglement of Two Individual Neutral Atoms Using Rydberg Blockade”. In: *Phys. Rev. Lett.* 104.1 (Jan. 8, 2010), p. 010502. doi: [10.1103/PhysRevLett.104.010502](https://doi.org/10.1103/PhysRevLett.104.010502).
- [306] J. B. Balewski et al. “Rydberg Dressing: Understanding of Collective Many-Body Effects and Implications for Experiments”. In: *New J. Phys.* 16.6 (June 2014), p. 063012. ISSN: 1367-2630. doi: [10.1088/1367-2630/16/6/063012](https://doi.org/10.1088/1367-2630/16/6/063012).
- [307] Y.-Y. Jau et al. “Entangling Atomic Spins with a Rydberg-dressed Spin-Flip Blockade”. In: *Nature Phys* 12.1 (1 Jan. 2016), pp. 71–74. ISSN: 1745-2481. doi: [10.1038/nphys3487](https://doi.org/10.1038/nphys3487).
- [308] J. Zeiher et al. “Many-Body Interferometry of a Rydberg-dressed Spin Lattice”. In: *Nature Phys* 12.12 (12 Dec. 2016), pp. 1095–1099. ISSN: 1745-2481. doi: [10.1038/nphys3835](https://doi.org/10.1038/nphys3835).
- [309] C. H. Greene, A. S. Dickinson, and H. R. Sadeghpour. “Creation of Polar and Non-polar Ultra-Long-Range Rydberg Molecules”. In: *Phys. Rev. Lett.* 85.12 (Sept. 18, 2000), pp. 2458–2461. doi: [10.1103/PhysRevLett.85.2458](https://doi.org/10.1103/PhysRevLett.85.2458).
- [310] V. Bendkowsky et al. “Observation of Ultralong-Range Rydberg Molecules”. In: *Nature* 458.7241 (7241 Apr. 2009), pp. 1005–1008. ISSN: 1476-4687. doi: [10.1038/nature07945](https://doi.org/10.1038/nature07945).
- [311] V. Bendkowsky et al. “Rydberg Trimers and Excited Dimers Bound by Internal Quantum Reflection”. In: *Phys. Rev. Lett.* 105.16 (Oct. 12, 2010), p. 163201. doi: [10.1103/PhysRevLett.105.163201](https://doi.org/10.1103/PhysRevLett.105.163201).
- [312] W. Li et al. “A Homonuclear Molecule with a Permanent Electric Dipole Moment”. In: *Science* 334.6059 (Nov. 25, 2011), pp. 1110–1114. doi: [10.1126/science.1211255](https://doi.org/10.1126/science.1211255).
- [313] C. Fey, F. Hummel, and P. Schmelcher. “Ultralong-Range Rydberg Molecules”. In: *Mol. Phys.* 118.2 (Jan. 17, 2020), e1679401. ISSN: 0026-8976. doi: [10.1080/00268976.2019.1679401](https://doi.org/10.1080/00268976.2019.1679401).
- [314] C. L. Degen, F. Reinhard, and P. Cappellaro. “Quantum Sensing”. In: *Rev. Mod. Phys.* 89.3 (July 25, 2017), p. 035002. doi: [10.1103/RevModPhys.89.035002](https://doi.org/10.1103/RevModPhys.89.035002).
- [315] M. Saffman and T. G. Walker. “Creating Single-Atom and Single-Photon Sources from Entangled Atomic Ensembles”. In: *Phys. Rev. A* 66.6 (Dec. 16, 2002), p. 065403. doi: [10.1103/PhysRevA.66.065403](https://doi.org/10.1103/PhysRevA.66.065403).
- [316] J. Honer et al. “Artificial Atoms Can Do More Than Atoms: Deterministic Single Photon Subtraction from Arbitrary Light Fields”. In: *Phys. Rev. Lett.* 107.9 (Aug. 25, 2011), p. 093601. doi: [10.1103/PhysRevLett.107.093601](https://doi.org/10.1103/PhysRevLett.107.093601).
- [317] S. Baur et al. “Single-Photon Switch Based on Rydberg Blockade”. In: *Phys. Rev. Lett.* 112.7 (Feb. 18, 2014), p. 073901. doi: [10.1103/PhysRevLett.112.073901](https://doi.org/10.1103/PhysRevLett.112.073901).
-

- [318] H. Gorniaczyk et al. “Single-Photon Transistor Mediated by Interstate Rydberg Interactions”. In: *Phys. Rev. Lett.* 113.5 (July 28, 2014), p. 053601. doi: [10.1103/PhysRevLett.113.053601](https://doi.org/10.1103/PhysRevLett.113.053601).
- [319] O. Firstenberg, C. S. Adams, and S. Hofferberth. “Nonlinear Quantum Optics Mediated by Rydberg Interactions”. In: *J. Phys. B: At. Mol. Opt. Phys.* 49.15 (June 2016), p. 152003. issn: 0953-4075. doi: [10.1088/0953-4075/49/15/152003](https://doi.org/10.1088/0953-4075/49/15/152003).
- [320] T. M. Graham et al. “Rydberg-Mediated Entanglement in a Two-Dimensional Neutral Atom Qubit Array”. In: *Phys. Rev. Lett.* 123.23 (Dec. 4, 2019), p. 230501. doi: [10.1103/PhysRevLett.123.230501](https://doi.org/10.1103/PhysRevLett.123.230501).
- [321] D. Tiarks et al. “A Photon–Photon Quantum Gate Based on Rydberg Interactions”. In: *Nat. Phys.* 15.2 (2 Feb. 2019), pp. 124–126. issn: 1745-2481. doi: [10.1038/s41567-018-0313-7](https://doi.org/10.1038/s41567-018-0313-7).
- [322] J. L. O’Brien, A. Furusawa, and J. Vučković. “Photonic Quantum Technologies”. In: *Nat. Photonics* 3.12 (12 Dec. 2009), pp. 687–695. issn: 1749-4893. doi: [10.1038/nphoton.2009.229](https://doi.org/10.1038/nphoton.2009.229).
- [323] A. Aspuru-Guzik and P. Walther. “Photonic Quantum Simulators”. In: *Nat. Phys.* 8.4 (4 Apr. 2012), pp. 285–291. issn: 1745-2481. doi: [10.1038/nphys2253](https://doi.org/10.1038/nphys2253).
- [324] S. Slussarenko and G. J. Pryde. “Photonic Quantum Information Processing: A Concise Review”. In: *Appl. Phys. Rev.* 6.4 (Oct. 14, 2019), p. 041303. issn: 1931-9401. doi: [10.1063/1.5115814](https://doi.org/10.1063/1.5115814).
- [325] H. Weimer et al. “A Rydberg Quantum Simulator”. In: *Nat. Phys.* 6.5 (5 May 2010), pp. 382–388. issn: 1745-2481. doi: [10.1038/nphys1614](https://doi.org/10.1038/nphys1614).
- [326] L. Henriët et al. “Quantum Computing with Neutral Atoms”. In: *Quantum* 4 (Sept. 21, 2020), p. 327. doi: [10.22331/q-2020-09-21-327](https://doi.org/10.22331/q-2020-09-21-327).
- [327] W. Li. “A Boost to Rydberg Quantum Computing”. In: *Nat. Phys.* 16.8 (8 Aug. 2020), pp. 820–821. issn: 1745-2481. doi: [10.1038/s41567-020-0907-8](https://doi.org/10.1038/s41567-020-0907-8).
- [328] M. F. Serret, B. Marchand, and T. Ayrál. “Solving Optimization Problems with Rydberg Analog Quantum Computers: Realistic Requirements for Quantum Advantage Using Noisy Simulation and Classical Benchmarks”. In: *Phys. Rev. A* 102.5 (Nov. 23, 2020), p. 052617. doi: [10/gfq6tx](https://doi.org/10/gfq6tx).
- [329] M. Morgado and S. Whitlock. “Quantum Simulation and Computing with Rydberg-interacting Qubits”. In: *AVS Quantum Science* 3.2 (May 3, 2021), p. 023501. issn: 2639-0213. doi: [10.1116/5.0036562](https://doi.org/10.1116/5.0036562).
- [330] H. Labuhn et al. “Tunable Two-Dimensional Arrays of Single Rydberg Atoms for Realizing Quantum Ising Models”. In: *Nature (London)* 534.7609 (7609 June 2016), pp. 667–670. issn: 1476-4687. doi: [10.1038/nature18274](https://doi.org/10.1038/nature18274).
- [331] H. Bernien et al. “Probing Many-Body Dynamics on a 51-Atom Quantum Simulator”. In: *Nature* 551.7682 (7682 Nov. 2017), pp. 579–584. issn: 1476-4687. doi: [10.1038/nature24622](https://doi.org/10.1038/nature24622).
- [332] K.-N. Schymik et al. “Enhanced Atom-by-Atom Assembly of Arbitrary Tweezer Arrays”. In: *Phys. Rev. A* 102.6 (Dec. 10, 2020), p. 063107. doi: [10/gj9xvv](https://doi.org/10/gj9xvv).
- [333] D. Bluvstein et al. “Controlling Quantum Many-Body Dynamics in Driven Rydberg Atom Arrays”. In: *Science* 371.6536 (Mar. 26, 2021), pp. 1355–1359. doi: [10.1126/science.abg2530](https://doi.org/10.1126/science.abg2530).

- 
- [334] S. Ebadi et al. “Quantum Phases of Matter on a 256-Atom Programmable Quantum Simulator”. In: *Nature* 595.7866 (7866 July 2021), pp. 227–232. ISSN: 1476-4687. DOI: [10.1038/s41586-021-03582-4](https://doi.org/10.1038/s41586-021-03582-4).
- [335] P. Scholl et al. “Quantum Simulation of 2D Antiferromagnets with Hundreds of Rydberg Atoms”. In: *Nature* 595.7866 (7866 July 2021), pp. 233–238. ISSN: 1476-4687. DOI: [10.1038/s41586-021-03585-1](https://doi.org/10.1038/s41586-021-03585-1).
- [336] S. Ebadi et al. “Quantum Optimization of Maximum Independent Set Using Rydberg Atom Arrays”. In: *Science* 376.6598 (June 10, 2022), pp. 1209–1215. DOI: [10.1126/science.abo6587](https://doi.org/10.1126/science.abo6587).
- [337] E. Farhi, J. Goldstone, and S. Gutmann. “A Quantum Approximate Optimization Algorithm”. Nov. 14, 2014. URL: <http://arxiv.org/abs/1411.4028>.
- [338] A. W. Glaetzle et al. “Quantum Spin-Ice and Dimer Models with Rydberg Atoms”. In: *Phys. Rev. X* 4.4 (Nov. 25, 2014), p. 041037. DOI: [10.1103/PhysRevX.4.041037](https://doi.org/10.1103/PhysRevX.4.041037).
- [339] M. Marcuzzi et al. “Facilitation Dynamics and Localization Phenomena in Rydberg Lattice Gases with Position Disorder”. In: *Phys. Rev. Lett.* 118.6 (Feb. 10, 2017), p. 063606. DOI: [10.1103/PhysRevLett.118.063606](https://doi.org/10.1103/PhysRevLett.118.063606).
- [340] T. L. Nguyen et al. “Towards Quantum Simulation with Circular Rydberg Atoms”. In: *Phys. Rev. X* 8.1 (Feb. 26, 2018), p. 011032. DOI: [10.1103/PhysRevX.8.011032](https://doi.org/10.1103/PhysRevX.8.011032).
- [341] A. Signoles et al. “Glassy Dynamics in a Disordered Heisenberg Quantum Spin System”. In: *Phys. Rev. X* 11.1 (Jan. 19, 2021), p. 011011. DOI: [10.1103/PhysRevX.11.011011](https://doi.org/10.1103/PhysRevX.11.011011).
- [342] G. Lindblad. “On the Generators of Quantum Dynamical Semigroups”. In: *Commun. Math. Phys.* 48.2 (June 1, 1976), pp. 119–130. ISSN: 1432-0916. DOI: [10.1007/BF01608499](https://doi.org/10.1007/BF01608499).
- [343] V. Gorini, A. Kossakowski, and E. C. G. Sudarshan. “Completely Positive Dynamical Semigroups of N-level Systems”. In: *J. Math. Phys.* 17.5 (May 1976), pp. 821–825. ISSN: 0022-2488. DOI: [10.1063/1.522979](https://doi.org/10.1063/1.522979).
- [344] H.-P. Breuer. *The Theory of Open Quantum Systems*. Oxford: Oxford University Press, USA, Mar. 29, 2007. 636 pp. ISBN: 978-0-19-921390-0.
- [345] H. Pichler, A. J. Daley, and P. Zoller. “Nonequilibrium Dynamics of Bosonic Atoms in Optical Lattices: Decoherence of Many-Body States Due to Spontaneous Emission”. In: *Phys. Rev. A* 82.6 (Dec. 6, 2010), p. 063605. DOI: [10.1103/PhysRevA.82.063605](https://doi.org/10.1103/PhysRevA.82.063605).
- [346] M. Müller et al. “Engineered Open Systems and Quantum Simulations with Atoms and Ions”. In: *Advances In Atomic, Molecular, and Optical Physics*. Ed. by P. Berman, E. Arimondo, and C. Lin. Vol. 61. Advances in Atomic, Molecular, and Optical Physics. Academic Press, July 1, 2012, pp. 1–80. DOI: [10.1016/B978-0-12-396482-3.00001-6](https://doi.org/10.1016/B978-0-12-396482-3.00001-6).
- [347] E. Schrödinger. “An Undulatory Theory of the Mechanics of Atoms and Molecules”. In: *Phys. Rev.* 28.6 (Dec. 1, 1926), pp. 1049–1070. DOI: [10.1103/PhysRev.28.1049](https://doi.org/10.1103/PhysRev.28.1049).
- [348] C. Gogolin and J. Eisert. “Equilibration, Thermalisation, and the Emergence of Statistical Mechanics in Closed Quantum Systems”. In: *Rep. Prog. Phys.* 79.5 (Apr. 2016), p. 056001. ISSN: 0034-4885. DOI: [10.1088/0034-4885/79/5/056001](https://doi.org/10.1088/0034-4885/79/5/056001).
-

- [349] N. Khaneja et al. "Optimal Control of Coupled Spin Dynamics: Design of NMR Pulse Sequences by Gradient Ascent Algorithms". In: *J. Magn. Reson.* 172.2 (Feb. 1, 2005), pp. 296–305. ISSN: 1090-7807. DOI: [10.1016/j.jmr.2004.11.004](https://doi.org/10.1016/j.jmr.2004.11.004).
- [350] A. Omran et al. "Generation and Manipulation of Schrödinger Cat States in Rydberg Atom Arrays". In: *Science* 365.6453 (Aug. 9, 2019), pp. 570–574. DOI: [10.1126/science.aax9743](https://doi.org/10.1126/science.aax9743).
- [351] L. Pitaevskii and S. Stringari. *Bose-Einstein Condensation*. 1st ed. International Series of Monographs on Physics 116. Oxford: Oxford University Press, 2003. 382 pp. ISBN: 0-19-850719-4.
- [352] K. Huang and C. N. Yang. "Quantum-Mechanical Many-Body Problem with Hard-Sphere Interaction". In: *Phys. Rev.* 105.3 (Feb. 1, 1957), pp. 767–775. DOI: [10.1103/PhysRev.105.767](https://doi.org/10.1103/PhysRev.105.767).
- [353] T. Busch et al. "Two Cold Atoms in a Harmonic Trap". In: *Found. Phys.* 28.4 (Apr. 1, 1998), pp. 549–559. ISSN: 1572-9516. DOI: [10.1023/A:1018705520999](https://doi.org/10.1023/A:1018705520999).
- [354] M. Olshanii and L. Pricoupenko. "Rigorous Approach to the Problem of Ultraviolet Divergencies in Dilute Bose Gases". In: *Phys. Rev. Lett.* 88.1 (Dec. 17, 2001), p. 010402. DOI: [10.1103/PhysRevLett.88.010402](https://doi.org/10.1103/PhysRevLett.88.010402).
- [355] Y. Castin. "Bose-Einstein Condensates in Atomic Gases: Simple Theoretical Results". In: *Coherent Atomic Matter Waves: 27 July–27 August 1999*. Springer, 2002, pp. 1–136. URL: [https://link.springer.com/chapter/10.1007/3-540-45338-5\\_1](https://link.springer.com/chapter/10.1007/3-540-45338-5_1).
- [356] A. Derevianko. "Revised Huang-Yang Multipolar Pseudopotential". In: *Phys. Rev. A* 72.4 (Oct. 5, 2005), p. 044701. DOI: [10.1103/PhysRevA.72.044701](https://doi.org/10.1103/PhysRevA.72.044701).
- [357] R. Stock et al. "Generalized Pseudopotentials for Higher Partial Wave Scattering". In: *Phys. Rev. Lett.* 94.2 (Jan. 19, 2005), p. 023202. DOI: [10.1103/PhysRevLett.94.023202](https://doi.org/10.1103/PhysRevLett.94.023202).
- [358] Z. Idziaszek and T. Calarco. "Analytical Solutions for the Dynamics of Two Trapped Interacting Ultracold Atoms". In: *Phys. Rev. A* 74.2 (Aug. 8, 2006), p. 022712. DOI: [10.1103/PhysRevA.74.022712](https://doi.org/10.1103/PhysRevA.74.022712).
- [359] A. Farrell and B. P. van Zyl. "S-Wave Scattering and the Zero-Range Limit of the Finite Square Well in Arbitrary Dimensions". In: *Can. J. Phys.* 88.11 (Nov. 2010), pp. 817–824. ISSN: 0008-4204. DOI: [10.1139/P10-061](https://doi.org/10.1139/P10-061).
- [360] E. H. Lieb and W. Liniger. "Exact Analysis of an Interacting Bose Gas. I. The General Solution and the Ground State". In: *Phys. Rev.* 130.4 (May 15, 1963), pp. 1605–1616. DOI: [10/dhgb9j](https://doi.org/10/dhgb9j).
- [361] E. H. Lieb. "Exact Analysis of an Interacting Bose Gas. II. The Excitation Spectrum". In: *Phys. Rev.* 130.4 (May 15, 1963), pp. 1616–1624. DOI: [10/b2n7sm](https://doi.org/10/b2n7sm).
- [362] H. Bethe. "Zur Theorie der Metalle". In: *Z. Phys.* 71.3 (Mar. 1, 1931), pp. 205–226. ISSN: 0044-3328. DOI: [10.1007/BF01341708](https://doi.org/10.1007/BF01341708).
- [363] T. C. Dorlas. "Orthogonality and Completeness of the Bethe Ansatz Eigenstates of the Nonlinear Schroedinger Model". In: *Commun. Math. Phys.* 154.2 (June 1, 1993), pp. 347–376. ISSN: 1432-0916. DOI: [10.1007/BF02097001](https://doi.org/10.1007/BF02097001).

- 
- [364] V. Y. Pan and Z. Q. Chen. “The Complexity of the Matrix Eigenproblem”. In: *Proceedings of the Thirty-First Annual ACM Symposium on Theory of Computing*. STOC '99. New York, NY, USA: Association for Computing Machinery, May 1, 1999, pp. 507–516. ISBN: 978-1-58113-067-6. DOI: [10.1145/301250.301389](https://doi.org/10.1145/301250.301389).
- [365] W. H. Press et al. *Numerical Recipes 3rd Edition: The Art of Scientific Computing*. 3rd ed. Cambridge, UK ; New York: Cambridge University Press, Sept. 6, 2007. 1256 pp. ISBN: 978-0-521-88068-8.
- [366] D. Calvetti, L. Reichel, and D. C. Sorensen. “An Implicitly Restarted Lanczos Method for Large Symmetric Eigenvalue Problems”. In: *Electron. T. Numer. Ana.* 2.1 (1994), p. 21.
- [367] E. R. Davidson. “The Iterative Calculation of a Few of the Lowest Eigenvalues and Corresponding Eigenvectors of Large Real-Symmetric Matrices”. In: *J. Comput. Phys.* 17.1 (Jan. 1, 1975), pp. 87–94. ISSN: 0021-9991. DOI: [10/fh9h3z](https://doi.org/10/fh9h3z).
- [368] M. A. García-March et al. “Distinguishability, Degeneracy, and Correlations in Three Harmonically Trapped Bosons in One Dimension”. In: *Phys. Rev. A* 90.6 (Dec. 1, 2014), p. 063605. DOI: [10.1103/PhysRevA.90.063605](https://doi.org/10.1103/PhysRevA.90.063605).
- [369] P. Mujal et al. “Quantum Correlations and Degeneracy of Identical Bosons in a Two-Dimensional Harmonic Trap”. In: *Phys. Rev. A* 96.4 (Oct. 16, 2017), p. 043614. DOI: [10.1103/PhysRevA.96.043614](https://doi.org/10.1103/PhysRevA.96.043614).
- [370] M. Pyzh et al. “Spectral Properties and Breathing Dynamics of a Few-Body Bose–Bose Mixture in a 1D Harmonic Trap”. In: *New J. Phys.* 20.1 (Jan. 2018), p. 015006. ISSN: 1367-2630. DOI: [10.1088/1367-2630/aa9cb2](https://doi.org/10.1088/1367-2630/aa9cb2).
- [371] J. F. Corney and P. D. Drummond. “Gaussian Quantum Monte Carlo Methods for Fermions and Bosons”. In: *Phys. Rev. Lett.* 93.26 (Dec. 20, 2004), p. 260401. DOI: [10.1103/PhysRevLett.93.260401](https://doi.org/10.1103/PhysRevLett.93.260401).
- [372] F. F. Assaad et al. “Symmetry Projection Schemes for Gaussian Monte Carlo Methods”. In: *Phys. Rev. B* 72.22 (Dec. 30, 2005), p. 224518. DOI: [10.1103/PhysRevB.72.224518](https://doi.org/10.1103/PhysRevB.72.224518).
- [373] J. B. Anderson. “A Random-walk Simulation of the Schrödinger Equation: H+3”. In: *J. Chem. Phys.* 63.4 (Sept. 3, 2008), pp. 1499–1503. ISSN: 0021-9606. DOI: [10.1063/1.431514](https://doi.org/10.1063/1.431514).
- [374] R. J. Needs et al. “Continuum Variational and Diffusion Quantum Monte Carlo Calculations”. In: *J. Phys.: Condens. Mat.* 22.2 (Dec. 2009), p. 023201. ISSN: 0953-8984. DOI: [10.1088/0953-8984/22/2/023201](https://doi.org/10.1088/0953-8984/22/2/023201).
- [375] D. Ceperley, G. V. Chester, and M. H. Kalos. “Monte Carlo Simulation of a Many-Fermion Study”. In: *Phys. Rev. B* 16.7 (Oct. 1, 1977), pp. 3081–3099. DOI: [10.1103/PhysRevB.16.3081](https://doi.org/10.1103/PhysRevB.16.3081).
- [376] R. Blankenbecler, D. J. Scalapino, and R. L. Sugar. “Monte Carlo Calculations of Coupled Boson-Fermion Systems. I”. In: *Phys. Rev. D* 24.8 (Oct. 15, 1981), pp. 2278–2286. DOI: [10.1103/PhysRevD.24.2278](https://doi.org/10.1103/PhysRevD.24.2278).
- [377] W. Krauth. “Quantum Monte Carlo Calculations for a Large Number of Bosons in a Harmonic Trap”. In: *Phys. Rev. Lett.* 77.18 (Oct. 28, 1996), pp. 3695–3699. DOI: [10.1103/PhysRevLett.77.3695](https://doi.org/10.1103/PhysRevLett.77.3695).
-

- [378] V. G. Rousseau. “Stochastic Green Function Algorithm”. In: *Phys. Rev. E* 77.5 (May 20, 2008), p. 056705. DOI: [10.1103/PhysRevE.77.056705](https://doi.org/10.1103/PhysRevE.77.056705).
- [379] G. G. Batrouni and R. T. Scalettar. “World-Line Quantum Monte Carlo Algorithm for a One-Dimensional Bose Model”. In: *Phys. Rev. B* 46.14 (Oct. 1, 1992), pp. 9051–9062. DOI: [10.1103/PhysRevB.46.9051](https://doi.org/10.1103/PhysRevB.46.9051).
- [380] G. Carleo et al. “Localization and Glassy Dynamics Of Many-Body Quantum Systems”. In: *Sci. Rep.* 2 (Feb. 6, 2012), p. 243. ISSN: 2045-2322. DOI: [10.1038/srep00243](https://doi.org/10.1038/srep00243).
- [381] G. Carleo et al. “Light-Cone Effect and Supersonic Correlations in One- and Two-Dimensional Bosonic Superfluids”. In: *Phys. Rev. A* 89.3 (Mar. 27, 2014), p. 031602. DOI: [10.1103/PhysRevA.89.031602](https://doi.org/10.1103/PhysRevA.89.031602).
- [382] M. Troyer and U.-J. Wiese. “Computational Complexity and Fundamental Limitations to Fermionic Quantum Monte Carlo Simulations”. In: *Phys. Rev. Lett.* 94.17 (May 4, 2005), p. 170201. DOI: [10.1103/PhysRevLett.94.170201](https://doi.org/10.1103/PhysRevLett.94.170201).
- [383] D. R. Hartree. “The Wave Mechanics of an Atom with a Non-Coulomb Central Field. Part I. Theory and Methods”. In: *Math. Proc. Cambridge* 24.1 (Jan. 1928), pp. 89–110. ISSN: 1469-8064, 0305-0041. DOI: [10/d4fnqc](https://doi.org/10/d4fnqc).
- [384] D. R. Hartree. “The Wave Mechanics of an Atom with a Non-Coulomb Central Field. Part II. Some Results and Discussion”. In: *Math. Proc. Cambridge* 24.1 (Jan. 1928), pp. 111–132. ISSN: 1469-8064, 0305-0041. DOI: [10.1017/S0305004100011920](https://doi.org/10.1017/S0305004100011920).
- [385] V. Fock. “Näherungsmethode zur Lösung des quantenmechanischen Mehrkörperproblems”. In: *Z. Phys.* 61.1 (Jan. 1, 1930), pp. 126–148. ISSN: 0044-3328. DOI: [10/cv2qt6](https://doi.org/10/cv2qt6).
- [386] J. C. Slater. “Note on Hartree’s Method”. In: *Phys. Rev.* 35.2 (Jan. 15, 1930), pp. 210–211. DOI: [10.1103/PhysRev.35.210.2](https://doi.org/10.1103/PhysRev.35.210.2).
- [387] W. Pauli. “Über den Zusammenhang des Abschlusses der Elektronengruppen im Atom mit der Komplexstruktur der Spektren”. In: *Z. Phys.* 31.1 (Feb. 1, 1925), pp. 765–783. ISSN: 0044-3328. DOI: [10.1007/BF02980631](https://doi.org/10.1007/BF02980631).
- [388] E. P. Gross. “Structure of a Quantized Vortex in Boson Systems”. In: *Nuovo Cimento* 20.3 (1961), pp. 454–477. ISSN: 1827-6121. DOI: [10/bj4ntt](https://doi.org/10/bj4ntt).
- [389] L. P. Pitaevskii. “Vortex Lines in an Imperfect Bose Gas”. In: *Sov. Phys. JETP*. 13.2 (Aug. 1961), pp. 451–454.
- [390] E. P. Gross. “Hydrodynamics of a Superfluid Condensate”. In: *J. Math. Phys.* 4.2 (Feb. 1963), pp. 195–207. ISSN: 0022-2488. DOI: [10.1063/1.1703944](https://doi.org/10.1063/1.1703944).
- [391] O. Penrose and L. Onsager. “Bose-Einstein Condensation and Liquid Helium”. In: *Phys. Rev.* 104.3 (Nov. 1, 1956), pp. 576–584. DOI: [10/b2cqrn](https://doi.org/10/b2cqrn).
- [392] W. Bao, D. Jaksch, and P. A. Markowich. “Numerical Solution of the Gross-Pitaevskii Equation for Bose-Einstein Condensation”. In: *J. Comput. Phys.* 187.1 (May 1, 2003), pp. 318–342. ISSN: 0021-9991. DOI: [10/chhzpp](https://doi.org/10/chhzpp).
- [393] N. Bogoliubov. “On the Theory of Superfluidity”. In: *J. Phys.-USSR* 11.1 (1947), pp. 23–32.

- 
- [394] C. W. Gardiner. “Particle-Number-Conserving Bogoliubov Method Which Demonstrates the Validity of the Time-Dependent Gross-Pitaevskii Equation for a Highly Condensed Bose Gas”. In: *Phys. Rev. A* 56.2 (Aug. 1, 1997), pp. 1414–1423. doi: [10.1103/PhysRevA.56.1414](https://doi.org/10.1103/PhysRevA.56.1414).
- [395] A. Weller et al. “Experimental Observation of Oscillating and Interacting Matter Wave Dark Solitons”. In: *Phys. Rev. Lett.* 101.13 (Sept. 22, 2008), p. 130401. doi: [10.1103/PhysRevLett.101.130401](https://doi.org/10.1103/PhysRevLett.101.130401).
- [396] G. Theocharis et al. “Multiple Atomic Dark Solitons in Cigar-Shaped Bose-Einstein Condensates”. In: *Phys. Rev. A* 81.6 (June 3, 2010), p. 063604. doi: [10.1103/PhysRevA.81.063604](https://doi.org/10.1103/PhysRevA.81.063604).
- [397] H. Sakaguchi and B. A. Malomed. “Matter-Wave Solitons in Nonlinear Optical Lattices”. In: *Phys. Rev. E* 72.4 (Oct. 24, 2005), p. 046610. doi: [10.1103/PhysRevE.72.046610](https://doi.org/10.1103/PhysRevE.72.046610).
- [398] O. V. Borovkova et al. “Bright Solitons from Defocusing Nonlinearities”. In: *Phys. Rev. E* 84.3 (Sept. 19, 2011), p. 035602. doi: [10.1103/PhysRevE.84.035602](https://doi.org/10.1103/PhysRevE.84.035602).
- [399] F. Bethuel, G. Orlandi, and D. Smets. “Vortex Rings for the Gross-Pitaevskii Equation”. In: *J. Eur. Math. Soc.* 006.1 (2004), pp. 17–94. issn: 1435-9855. url: <https://eudml.org/doc/277427>.
- [400] H. Sakaguchi and B. Li. “Vortex Lattice Solutions to the Gross-Pitaevskii Equation with Spin-Orbit Coupling in Optical Lattices”. In: *Phys. Rev. A* 87.1 (Jan. 25, 2013), p. 015602. doi: [10.1103/PhysRevA.87.015602](https://doi.org/10.1103/PhysRevA.87.015602).
- [401] T. D. Lee and C. N. Yang. “Many-Body Problem in Quantum Mechanics and Quantum Statistical Mechanics”. In: *Phys. Rev.* 105.3 (Feb. 1, 1957), pp. 1119–1120. doi: [10/cbvcv4](https://doi.org/10/cbvcv4).
- [402] R. N. Bisset et al. “Ground-State Phase Diagram of a Dipolar Condensate with Quantum Fluctuations”. In: *Phys. Rev. A* 94.3 (Sept. 15, 2016), p. 033619. doi: [10.1103/PhysRevA.94.033619](https://doi.org/10.1103/PhysRevA.94.033619).
- [403] F. Wächtler and L. Santos. “Quantum Filaments in Dipolar Bose-Einstein Condensates”. In: *Phys. Rev. A* 93.6 (June 24, 2016), p. 061603. doi: [10.1103/PhysRevA.93.061603](https://doi.org/10.1103/PhysRevA.93.061603).
- [404] Th. Busch and J. R. Anglin. “Dark-Bright Solitons in Inhomogeneous Bose-Einstein Condensates”. In: *Phys. Rev. Lett.* 87.1 (June 15, 2001), p. 010401. doi: [10.1103/PhysRevLett.87.010401](https://doi.org/10.1103/PhysRevLett.87.010401).
- [405] D. Yan et al. “Multiple Dark-Bright Solitons in Atomic Bose-Einstein Condensates”. In: *Phys. Rev. A* 84.5 (Nov. 28, 2011), p. 053630. doi: [10.1103/PhysRevA.84.053630](https://doi.org/10.1103/PhysRevA.84.053630).
- [406] A. Álvarez et al. “Scattering of Atomic Dark–Bright Solitons from Narrow Impurities”. In: *J. Phys. B: At. Mol. Opt. Phys.* 46.6 (Mar. 2013), p. 065302. issn: 0953-4075. doi: [10.1088/0953-4075/46/6/065302](https://doi.org/10.1088/0953-4075/46/6/065302).
- [407] D. Dagnino et al. “Vortex Nucleation as a Case Study of Symmetry Breaking in Quantum Systems”. In: *Nat. Phys.* 5.6 (6 June 2009), pp. 431–437. issn: 1745-2481. doi: [10.1038/nphys1277](https://doi.org/10.1038/nphys1277).
-

- [408] T. Stöferle et al. "Transition from a Strongly Interacting 1D Superfluid to a Mott Insulator". In: *Phys. Rev. Lett.* 92.13 (Mar. 31, 2004), p. 130403. doi: [10.1103/PhysRevLett.92.130403](https://doi.org/10.1103/PhysRevLett.92.130403).
- [409] L. S. Cederbaum and A. I. Streltsov. "Best Mean-Field for Condensates". In: *Physics Letters A* 318.6 (Nov. 24, 2003), pp. 564–569. issn: 0375-9601. doi: [10.1016/j.physleta.2003.09.058](https://doi.org/10.1016/j.physleta.2003.09.058).
- [410] L. S. Cederbaum and A. I. Streltsov. "Self-Consistent Fragmented Excited States of Trapped Condensates". In: *Phys. Rev. A* 70.2 (Aug. 27, 2004), p. 023610. doi: [10.1103/PhysRevA.70.023610](https://doi.org/10.1103/PhysRevA.70.023610).
- [411] O. E. Alon, A. I. Streltsov, and L. S. Cederbaum. "Zoo of Quantum Phases and Excitations of Cold Bosonic Atoms in Optical Lattices". In: *Phys. Rev. Lett.* 95.3 (July 15, 2005), p. 030405. doi: [10.1103/PhysRevLett.95.030405](https://doi.org/10.1103/PhysRevLett.95.030405).
- [412] A. I. Streltsov and L. S. Cederbaum. "Properties of Fragmented Repulsive Condensates". In: *Phys. Rev. A* 71.6 (June 22, 2005), p. 063612. doi: [10.1103/PhysRevA.71.063612](https://doi.org/10.1103/PhysRevA.71.063612).
- [413] O. E. Alon, A. I. Streltsov, and L. S. Cederbaum. "Demixing of Bosonic Mixtures in Optical Lattices from Macroscopic to Microscopic Scales". In: *Phys. Rev. Lett.* 97.23 (Dec. 6, 2006), p. 230403. doi: [10.1103/PhysRevLett.97.230403](https://doi.org/10.1103/PhysRevLett.97.230403).
- [414] O. E. Alon, A. I. Streltsov, and L. S. Cederbaum. "Time-Dependent Multi-Orbital Mean-Field for Fragmented Bose–Einstein Condensates". In: *Phys. Lett. A* 362.5 (Mar. 12, 2007), pp. 453–459. issn: 0375-9601. doi: [10.1016/j.physleta.2006.10.048](https://doi.org/10.1016/j.physleta.2006.10.048).
- [415] L. S. Cederbaum et al. "Interferences in the Density of Two Bose-Einstein Condensates Consisting of Identical or Different Atoms". In: *Phys. Rev. Lett.* 98.11 (Mar. 14, 2007), p. 110405. doi: [10.1103/PhysRevLett.98.110405](https://doi.org/10.1103/PhysRevLett.98.110405).
- [416] S. I. Mistakidis, L. Cao, and P. Schmelcher. "Interaction Quench Induced Multi-mode Dynamics of Finite Atomic Ensembles". In: *J. Phys. B: At. Mol. Opt. Phys.* 47.22 (Nov. 2014), p. 225303. issn: 0953-4075. doi: [10/gft7mv](https://doi.org/10/gft7mv).
- [417] S. I. Mistakidis, L. Cao, and P. Schmelcher. "Negative-Quench-Induced Excitation Dynamics for Ultracold Bosons in One-Dimensional Lattices". In: *Phys. Rev. A* 91.3 (Mar. 10, 2015), p. 033611. doi: [10/gffmkg](https://doi.org/10/gffmkg).
- [418] S. I. Mistakidis and P. Schmelcher. "Mode Coupling of Interaction Quenched Ultracold Few-Boson Ensembles in Periodically Driven Lattices". In: *Phys. Rev. A* 95.1 (Jan. 24, 2017), p. 013625. doi: [10/gffmkr](https://doi.org/10/gffmkr).
- [419] G. M. Koutentakis, S. I. Mistakidis, and P. Schmelcher. "Quench-Induced Resonant Tunneling Mechanisms of Bosons in an Optical Lattice with Harmonic Confinement". In: *Phys. Rev. A* 95.1 (Jan. 18, 2017), p. 013617. doi: [10/gfwrsu](https://doi.org/10/gfwrsu).
- [420] M. Beck et al. "The Multiconfiguration Time-Dependent Hartree (MCTDH) Method: A Highly Efficient Algorithm for Propagating Wavepackets". In: *Phys. Rep.* 324.1 (Jan. 2000), pp. 1–105. issn: 0370-1573. doi: [10.1016/S0370-1573\(99\)00047-2](https://doi.org/10.1016/S0370-1573(99)00047-2).
- [421] U. Manthe. "A Multilayer Multiconfigurational Time-Dependent Hartree Approach for Quantum Dynamics on General Potential Energy Surfaces". In: *J. Chem. Phys.* 128.16 (Apr. 28, 2008), p. 164116. issn: 0021-9606. doi: [10/c2fcph](https://doi.org/10/c2fcph).



- 
- [422] O. Vendrell and H.-D. Meyer. "Multilayer Multiconfiguration Time-Dependent Hartree Method: Implementation and Applications to a Henon–Heiles Hamiltonian and to Pyrazine". In: *J. Chem. Phys.* 134.4 (Jan. 28, 2011), p. 044135. ISSN: 0021-9606. DOI: [10/cbmwsc](https://doi.org/10/cbmwsc).
- [423] F. Gatti et al. *Applications of Quantum Dynamics in Chemistry*. 1st ed. 2017 edition. New York, NY: Springer, Dec. 25, 2017. 429 pp. ISBN: 978-3-319-53921-8.
- [424] H.-D. Meyer, U. Manthe, and L. Cederbaum. "The Multi-Configurational Time-Dependent Hartree Approach". In: *Chem. Phys. Lett.* 165.1 (Jan. 5, 1990), pp. 73–78. ISSN: 0009-2614. DOI: [10/b54n8q](https://doi.org/10/b54n8q).
- [425] U. Manthe, H.-D. Meyer, and L. S. Cederbaum. "Wave-packet Dynamics within the Multiconfiguration Hartree Framework: General Aspects and Application to NOCl". In: *J. Chem. Phys.* 97.5 (Sept. 1, 1992), pp. 3199–3213. ISSN: 0021-9606. DOI: [10/bqsw54](https://doi.org/10/bqsw54).
- [426] H.-D. Meyer and G. A. Worth. "Quantum Molecular Dynamics: Propagating Wavepackets and Density Operators Using the Multiconfiguration Time-Dependent Hartree Method". In: *Theor. Chem. Acc.* 109.5 (2003), pp. 251–267. ISSN: 1432-2234. DOI: [10/b83jqb](https://doi.org/10/b83jqb).
- [427] H.-D. Meyer, F. Gatti, and G. A. Worth. *Multidimensional Quantum Dynamics: MCTDH Theory and Applications*. 1. edition. Weinheim : Chichester: Wiley-VCH, Apr. 15, 2009. 442 pp. ISBN: 978-3-527-32018-9.
- [428] H.-D. Meyer. "Studying Molecular Quantum Dynamics with the Multiconfiguration Time-Dependent Hartree Method". In: *Wiley Interdiscip. Rev. Comput. Mol. Sci.* 2.2 (2012), pp. 351–374. ISSN: 1759-0884. DOI: [10/bdq69c](https://doi.org/10/bdq69c).
- [429] H. Wang and M. Thoss. "Multilayer Formulation of the Multiconfiguration Time-Dependent Hartree Theory". In: *J. Chem. Phys.* 119.3 (July 15, 2003), pp. 1289–1299. ISSN: 0021-9606. DOI: [10.1063/1.1580111](https://doi.org/10.1063/1.1580111).
- [430] O. E. Alon, A. I. Streltsov, and L. S. Cederbaum. "Unified View on Multiconfigurational Time Propagation for Systems Consisting of Identical Particles". In: *J. Chem. Phys.* 127.15 (Oct. 16, 2007), p. 154103. ISSN: 0021-9606. DOI: [10/ckgg9c](https://doi.org/10/ckgg9c).
- [431] A. I. Streltsov, O. E. Alon, and L. S. Cederbaum. "Role of Excited States in the Splitting of a Trapped Interacting Bose-Einstein Condensate by a Time-Dependent Barrier". In: *Phys. Rev. Lett.* 99.3 (July 20, 2007), p. 030402. DOI: [10/d3jxrf](https://doi.org/10/d3jxrf).
- [432] O. E. Alon, A. I. Streltsov, and L. S. Cederbaum. "Multiconfigurational Time-Dependent Hartree Method for Bosons: Many-body Dynamics of Bosonic Systems". In: *Phys. Rev. A* 77.3 (Mar. 14, 2008), p. 033613. DOI: [10/ff83pq](https://doi.org/10/ff83pq).
- [433] J. Zanghellini et al. "An MCTDHF Approach to Multielectron Dynamics in Laser Fields". In: *Laser Phys.* 13.8 (2003), pp. 1064–1068.
- [434] T. Kato and H. Kono. "Time-Dependent Multiconfiguration Theory for Electronic Dynamics of Molecules in an Intense Laser Field". In: *Chem. Phys. Lett.* 392.4 (July 11, 2004), pp. 533–540. ISSN: 0009-2614. DOI: [10.1016/j.cplett.2004.05.106](https://doi.org/10.1016/j.cplett.2004.05.106).
- [435] M. Kitzler et al. "Ionization Dynamics of Extended Multielectron Systems". In: *Phys. Rev. A* 70.4 (Oct. 15, 2004), p. 041401. DOI: [10.1103/PhysRevA.70.041401](https://doi.org/10.1103/PhysRevA.70.041401).
-

- [436] J. Caillat et al. "Correlated Multielectron Systems in Strong Laser Fields: A Multiconfiguration Time-Dependent Hartree-Fock Approach". In: *Phys. Rev. A* 71.1 (Jan. 21, 2005), p. 012712. DOI: [10/d5pg4p](https://doi.org/10/d5pg4p).
- [437] M. Nest, T. Klamroth, and P. Saalfrank. "The Multiconfiguration Time-Dependent Hartree-Fock Method for Quantum Chemical Calculations". In: *J. Chem. Phys.* 122.12 (Mar. 28, 2005), p. 124102. ISSN: 0021-9606. DOI: [10.1063/1.1862243](https://doi.org/10.1063/1.1862243).
- [438] M. Nest, R. Padmanaban, and P. Saalfrank. "Time-Dependent Approach to Electronically Excited States of Molecules with the Multiconfiguration Time-Dependent Hartree-Fock Method". In: *J. Chem. Phys.* 126.21 (June 7, 2007), p. 214106. ISSN: 0021-9606. DOI: [10.1063/1.2743007](https://doi.org/10.1063/1.2743007).
- [439] T. Kato and H. Kono. "Time-Dependent Multiconfiguration Theory for Electronic Dynamics of Molecules in Intense Laser Fields: A Description in Terms of Numerical Orbital Functions". In: *J. Chem. Phys.* 128.18 (May 9, 2008), p. 184102. ISSN: 0021-9606. DOI: [10.1063/1.2912066](https://doi.org/10.1063/1.2912066).
- [440] M. Nest, F. Remacle, and R. D. Levine. "Pump and Probe Ultrafast Electron Dynamics in LiH: A Computational Study". In: *New J. Phys.* 10.2 (Feb. 2008), p. 025019. ISSN: 1367-2630. DOI: [10.1088/1367-2630/10/2/025019](https://doi.org/10.1088/1367-2630/10/2/025019).
- [441] O. E. Alon, A. I. Streltsov, and L. S. Cederbaum. "Many-Body Theory for Systems with Particle Conversion: Extending the Multiconfigurational Time-Dependent Hartree Method". In: *Phys. Rev. A* 79.2 (Feb. 4, 2009), p. 022503. DOI: [10/fc6zs6](https://doi.org/10/fc6zs6).
- [442] D. J. Haxton, K. V. Lawler, and C. W. McCurdy. "Multiconfiguration Time-Dependent Hartree-Fock Treatment of Electronic and Nuclear Dynamics in Diatomic Molecules". In: *Phys. Rev. A* 83.6 (June 24, 2011), p. 063416. DOI: [10.1103/PhysRevA.83.063416](https://doi.org/10.1103/PhysRevA.83.063416).
- [443] G. Evenbly and G. Vidal. "Tensor Network States and Geometry". In: *J. Stat. Phys.* 145.4 (Nov. 1, 2011), pp. 891–918. ISSN: 1572-9613. DOI: [10.1007/s10955-011-0237-4](https://doi.org/10.1007/s10955-011-0237-4).
- [444] R. Orús. "A Practical Introduction to Tensor Networks: Matrix Product States and Projected Entangled Pair States". In: *Ann. Phys.* 349 (Oct. 1, 2014), pp. 117–158. ISSN: 0003-4916. DOI: [10.1016/j.aop.2014.06.013](https://doi.org/10.1016/j.aop.2014.06.013).
- [445] R. Orús. "Tensor Networks for Complex Quantum Systems". In: *Nat Rev Phys* 1.9 (9 Sept. 2019), pp. 538–550. ISSN: 2522-5820. DOI: [10.1038/s42254-019-0086-7](https://doi.org/10.1038/s42254-019-0086-7).
- [446] M. Fannes, B. Nachtergaele, and R. F. Werner. "Finitely Correlated States on Quantum Spin Chains". In: *Commun.Math. Phys.* 144.3 (Mar. 1, 1992), pp. 443–490. ISSN: 1432-0916. DOI: [10.1007/BF02099178](https://doi.org/10.1007/BF02099178).
- [447] S. Östlund and S. Rommer. "Thermodynamic Limit of Density Matrix Renormalization". In: *Phys. Rev. Lett.* 75.19 (Nov. 6, 1995), pp. 3537–3540. DOI: [10.1103/PhysRevLett.75.3537](https://doi.org/10.1103/PhysRevLett.75.3537).
- [448] S. Rommer and S. Östlund. "Class of Ansatz Wave Functions for One-Dimensional Spin Systems and Their Relation to the Density Matrix Renormalization Group". In: *Phys. Rev. B* 55.4 (Jan. 15, 1997), pp. 2164–2181. DOI: [10.1103/PhysRevB.55.2164](https://doi.org/10.1103/PhysRevB.55.2164).
- [449] D. Perez-Garcia et al. "Matrix Product State Representations". In: *Quant. Inf. Comput.* 7 (5&6 July 2007), pp. 401–430. ISSN: 1533-7146. DOI: [10.26421/QIC7.5-6-1](https://doi.org/10.26421/QIC7.5-6-1).

- 
- [450] S. R. White. “Density Matrix Formulation for Quantum Renormalization Groups”. In: *Phys. Rev. Lett.* 69.19 (Nov. 9, 1992), pp. 2863–2866. doi: [10/bbvnr8](https://doi.org/10/bbvnr8).
- [451] S. R. White. “Density-Matrix Algorithms for Quantum Renormalization Groups”. In: *Phys. Rev. B* 48.14 (Oct. 1, 1993), pp. 10345–10356. doi: [10/cnpjkn](https://doi.org/10/cnpjkn).
- [452] U. Schollwöck. “The Density-Matrix Renormalization Group”. In: *Rev. Mod. Phys.* 77.1 (Apr. 26, 2005), pp. 259–315. doi: [10/bx4jbr](https://doi.org/10/bx4jbr).
- [453] U. Schollwöck. “The Density-Matrix Renormalization Group in the Age of Matrix Product States”. In: *Ann. Phys.* January 2011 Special Issue 326.1 (Jan. 1, 2011), pp. 96–192. issn: 0003-4916. doi: [10.1016/j.aop.2010.09.012](https://doi.org/10.1016/j.aop.2010.09.012).
- [454] G. Vidal. “Entanglement Renormalization”. In: *Phys. Rev. Lett.* 99.22 (Nov. 28, 2007), p. 220405. doi: [10.1103/PhysRevLett.99.220405](https://doi.org/10.1103/PhysRevLett.99.220405).
- [455] V. Giovannetti, S. Montangero, and R. Fazio. “Quantum Multiscale Entanglement Renormalization Ansatz Channels”. In: *Phys. Rev. Lett.* 101.18 (Oct. 30, 2008), p. 180503. doi: [10.1103/PhysRevLett.101.180503](https://doi.org/10.1103/PhysRevLett.101.180503).
- [456] G. Vidal. “Class of Quantum Many-Body States That Can Be Efficiently Simulated”. In: *Phys. Rev. Lett.* 101.11 (Sept. 12, 2008), p. 110501. doi: [10.1103/PhysRevLett.101.110501](https://doi.org/10.1103/PhysRevLett.101.110501).
- [457] G. Evenbly and G. Vidal. “Algorithms for Entanglement Renormalization”. In: *Phys. Rev. B* 79.14 (Apr. 7, 2009), p. 144108. doi: [10.1103/PhysRevB.79.144108](https://doi.org/10.1103/PhysRevB.79.144108).
- [458] R. N. C. Pfeifer, G. Evenbly, and G. Vidal. “Entanglement Renormalization, Scale Invariance, and Quantum Criticality”. In: *Phys. Rev. A* 79.4 (Apr. 6, 2009), p. 040301. doi: [10.1103/PhysRevA.79.040301](https://doi.org/10.1103/PhysRevA.79.040301).
- [459] T. Nishino and K. Okunishi. “A Density Matrix Algorithm for 3D Classical Models”. In: *J. Phys. Soc. Jpn.* 67.9 (1998), pp. 3066–3072.
- [460] G. Sierra and M. A. Martin-Delgado. *The Density Matrix Renormalization Group, Quantum Groups and Conformal Field Theory*. Version 3. Nov. 30, 1998. doi: [10.48550/arXiv.cond-mat/9811170](https://doi.org/10.48550/arXiv.cond-mat/9811170). preprint.
- [461] Y. Nishio et al. *Tensor Product Variational Formulation for Quantum Systems*. Jan. 8, 2004. doi: [10.48550/arXiv.cond-mat/0401115](https://doi.org/10.48550/arXiv.cond-mat/0401115). preprint.
- [462] F. Verstraete and J. I. Cirac. *Renormalization Algorithms for Quantum-Many Body Systems in Two and Higher Dimensions*. July 2, 2004. doi: [10.48550/arXiv.cond-mat/0407066](https://doi.org/10.48550/arXiv.cond-mat/0407066). preprint.
- [463] F. Verstraete and J. I. Cirac. “Valence-Bond States for Quantum Computation”. In: *Phys. Rev. A* 70.6 (Dec. 14, 2004), p. 060302. doi: [10.1103/PhysRevA.70.060302](https://doi.org/10.1103/PhysRevA.70.060302).
- [464] V. Murg, F. Verstraete, and J. I. Cirac. “Variational Study of Hard-Core Bosons in a Two-Dimensional Optical Lattice Using Projected Entangled Pair States”. In: *Phys. Rev. A* 75.3 (Mar. 13, 2007), p. 033605. doi: [10.1103/PhysRevA.75.033605](https://doi.org/10.1103/PhysRevA.75.033605).
- [465] Z.-C. Gu, M. Levin, and X.-G. Wen. “Tensor-Entanglement Renormalization Group Approach as a Unified Method for Symmetry Breaking and Topological Phase Transitions”. In: *Phys. Rev. B* 78.20 (Nov. 24, 2008), p. 205116. doi: [10.1103/PhysRevB.78.205116](https://doi.org/10.1103/PhysRevB.78.205116).
- [466] H. C. Jiang, Z. Y. Weng, and T. Xiang. “Accurate Determination of Tensor Network State of Quantum Lattice Models in Two Dimensions”. In: *Phys. Rev. Lett.* 101.9 (Aug. 29, 2008), p. 090603. doi: [10.1103/PhysRevLett.101.090603](https://doi.org/10.1103/PhysRevLett.101.090603).
-

- [467] J. Jordan et al. "Classical Simulation of Infinite-Size Quantum Lattice Systems in Two Spatial Dimensions". In: *Phys. Rev. Lett.* 101.25 (Dec. 18, 2008), p. 250602. DOI: [10.1103/PhysRevLett.101.250602](https://doi.org/10.1103/PhysRevLett.101.250602).
- [468] V. Murg, F. Verstraete, and J. I. Cirac. "Exploring Frustrated Spin Systems Using Projected Entangled Pair States". In: *Phys. Rev. B* 79.19 (May 20, 2009), p. 195119. DOI: [10.1103/PhysRevB.79.195119](https://doi.org/10.1103/PhysRevB.79.195119).
- [469] Z. Y. Xie et al. "Second Renormalization of Tensor-Network States". In: *Phys. Rev. Lett.* 103.16 (Oct. 12, 2009), p. 160601. DOI: [10.1103/PhysRevLett.103.160601](https://doi.org/10.1103/PhysRevLett.103.160601).
- [470] C. Cohen-Tannoudji, B. Diu, and F. Laloë. *Quantum Mechanics, Volume 1: Basic Concepts, Tools, and Applications*. 2nd edition. Weinheim: Wiley-VCH, Dec. 4, 2019. 944 pp. ISBN: 978-3-527-34553-3.
- [471] D. J. Tannor. *Introduction to Quantum Mechanics: A Time-Dependent Perspective*. University Science Books, 2006. ISBN: 978-1-891389-23-8.
- [472] P. Kramer and M. Saraceno. *Geometry of the Time-Dependent Variational Principle in Quantum Mechanics*. Vol. 140. Lecture Notes in Physics. Springer, Berlin, 1981. 101 pp. ISBN: 978-3-540-38576-9.
- [473] P. Kramer. "A Review of the Time-Dependent Variational Principle". In: *J. Phys.: Conf. Ser.* 99.1 (Feb. 2008), p. 012009. ISSN: 1742-6596. DOI: [10.1088/1742-6596/99/1/012009](https://doi.org/10.1088/1742-6596/99/1/012009).
- [474] P. A. M. Dirac. "Note on Exchange Phenomena in the Thomas Atom". In: *Math. Proc. Cambridge* 26.3 (1930), pp. 376–385. DOI: [10/d6d4m4](https://doi.org/10/d6d4m4).
- [475] J. Frenkel. *Wave Mechanics - Advanced General Theory*. Oxford: Oxford University Press, 1934.
- [476] A. McLachlan. "A Variational Solution of the Time-Dependent Schrodinger Equation". In: *Mol. Phys.* 8.1 (Jan. 1, 1964), pp. 39–44. ISSN: 0026-8976. DOI: [10/dkdc45](https://doi.org/10/dkdc45).
- [477] J. Broeckhove et al. "On the Equivalence of Time-Dependent Variational Principles". In: *Chem. Phys. Lett.* 149.5 (Sept. 2, 1988), pp. 547–550. ISSN: 0009-2614. DOI: [10/c3gfrc](https://doi.org/10/c3gfrc).
- [478] A. Raab. "On the Dirac–Frenkel/McLachlan Variational Principle". In: *Chem. Phys. Lett.* 319.5 (Mar. 24, 2000), pp. 674–678. ISSN: 0009-2614. DOI: [10.1016/S0009-2614\(00\)00200-1](https://doi.org/10.1016/S0009-2614(00)00200-1).
- [479] A. McLachlan and M. A. Ball. "Time-Dependent Hartree-Fock Theory for Molecules". In: *Rev. Mod. Phys.* 36.3 (July 1, 1964), pp. 844–855. DOI: [10.1103/RevModPhys.36.844](https://doi.org/10.1103/RevModPhys.36.844).
- [480] R. B. Gerber, V. Buch, and M. A. Ratner. "Time-dependent Self-consistent Field Approximation for Intramolecular Energy Transfer. I. Formulation and Application to Dissociation of van Der Waals Molecules". In: *J. Chem. Phys.* 77.6 (Sept. 15, 1982), pp. 3022–3030. ISSN: 0021-9606. DOI: [10.1063/1.444225](https://doi.org/10.1063/1.444225).
- [481] R. B. Gerber, M. A. Ratner, and V. Buch. "Simplified Time-Dependent Self-Consistent Field Approximation for Intramolecular Dynamics". In: *Chem. Phys. Lett.* 91.3 (Sept. 10, 1982), pp. 173–177. ISSN: 0009-2614. DOI: [10.1016/0009-2614\(82\)83635-X](https://doi.org/10.1016/0009-2614(82)83635-X).

- 
- [482] G. C. Schatz et al. "Dissociation Dynamics of Vibrationally Excited van Der Waals Clusters:  $I_2XY \rightarrow I_2+X+Y$  ( $X, Y=He, Ne$ )". In: *J. Chem. Phys.* 79.4 (Aug. 15, 1983), pp. 1808–1822. ISSN: 0021-9606. DOI: [10.1063/1.446026](https://doi.org/10.1063/1.446026).
- [483] R. H. Bisseling et al. "Exact Time-dependent Quantum Mechanical Dissociation Dynamics of  $I_2He$ : Comparison of Exact Time-dependent Quantum Calculation with the Quantum Time-dependent Self-consistent Field (TDSCF) Approximation". In: *J. Chem. Phys.* 87.5 (Sept. 1987), pp. 2760–2765. ISSN: 0021-9606. DOI: [10.1063/1.453063](https://doi.org/10.1063/1.453063).
- [484] M. Messina and R. D. Coalson. "Time-dependent Hartree Wave Packet Dynamical Techniques for Computation of Electronically Excited State Optical Spectra of Many-body Quantum Systems". In: *J. Chem. Phys.* 90.8 (Apr. 15, 1989), pp. 4015–4030. ISSN: 0021-9606. DOI: [10.1063/1.455812](https://doi.org/10.1063/1.455812).
- [485] J. Kucar, H.-D. Meyer, and L. Cederbaum. "Time-Dependent Rotated Hartree Approach". In: *Chem. Phys. Lett.* 140.5 (Jan. 1, 1987), pp. 525–530. ISSN: 0009-2614. DOI: [10/bw9pdr](https://doi.org/10/bw9pdr).
- [486] H.-D. Meyer, J. Kučar, and L. S. Cederbaum. "Time-dependent Rotated Hartree: Formal Development". In: *J. Math. Phys.* 29.6 (June 1988), pp. 1417–1430. ISSN: 0022-2488. DOI: [10.1063/1.527934](https://doi.org/10.1063/1.527934).
- [487] N. Makri and W. H. Miller. "Time-dependent Self-consistent Field (TDSCF) Approximation for a Reaction Coordinate Coupled to a Harmonic Bath: Single and Multiple Configuration Treatments". In: *J. Chem. Phys.* 87.10 (Nov. 15, 1987), pp. 5781–5787. ISSN: 0021-9606. DOI: [10.1063/1.453501](https://doi.org/10.1063/1.453501).
- [488] R. Kosloff. "Time-Dependent Quantum-Mechanical Methods for Molecular Dynamics". In: *J. Phys. Chem.* 92.8 (Apr. 1, 1988), pp. 2087–2100. ISSN: 0022-3654. DOI: [10/dgnh2n](https://doi.org/10/dgnh2n).
- [489] Z. Kotler, A. Nitzan, and R. Kosloff. "Multiconfiguration Time-Dependent Self-Consistent Field Approximation for Curve Crossing in Presence of a Bath. A Fast Fourier Transform Study". In: *Chem. Phys. Lett.* 153.6 (Dec. 30, 1988), pp. 483–489. ISSN: 0009-2614. DOI: [10.1016/0009-2614\(88\)85247-3](https://doi.org/10.1016/0009-2614(88)85247-3).
- [490] A. Raab et al. "Molecular Dynamics of Pyrazine after Excitation to the S2 Electronic State Using a Realistic 24-Mode Model Hamiltonian". In: *J. Chem. Phys.* 110.2 (Jan. 8, 1999), pp. 936–946. ISSN: 0021-9606. DOI: [10.1063/1.478061](https://doi.org/10.1063/1.478061).
- [491] H. Wang. "Basis Set Approach to the Quantum Dissipative Dynamics: Application of the Multiconfiguration Time-Dependent Hartree Method to the Spin-Boson Problem". In: *J. Chem. Phys.* 113.22 (Dec. 8, 2000), pp. 9948–9956. ISSN: 0021-9606. DOI: [10.1063/1.1323746](https://doi.org/10.1063/1.1323746).
- [492] H. Wang, M. Thoss, and W. H. Miller. "Systematic Convergence in the Dynamical Hybrid Approach for Complex Systems: A Numerically Exact Methodology". In: *J. Chem. Phys.* 115.7 (Aug. 15, 2001), pp. 2979–2990. ISSN: 0021-9606. DOI: [10.1063/1.1385561](https://doi.org/10.1063/1.1385561).
- [493] M. Thoss and H. Wang. "Quantum Dynamical Simulation of Ultrafast Photoinduced Electron Transfer Processes in a Mixed-Valence Compound". In: *Chem. Phys. Lett.* 358.3 (May 31, 2002), pp. 298–306. ISSN: 0009-2614. DOI: [10.1016/S0009-2614\(02\)00624-3](https://doi.org/10.1016/S0009-2614(02)00624-3).
-

- [494] H. Wang and M. Thoss. "Theoretical Study of Ultrafast Photoinduced Electron Transfer Processes in Mixed-Valence Systems". In: *J. Phys. Chem. A* 107.13 (Apr. 1, 2003), pp. 2126–2136. ISSN: 1089-5639. DOI: [10.1021/jp0272668](https://doi.org/10.1021/jp0272668).
- [495] O. Vendrell et al. "Full-Dimensional (15-Dimensional) Quantum-Dynamical Simulation of the Protonated Water Dimer. I. Hamiltonian Setup and Analysis of the Ground Vibrational State". In: *J. Chem. Phys.* 127.18 (Nov. 14, 2007), p. 184302. ISSN: 0021-9606. DOI: [10.1063/1.2787588](https://doi.org/10.1063/1.2787588).
- [496] O. Vendrell, F. Gatti, and H.-D. Meyer. "Full Dimensional (15-Dimensional) Quantum-Dynamical Simulation of the Protonated Water Dimer. II. Infrared Spectrum and Vibrational Dynamics". In: *J. Chem. Phys.* 127.18 (Nov. 14, 2007), p. 184303. ISSN: 0021-9606. DOI: [10.1063/1.2787596](https://doi.org/10.1063/1.2787596).
- [497] O. Vendrell et al. "Full Dimensional (15-Dimensional) Quantum-Dynamical Simulation of the Protonated Water-Dimer III: Mixed Jacobi-valence Parametrization and Benchmark Results for the Zero Point Energy, Vibrationally Excited States, and Infrared Spectrum". In: *J. Chem. Phys.* 130.23 (June 16, 2009), p. 234305. ISSN: 0021-9606. DOI: [10.1063/1.3152488](https://doi.org/10.1063/1.3152488).
- [498] O. Vendrell, F. Gatti, and H.-D. Meyer. "Full Dimensional (15 Dimensional) Quantum-Dynamical Simulation of the Protonated Water-Dimer IV: Isotope Effects in the Infrared Spectra of  $D(D_2O)_2^+$ ,  $H(D_2O)_2^+$ , and  $D(H_2O)_2^+$  Isotopologues". In: *J. Chem. Phys.* 131.3 (July 17, 2009), p. 034308. ISSN: 0021-9606. DOI: [10.1063/1.3183166](https://doi.org/10.1063/1.3183166).
- [499] G. Schiffl and U. Manthe. "Quantum Dynamics of the  $H+CH_4 \rightarrow H_2+CH_3$  Reaction in Curvilinear Coordinates: Full-dimensional and Reduced Dimensional Calculations of Reaction Rates". In: *J. Chem. Phys.* 132.8 (Feb. 23, 2010), p. 084103. ISSN: 0021-9606. DOI: [10.1063/1.3304920](https://doi.org/10.1063/1.3304920).
- [500] M. Schröder, F. Gatti, and H.-D. Meyer. "Theoretical Studies of the Tunneling Splitting of Malonaldehyde Using the Multiconfiguration Time-Dependent Hartree Approach". In: *J. Chem. Phys.* 134.23 (June 17, 2011), p. 234307. ISSN: 0021-9606. DOI: [10.1063/1.3600343](https://doi.org/10.1063/1.3600343).
- [501] T. Hammer and U. Manthe. "Intramolecular Proton Transfer in Malonaldehyde: Accurate Multilayer Multi-Configurational Time-Dependent Hartree Calculations". In: *J. Chem. Phys.* 134.22 (June 13, 2011), p. 224305. ISSN: 0021-9606. DOI: [10.1063/1.3598110](https://doi.org/10.1063/1.3598110).
- [502] T. Hammer and U. Manthe. "Iterative Diagonalization in the State-Averaged Multi-Configurational Time-Dependent Hartree Approach: Excited State Tunneling Splittings in Malonaldehyde". In: *J. Chem. Phys.* 136.5 (Feb. 3, 2012), p. 054105. ISSN: 0021-9606. DOI: [10.1063/1.3681166](https://doi.org/10.1063/1.3681166).
- [503] R. Welsch and U. Manthe. "Reaction Dynamics with the Multi-Layer Multi-Configurational Time-Dependent Hartree Approach:  $H+CH_4 \rightarrow H_2+CH_3$  Rate Constants for Different Potentials". In: *J. Chem. Phys.* 137.24 (Dec. 27, 2012), p. 244106. ISSN: 0021-9606. DOI: [10.1063/1.4772585](https://doi.org/10.1063/1.4772585).
- [504] M. Schröder and H.-D. Meyer. "Calculation of the Vibrational Excited States of Malonaldehyde and Their Tunneling Splittings with the Multi-Configuration Time-Dependent Hartree Method". In: *J. Chem. Phys.* 141.3 (July 21, 2014), p. 034116. ISSN: 0021-9606. DOI: [10.1063/1.4890116](https://doi.org/10.1063/1.4890116).

- 
- [505] R. Welsch and U. Manthe. "The Role of the Transition State in Polyatomic Reactions: Initial State-Selected Reaction Probabilities of the  $\text{H} + \text{CH}_4 \rightarrow \text{H}_2 + \text{CH}_3$  Reaction". In: *J. Chem. Phys.* 141.17 (Nov. 5, 2014), p. 174313. issn: 0021-9606. doi: [10.1063/1.4900735](https://doi.org/10.1063/1.4900735).
- [506] F. Huarte-Larrañaga and U. Manthe. "Full Dimensional Quantum Calculations of the  $\text{CH}_4 + \text{H} \rightarrow \text{CH}_3 + \text{H}_2$  Reaction Rate". In: *J. Chem. Phys.* 113.13 (Oct. 2000), pp. 5115–5118. issn: 0021-9606. doi: [10.1063/1.1311802](https://doi.org/10.1063/1.1311802).
- [507] F. Huarte-Larrañaga and U. Manthe. "Quantum Dynamics of the  $\text{CH}_4 + \text{H} \rightarrow \text{CH}_3 + \text{H}_2$  Reaction: Full-Dimensional and Reduced Dimensionality Rate Constant Calculations". In: *J. Phys. Chem. A* 105.12 (Mar. 1, 2001), pp. 2522–2529. issn: 1089-5639. doi: [10.1021/jp003579w](https://doi.org/10.1021/jp003579w).
- [508] F. Huarte-Larrañaga and U. Manthe. "Vibrational Excitation in the Transition State: The  $\text{CH}_4 + \text{H} \rightarrow \text{CH}_3 + \text{H}_2$  Reaction Rate Constant in an Extended Temperature Interval". In: *J. Chem. Phys.* 116.7 (Feb. 15, 2002), pp. 2863–2869. issn: 0021-9606. doi: [10.1063/1.1436307](https://doi.org/10.1063/1.1436307).
- [509] T. Wu, H.-J. Werner, and U. Manthe. "First-Principles Theory for the  $\text{H} + \text{CH}_4 \rightarrow \text{H}_2 + \text{CH}_3$  Reaction". In: *Science* 306.5705 (Dec. 24, 2004), pp. 2227–2229. doi: [10.1126/science.1104085](https://doi.org/10.1126/science.1104085).
- [510] A. Leclerc and T. Carrington. "Calculating Vibrational Spectra with Sum of Product Basis Functions without Storing Full-Dimensional Vectors or Matrices". In: *J. Chem. Phys.* 140.17 (May 6, 2014), p. 174111. issn: 0021-9606. doi: [10.1063/1.4871981](https://doi.org/10.1063/1.4871981).
- [511] P. S. Thomas and T. J. Carrington. "Using Nested Contractions and a Hierarchical Tensor Format To Compute Vibrational Spectra of Molecules with Seven Atoms". In: *J. Phys. Chem. A* 119.52 (Dec. 31, 2015), pp. 13074–13091. issn: 1089-5639. doi: [10.1021/acs.jpca.5b10015](https://doi.org/10.1021/acs.jpca.5b10015).
- [512] M. Rakhuba and I. Oseledets. "Calculating Vibrational Spectra of Molecules Using Tensor Train Decomposition". In: *J. Chem. Phys.* 145.12 (Sept. 22, 2016), p. 124101. issn: 0021-9606. doi: [10.1063/1.4962420](https://doi.org/10.1063/1.4962420).
- [513] H. R. Larsson. "Computing Vibrational Eigenstates with Tree Tensor Network States (TTNS)". In: *J. Chem. Phys.* 151.20 (Nov. 28, 2019), p. 204102. issn: 0021-9606. doi: [10.1063/1.5130390](https://doi.org/10.1063/1.5130390).
- [514] A. Jäckle and H.-D. Meyer. "Product Representation of Potential Energy Surfaces". In: *J. Chem. Phys.* 104.20 (May 22, 1996), pp. 7974–7984. issn: 0021-9606. doi: [10/d6nqw8](https://doi.org/10/d6nqw8).
- [515] A. Jäckle and H.-D. Meyer. "Product Representation of Potential Energy Surfaces. II". In: *J. Chem. Phys.* 109.10 (Sept. 8, 1998), pp. 3772–3779. issn: 0021-9606. doi: [10.1063/1.476977](https://doi.org/10.1063/1.476977).
- [516] L. De Lathauwer, B. De Moor, and J. Vandewalle. "A Multilinear Singular Value Decomposition". In: *SIAM J. Matrix Anal. Appl.* 21.4 (Jan. 2000), pp. 1253–1278. issn: 0895-4798. doi: [10.1137/S0895479896305696](https://doi.org/10.1137/S0895479896305696).
- [517] L. De Lathauwer, B. De Moor, and J. Vandewalle. "On the Best Rank-1 and Rank-( $R_1, R_2, \dots, R_N$ ) Approximation of Higher-Order Tensors". In: *SIAM J. Matrix Anal. Appl.* 21.4 (Jan. 2000), pp. 1324–1342. issn: 0895-4798. doi: [10.1137/S0895479898346995](https://doi.org/10.1137/S0895479898346995).
-

- [518] J. O. Jung and R. B. Gerber. "Vibrational Wave Functions and Spectroscopy of (H<sub>2</sub>O)<sub>n</sub>, N=2,3,4,5: Vibrational Self-consistent Field with Correlation Corrections". In: *J. Chem. Phys.* 105.23 (Dec. 15, 1996), pp. 10332–10348. ISSN: 0021-9606. DOI: [10.1063/1.472960](https://doi.org/10.1063/1.472960).
- [519] S. Carter, S. J. Culik, and J. M. Bowman. "Vibrational Self-Consistent Field Method for Many-Mode Systems: A New Approach and Application to the Vibrations of CO Adsorbed on Cu(100)". In: *J. Chem. Phys.* 107.24 (Dec. 22, 1997), pp. 10458–10469. ISSN: 0021-9606. DOI: [10.1063/1.474210](https://doi.org/10.1063/1.474210).
- [520] G. Li et al. "High Dimensional Model Representations Generated from Low Dimensional Data Samples. I. Mp-Cut-HDMR". In: *Journal of Mathematical Chemistry* 30.1 (July 1, 2001), pp. 1–30. ISSN: 1572-8897. DOI: [10.1023/A:1013172329778](https://doi.org/10.1023/A:1013172329778).
- [521] G. Li et al. "High-Dimensional Model Representations Generated from Low Order Terms—Lp-RS-HDMR". In: *Journal of Computational Chemistry* 24.5 (2003), pp. 647–656. ISSN: 1096-987X. DOI: [10.1002/jcc.10232](https://doi.org/10.1002/jcc.10232).
- [522] M. Beck and H.-D. Meyer. "An Efficient and Robust Integration Scheme for the Equations of Motion of the Multiconfiguration Time-Dependent Hartree (MCTDH) Method". In: *Z. Phys. D - Atom. Mol. Cl.* 42.2 (June 1, 1997), pp. 113–129. ISSN: 1431-5866. DOI: [10.1007/s004600050342](https://doi.org/10.1007/s004600050342).
- [523] A. P. J. Jansen. "A Multiconfiguration Time-dependent Hartree Approximation Based on Natural Single-particle States". In: *J. Chem. Phys.* 99.5 (Sept. 1, 1993), pp. 4055–4063. ISSN: 0021-9606. DOI: [10/btz5tm](https://doi.org/10/btz5tm).
- [524] U. Manthe. "Comment on 'A Multiconfiguration Time-dependent Hartree Approximation Based on Natural Single-particle States' [J. Chem. Phys. 99, 4055 (1993)]". In: *J. Chem. Phys.* 101.3 (Aug. 1, 1994), pp. 2652–2653. ISSN: 0021-9606. DOI: [10/cc75r2](https://doi.org/10/cc75r2).
- [525] A. P. J. Jansen. "Response to 'Comment on 'A Multiconfiguration Time-dependent Hartree Approximation Based on Natural Single-particle States' " [J. Chem. Phys. 101, 2652 (1994)]". In: *J. Chem. Phys.* 101.3 (Aug. 1, 1994), pp. 2654–2654. ISSN: 0021-9606. DOI: [10/dq9w3k](https://doi.org/10/dq9w3k).
- [526] G. A. Worth, H.-D. Meyer, and L. S. Cederbaum. "The Effect of a Model Environment on the S<sub>2</sub> Absorption Spectrum of Pyrazine: A Wave Packet Study Treating All 24 Vibrational Modes". In: *J. Chem. Phys.* 105.11 (Sept. 15, 1996), pp. 4412–4426. ISSN: 0021-9606. DOI: [10.1063/1.472327](https://doi.org/10.1063/1.472327).
- [527] E. Hairer, S. P. Nørsett, and G. Wanner. *Solving Ordinary Differential Equations I: Nonstiff Problems*. 2nd ed. Springer Series in Computational Mathematics. Berlin Heidelberg: Springer-Verlag, 1993. ISBN: 978-3-540-56670-0. DOI: [10.1007/978-3-540-78862-1](https://doi.org/10.1007/978-3-540-78862-1).
- [528] E. Hairer and G. Wanner. *Solving Ordinary Differential Equations II: Stiff and Differential-Algebraic Problems*. 2nd ed. Springer Series in Computational Mathematics. Berlin Heidelberg: Springer-Verlag, 1996. ISBN: 978-3-540-60452-5. DOI: [10.1007/978-3-642-05221-7](https://doi.org/10.1007/978-3-642-05221-7).
- [529] U. Manthe. "On the Integration of the Multi-Configurational Time-Dependent Hartree (MCTDH) Equations of Motion". In: *Chem. Phys. Electron Correlation and Multimode Dynamics in Molecules* 329.1 (Oct. 26, 2006), pp. 168–178. ISSN: 0301-0104. DOI: [10.1016/j.chemphys.2006.05.028](https://doi.org/10.1016/j.chemphys.2006.05.028).



- 
- [530] C. Leforestier et al. "A Comparison of Different Propagation Schemes for the Time Dependent Schrödinger Equation". In: *J. Comput. Phys.* 94.1 (May 1, 1991), pp. 59–80. ISSN: 0021-9991. DOI: [10.1016/0021-9991\(91\)90137-A](https://doi.org/10.1016/0021-9991(91)90137-A).
- [531] M. D. Feit, J. A. Fleck, and A. Steiger. "Solution of the Schrödinger Equation by a Spectral Method". In: *J. Comput. Phys.* 47.3 (Sept. 1, 1982), pp. 412–433. ISSN: 0021-9991. DOI: [10.1016/0021-9991\(82\)90091-2](https://doi.org/10.1016/0021-9991(82)90091-2).
- [532] M. D. Feit and J. A. Fleck Jr. "Solution of the Schrödinger Equation by a Spectral Method II: Vibrational Energy Levels of Triatomic Molecules". In: *J. Chem. Phys.* 78.1 (Jan. 1, 1983), pp. 301–308. ISSN: 0021-9606. DOI: [10.1063/1.444501](https://doi.org/10.1063/1.444501).
- [533] M. D. Feit and J. A. Fleck Jr. "Wave Packet Dynamics and Chaos in the Hénon–Heiles System". In: *J. Chem. Phys.* 80.6 (Mar. 15, 1984), pp. 2578–2584. ISSN: 0021-9606. DOI: [10.1063/1.447051](https://doi.org/10.1063/1.447051).
- [534] H. Tal-Ezer and R. Kosloff. "An Accurate and Efficient Scheme for Propagating the Time Dependent Schrödinger Equation". In: *J. Chem. Phys.* 81.9 (Nov. 1, 1984), pp. 3967–3971. ISSN: 0021-9606. DOI: [10.1063/1.448136](https://doi.org/10.1063/1.448136).
- [535] T. J. Park and J. C. Light. "Unitary Quantum Time Evolution by Iterative Lanczos Reduction". In: *J. Chem. Phys.* 85.10 (Nov. 15, 1986), pp. 5870–5876. ISSN: 0021-9606. DOI: [10.1063/1.451548](https://doi.org/10.1063/1.451548).
- [536] M. Ehara, H.-D. Meyer, and L. S. Cederbaum. "Multiconfiguration Time-dependent Hartree (MCTDH) Study on Rotational and Diffractive Inelastic Molecule-surface Scattering". In: *J. Chem. Phys.* 105.19 (Nov. 15, 1996), pp. 8865–8877. ISSN: 0021-9606. DOI: [10.1063/1.472616](https://doi.org/10.1063/1.472616).
- [537] G. A. Worth, H.-D. Meyer, and L. S. Cederbaum. "Relaxation of a System with a Conical Intersection Coupled to a Bath: A Benchmark 24-Dimensional Wave Packet Study Treating the Environment Explicitly". In: *J. Chem. Phys.* 109.9 (Sept. 1998), pp. 3518–3529. ISSN: 0021-9606. DOI: [10.1063/1.476947](https://doi.org/10.1063/1.476947).
- [538] M. Nest and H.-D. Meyer. "Dissipative Quantum Dynamics of Anharmonic Oscillators with the Multiconfiguration Time-Dependent Hartree Method". In: *J. Chem. Phys.* 119.1 (July 2003), pp. 24–33. ISSN: 0021-9606. DOI: [10.1063/1.1576384](https://doi.org/10.1063/1.1576384).
- [539] Chr. Cattarius et al. "All Mode Dynamics at the Conical Intersection of an Octa-Atomic Molecule: Multi-configuration Time-Dependent Hartree (MCTDH) Investigation on the Butatriene Cation". In: *J. Chem. Phys.* 115.5 (Aug. 2001), pp. 2088–2100. ISSN: 0021-9606. DOI: [10.1063/1.1384872](https://doi.org/10.1063/1.1384872).
- [540] H. Wang, D. E. Skinner, and M. Thoss. "Calculation of Reactive Flux Correlation Functions for Systems in a Condensed Phase Environment: A Multilayer Multiconfiguration Time-Dependent Hartree Approach". In: *J. Chem. Phys.* 125.17 (Nov. 7, 2006), p. 174502. ISSN: 0021-9606. DOI: [10.1063/1.2363195](https://doi.org/10.1063/1.2363195).
- [541] I. R. Craig, M. Thoss, and H. Wang. "Proton Transfer Reactions in Model Condensed-Phase Environments: Accurate Quantum Dynamics Using the Multilayer Multiconfiguration Time-Dependent Hartree Approach". In: *J. Chem. Phys.* 127.14 (Oct. 14, 2007), p. 144503. ISSN: 0021-9606. DOI: [10.1063/1.2772265](https://doi.org/10.1063/1.2772265).
-

- [542] I. Kondov et al. "Quantum Dynamics of Photoinduced Electron-Transfer Reactions in Dye–Semiconductor Systems: First-Principles Description and Application to Coumarin 343–TiO<sub>2</sub>". In: *J. Phys. Chem. C* 111.32 (Aug. 1, 2007), pp. 11970–11981. ISSN: 1932-7447. DOI: [10.1021/jp072217m](https://doi.org/10.1021/jp072217m).
- [543] H. Wang and M. Thoss. "Quantum Dynamical Simulation of Electron-Transfer Reactions in an Anharmonic Environment". In: *J. Phys. Chem. A* 111.41 (Oct. 1, 2007), pp. 10369–10375. ISSN: 1089-5639. DOI: [10.1021/jp072367x](https://doi.org/10.1021/jp072367x).
- [544] I. R. Craig, M. Thoss, and H. Wang. "Accurate Quantum-Mechanical Rate Constants for a Linear Response Azzouz-Borgis Proton Transfer Model Employing the Multilayer Multiconfiguration Time-Dependent Hartree Approach". In: *J. Chem. Phys.* 135.6 (Aug. 14, 2011), p. 064504. ISSN: 0021-9606. DOI: [10.1063/1.3624342](https://doi.org/10.1063/1.3624342).
- [545] H. Wang et al. "Numerically Exact, Time-Dependent Treatment of Vibrationally Coupled Electron Transport in Single-Molecule Junctions". In: *J. Chem. Phys.* 135.24 (Dec. 29, 2011), p. 244506. ISSN: 0021-9606. DOI: [10.1063/1.3660206](https://doi.org/10.1063/1.3660206).
- [546] S. Mainali et al. "Comparison of the Multi-Layer Multi-Configuration Time-Dependent Hartree (ML-MCTDH) Method and the Density Matrix Renormalization Group (DMRG) for Ground State Properties of Linear Rotor Chains". In: *J. Chem. Phys.* 154.17 (May 7, 2021), p. 174106. ISSN: 0021-9606. DOI: [10.1063/5.0047090](https://doi.org/10.1063/5.0047090).
- [547] H. Wang and H.-D. Meyer. "On Regularizing the ML-MCTDH Equations of Motion". In: *J. Chem. Phys.* 149.4 (July 27, 2018), p. 044119. ISSN: 0021-9606. DOI: [10/gdzsts](https://doi.org/10/gdzsts).
- [548] T. Weike and U. Manthe. "Symmetries in the Multi-Configurational Time-Dependent Hartree Wavefunction Representation and Propagation". In: *J. Chem. Phys.* 154.19 (May 21, 2021), p. 194108. ISSN: 0021-9606. DOI: [10.1063/5.0054105](https://doi.org/10.1063/5.0054105).
- [549] R. Penrose. "Applications of Negative Dimensional Tensors". In: *Combinatorial Mathematics and Its Applications*. Vol. 1. 1971, pp. 221–244. ISBN: 978-0-8078-7820-0.
- [550] J. C. Bridgeman and C. T. Chubb. "Hand-Waving and Interpretive Dance: An Introductory Course on Tensor Networks". In: *J. Phys. A: Math. Theor.* 50.22 (May 2017), p. 223001. ISSN: 1751-8121. DOI: [10.1088/1751-8121/aa6dc3](https://doi.org/10.1088/1751-8121/aa6dc3).
- [551] F. L. Hitchcock. "The Expression of a Tensor or a Polyadic as a Sum of Products". In: *J. Math. Phys. Camb.* 6.1-4 (1927), pp. 164–189. ISSN: 1467-9590. DOI: [10.1002/sapm192761164](https://doi.org/10.1002/sapm192761164).
- [552] L. R. Tucker. "Implications of Factor Analysis of Three-Way Matrices for Measurement of Change". In: *Problems in measuring change* 15.122-137 (1963), p. 3.
- [553] L. R. Tucker et al. "The Extension of Factor Analysis to Three-Dimensional Matrices". In: *Contributions to mathematical psychology* 110119 (1964).
- [554] L. R. Tucker. "Some Mathematical Notes on Three-Mode Factor Analysis". In: *Psychometrika* 31.3 (Sept. 1, 1966), pp. 279–311. ISSN: 1860-0980. DOI: [10.1007/BF02289464](https://doi.org/10.1007/BF02289464).
- [555] T. G. Kolda and B. W. Bader. "Tensor Decompositions and Applications". In: *SIAM Rev.* 51.3 (Aug. 6, 2009), pp. 455–500. ISSN: 0036-1445. DOI: [10.1137/07070111X](https://doi.org/10.1137/07070111X).

- 
- [556] M. A. Nielsen and I. L. Chuang. *Quantum Computation and Quantum Information: 10th Anniversary Edition*. Cambridge: Cambridge University Press, 2010. ISBN: 978-1-107-00217-3. DOI: [10.1017/CB09780511976667](https://doi.org/10.1017/CB09780511976667).
- [557] W. Hackbusch and S. Kühn. “A New Scheme for the Tensor Representation”. In: *J Fourier Anal Appl* 15.5 (Oct. 1, 2009), pp. 706–722. ISSN: 1531-5851. DOI: [10.1007/s00041-009-9094-9](https://doi.org/10.1007/s00041-009-9094-9).
- [558] L. Grasedyck. “Hierarchical Singular Value Decomposition of Tensors”. In: *SIAM J. Matrix Anal. Appl.* 31.4 (Jan. 2010), pp. 2029–2054. ISSN: 0895-4798. DOI: [10.1137/090764189](https://doi.org/10.1137/090764189).
- [559] W. Hackbusch. *Tensor Spaces and Numerical Tensor Calculus*. 2nd ed. 2019 edition. Cham, Switzerland: Springer, Jan. 24, 2020. 633 pp. ISBN: 978-3-030-35553-1.
- [560] Y.-Y. Shi, L.-M. Duan, and G. Vidal. “Classical Simulation of Quantum Many-Body Systems with a Tree Tensor Network”. In: *Phys. Rev. A* 74.2 (Aug. 23, 2006), p. 022320. DOI: [10.1103/PhysRevA.74.022320](https://doi.org/10.1103/PhysRevA.74.022320).
- [561] L. Tagliacozzo, G. Evenbly, and G. Vidal. “Simulation of Two-Dimensional Quantum Systems Using a Tree Tensor Network That Exploits the Entropic Area Law”. In: *Phys. Rev. B* 80.23 (Dec. 18, 2009), p. 235127. DOI: [10.1103/PhysRevB.80.235127](https://doi.org/10.1103/PhysRevB.80.235127).
- [562] V. Murg et al. “Simulating Strongly Correlated Quantum Systems with Tree Tensor Networks”. In: *Phys. Rev. B* 82.20 (Nov. 3, 2010), p. 205105. DOI: [10.1103/PhysRevB.82.205105](https://doi.org/10.1103/PhysRevB.82.205105).
- [563] V. Alba, L. Tagliacozzo, and P. Calabrese. “Entanglement Entropy of Two Disjoint Intervals in C=1 Theories”. In: *J. Stat. Mech.* 2011.06 (June 2011), P06012. ISSN: 1742-5468. DOI: [10.1088/1742-5468/2011/06/P06012](https://doi.org/10.1088/1742-5468/2011/06/P06012).
- [564] N. Nakatani and G. K.-L. Chan. “Efficient Tree Tensor Network States (TTNS) for Quantum Chemistry: Generalizations of the Density Matrix Renormalization Group Algorithm”. In: *J. Chem. Phys.* 138.13 (Apr. 4, 2013), p. 134113. ISSN: 0021-9606. DOI: [10.1063/1.4798639](https://doi.org/10.1063/1.4798639).
- [565] I. V. Oseledets. “Tensor-Train Decomposition”. In: *SIAM J. Sci. Comput.* 33.5 (Jan. 2011), pp. 2295–2317. ISSN: 1064-8275. DOI: [10.1137/090752286](https://doi.org/10.1137/090752286).
- [566] N. Shibata. “Thermodynamics of the Anisotropic Heisenberg Chain Calculated by the Density Matrix Renormalization Group Method”. In: *J. Phys. Soc. Jpn.* 66.8 (Aug. 15, 1997), pp. 2221–2223. ISSN: 0031-9015. DOI: [10.1143/JPSJ.66.2221](https://doi.org/10.1143/JPSJ.66.2221).
- [567] T. D. Kühner and H. Monien. “Phases of the One-Dimensional Bose-Hubbard Model”. In: *Phys. Rev. B* 58.22 (Dec. 1, 1998), R14741–R14744. DOI: [10/cdfmhs](https://doi.org/10/cdfmhs).
- [568] A. Mering and M. Fleischhauer. “One-Dimensional Bose-Fermi-Hubbard Model in the Heavy-Fermion Limit”. In: *Phys. Rev. A* 77.2 (Feb. 1, 2008), p. 023601. DOI: [10.1103/PhysRevA.77.023601](https://doi.org/10.1103/PhysRevA.77.023601).
- [569] M. Tezuka and M. Ueda. “Density-Matrix Renormalization Group Study of Trapped Imbalanced Fermi Condensates”. In: *Phys. Rev. Lett.* 100.11 (Mar. 19, 2008), p. 110403. DOI: [10.1103/PhysRevLett.100.110403](https://doi.org/10.1103/PhysRevLett.100.110403).
- [570] A. W. Sandvik. “Ground States of a Frustrated Quantum Spin Chain with Long-Range Interactions”. In: *Phys. Rev. Lett.* 104.13 (Mar. 31, 2010), p. 137204. DOI: [10.1103/PhysRevLett.104.137204](https://doi.org/10.1103/PhysRevLett.104.137204).
-

- [571] Z.-X. Gong et al. "Kaleidoscope of Quantum Phases in a Long-Range Interacting Spin-1 Chain". In: *Phys. Rev. B* 93.20 (May 11, 2016), p. 205115. doi: [10.1103/PhysRevB.93.205115](https://doi.org/10.1103/PhysRevB.93.205115).
- [572] Ö. Legeza, J. Röder, and B. A. Hess. "QC-DMRG Study of the Ionic-Neutral Curve Crossing of LiF". In: *Mol. Phys.* 101.13 (July 10, 2003), pp. 2019–2028. issn: 0026-8976. doi: [10.1080/0026897031000155625](https://doi.org/10.1080/0026897031000155625).
- [573] G. Moritz, A. Wolf, and M. Reiher. "Relativistic DMRG Calculations on the Curve Crossing of Cesium Hydride". In: *J. Chem. Phys.* 123.18 (Nov. 8, 2005), p. 184105. issn: 0021-9606. doi: [10.1063/1.2104447](https://doi.org/10.1063/1.2104447).
- [574] F. Liu et al. "Multireference Ab Initio Density Matrix Renormalization Group (DMRG)-CASSCF and DMRG-CASPT2 Study on the Photochromic Ring Opening of Spiropyran". In: *J. Chem. Theory Comput.* 9.10 (Oct. 8, 2013), pp. 4462–4469. issn: 1549-9618. doi: [10.1021/ct400707k](https://doi.org/10.1021/ct400707k).
- [575] S. Wouters et al. "Communication: Dmrg-Scf Study of the Singlet, Triplet, and Quintet States of Oxo-Mn(Salen)". In: *J. Chem. Phys.* 140.24 (June 28, 2014), p. 241103. issn: 0021-9606. doi: [10.1063/1.4885815](https://doi.org/10.1063/1.4885815).
- [576] S. Wouters, V. Van Speybroeck, and D. Van Neck. "DMRG-CASPT2 Study of the Longitudinal Static Second Hyperpolarizability of All-Trans Polyenes". In: *J. Chem. Phys.* 145.5 (Aug. 7, 2016), p. 054120. issn: 0021-9606. doi: [10.1063/1.4959817](https://doi.org/10.1063/1.4959817).
- [577] S. Guo, Z. Li, and G. K.-L. Chan. "A Perturbative Density Matrix Renormalization Group Algorithm for Large Active Spaces". In: *J. Chem. Theory Comput.* 14.8 (Aug. 14, 2018), pp. 4063–4071. issn: 1549-9618. doi: [10.1021/acs.jctc.8b00273](https://doi.org/10.1021/acs.jctc.8b00273).
- [578] A. Baiardi and M. Reiher. "The Density Matrix Renormalization Group in Chemistry and Molecular Physics: Recent Developments and New Challenges". In: *J. Chem. Phys.* 152.4 (Jan. 31, 2020), p. 040903. issn: 0021-9606. doi: [10.1063/1.5129672](https://doi.org/10.1063/1.5129672).
- [579] S. R. White. "Spin Gaps in a Frustrated Heisenberg Model for  $\text{CaV}_4\text{O}_9$ ". In: *Phys. Rev. Lett.* 77.17 (Oct. 21, 1996), pp. 3633–3636. doi: [10.1103/PhysRevLett.77.3633](https://doi.org/10.1103/PhysRevLett.77.3633).
- [580] E. Stoudenmire and S. R. White. "Studying Two-Dimensional Systems with the Density Matrix Renormalization Group". In: *Annu. Rev. Condens. Ma. P.* 3.1 (2012), pp. 111–128. doi: [10.1146/annurev-conmatphys-020911-125018](https://doi.org/10.1146/annurev-conmatphys-020911-125018).
- [581] Y. Iqbal et al. "Spin Liquid Nature in the Heisenberg J1-J2 Triangular Antiferromagnet". In: *Phys. Rev. B* 93.14 (Apr. 11, 2016), p. 144411. doi: [10.1103/PhysRevB.93.144411](https://doi.org/10.1103/PhysRevB.93.144411).
- [582] Y.-C. He et al. "Signatures of Dirac Cones in a DMRG Study of the Kagome Heisenberg Model". In: *Phys. Rev. X* 7.3 (July 28, 2017), p. 031020. doi: [10.1103/PhysRevX.7.031020](https://doi.org/10.1103/PhysRevX.7.031020).
- [583] G. Vidal et al. "Entanglement in Quantum Critical Phenomena". In: *Phys. Rev. Lett.* 90.22 (June 2, 2003), p. 227902. doi: [10.1103/PhysRevLett.90.227902](https://doi.org/10.1103/PhysRevLett.90.227902).
- [584] A. J. Daley et al. "Time-Dependent Density-Matrix Renormalization-Group Using Adaptive Effective Hilbert Spaces". In: *J. Stat. Mech.: Theory E.* 2004.04 (2004), P04005. issn: 1742-5468. doi: [10/b8kdqf](https://doi.org/10/b8kdqf).

- 
- [585] G. Vidal. “Efficient Simulation of One-Dimensional Quantum Many-Body Systems”. In: *Phys. Rev. Lett.* 93.4 (July 19, 2004), p. 040502. DOI: [10.1103/PhysRevLett.93.040502](https://doi.org/10.1103/PhysRevLett.93.040502).
- [586] S. R. White and A. E. Feiguin. “Real-Time Evolution Using the Density Matrix Renormalization Group”. In: *Phys. Rev. Lett.* 93.7 (Aug. 2004), p. 076401. DOI: [10/fwdhbm](https://doi.org/10/fwdhbm).
- [587] H. F. Trotter. “On the Product of Semi-Groups of Operators”. In: *Proc. Amer. Math. Soc.* 10.4 (1959), pp. 545–551. ISSN: 0002-9939, 1088-6826. DOI: [10.1090/S0002-9939-1959-0108732-6](https://doi.org/10.1090/S0002-9939-1959-0108732-6).
- [588] M. Suzuki. “Generalized Trotter’s Formula and Systematic Approximants of Exponential Operators and Inner Derivations with Applications to Many-Body Problems”. In: *Commun. Math. Phys.* 51.2 (June 1, 1976), pp. 183–190. ISSN: 1432-0916. DOI: [10.1007/BF01609348](https://doi.org/10.1007/BF01609348).
- [589] M. Urbanek and P. Soldán. “Parallel Implementation of the Time-Evolving Block Decimation Algorithm for the Bose–Hubbard Model”. In: *Comput. Phys. Commun.* 199 (Feb. 1, 2016), pp. 170–177. ISSN: 0010-4655. DOI: [10.1016/j.cpc.2015.10.016](https://doi.org/10.1016/j.cpc.2015.10.016).
- [590] E. M. Stoudenmire and S. R. White. “Minimally Entangled Typical Thermal State Algorithms”. In: *New J. Phys.* 12.5 (May 2010), p. 055026. ISSN: 1367-2630. DOI: [10.1088/1367-2630/12/5/055026](https://doi.org/10.1088/1367-2630/12/5/055026).
- [591] J. Haegeman et al. “Time-Dependent Variational Principle for Quantum Lattices”. In: *Phys. Rev. Lett.* 107.7 (Aug. 10, 2011), p. 070601. DOI: [10.1103/PhysRevLett.107.070601](https://doi.org/10.1103/PhysRevLett.107.070601).
- [592] J. Haegeman, T. J. Osborne, and F. Verstraete. “Post-Matrix Product State Methods: To Tangent Space and Beyond”. In: *Phys. Rev. B* 88.7 (Aug. 20, 2013), p. 075133. DOI: [10.1103/PhysRevB.88.075133](https://doi.org/10.1103/PhysRevB.88.075133).
- [593] C. Lubich et al. “Dynamical Approximation by Hierarchical Tucker and Tensor-Train Tensors”. In: *SIAM J. Matrix Anal. Appl.* 34.2 (Jan. 2013), pp. 470–494. ISSN: 0895-4798. DOI: [10.1137/120885723](https://doi.org/10.1137/120885723).
- [594] J. Haegeman et al. “Unifying Time Evolution and Optimization with Matrix Product States”. In: *Phys. Rev. B* 94.16 (Oct. 10, 2016), p. 165116. DOI: [10.1103/PhysRevB.94.165116](https://doi.org/10.1103/PhysRevB.94.165116).
- [595] M. Yang and S. R. White. “Time-Dependent Variational Principle with Ancillary Krylov Subspace”. In: *Phys. Rev. B* 102.9 (Sept. 29, 2020), p. 094315. DOI: [10.1103/PhysRevB.102.094315](https://doi.org/10.1103/PhysRevB.102.094315).
- [596] Y. Kurashige. “Matrix Product State Formulation of the Multiconfiguration Time-Dependent Hartree Theory”. In: *J. Chem. Phys.* 149.19 (Nov. 21, 2018), p. 194114. ISSN: 0021-9606. DOI: [10.1063/1.5051498](https://doi.org/10.1063/1.5051498).
- [597] F. A. Y. N. Schröder et al. “Tensor Network Simulation of Multi-Environmental Open Quantum Dynamics via Machine Learning and Entanglement Renormalisation”. In: *Nat. Commun.* 10.1 (1 Mar. 5, 2019), p. 1062. ISSN: 2041-1723. DOI: [10.1038/s41467-019-09039-7](https://doi.org/10.1038/s41467-019-09039-7).
- [598] D. Bauernfeind and M. Aichhorn. “Time Dependent Variational Principle for Tree Tensor Networks”. In: *SciPost Phys.* 8.2 (Feb. 7, 2020), p. 024. ISSN: 2542-4653. DOI: [10.21468/SciPostPhys.8.2.024](https://doi.org/10.21468/SciPostPhys.8.2.024).
-

- [599] D. Kosloff and R. Kosloff. "A Fourier Method Solution for the Time Dependent Schrödinger Equation as a Tool in Molecular Dynamics". In: *J. Comput. Phys.* 52.1 (Oct. 1, 1983), pp. 35–53. ISSN: 0021-9991. DOI: [10/bdmt8m](https://doi.org/10/bdmt8m).
- [600] J. C. Light, I. P. Hamilton, and J. V. Lill. "Generalized Discrete Variable Approximation in Quantum Mechanics". In: *J. Chem. Phys.* 82.3 (1985), pp. 1400–1409. DOI: [10/cjdkj2](https://doi.org/10/cjdkj2).
- [601] R. Kosloff and H. Tal-Ezer. "A Direct Relaxation Method for Calculating Eigenfunctions and Eigenvalues of the Schrödinger Equation on a Grid". In: *Chem. Phys. Lett.* 127.3 (June 13, 1986), pp. 223–230. ISSN: 0009-2614. DOI: [10/bq4zmn](https://doi.org/10/bq4zmn).
- [602] J. V. Lill, G. A. Parker, and J. C. Light. "The Discrete Variable–Finite Basis Approach to Quantum Scattering". In: *J. Chem. Phys.* 85.2 (July 15, 1986), pp. 900–910. ISSN: 0021-9606. DOI: [10.1063/1.451245](https://doi.org/10.1063/1.451245).
- [603] G. C. Corey and D. Lemoine. "Pseudospectral Method for Solving the Time-dependent Schrödinger Equation in Spherical Coordinates". In: *J. Chem. Phys.* 97.6 (Sept. 15, 1992), pp. 4115–4126. ISSN: 0021-9606. DOI: [10.1063/1.463916](https://doi.org/10.1063/1.463916).
- [604] M. J. Bramley et al. "Efficient Calculation of Highly Excited Vibrational Energy Levels of Floppy Molecules: The Band Origins of  $\text{H}^+_3$  up to  $35000\text{ cm}^{-1}$ ". In: *J. Chem. Phys.* 100.9 (May 1994), pp. 6175–6194. ISSN: 0021-9606. DOI: [10.1063/1.467273](https://doi.org/10.1063/1.467273).
- [605] D. Lemoine. "The Finite Basis Representation as the Primary Space in Multidimensional Pseudospectral Schemes". In: *J. Chem. Phys.* 101.12 (Dec. 15, 1994), pp. 10526–10532. ISSN: 0021-9606. DOI: [10.1063/1.467870](https://doi.org/10.1063/1.467870).
- [606] R. Kosloff. "Quantum Molecular Dynamics on Grids". In: *Dynamics of Molecules and Chemical Reactions*. Ed. by R. E. Wyatt and J. Z. H. Zhang. 1st edition. New York: CRC Press, June 27, 1996, pp. 185–230. ISBN: 978-0-8247-9538-2.
- [607] J. C. Light and T. Carrington Jr. "Discrete-Variable Representations and Their Utilization". In: *Advances in Chemical Physics*. John Wiley & Sons, Ltd, 2000, pp. 263–310. ISBN: 978-0-470-14173-1. DOI: [10.1002/9780470141731.ch4](https://doi.org/10.1002/9780470141731.ch4).
- [608] D. O. Harris, G. G. Engerholm, and W. D. Gwinn. "Calculation of Matrix Elements for One-Dimensional Quantum-Mechanical Problems and the Application to Anharmonic Oscillators". In: *J. Chem. Phys.* 43.5 (Sept. 1965), pp. 1515–1517. ISSN: 0021-9606. DOI: [10.1063/1.1696963](https://doi.org/10.1063/1.1696963).
- [609] A. S. Dickinson and P. R. Certain. "Calculation of Matrix Elements for One-Dimensional Quantum-Mechanical Problems". In: *J. Chem. Phys.* 49.9 (Nov. 1968), pp. 4209–4211. ISSN: 0021-9606. DOI: [10.1063/1.1670738](https://doi.org/10.1063/1.1670738).
- [610] R. Kosloff. "Dynamics of Molecules and Chemical Reactions". In: *Mercel Dekker, New York* (1996), p. 185.
- [611] R. Dawes and T. Carrington Jr. "A Multidimensional Discrete Variable Representation Basis Obtained by Simultaneous Diagonalization". In: *J. Chem. Phys.* 121.2 (June 24, 2004), pp. 726–736. ISSN: 0021-9606. DOI: [10.1063/1.1758941](https://doi.org/10.1063/1.1758941).
- [612] J. Li et al. "High-Level, First-Principles, Full-Dimensional Quantum Calculation of the Ro-vibrational Spectrum of the Simplest Criegee Intermediate ( $\text{CH}_2\text{OO}$ )". In: *J. Phys. Chem. Lett.* 5.13 (July 3, 2014), pp. 2364–2369. DOI: [10.1021/jz501059m](https://doi.org/10.1021/jz501059m).

- 
- [613] U. Manthe. "A Time-dependent Discrete Variable Representation for (Multiconfiguration) Hartree Methods". In: *J. Chem. Phys.* 105.16 (Oct. 22, 1996), pp. 6989–6994. ISSN: 0021-9606. DOI: [10.1063/1.471847](https://doi.org/10.1063/1.471847).
- [614] R. van Harrevelt and U. Manthe. "Degeneracy in Discrete Variable Representations: General Considerations and Application to the Multiconfigurational Time-Dependent Hartree Approach". In: *J. Chem. Phys.* 121.12 (Sept. 14, 2004), pp. 5623–5628. ISSN: 0021-9606. DOI: [10.1063/1.1782811](https://doi.org/10.1063/1.1782811).
- [615] R. van Harrevelt and U. Manthe. "Multidimensional Time-Dependent Discrete Variable Representations in Multiconfiguration Hartree Calculations". In: *J. Chem. Phys.* 123.6 (Aug. 16, 2005), p. 064106. ISSN: 0021-9606. DOI: [10.1063/1.1995692](https://doi.org/10.1063/1.1995692).
- [616] D. Gottlieb and S. A. Orszag. *Numerical Analysis of Spectral Methods*. Society for Industrial and Applied Mathematics, 1977. DOI: [10.1137/1.9781611970425](https://doi.org/10.1137/1.9781611970425).
- [617] W. Yang and A. C. Peet. "The Collocation Method for Bound Solutions of the Schrödinger Equation". In: *Chem. Phys. Lett.* 153.1 (Dec. 2, 1988), pp. 98–104. ISSN: 0009-2614. DOI: [10.1016/0009-2614\(88\)80139-8](https://doi.org/10.1016/0009-2614(88)80139-8).
- [618] B. W. Shore. "Solving the Radial Schrödinger Equation by Using Cubic-spline Basis Functions". In: *J. Chem. Phys.* 58.9 (Aug. 22, 2003), pp. 3855–3866. ISSN: 0021-9606. DOI: [10.1063/1.1679740](https://doi.org/10.1063/1.1679740).
- [619] S. Manzhos and T. Carrington. "An Improved Neural Network Method for Solving the Schrödinger Equation". In: *Can. J. Chem.* 87.7 (July 2009), pp. 864–871. ISSN: 0008-4042. DOI: [10.1139/V09-025](https://doi.org/10.1139/V09-025).
- [620] S. Manzhos, M. Chan, and T. Carrington Jr. "Communication: Favorable Dimensionality Scaling of Rectangular Collocation with Adaptable Basis Functions up to 7 Dimensions". In: *J. Chem. Phys.* 139.5 (Aug. 1, 2013), p. 051101. ISSN: 0021-9606. DOI: [10.1063/1.4817182](https://doi.org/10.1063/1.4817182).
- [621] G. Avila and T. Carrington Jr. "A Multi-Dimensional Smolyak Collocation Method in Curvilinear Coordinates for Computing Vibrational Spectra". In: *J. Chem. Phys.* 143.21 (Dec. 2, 2015), p. 214108. ISSN: 0021-9606. DOI: [10.1063/1.4936294](https://doi.org/10.1063/1.4936294).
- [622] G. Avila and T. Carrington Jr. "Reducing the Cost of Using Collocation to Compute Vibrational Energy Levels: Results for CH<sub>2</sub>NH". In: *J. Chem. Phys.* 147.6 (Aug. 8, 2017), p. 064103. ISSN: 0021-9606. DOI: [10.1063/1.4994920](https://doi.org/10.1063/1.4994920).
- [623] R. Wodraszka and T. Carrington. "A New Collocation-Based Multi-Configuration Time-Dependent Hartree (MCTDH) Approach for Solving the Schrödinger Equation with a General Potential Energy Surface". In: *J. Chem. Phys.* 148.4 (Jan. 30, 2018), p. 044115. ISSN: 0021-9606. DOI: [10.1063/1.5018793](https://doi.org/10.1063/1.5018793).
- [624] R. Wodraszka and T. Carrington Jr. "A Pruned Collocation-Based Multiconfiguration Time-Dependent Hartree Approach Using a Smolyak Grid for Solving the Schrödinger Equation with a General Potential Energy Surface". In: *J. Chem. Phys.* 150.15 (Apr. 16, 2019), p. 154108. ISSN: 0021-9606. DOI: [10.1063/1.5093317](https://doi.org/10.1063/1.5093317).
- [625] R. Wodraszka and T. Carrington Jr. "A Collocation-Based Multi-Configuration Time-Dependent Hartree Method Using Mode Combination and Improved Relaxation". In: *J. Chem. Phys.* 152.16 (Apr. 30, 2020), p. 164117. ISSN: 0021-9606. DOI: [10.1063/5.0006081](https://doi.org/10.1063/5.0006081).
-

- [626] R. Wodraszka and T. Carrington Jr. “A Rectangular Collocation Multi-Configuration Time-Dependent Hartree (MCTDH) Approach with Time-Independent Points for Calculations on General Potential Energy Surfaces”. In: *J. Chem. Phys.* 154.11 (Mar. 16, 2021), p. 114107. ISSN: 0021-9606. DOI: [10.1063/5.0046425](https://doi.org/10.1063/5.0046425).
- [627] J. W. Cooley and J. W. Tukey. “An Algorithm for the Machine Calculation of Complex Fourier Series”. In: *Math. Comput.* 19.90 (1965), pp. 297–301. ISSN: 00255718, 10886842. DOI: [10/fhm9cr](https://doi.org/10/fhm9cr).
- [628] J. W. Cooley, P. A. W. Lewis, and P. D. Welch. “The Fast Fourier Transform and Its Applications”. In: *IEEE T. Educ.* 12.1 (Mar. 1969), pp. 27–34. ISSN: 1557-9638. DOI: [10.1109/TE.1969.4320436](https://doi.org/10.1109/TE.1969.4320436).
- [629] W. Pauli. “Zur Quantenmechanik des magnetischen Elektrons”. In: *Z. Phys.* 43.9 (Sept. 1, 1927), pp. 601–623. ISSN: 0044-3328. DOI: [10.1007/BF01397326](https://doi.org/10.1007/BF01397326).
- [630] L. H. Thomas. “The Motion of the Spinning Electron”. In: *Nature* 117.2945 (2945 Apr. 1926), pp. 514–514. ISSN: 1476-4687. DOI: [10.1038/117514a0](https://doi.org/10.1038/117514a0).
- [631] C. Moller. *The Theory Of Relativity*. In collab. with Osmania University and Digital Library Of India. At The Clarendon Press, 1952. 409 pp. URL: <http://archive.org/details/theoryofrelativi029229mbp>.
- [632] V. Galitski and I. B. Spielman. “Spin–Orbit Coupling in Quantum Gases”. In: *Nature* 494.7435 (7435 Feb. 2013), pp. 49–54. ISSN: 1476-4687. DOI: [10.1038/nature11841](https://doi.org/10.1038/nature11841).
- [633] A. U. J. Lode, B. Chakrabarti, and V. K. B. Kota. “Many-Body Entropies, Correlations, and Emergence of Statistical Relaxation in Interaction Quench Dynamics of Ultracold Bosons”. In: *Phys. Rev. A* 92.3 (Sept. 23, 2015), p. 033622. DOI: [10/gffmkh](https://doi.org/10/gffmkh).
- [634] J. Neuhaus-Steinmetz, S. I. Mistakidis, and P. Schmelcher. “Quantum Dynamical Response of Ultracold Few-Boson Ensembles in Finite Optical Lattices to Multiple Interaction Quenches”. In: *Phys. Rev. A* 95.5 (May 10, 2017), p. 053610. DOI: [10/gfwrst](https://doi.org/10/gfwrst).
- [635] S. I. Mistakidis, G. M. Koutentakis, and P. Schmelcher. “Bosonic Quantum Dynamics Following a Linear Interaction Quench in Finite Optical Lattices of Unit Filling”. In: *Chem. Phys.* 509 (June 15, 2018), pp. 106–115. ISSN: 0301-0104. DOI: [10/gdvdp2](https://doi.org/10/gdvdp2).
- [636] T. Plaßmann, S. I. Mistakidis, and P. Schmelcher. “Quench Dynamics of Finite Bosonic Ensembles in Optical Lattices with Spatially Modulated Interactions”. In: *J. Phys. B: At. Mol. Opt. Phys.* 51.22 (Oct. 2018), p. 225001. ISSN: 0953-4075. DOI: [10/gfwrq6](https://doi.org/10/gfwrq6).
- [637] A. U. J. Lode et al. “Numerically Exact Quantum Dynamics of Bosons with Time-Dependent Interactions of Harmonic Type”. In: *Phys. Rev. A* 86.6 (Dec. 6, 2012), p. 063606. DOI: [10/gffmkg](https://doi.org/10/gffmkg).
- [638] R. Schmitz et al. “Quantum Breathing Dynamics of Ultracold Bosons in One-Dimensional Harmonic Traps: Unraveling the Pathway from Few- to Many-Body Systems”. In: *Phys. Rev. A* 88.4 (Oct. 2013), p. 043601. DOI: [10/gffmk4](https://doi.org/10/gffmk4).
- [639] M. Theisen and A. I. Streltsov. “Many-Body Excitations and Deexcitations in Trapped Ultracold Bosonic Clouds”. In: *Phys. Rev. A* 94.5 (Nov. 22, 2016), p. 053622. DOI: [10.1103/PhysRevA.94.053622](https://doi.org/10.1103/PhysRevA.94.053622).



- 
- [640] K. Sakmann et al. “Universality of Fragmentation in the Schrödinger Dynamics of Bosonic Josephson Junctions”. In: *Phys. Rev. A* 89.2 (Feb. 5, 2014), p. 023602. doi: [10/gft3dp](https://doi.org/10/gft3dp).
- [641] J. G. Cosme, M. F. Andersen, and J. Brand. “Interaction Blockade for Bosons in an Asymmetric Double Well”. In: *Phys. Rev. A* 96.1 (July 14, 2017), p. 013616. doi: [10.1103/PhysRevA.96.013616](https://doi.org/10.1103/PhysRevA.96.013616).
- [642] C. Menotti et al. “Dynamic Splitting of a Bose-Einstein Condensate”. In: *Phys. Rev. A* 63.2 (Jan. 4, 2001), p. 023601. doi: [10.1103/PhysRevA.63.023601](https://doi.org/10.1103/PhysRevA.63.023601).
- [643] D. J. Masiello and W. P. Reinhardt. “Time-Dependent Quantum Many-Body Theory of Identical Bosons in a Double Well: Early-time Ballistic Interferences of Fragmented and Number Entangled States”. In: *Phys. Rev. A* 76.4 (Oct. 11, 2007), p. 043612. doi: [10.1103/PhysRevA.76.043612](https://doi.org/10.1103/PhysRevA.76.043612).
- [644] J. Zanghellini et al. “Testing the Multi-Configuration Time-Dependent Hartree-Fock Method”. In: *J. Phys. B: At. Mol. Opt. Phys.* 37.4 (2004), p. 763. issn: 0953-4075. doi: [10/cdtfss](https://doi.org/10/cdtfss).
- [645] B. Diu, C. Cohen-Tannoudji, and F. Laloë. *Quantum Mechanics, Volume 3: Fermions, Bosons, Photons, Correlations, and Entanglement*. 1st edition. Weinheim: Wiley-VCH, Dec. 16, 2019. 784 pp. isbn: 978-3-527-34555-7.
- [646] P. A. M. Dirac. “The Quantum Theory of the Emission and Absorption of Radiation”. In: *P. R. Soc. London* 114.767 (Mar. 1, 1927), p. 243. doi: [10/d57ttp](https://doi.org/10/d57ttp).
- [647] A. I. Streltsov et al. “Accurate Multi-Boson Long-Time Dynamics in Triple-Well Periodic Traps”. In: *Phys. Rev. A* 83.4 (Apr. 6, 2011), p. 043604. doi: [10.1103/PhysRevA.83.043604](https://doi.org/10.1103/PhysRevA.83.043604).
- [648] A. I. Streltsov, O. E. Alon, and L. S. Cederbaum. “Swift Loss of Coherence of Soliton Trains in Attractive Bose-Einstein Condensates”. In: *Phys. Rev. Lett.* 106.24 (June 14, 2011), p. 240401. doi: [10.1103/PhysRevLett.106.240401](https://doi.org/10.1103/PhysRevLett.106.240401).
- [649] S. Bera et al. “Probing Relaxation Dynamics of a Few Strongly Correlated Bosons in a 1D Triple Well Optical Lattice”. In: *J. Phys. B: At. Mol. Opt. Phys.* 52.21 (Oct. 2019), p. 215303. issn: 0953-4075. doi: [10.1088/1361-6455/ab2999](https://doi.org/10.1088/1361-6455/ab2999).
- [650] S. Bera et al. “Sorting Fermionization from Crystallization in Many-Boson Wavefunctions”. In: *Sci. Rep.* 9.1 (1 Nov. 29, 2019), p. 17873. issn: 2045-2322. doi: [10.1038/s41598-019-53179-1](https://doi.org/10.1038/s41598-019-53179-1).
- [651] E. Fasshauer and A. U. J. Lode. “Multiconfigurational Time-Dependent Hartree Method for Fermions: Implementation, Exactness, and Few-Fermion Tunneling to Open Space”. In: *Phys. Rev. A* 93.3 (Mar. 21, 2016), p. 033635. doi: [10.1103/PhysRevA.93.033635](https://doi.org/10.1103/PhysRevA.93.033635).
- [652] B. D. Esry, C. H. Greene, and J. P. Burke. “Recombination of Three Atoms in the Ultracold Limit”. In: *Phys. Rev. Lett.* 83.9 (Aug. 30, 1999), pp. 1751–1754. doi: [10.1103/PhysRevLett.83.1751](https://doi.org/10.1103/PhysRevLett.83.1751).
- [653] D. S. Petrov, C. Salomon, and G. V. Shlyapnikov. “Scattering Properties of Weakly Bound Dimers of Fermionic Atoms”. In: *Phys. Rev. A* 71.1 (Jan. 14, 2005), p. 012708. doi: [10.1103/PhysRevA.71.012708](https://doi.org/10.1103/PhysRevA.71.012708).
-

- [654] H. P. Büchler, A. Micheli, and P. Zoller. “Three-Body Interactions with Cold Polar Molecules”. In: *Nature Phys* 3.10 (10 Oct. 2007), pp. 726–731. issn: 1745-2481. doi: [10.1038/nphys678](https://doi.org/10.1038/nphys678).
- [655] B.-l. Chen et al. “Mott-Hubbard Transition of Bosons in Optical Lattices with Three-Body Interactions”. In: *Phys. Rev. A* 78.4 (Oct. 7, 2008), p. 043603. doi: [10.1103/PhysRevA.78.043603](https://doi.org/10.1103/PhysRevA.78.043603).
- [656] K. P. Schmidt, J. Dorier, and A. M. Läuchli. “Solids and Supersolids of Three-Body Interacting Polar Molecules on an Optical Lattice”. In: *Phys. Rev. Lett.* 101.15 (Oct. 7, 2008), p. 150405. doi: [10.1103/PhysRevLett.101.150405](https://doi.org/10.1103/PhysRevLett.101.150405).
- [657] B. Capogrosso-Sansone et al. “Phase Diagram of One-Dimensional Hard-Core Bosons with Three-Body Interactions”. In: *Phys. Rev. B* 79.2 (Jan. 9, 2009), p. 020503. doi: [10.1103/PhysRevB.79.020503](https://doi.org/10.1103/PhysRevB.79.020503).
- [658] J. H. Huckans et al. “Three-Body Recombination in a Three-State Fermi Gas with Widely Tunable Interactions”. In: *Phys. Rev. Lett.* 102.16 (Apr. 24, 2009), p. 165302. doi: [10.1103/PhysRevLett.102.165302](https://doi.org/10.1103/PhysRevLett.102.165302).
- [659] P. R. Johnson et al. “Effective Three-Body Interactions of Neutral Bosons in Optical Lattices”. In: *New J. Phys.* 11.9 (Sept. 2009), p. 093022. issn: 1367-2630. doi: [10.1088/1367-2630/11/9/093022](https://doi.org/10.1088/1367-2630/11/9/093022).
- [660] L. Platter, H.-W. Hammer, and U.-G. Meißner. “Four-Boson System with Short-Range Interactions”. In: *Phys. Rev. A* 70.5 (Nov. 5, 2004), p. 052101. doi: [10.1103/PhysRevA.70.052101](https://doi.org/10.1103/PhysRevA.70.052101).
- [661] M. T. Yamashita et al. “Four-Boson Scale near a Feshbach Resonance”. In: *Europhys. Lett.* 75.4 (July 7, 2006), p. 555. issn: 0295-5075. doi: [10.1209/ep1/i2006-10141-6](https://doi.org/10.1209/ep1/i2006-10141-6).
- [662] F. Ferlaino et al. “Collisions between Tunable Halo Dimers: Exploring an Elementary Four-Body Process with Identical Bosons”. In: *Phys. Rev. Lett.* 101.2 (July 9, 2008), p. 023201. doi: [10.1103/PhysRevLett.101.023201](https://doi.org/10.1103/PhysRevLett.101.023201).
- [663] F. Ferlaino et al. “Evidence for Universal Four-Body States Tied to an Efimov Trimer”. In: *Phys. Rev. Lett.* 102.14 (Apr. 6, 2009), p. 140401. doi: [10.1103/PhysRevLett.102.140401](https://doi.org/10.1103/PhysRevLett.102.140401).
- [664] M. Stoll and T. Köhler. “Production of Three-Body Efimov Molecules in an Optical Lattice”. In: *Phys. Rev. A* 72.2 (Aug. 17, 2005), p. 022714. doi: [10.1103/PhysRevA.72.022714](https://doi.org/10.1103/PhysRevA.72.022714).
- [665] M. Bonkhoff et al. “Bosonic Continuum Theory of One-Dimensional Lattice Anyons”. In: *Phys. Rev. Lett.* 126.16 (Apr. 19, 2021), p. 163201. doi: [10.1103/PhysRevLett.126.163201](https://doi.org/10.1103/PhysRevLett.126.163201).
- [666] P. Jordan and E. Wigner. “Über das Paulische Äquivalenzverbot”. In: *Z. Phys.* 47.9 (Sept. 1, 1928), pp. 631–651. issn: 0044-3328. doi: [10/d4dxmd](https://doi.org/10/d4dxmd).
- [667] V. Fock. “Konfigurationsraum Und Zweite Quantelung”. In: *Z. Phys.* 75.9 (1932), pp. 622–647. issn: 0044-3328. doi: [10/d64q83](https://doi.org/10/d64q83).
- [668] B. D. Esry and C. H. Greene. “Validity of the Shape-Independent Approximation for Bose-Einstein Condensates”. In: *Phys. Rev. A* 60.2 (Aug. 1, 1999), pp. 1451–1462. doi: [10.1103/PhysRevA.60.1451](https://doi.org/10.1103/PhysRevA.60.1451).

- 
- [669] Y. Castin. “Simple Theoretical Tools for Low Dimension Bose Gases”. In: *J. Phys. IV* 116 (Oct. 1, 2004), pp. 89–132. ISSN: 1155-4339. DOI: [10.1051/jp4:2004116004](https://doi.org/10.1051/jp4:2004116004).
- [670] R. A. Doganov et al. “Two Trapped Particles Interacting by a Finite-Range Two-Body Potential in Two Spatial Dimensions”. In: *Phys. Rev. A* 87.3 (Mar. 28, 2013), p. 033631. DOI: [10.1103/PhysRevA.87.033631](https://doi.org/10.1103/PhysRevA.87.033631).
- [671] V. J. Bolsinger, S. Krönke, and P. Schmelcher. “Beyond Mean-Field Dynamics of Ultra-Cold Bosonic Atoms in Higher Dimensions: Facing the Challenges with a Multi-Configurational Approach”. In: *J. Phys. B: At. Mol. Opt. Phys.* 50.3 (2017), p. 034003. ISSN: 0953-4075. DOI: [10/gffmmg](https://doi.org/10/gffmmg).
- [672] I. Mitra, A. DasGupta, and B. Dutta-Roy. “Regularization and Renormalization in Scattering from Dirac Delta Potentials”. In: *Am. J. Phys.* 66.12 (Dec. 1, 1998), pp. 1101–1109. ISSN: 0002-9505. DOI: [10.1119/1.19051](https://doi.org/10.1119/1.19051).
- [673] R. M. Cavalcanti. “Exact Green’s Functions for Delta Function Potentials and Renormalization in Quantum Mechanics”. In: *Rev. Bras. Ens. Fis.* 21.arXiv:quant-ph/9801033 (1999), p. 336. URL: <https://inspirehep.net/literature/466300>.
- [674] T. Ernst et al. “Simulating Strongly Correlated Multiparticle Systems in a Truncated Hilbert Space”. In: *Phys. Rev. A* 84.2 (Aug. 16, 2011), p. 023623. DOI: [10.1103/PhysRevA.84.023623](https://doi.org/10.1103/PhysRevA.84.023623).
- [675] N. T. Zinner. “Universal Two-Body Spectra of Ultracold Harmonically Trapped Atoms in Two and Three Dimensions”. In: *J. Phys. A: Math. Theor.* 45.20 (May 2012), p. 205302. ISSN: 1751-8121. DOI: [10.1088/1751-8113/45/20/205302](https://doi.org/10.1088/1751-8113/45/20/205302).
- [676] M. Rontani et al. “On the Renormalization of Contact Interactions for the Configuration-Interaction Method in Two-Dimensions”. In: *J. Phys. B: At. Mol. Opt. Phys.* 50.6 (Mar. 2017), p. 065301. ISSN: 0953-4075. DOI: [10/f9r5xg](https://doi.org/10/f9r5xg).
- [677] O. E. Alon, A. I. Streltsov, and L. S. Cederbaum. “Multiconfigurational Time-Dependent Hartree Method for Mixtures Consisting of Two Types of Identical Particles”. In: *Phys. Rev. A* 76.6 (Dec. 7, 2007), p. 062501. DOI: [10.1103/PhysRevA.76.062501](https://doi.org/10.1103/PhysRevA.76.062501).
- [678] O. E. Alon et al. “Recursive Formulation of the Multiconfigurational Time-Dependent Hartree Method for Fermions, Bosons and Mixtures Thereof in Terms of One-Body Density Operators”. In: *Chem. Phys.* 401 (June 5, 2012), pp. 2–14. ISSN: 0301-0104. DOI: [10/frxsz4](https://doi.org/10/frxsz4).
- [679] L. Cao et al. “The Multi-Layer Multi-Configuration Time-Dependent Hartree Method for Bosons: Theory, Implementation, and Applications”. In: *J. Chem. Phys.* 139.13 (Oct. 2013), p. 134103. ISSN: 0021-9606, 1089-7690. DOI: [10/gffmjv](https://doi.org/10/gffmjv).
- [680] S. Krönke et al. “Non-Equilibrium Quantum Dynamics of Ultra-Cold Atomic Mixtures: The Multi-Layer Multi-Configuration Time-Dependent Hartree Method for Bosons”. In: *New J. Phys.* 15.6 (2013), p. 063018. ISSN: 1367-2630. DOI: [10/gffmj9](https://doi.org/10/gffmj9).
- [681] L. Cao et al. “A Unified Ab Initio Approach to the Correlated Quantum Dynamics of Ultracold Fermionic and Bosonic Mixtures”. In: *J. Chem. Phys.* 147.4 (July 26, 2017), p. 044106. ISSN: 0021-9606. DOI: [10/gbqn8w](https://doi.org/10/gbqn8w).
- [682] F. Theel et al. “Many-Body Collisional Dynamics of Impurities Injected into a Double-Well Trapped Bose-Einstein Condensate”. In: *Phys. Rev. Res.* 3.2 (Apr. 23, 2021), p. 023068. DOI: [10.1103/PhysRevResearch.3.023068](https://doi.org/10.1103/PhysRevResearch.3.023068).
-

- [683] M. Pyzh et al. “Entangling Lattice-Trapped Bosons with a Free Impurity: Impact on Stationary and Dynamical Properties”. In: *Entropy* 23.3 (3 Mar. 2021), p. 290. DOI: [10.3390/e23030290](https://doi.org/10.3390/e23030290).
- [684] S. Krönke and P. Schmelcher. “Many-Body Processes in Black and Gray Matter-Wave Solitons”. In: *Phys. Rev. A* 91.5 (May 15, 2015), p. 053614. DOI: [10.1103/PhysRevA.91.053614](https://doi.org/10.1103/PhysRevA.91.053614).
- [685] G. C. Katsimiga et al. “Many-Body Quantum Dynamics in the Decay of Bent Dark Solitons of Bose–Einstein Condensates”. In: *New J. Phys.* 19.12 (Dec. 2017), p. 123012. ISSN: 1367-2630. DOI: [10/gg5fv9](https://doi.org/10/gg5fv9).
- [686] F. Theel, S. I. Mistakidis, and P. Schmelcher. *Crossover from Attractive to Repulsive Induced Interactions and Bound States of Two Distinguishable Bose Polarons*. Mar. 8, 2023. DOI: [10.48550/arXiv.2303.04699](https://doi.org/10.48550/arXiv.2303.04699). preprint.
- [687] H. Wang and M. Thoss. “Numerically Exact Quantum Dynamics for Indistinguishable Particles: The Multilayer Multiconfiguration Time-Dependent Hartree Theory in Second Quantization Representation”. In: *J. Chem. Phys.* 131.2 (2009), p. 024114. DOI: [10/b8zmvk](https://doi.org/10/b8zmvk).
- [688] H. Wang. “Multilayer Multiconfiguration Time-Dependent Hartree Theory”. In: *J. Phys. Chem. A* 119.29 (July 23, 2015), pp. 7951–7965. ISSN: 1089-5639. DOI: [10.1021/acs.jpca.5b03256](https://doi.org/10.1021/acs.jpca.5b03256).
- [689] K. F. Albrecht et al. “Bistability Signatures in Nonequilibrium Charge Transport through Molecular Quantum Dots”. In: *Phys. Rev. B* 86.8 (Aug. 17, 2012), p. 081412. DOI: [10.1103/PhysRevB.86.081412](https://doi.org/10.1103/PhysRevB.86.081412).
- [690] H. Wang and M. Thoss. “Multilayer Multiconfiguration Time-Dependent Hartree Study of Vibrationally Coupled Electron Transport Using the Scattering-State Representation”. In: *J. Phys. Chem. A* 117.32 (Aug. 15, 2013), pp. 7431–7441. ISSN: 1089-5639. DOI: [10.1021/jp401464b](https://doi.org/10.1021/jp401464b).
- [691] E. Y. Wilner et al. “Bistability in a Nonequilibrium Quantum System with Electron-Phonon Interactions”. In: *Phys. Rev. B* 88.4 (July 31, 2013), p. 045137. DOI: [10.1103/PhysRevB.88.045137](https://doi.org/10.1103/PhysRevB.88.045137).
- [692] E. Y. Wilner et al. “Nonequilibrium Quantum Systems with Electron-Phonon Interactions: Transient Dynamics and Approach to Steady State”. In: *Phys. Rev. B* 89.20 (May 27, 2014), p. 205129. DOI: [10.1103/PhysRevB.89.205129](https://doi.org/10.1103/PhysRevB.89.205129).
- [693] S. Sasmal and O. Vendrell. “Non-Adiabatic Quantum Dynamics without Potential Energy Surfaces Based on Second-Quantized Electrons: Application within the Framework of the MCTDH Method”. In: *J. Chem. Phys.* 153.15 (Oct. 21, 2020), p. 154110. ISSN: 0021-9606. DOI: [10.1063/5.0028116](https://doi.org/10.1063/5.0028116).
- [694] U. Manthe and T. Weike. “On the Multi-Layer Multi-Configurational Time-Dependent Hartree Approach for Bosons and Fermions”. In: *J. Chem. Phys.* 146.6 (2017), p. 064117. DOI: [10/f9qz7h](https://doi.org/10/f9qz7h).
- [695] T. Weike and U. Manthe. “The Multi-Configurational Time-Dependent Hartree Approach in Optimized Second Quantization: Imaginary Time Propagation and Particle Number Conservation”. In: *J. Chem. Phys.* 152.3 (Jan. 16, 2020), p. 034101. ISSN: 0021-9606. DOI: [10/gj9xwh](https://doi.org/10/gj9xwh).
- [696] H. Q. Lin. “Exact Diagonalization of Quantum-Spin Models”. In: *Phys. Rev. B* 42.10 (Oct. 1, 1990), pp. 6561–6567. DOI: [10.1103/PhysRevB.42.6561](https://doi.org/10.1103/PhysRevB.42.6561).

- 
- [697] T. Haugset and H. Haugerud. "Exact Diagonalization of the Hamiltonian for Trapped Interacting Bosons in Lower Dimensions". In: *Phys. Rev. A* 57.5 (May 1, 1998), pp. 3809–3817. doi: [10.1103/PhysRevA.57.3809](https://doi.org/10.1103/PhysRevA.57.3809).
- [698] F. Deuretzbacher et al. "Evolution from a Bose-Einstein Condensate to a Tonks-Girardeau Gas: An Exact Diagonalization Study". In: *Phys. Rev. A* 75.1 (Jan. 12, 2007), p. 013614. doi: [10.1103/PhysRevA.75.013614](https://doi.org/10.1103/PhysRevA.75.013614).
- [699] S. Capponi and A. M. Läuchli. "Phase Diagram of Interacting Spinless Fermions on the Honeycomb Lattice: A Comprehensive Exact Diagonalization Study". In: *Phys. Rev. B* 92.8 (Aug. 26, 2015), p. 085146. doi: [10.1103/PhysRevB.92.085146](https://doi.org/10.1103/PhysRevB.92.085146).
- [700] D. Raventós et al. "Cold Bosons in Optical Lattices: A Tutorial for Exact Diagonalization". In: *J. Phys. B: At. Mol. Opt. Phys.* 50.11 (May 2017), p. 113001. issn: 0953-4075. doi: [10.1088/1361-6455/aa68b1](https://doi.org/10.1088/1361-6455/aa68b1).
- [701] H. Wang. "Iterative Calculation of Energy Eigenstates Employing the Multilayer Multiconfiguration Time-Dependent Hartree Theory". In: *J. Phys. Chem. A* 118.39 (Oct. 2, 2014), pp. 9253–9261. issn: 1089-5639. doi: [10.1021/jp503351t](https://doi.org/10.1021/jp503351t).
- [702] J. Hinze. "MC-SCF. I. The Multi-Configuration Self-Consistent-Field Method". In: *J. Chem. Phys.* 59.12 (Dec. 15, 1973), pp. 6424–6432. issn: 0021-9606. doi: [10.1063/1.1680022](https://doi.org/10.1063/1.1680022).
- [703] R. Lehoucq, D. Sorensen, and C. Yang. *ARPACK Users' Guide*. Software, Environments and Tools. Philadelphia: Society for Industrial and Applied Mathematics, Jan. 1, 1998. 150 pp. isbn: 978-0-89871-407-4. doi: [10.1137/1.9780898719628](https://doi.org/10.1137/1.9780898719628).
- [704] D. Jaksch and P. Zoller. "The Cold Atom Hubbard Toolbox". In: *Ann. Phys. Special Issue* 315.1 (Jan. 1, 2005), pp. 52–79. issn: 0003-4916. doi: [10/dv3ws6](https://doi.org/10/dv3ws6).
- [705] G. A. Worth. "Accurate Wave Packet Propagation for Large Molecular Systems: The Multiconfiguration Time-Dependent Hartree (MCTDH) Method with Selected Configurations". In: *J. Chem. Phys.* 112.19 (May 15, 2000), pp. 8322–8329. issn: 0021-9606, 1089-7690. doi: [10.1063/1.481438](https://doi.org/10.1063/1.481438).
- [706] R. Wodraszka and T. Carrington. "Using a Pruned, Nondirect Product Basis in Conjunction with the Multi-Configuration Time-Dependent Hartree (MCTDH) Method". In: *J. Chem. Phys.* 145.4 (July 27, 2016), p. 044110. issn: 0021-9606. doi: [10/gfzj42](https://doi.org/10/gfzj42).
- [707] H. Miyagi and L. B. Madsen. "Time-Dependent Restricted-Active-Space Self-Consistent-Field Theory for Laser-Driven Many-Electron Dynamics". In: *Phys. Rev. A* 87.6 (June 21, 2013), p. 062511. doi: [10.1103/PhysRevA.87.062511](https://doi.org/10.1103/PhysRevA.87.062511).
- [708] H. Miyagi and L. B. Madsen. "Time-Dependent Restricted-Active-Space Self-Consistent-Field Singles Method for Many-Electron Dynamics". In: *J. Chem. Phys.* 140.16 (Apr. 25, 2014), p. 164309. issn: 0021-9606. doi: [10/gffmkq](https://doi.org/10/gffmkq).
- [709] H. Miyagi and L. B. Madsen. "Time-Dependent Restricted-Active-Space Self-Consistent-Field Theory for Laser-Driven Many-Electron Dynamics. II. Extended Formulation and Numerical Analysis". In: *Phys. Rev. A* 89.6 (June 25, 2014), p. 063416. doi: [10.1103/PhysRevA.89.063416](https://doi.org/10.1103/PhysRevA.89.063416).
- [710] D. J. Haxton and C. W. McCurdy. "Two Methods for Restricted Configuration Spaces within the Multiconfiguration Time-Dependent Hartree-Fock Method". In: *Phys. Rev. A* 91.1 (Jan. 20, 2015), p. 012509. doi: [10/gffmj7](https://doi.org/10/gffmj7).
-

- [711] C. Lévêque and L. B. Madsen. “Time-Dependent Restricted-Active-Space Self-Consistent-Field Theory for Bosonic Many-Body Systems”. In: *New J. Phys.* 19.4 (2017), p. 043007. ISSN: 1367-2630. DOI: [10/gffmkf](https://doi.org/10/gffmkf).
- [712] H. R. Larsson, B. Hartke, and D. J. Tannor. “Efficient Molecular Quantum Dynamics in Coordinate and Phase Space Using Pruned Bases”. In: *J. Chem. Phys.* 145.20 (Nov. 28, 2016), p. 204108. ISSN: 0021-9606. DOI: [10/gffmkd](https://doi.org/10/gffmkd).
- [713] H. R. Larsson and D. J. Tannor. “Dynamical Pruning of the Multiconfiguration Time-Dependent Hartree (DP-MCTDH) Method: An Efficient Approach for Multidimensional Quantum Dynamics”. In: *J. Chem. Phys.* 147.4 (July 25, 2017), p. 044103. ISSN: 0021-9606. DOI: [10/gbqmdq](https://doi.org/10/gbqmdq).
- [714] J. Akram and A. Pelster. “Statics and Dynamics of Quasi One-Dimensional Bose–Einstein Condensate in Harmonic and Dimple Trap”. In: *Laser Phys.* 26.6 (May 2016), p. 065501. ISSN: 1555-6611. DOI: [10/gft2mt](https://doi.org/10/gft2mt).
- [715] C. C. Bradley et al. “Evidence of Bose-Einstein Condensation in an Atomic Gas with Attractive Interactions”. In: *Phys. Rev. Lett.* 75.9 (Aug. 28, 1995), pp. 1687–1690. DOI: [10/b2tp84](https://doi.org/10/b2tp84).
- [716] R. Senaratne et al. “Quantum Simulation of Ultrafast Dynamics Using Trapped Ultracold Atoms”. In: *Nat. Commun.* 9.1 (1 May 25, 2018), p. 2065. ISSN: 2041-1723. DOI: [10/gdn9nk](https://doi.org/10/gdn9nk).
- [717] Y. D. Wang et al. “Theory of Projectile Ionization by Molecular Hydrogen Targets”. In: *Nucl. Instrum. Meth. B* 79.1 (June 2, 1993), pp. 124–127. ISSN: 0168-583X. DOI: [10/dtnqq5](https://doi.org/10/dtnqq5).
- [718] E. C. Montenegro, W. E. Meyerhof, and J. H. McGuire. “Role of Two-Center Electron–Electron Interaction in Projectile Electron Excitation and Loss”. In: *Adv. At. Mol. Opt. Phys.* 34 (Jan. 1, 1994). Ed. by B. Bederson and H. Walther, pp. 249–300. DOI: [10.1016/S1049-250X\(08\)60079-8](https://doi.org/10.1016/S1049-250X(08)60079-8).
- [719] W. L. Fite et al. “Ionization and Charge Transfer in Proton-Hydrogen Atom Collisions”. In: *Phys. Rev.* 119.2 (July 15, 1960), pp. 663–668. DOI: [10/czf25w](https://doi.org/10/czf25w).
- [720] R. E. Olson and A. Salop. “Charge-Transfer and Impact-Ionization Cross Sections for Fully and Partially Stripped Positive Ions Colliding with Atomic Hydrogen”. In: *Phys. Rev. A* 16.2 (Aug. 1, 1977), pp. 531–541. DOI: [10/cx8dqf](https://doi.org/10/cx8dqf).
- [721] T. Calarco et al. “Quantum Gates with Neutral Atoms: Controlling Collisional Interactions in Time-Dependent Traps”. In: *Phys. Rev. A* 61.2 (Jan. 10, 2000), p. 022304. DOI: [10/ctjhtt](https://doi.org/10/ctjhtt).
- [722] D. P. DiVincenzo. “The Physical Implementation of Quantum Computation”. In: *Fortschr. Phys.* 48.9-11 (2000), pp. 771–783. ISSN: 1521-3978. DOI: [10.1002/1521-3978\(200009\)48:9/11<771::AID-PROP771>3.0.CO;2-E](https://doi.org/10.1002/1521-3978(200009)48:9/11<771::AID-PROP771>3.0.CO;2-E).
- [723] R. Jozsa and N. Linden. “On the Role of Entanglement in Quantum-Computational Speed-Up”. In: *P. Roy. Soc. Lond. A Mat.* 459.2036 (Aug. 8, 2003), pp. 2011–2032. DOI: [10/fhs6c2](https://doi.org/10/fhs6c2).
- [724] A. Ashkin. “Acceleration and Trapping of Particles by Radiation Pressure”. In: *Phys. Rev. Lett.* 24.4 (Jan. 1970), pp. 156–159. DOI: [10/bxxnjn](https://doi.org/10/bxxnjn).

- 
- [725] A. Ashkin et al. "Observation of a Single-Beam Gradient Force Optical Trap for Dielectric Particles". In: *Opt. Lett.* 11.5 (May 1, 1986), pp. 288–290. ISSN: 1539-4794. DOI: [10/c92str](https://doi.org/10/c92str).
- [726] A. Gaëtan et al. "Observation of Collective Excitation of Two Individual Atoms in the Rydberg Blockade Regime". In: *Nat. Phys.* 5.2 (2 Feb. 2009), pp. 115–118. ISSN: 1745-2481. DOI: [10/ctz867](https://doi.org/10/ctz867).
- [727] S. Sashkin et al. "Narrow-Line Cooling and Imaging of Ytterbium Atoms in an Optical Tweezer Array". In: *Phys. Rev. Lett.* 122.14 (Apr. 10, 2019), p. 143002. ISSN: 0031-9007, 1079-7114. DOI: [10/gfzbt5](https://doi.org/10/gfzbt5).
- [728] A. Ashkin and J. M. Dziedzic. "Optical Trapping and Manipulation of Viruses and Bacteria". In: *Science* 235.4795 (Mar. 20, 1987), pp. 1517–1520. ISSN: 0036-8075, 1095-9203. DOI: [10/bv3h5k](https://doi.org/10/bv3h5k).
- [729] K. Sakmann et al. "Reduced Density Matrices and Coherence of Trapped Interacting Bosons". In: *Phys. Rev. A* 78.2 (Aug. 8, 2008), p. 023615. DOI: [10/d93k6m](https://doi.org/10/d93k6m).
- [730] J. von Neumann. "Thermodynamik Quantenmechanischer Gesamtheiten". In: *Nachr. Akad. Wiss. Göttingen Math. Phys. Kl.* 1927 (1927), pp. 273–291. URL: <https://eudml.org/doc/59231>.
- [731] F. Bloch. "Zur Theorie des Ferromagnetismus". In: *Z. Phys.* 61.3 (Mar. 1, 1930), pp. 206–219. ISSN: 0044-3328. DOI: [10.1007/BF01339661](https://doi.org/10.1007/BF01339661).
- [732] J. C. Slater. "Cohesion in Monovalent Metals". In: *Phys. Rev.* 35.5 (Mar. 1, 1930), pp. 509–529. DOI: [10.1103/PhysRev.35.509](https://doi.org/10.1103/PhysRev.35.509).
- [733] W. Nolting and A. Ramakanth. *Quantum Theory of Magnetism*. 2010th edition. Heidelberg ; New York: Springer, Oct. 15, 2009. 765 pp. ISBN: 978-3-540-85415-9.
- [734] A. Auerbach. *Interacting Electrons and Quantum Magnetism*. Springer Science & Business Media, Sept. 11, 1998. 282 pp. ISBN: 978-0-387-94286-5.
- [735] F. Schäfer et al. "Tools for Quantum Simulation with Ultracold Atoms in Optical Lattices". In: *Nat Rev Phys* 2.8 (8 Aug. 2020), pp. 411–425. ISSN: 2522-5820. DOI: [10.1038/s42254-020-0195-3](https://doi.org/10.1038/s42254-020-0195-3).
- [736] G. Vidal. "Efficient Classical Simulation of Slightly Entangled Quantum Computations". In: *Phys. Rev. Lett.* 91.14 (Oct. 1, 2003), p. 147902. DOI: [10.1103/PhysRevLett.91.147902](https://doi.org/10.1103/PhysRevLett.91.147902).
- [737] N. Matsudaira. "Ising Ferromagnets with Random Impurities". In: *J. Phys. Soc. Jpn.* 35.6 (Dec. 15, 1973), pp. 1593–1599. ISSN: 0031-9015. DOI: [10.1143/JPSJ.35.1593](https://doi.org/10.1143/JPSJ.35.1593).
- [738] H. Frahm and A. A. Zvyagin. "The Open Spin Chain with Impurity: An Exact Solution". In: *J. Phys.: Condens. Mat.* 9.45 (Nov. 1997), pp. 9939–9946. ISSN: 0953-8984. DOI: [10.1088/0953-8984/9/45/021](https://doi.org/10.1088/0953-8984/9/45/021).
- [739] M. Oshikawa and I. Affleck. "Boundary Conformal Field Theory Approach to the Critical Two-Dimensional Ising Model with a Defect Line". In: *Nucl. Phys. B* 495.3 (June 30, 1997), pp. 533–582. ISSN: 0550-3213. DOI: [10.1016/S0550-3213\(97\)00219-8](https://doi.org/10.1016/S0550-3213(97)00219-8).
- [740] D. C. Tsui, H. L. Stormer, and A. C. Gossard. "Two-Dimensional Magnetotransport in the Extreme Quantum Limit". In: *Phys. Rev. Lett.* 48.22 (May 31, 1982), pp. 1559–1562. DOI: [10.1103/PhysRevLett.48.1559](https://doi.org/10.1103/PhysRevLett.48.1559).
-

- [741] R. B. Laughlin. “Anomalous Quantum Hall Effect: An Incompressible Quantum Fluid with Fractionally Charged Excitations”. In: *Phys. Rev. Lett.* 50.18 (May 2, 1983), pp. 1395–1398. doi: [10.1103/PhysRevLett.50.1395](https://doi.org/10.1103/PhysRevLett.50.1395).
- [742] H. L. Stormer. “Nobel Lecture: The Fractional Quantum Hall Effect”. In: *Rev. Mod. Phys.* 71.4 (July 1, 1999), pp. 875–889. doi: [10.1103/RevModPhys.71.875](https://doi.org/10.1103/RevModPhys.71.875).
- [743] S. F. Edwards and P. W. Anderson. “Theory of Spin Glasses”. In: *J. Phys. F: Met. Phys.* 5.5 (May 1975), pp. 965–974. issn: 0305-4608. doi: [10.1088/0305-4608/5/5/017](https://doi.org/10.1088/0305-4608/5/5/017).
- [744] D. Sherrington and S. Kirkpatrick. “Solvable Model of a Spin-Glass”. In: *Phys. Rev. Lett.* 35.26 (Dec. 29, 1975), pp. 1792–1796. doi: [10.1103/PhysRevLett.35.1792](https://doi.org/10.1103/PhysRevLett.35.1792).
- [745] K. Binder and A. P. Young. “Spin Glasses: Experimental Facts, Theoretical Concepts, and Open Questions”. In: *Rev. Mod. Phys.* 58.4 (Oct. 1, 1986), pp. 801–976. doi: [10.1103/RevModPhys.58.801](https://doi.org/10.1103/RevModPhys.58.801).
- [746] P. W. Anderson. “Absence of Diffusion in Certain Random Lattices”. In: *Phys. Rev.* 109.5 (Mar. 1, 1958), pp. 1492–1505. doi: [10.1103/PhysRev.109.1492](https://doi.org/10.1103/PhysRev.109.1492).
- [747] E. Abrahams et al. “Scaling Theory of Localization: Absence of Quantum Diffusion in Two Dimensions”. In: *Phys. Rev. Lett.* 42.10 (Mar. 5, 1979), pp. 673–676. doi: [10.1103/PhysRevLett.42.673](https://doi.org/10.1103/PhysRevLett.42.673).
- [748] G. Roati et al. “Anderson Localization of a Non-Interacting Bose–Einstein Condensate”. In: *Nature (London)* 453.7197 (7197 June 2008), pp. 895–898. issn: 1476-4687. doi: [10.1038/nature07071](https://doi.org/10.1038/nature07071).
- [749] A. Pal and D. A. Huse. “Many-Body Localization Phase Transition”. In: *Phys. Rev. B* 82.17 (Nov. 9, 2010), p. 174411. doi: [10.1103/PhysRevB.82.174411](https://doi.org/10.1103/PhysRevB.82.174411).
- [750] D. A. Huse, R. Nandkishore, and V. Oganesyan. “Phenomenology of Fully Many-Body-Localized Systems”. In: *Phys. Rev. B* 90.17 (Nov. 13, 2014), p. 174202. doi: [10.1103/PhysRevB.90.174202](https://doi.org/10.1103/PhysRevB.90.174202).
- [751] D. J. Luitz, N. Laflorencie, and F. Alet. “Many-Body Localization Edge in the Random-Field Heisenberg Chain”. In: *Phys. Rev. B* 91.8 (Feb. 9, 2015), p. 081103. doi: [10.1103/PhysRevB.91.081103](https://doi.org/10.1103/PhysRevB.91.081103).
- [752] R. Vosk, D. A. Huse, and E. Altman. “Theory of the Many-Body Localization Transition in One-Dimensional Systems”. In: *Phys. Rev. X* 5.3 (Sept. 14, 2015), p. 031032. doi: [10.1103/PhysRevX.5.031032](https://doi.org/10.1103/PhysRevX.5.031032).
- [753] J.-y. Choi et al. “Exploring the Many-Body Localization Transition in Two Dimensions”. In: *Science* 352.6293 (June 24, 2016), pp. 1547–1552. doi: [10.1126/science.aaf8834](https://doi.org/10.1126/science.aaf8834).
- [754] F. Alet and N. Laflorencie. “Many-Body Localization: An Introduction and Selected Topics”. In: *Comptes Rendus Physique. Quantum Simulation / Simulation Quantique* 19.6 (Sept. 1, 2018), pp. 498–525. issn: 1631-0705. doi: [10.1016/j.crhy.2018.03.003](https://doi.org/10.1016/j.crhy.2018.03.003).
- [755] D. A. Abanin et al. “Colloquium: Many-body Localization, Thermalization, and Entanglement”. In: *Rev. Mod. Phys.* 91.2 (May 22, 2019), p. 021001. doi: [10.1103/RevModPhys.91.021001](https://doi.org/10.1103/RevModPhys.91.021001).
- [756] M. Srednicki. “Entropy and Area”. In: *Phys. Rev. Lett.* 71.5 (Aug. 2, 1993), pp. 666–669. doi: [10.1103/PhysRevLett.71.666](https://doi.org/10.1103/PhysRevLett.71.666).



- 
- [757] J. I. Latorre, E. Rico, and G. Vidal. “Ground State Entanglement in Quantum Spin Chains.” In: *Quant. Inf. Comput.* 4.1 (2004), pp. 48–92. doi: [10.26421/QIC4.1-4](https://doi.org/10.26421/QIC4.1-4).
- [758] M. B. Plenio et al. “Entropy, Entanglement, and Area: Analytical Results for Harmonic Lattice Systems”. In: *Phys. Rev. Lett.* 94.6 (Feb. 17, 2005), p. 060503. doi: [10.1103/PhysRevLett.94.060503](https://doi.org/10.1103/PhysRevLett.94.060503).
- [759] S. Bravyi, M. B. Hastings, and F. Verstraete. “Lieb-Robinson Bounds and the Generation of Correlations and Topological Quantum Order”. In: *Phys. Rev. Lett.* 97.5 (July 31, 2006), p. 050401. doi: [10.1103/PhysRevLett.97.050401](https://doi.org/10.1103/PhysRevLett.97.050401).
- [760] J. Eisert and T. J. Osborne. “General Entanglement Scaling Laws from Time Evolution”. In: *Phys. Rev. Lett.* 97.15 (Oct. 12, 2006), p. 150404. doi: [10.1103/PhysRevLett.97.150404](https://doi.org/10.1103/PhysRevLett.97.150404).
- [761] M. B. Hastings. “An Area Law for One-Dimensional Quantum Systems”. In: *J. Stat. Mech.* 2007.08 (Aug. 2007), P08024. issn: 1742-5468. doi: [10.1088/1742-5468/2007/08/P08024](https://doi.org/10.1088/1742-5468/2007/08/P08024).
- [762] L. Masanes. “Area Law for the Entropy of Low-Energy States”. In: *Phys. Rev. A* 80.5 (Nov. 10, 2009), p. 052104. doi: [10.1103/PhysRevA.80.052104](https://doi.org/10.1103/PhysRevA.80.052104).
- [763] J. Eisert, M. Cramer, and M. B. Plenio. “Colloquium: Area Laws for the Entanglement Entropy”. In: *Rev. Mod. Phys.* 82.1 (Feb. 4, 2010), pp. 277–306. doi: [10.1103/RevModPhys.82.277](https://doi.org/10.1103/RevModPhys.82.277).
- [764] C. Callan and F. Wilczek. “On Geometric Entropy”. In: *Phys. Lett. B* 333.1 (July 28, 1994), pp. 55–61. issn: 0370-2693. doi: [10.1016/0370-2693\(94\)91007-3](https://doi.org/10.1016/0370-2693(94)91007-3).
- [765] T. M. Fiola et al. “Black Hole Thermodynamics and Information Loss in Two Dimensions”. In: *Phys. Rev. D* 50.6 (Sept. 15, 1994), pp. 3987–4014. doi: [10.1103/PhysRevD.50.3987](https://doi.org/10.1103/PhysRevD.50.3987).
- [766] C. Holzhey, F. Larsen, and F. Wilczek. “Geometric and Renormalized Entropy in Conformal Field Theory”. In: *Nucl. Phys. B* 424.3 (Aug. 15, 1994), pp. 443–467. issn: 0550-3213. doi: [10.1016/0550-3213\(94\)90402-2](https://doi.org/10.1016/0550-3213(94)90402-2).
- [767] G. Refael and J. E. Moore. “Entanglement Entropy of Random Quantum Critical Points in One Dimension”. In: *Phys. Rev. Lett.* 93.26 (Dec. 21, 2004), p. 260602. doi: [10.1103/PhysRevLett.93.260602](https://doi.org/10.1103/PhysRevLett.93.260602).
- [768] T. Barthel, M.-C. Chung, and U. Schollwöck. “Entanglement Scaling in Critical Two-Dimensional Fermionic and Bosonic Systems”. In: *Phys. Rev. A* 74.2 (Aug. 29, 2006), p. 022329. doi: [10.1103/PhysRevA.74.022329](https://doi.org/10.1103/PhysRevA.74.022329).
- [769] D. Gioev and I. Klich. “Entanglement Entropy of Fermions in Any Dimension and the Widom Conjecture”. In: *Phys. Rev. Lett.* 96.10 (Mar. 14, 2006), p. 100503. doi: [10.1103/PhysRevLett.96.100503](https://doi.org/10.1103/PhysRevLett.96.100503).
- [770] W. Li et al. “Scaling Behavior of Entanglement in Two- and Three-Dimensional Free-Fermion Systems”. In: *Phys. Rev. B* 74.7 (Aug. 17, 2006), p. 073103. doi: [10.1103/PhysRevB.74.073103](https://doi.org/10.1103/PhysRevB.74.073103).
- [771] M. M. Wolf. “Violation of the Entropic Area Law for Fermions”. In: *Phys. Rev. Lett.* 96.1 (Jan. 12, 2006), p. 010404. doi: [10.1103/PhysRevLett.96.010404](https://doi.org/10.1103/PhysRevLett.96.010404).
- [772] O. I. Motrunich and M. P. A. Fisher. “D-Wave Correlated Critical Bose Liquids in Two Dimensions”. In: *Phys. Rev. B* 75.23 (June 21, 2007), p. 235116. doi: [10.1103/PhysRevB.75.235116](https://doi.org/10.1103/PhysRevB.75.235116).
-

- [773] T. Senthil. “Critical Fermi Surfaces and Non-Fermi Liquid Metals”. In: *Phys. Rev. B* 78.3 (July 3, 2008), p. 035103. doi: [10.1103/PhysRevB.78.035103](https://doi.org/10.1103/PhysRevB.78.035103).
- [774] B. Swingle. “Entanglement Entropy and the Fermi Surface”. In: *Phys. Rev. Lett.* 105.5 (July 30, 2010), p. 050502. doi: [10.1103/PhysRevLett.105.050502](https://doi.org/10.1103/PhysRevLett.105.050502).
- [775] H. Liu, J. McGreevy, and D. Vegh. “Non-Fermi Liquids from Holography”. In: *Phys. Rev. D* 83.6 (Mar. 28, 2011), p. 065029. doi: [10.1103/PhysRevD.83.065029](https://doi.org/10.1103/PhysRevD.83.065029).
- [776] B. Swingle. “Conformal Field Theory Approach to Fermi Liquids and Other Highly Entangled States”. In: *Phys. Rev. B* 86.3 (July 12, 2012), p. 035116. doi: [10.1103/PhysRevB.86.035116](https://doi.org/10.1103/PhysRevB.86.035116).
- [777] X. Turkeshi et al. “Entanglement Equipartition in Critical Random Spin Chains”. In: *Phys. Rev. B* 102.1 (July 30, 2020), p. 014455. doi: [10.1103/PhysRevB.102.014455](https://doi.org/10.1103/PhysRevB.102.014455).
- [778] P. Calabrese and J. Cardy. “Entanglement Entropy and Quantum Field Theory”. In: *J. Stat. Mech.* 2004.06 (June 2004), P06002. issn: 1742-5468. doi: [10.1088/1742-5468/2004/06/P06002](https://doi.org/10.1088/1742-5468/2004/06/P06002).
- [779] B.-Q. Jin and V. E. Korepin. “Quantum Spin Chain, Toeplitz Determinants and the Fisher—Hartwig Conjecture”. In: *J. Stat. Phys.* 116.1 (Aug. 1, 2004), pp. 79–95. issn: 1572-9613. doi: [10.1023/B:JOSS.0000037230.37166.42](https://doi.org/10.1023/B:JOSS.0000037230.37166.42).
- [780] P. Calabrese and J. Cardy. “Entanglement Entropy and Quantum Field Theory: A Non-Technical Introduction”. In: *Int. J. Quantum Inform.* 04.03 (June 2006), pp. 429–438. issn: 0219-7499. doi: [10.1142/S021974990600192X](https://doi.org/10.1142/S021974990600192X).
- [781] G. Vitagliano, A. Riera, and J. I. Latorre. “Volume-Law Scaling for the Entanglement Entropy in Spin-1/2 Chains”. In: *New J. Phys.* 12.11 (Nov. 2010), p. 113049. issn: 1367-2630. doi: [10.1088/1367-2630/12/11/113049](https://doi.org/10.1088/1367-2630/12/11/113049).
- [782] M. Pouranvari and K. Yang. “Maximally Entangled Mode, Metal-Insulator Transition, and Violation of Entanglement Area Law in Noninteracting Fermion Ground States”. In: *Phys. Rev. B* 89.11 (Mar. 5, 2014), p. 115104. doi: [10.1103/PhysRevB.89.115104](https://doi.org/10.1103/PhysRevB.89.115104).
- [783] N. Shiba and T. Takayanagi. “Volume Law for the Entanglement Entropy in Non-Local QFTs”. In: *J. High Energy Phys.* 2014.2 (Feb. 7, 2014), p. 33. issn: 1029-8479. doi: [10.1007/JHEP02\(2014\)033](https://doi.org/10.1007/JHEP02(2014)033).
- [784] G. Gori et al. “Explicit Hamiltonians Inducing Volume Law for Entanglement Entropy in Fermionic Lattices”. In: *Phys. Rev. B* 91.24 (June 17, 2015), p. 245138. doi: [10.1103/PhysRevB.91.245138](https://doi.org/10.1103/PhysRevB.91.245138).
- [785] N. Roy and A. Sharma. “Entanglement Contour Perspective for Strong Area-Law Violation in a Disordered Long-Range Hopping Model”. In: *Phys. Rev. B* 97.12 (Mar. 12, 2018), p. 125116. doi: [10.1103/PhysRevB.97.125116](https://doi.org/10.1103/PhysRevB.97.125116).
- [786] N. Roy, A. Sharma, and R. Mukherjee. “Quantum Simulation of Long-Range XY Quantum Spin Glass with Strong Area-Law Violation Using Trapped Ions”. In: *Phys. Rev. A* 99.5 (May 28, 2019), p. 052342. doi: [10.1103/PhysRevA.99.052342](https://doi.org/10.1103/PhysRevA.99.052342).
- [787] N. Roy, A. Sharma, and R. Mukherjee. “Erratum: Quantum Simulation of Long-Range XY Quantum Spin Glass with Strong Area-Law Violation Using Trapped Ions [Phys. Rev. A 99, 052342 (2019)]”. In: *Phys. Rev. A* 100.5 (Nov. 13, 2019), p. 059902. doi: [10.1103/PhysRevA.100.059902](https://doi.org/10.1103/PhysRevA.100.059902).

- 
- [788] G. Parisi. “Order Parameter for Spin-Glasses”. In: *Phys. Rev. Lett.* 50.24 (June 13, 1983), pp. 1946–1948. doi: [10.1103/PhysRevLett.50.1946](https://doi.org/10.1103/PhysRevLett.50.1946).
- [789] P. Pfeuty. “The One-Dimensional Ising Model with a Transverse Field”. In: *Ann. Phys.* 57.1 (Mar. 1, 1970), pp. 79–90. issn: 0003-4916. doi: [10.1016/0003-4916\(70\)90270-8](https://doi.org/10.1016/0003-4916(70)90270-8).
- [790] P. Pfeuty and R. J. Elliott. “The Ising Model with a Transverse Field. II. Ground State Properties”. In: *J. Phys. C: Solid State* 4.15 (Oct. 1971), pp. 2370–2385. issn: 0022-3719. doi: [10.1088/0022-3719/4/15/024](https://doi.org/10.1088/0022-3719/4/15/024).
- [791] S. Suzuki, J.-i. Inoue, and B. K. Chakrabarti. *Quantum Ising Phases and Transitions in Transverse Ising Models*. 2nd ed. 2013 edition. New York: Springer, Dec. 14, 2012. 414 pp. isbn: 978-3-642-33038-4.
- [792] D. Porras and J. I. Cirac. “Effective Quantum Spin Systems with Trapped Ions”. In: *Phys. Rev. Lett.* 92.20 (May 20, 2004), p. 207901. doi: [10.1103/PhysRevLett.92.207901](https://doi.org/10.1103/PhysRevLett.92.207901).
- [793] K. Kim et al. “Entanglement and Tunable Spin-Spin Couplings between Trapped Ions Using Multiple Transverse Modes”. In: *Phys. Rev. Lett.* 103.12 (Sept. 16, 2009), p. 120502. doi: [10.1103/PhysRevLett.103.120502](https://doi.org/10.1103/PhysRevLett.103.120502).
- [794] J. W. Britton et al. “Engineered Two-Dimensional Ising Interactions in a Trapped-Ion Quantum Simulator with Hundreds of Spins”. In: *Nature (London)* 484.7395 (7395 Apr. 2012), pp. 489–492. issn: 1476-4687. doi: [10.1038/nature10981](https://doi.org/10.1038/nature10981).
- [795] R. Islam et al. “Emergence and Frustration of Magnetism with Variable-Range Interactions in a Quantum Simulator”. In: *Science* 340.6132 (May 3, 2013), pp. 583–587. doi: [10.1126/science.1232296](https://doi.org/10.1126/science.1232296).
- [796] R. Coldea et al. “Quantum Criticality in an Ising Chain: Experimental Evidence for Emergent E8 Symmetry”. In: *Science* 327.5962 (Jan. 8, 2010), pp. 177–180. doi: [10.1126/science.1180085](https://doi.org/10.1126/science.1180085).
- [797] I. Lesanovsky. “Many-Body Spin Interactions and the Ground State of a Dense Rydberg Lattice Gas”. In: *Phys. Rev. Lett.* 106.2 (Jan. 11, 2011), p. 025301. doi: [10.1103/PhysRevLett.106.025301](https://doi.org/10.1103/PhysRevLett.106.025301).
- [798] P. Schauß et al. “Crystallization in Ising Quantum Magnets”. In: *Science* 347.6229 (Mar. 27, 2015), pp. 1455–1458. doi: [10.1126/science.1258351](https://doi.org/10.1126/science.1258351).
- [799] H. Albrecht et al. “Heisenberg, XY, and Ising Spin-Glass Behavior in Hexagonal Metallic Systems”. In: *Phys. Rev. Lett.* 48.12 (Mar. 22, 1982), pp. 819–822. doi: [10.1103/PhysRevLett.48.819](https://doi.org/10.1103/PhysRevLett.48.819).
- [800] L. De Cesare et al. “Two-Spin Cluster Approach to the Infinite-Range Quantum Transverse XY Spin-Glass Model”. In: *Physics Letters A* 145.5 (Apr. 16, 1990), pp. 291–295. issn: 0375-9601. doi: [10.1016/0375-9601\(90\)90368-X](https://doi.org/10.1016/0375-9601(90)90368-X).
- [801] L. De Cesare et al. “Cavity-Fields Approach to Quantum XY Spin-Glass Models in a Transverse Field”. In: *Phys. Rev. B* 45.2 (Jan. 1, 1992), pp. 1041–1044. doi: [10.1103/PhysRevB.45.1041](https://doi.org/10.1103/PhysRevB.45.1041).
- [802] A. P. Young and R. B. Stinchcombe. “Real-Space Renormalization Group Calculations for Spin Glasses and Dilute Magnets”. In: *J. Phys. C: Solid State* 9.24 (Dec. 1976), p. 4419. issn: 0022-3719. doi: [10.1088/0022-3719/9/24/012](https://doi.org/10.1088/0022-3719/9/24/012).
-

- [803] F. Iglói and C. Monthus. “Strong Disorder RG Approach of Random Systems”. In: *Phys. Rep.* 412.5 (June 1, 2005), pp. 277–431. ISSN: 0370-1573. DOI: [10.1016/j.physrep.2005.02.006](https://doi.org/10.1016/j.physrep.2005.02.006).
- [804] F. Iglói, Z. Szatmári, and Y.-C. Lin. “Entanglement Entropy Dynamics of Disordered Quantum Spin Chains”. In: *Phys. Rev. B* 85.9 (Mar. 12, 2012), p. 094417. DOI: [10.1103/PhysRevB.85.094417](https://doi.org/10.1103/PhysRevB.85.094417).
- [805] R. Vosk and E. Altman. “Dynamical Quantum Phase Transitions in Random Spin Chains”. In: *Phys. Rev. Lett.* 112.21 (May 29, 2014), p. 217204. DOI: [10.1103/PhysRevLett.112.217204](https://doi.org/10.1103/PhysRevLett.112.217204).
- [806] Y. LeCun, Y. Bengio, and G. Hinton. “Deep Learning”. In: *Nature (London)* 521.7553 (7553 May 2015), pp. 436–444. ISSN: 1476-4687. DOI: [10.1038/nature14539](https://doi.org/10.1038/nature14539).
- [807] I. Goodfellow, Y. Bengio, and A. Courville. *Deep Learning*. Ed. by F. Bach. Cambridge, MA: The MIT Press, Nov. 18, 2016. 775 pp. ISBN: 978-0-262-03561-3.
- [808] R. S. Sutton and A. G. Barto. *Reinforcement Learning, Second Edition: An Introduction*. Cambridge, MA: MIT Press, Nov. 13, 2018. 549 pp. ISBN: 978-0-262-35270-3.
- [809] D. Conte and C. Lubich. “An Error Analysis of the Multi-Configuration Time-Dependent Hartree Method of Quantum Dynamics”. In: *ESAIM: Math. Model. Num.* 44.4 (4 July 1, 2010), pp. 759–780. ISSN: 0764-583X, 1290-3841. DOI: [10.1051/m2an/2010018](https://doi.org/10.1051/m2an/2010018).
- [810] U. Manthe. “The Multi-Configurational Time-Dependent Hartree Approach Revisited”. In: *J. Chem. Phys.* 142.24 (June 29, 2015), p. 244109. ISSN: 0021-9606. DOI: [10.1063/1.4922889](https://doi.org/10.1063/1.4922889).
- [811] C. M. Hinz, S. Bauch, and M. Bonitz. “Instabilities and Inaccuracies of Multi-Configuration Time-Dependent Hartree-Fock”. In: *J. Phys.: Conf. Ser.* 696.1 (Mar. 2016), p. 012009. ISSN: 1742-6596. DOI: [10.1088/1742-6596/696/1/012009](https://doi.org/10.1088/1742-6596/696/1/012009).
- [812] H.-D. Meyer and H. Wang. “On Regularizing the MCTDH Equations of Motion”. In: *J. Chem. Phys.* 148.12 (Mar. 23, 2018), p. 124105. ISSN: 0021-9606. DOI: [10/gc9zvj](https://doi.org/10/gc9zvj).
- [813] H. Wang and H.-D. Meyer. “Importance of Appropriately Regularizing the ML-MCTDH Equations of Motion”. In: *J. Phys. Chem. A* 125.15 (Apr. 22, 2021), pp. 3077–3087. ISSN: 1089-5639. DOI: [10.1021/acs.jpca.0c11221](https://doi.org/10.1021/acs.jpca.0c11221).
- [814] R. Martinazzo and I. Burghardt. “Local-in-Time Error in Variational Quantum Dynamics”. In: *Phys. Rev. Lett.* 124.15 (Apr. 13, 2020), p. 150601. DOI: [10/ggwrcw](https://doi.org/10/ggwrcw).
- [815] D. Mendive-Tapia and H.-D. Meyer. “Regularizing the MCTDH Equations of Motion through an Optimal Choice On-the-Fly (i.e., Spawning) of Unoccupied Single-Particle Functions”. In: *J. Chem. Phys.* 153.23 (Dec. 21, 2020), p. 234114. ISSN: 0021-9606. DOI: [10/gj9xvq](https://doi.org/10/gj9xvq).
- [816] R. Martinazzo and I. Burghardt. “Comment on “Regularizing the MCTDH Equations of Motion through an Optimal Choice on-the-Fly (i.e., Spawning) of Unoccupied Single-Particle Functions” [D. Mendive-Tapia, H.-D. Meyer, *J. Chem. Phys.* 153, 234114 (2020)]”. Feb. 24, 2021. URL: <http://arxiv.org/abs/2102.12117>.

- 
- [817] C. Lubich. “Time Integration in the Multiconfiguration Time-Dependent Hartree Method of Molecular Quantum Dynamics”. In: *Applied Mathematics Research eXpress* 2015.2 (Jan. 1, 2015), pp. 311–328. ISSN: 1687-1200. DOI: [10.1093/amrx/abv006](https://doi.org/10.1093/amrx/abv006).
- [818] M. Bonfanti and I. Burghardt. “Tangent Space Formulation of the Multi-Configuration Time-Dependent Hartree Equations of Motion: The Projector-Splitting Algorithm Revisited”. In: *Chemical Physics*. Ultrafast Photoinduced Processes in Polyatomic Molecules: Electronic Structure, Dynamics and Spectroscopy (Dedicated to Wolfgang Domcke on the Occasion of His 70th Birthday) 515 (Nov. 14, 2018), pp. 252–261. ISSN: 0301-0104. DOI: [10.1016/j.chemphys.2018.05.029](https://doi.org/10.1016/j.chemphys.2018.05.029).
- [819] B. Kloss, I. Burghardt, and C. Lubich. “Implementation of a Novel Projector-Splitting Integrator for the Multi-Configurational Time-Dependent Hartree Approach”. In: *J. Chem. Phys.* 146.17 (May 7, 2017), p. 174107. ISSN: 0021-9606. DOI: [10.1063/1.4982065](https://doi.org/10.1063/1.4982065).
- [820] L. P. Lindoy, B. Kloss, and D. R. Reichman. “Time Evolution of ML-MCTDH Wavefunctions. I. Gauge Conditions, Basis Functions, and Singularities”. In: *J. Chem. Phys.* 155.17 (Nov. 7, 2021), p. 174108. ISSN: 0021-9606. DOI: [10.1063/5.0070042](https://doi.org/10.1063/5.0070042).
- [821] L. P. Lindoy, B. Kloss, and D. R. Reichman. “Time Evolution of ML-MCTDH Wavefunctions. II. Application of the Projector Splitting Integrator”. In: *J. Chem. Phys.* 155.17 (Nov. 7, 2021), p. 174109. ISSN: 0021-9606. DOI: [10.1063/5.0070043](https://doi.org/10.1063/5.0070043).
- [822] A. Paszke et al. “Automatic Differentiation in PyTorch”. In: (Oct. 28, 2017). URL: <https://openreview.net/forum?id=BJJsrmfCZ>.
- [823] A. Paszke et al. “PyTorch: An Imperative Style, High-Performance Deep Learning Library”. In: *Advances in Neural Information Processing Systems*. Vol. 32. Curran Associates, Inc., 2019. URL: <https://proceedings.neurips.cc/paper/2019/hash/bdbca288fee7f92f2bfa9f7012727740-Abstract.html>.
- [824] M. Abadi et al. “Tensorflow: A System for Large-Scale Machine Learning.” In: *Operating Systems Design and Implementation*. Vol. 16. 2016. Savannah, GA, USA, 2016, pp. 265–283.
- [825] M. Abadi et al. *TensorFlow: Large-Scale Machine Learning on Heterogeneous Distributed Systems*. Mar. 16, 2016. DOI: [10.48550/arXiv.1603.04467](https://doi.org/10.48550/arXiv.1603.04467). preprint.
- [826] N. Ng et al. “Localization Dynamics in a Centrally Coupled System”. In: *Phys. Rev. B* 103.13 (Apr. 2, 2021), p. 134201. DOI: [10.1103/PhysRevB.103.134201](https://doi.org/10.1103/PhysRevB.103.134201).
- [827] F. H. L. Essler and M. Fagotti. “Quench Dynamics and Relaxation in Isolated Integrable Quantum Spin Chains”. In: *J. Stat. Mech.* 2016.6 (June 2016), p. 064002. ISSN: 1742-5468. DOI: [10.1088/1742-5468/2016/06/064002](https://doi.org/10.1088/1742-5468/2016/06/064002).
- [828] E. Guardado-Sanchez et al. “Probing the Quench Dynamics of Antiferromagnetic Correlations in a 2D Quantum Ising Spin System”. In: *Phys. Rev. X* 8.2 (June 18, 2018), p. 021069. DOI: [10.1103/PhysRevX.8.021069](https://doi.org/10.1103/PhysRevX.8.021069).
- [829] N. Read and S. Sachdev. “Valence-Bond and Spin-Peierls Ground States of Low-Dimensional Quantum Antiferromagnets”. In: *Phys. Rev. Lett.* 62.14 (Apr. 3, 1989), pp. 1694–1697. DOI: [10.1103/PhysRevLett.62.1694](https://doi.org/10.1103/PhysRevLett.62.1694).
-

- [830] N. Kawashima and Y. Tanabe. “Ground States of the SU(N) Heisenberg Model”. In: *Phys. Rev. Lett.* 98.5 (Jan. 29, 2007), p. 057202. doi: [10.1103/PhysRevLett.98.057202](https://doi.org/10.1103/PhysRevLett.98.057202).
- [831] S. R. Manmana et al. “SU(N) Magnetism in Chains of Ultracold Alkaline-Earth-Metal Atoms: Mott Transitions and Quantum Correlations”. In: *Phys. Rev. A* 84.4 (Oct. 3, 2011), p. 043601. doi: [10.1103/PhysRevA.84.043601](https://doi.org/10.1103/PhysRevA.84.043601).
- [832] J. Lou, A. W. Sandvik, and N. Kawashima. “Antiferromagnetic to Valence-Bond-Solid Transitions in Two-Dimensional SU(N) Heisenberg Models with Multispin Interactions”. In: *Phys. Rev. B* 80.18 (Nov. 16, 2009), p. 180414. doi: [10.1103/PhysRevB.80.180414](https://doi.org/10.1103/PhysRevB.80.180414).
- [833] P. Nataf and F. Mila. “Exact Diagonalization of Heisenberg SU(N) Models”. In: *Phys. Rev. Lett.* 113.12 (Sept. 18, 2014), p. 127204. doi: [10.1103/PhysRevLett.113.127204](https://doi.org/10.1103/PhysRevLett.113.127204).
- [834] D. Banerjee et al. “Atomic Quantum Simulation of U(N) and SU(N) Non-Abelian Lattice Gauge Theories”. In: *Phys. Rev. Lett.* 110.12 (Mar. 21, 2013), p. 125303. doi: [10.1103/PhysRevLett.110.125303](https://doi.org/10.1103/PhysRevLett.110.125303).
- [835] A. V. Gorshkov et al. “Two-Orbital SU(N) Magnetism with Ultracold Alkaline-Earth Atoms”. In: *Nat. Phys.* 6.4 (4 Apr. 2010), pp. 289–295. issn: 1745-2481. doi: [10.1038/nphys1535](https://doi.org/10.1038/nphys1535).
- [836] M. A. Cazalilla and A. M. Rey. “Ultracold Fermi Gases with Emergent SU(N) Symmetry”. In: *Rep. Prog. Phys.* 77.12 (Nov. 2014), p. 124401. issn: 0034-4885. doi: [10.1088/0034-4885/77/12/124401](https://doi.org/10.1088/0034-4885/77/12/124401).
- [837] F. Scazza et al. “Observation of Two-Orbital Spin-Exchange Interactions with Ultracold SU(N)-Symmetric Fermions”. In: *Nat. Phys.* 10.10 (10 Oct. 2014), pp. 779–784. issn: 1745-2481. doi: [10.1038/nphys3061](https://doi.org/10.1038/nphys3061).
- [838] T. Keilmann et al. “Statistically Induced Phase Transitions and Anyons in 1D Optical Lattices”. In: *Nat. Commun.* 2.1 (1 June 21, 2011), p. 361. issn: 2041-1723. doi: [10.1038/ncomms1353](https://doi.org/10.1038/ncomms1353).
- [839] S. Greschner and L. Santos. “Anyon Hubbard Model in One-Dimensional Optical Lattices”. In: *Phys. Rev. Lett.* 115.5 (July 28, 2015), p. 053002. doi: [10.1103/PhysRevLett.115.053002](https://doi.org/10.1103/PhysRevLett.115.053002).
- [840] C. Sträter, S. C. L. Srivastava, and A. Eckardt. “Floquet Realization and Signatures of One-Dimensional Anyons in an Optical Lattice”. In: *Phys. Rev. Lett.* 117.20 (Nov. 10, 2016), p. 205303. doi: [10.1103/PhysRevLett.117.205303](https://doi.org/10.1103/PhysRevLett.117.205303).
- [841] F. Görg et al. “Realization of Density-Dependent Peierls Phases to Engineer Quantized Gauge Fields Coupled to Ultracold Matter”. In: *Nat. Phys.* 15.11 (11 Nov. 2019), pp. 1161–1167. issn: 1745-2481. doi: [10.1038/s41567-019-0615-4](https://doi.org/10.1038/s41567-019-0615-4).
- [842] C. Schweizer et al. “Floquet Approach to  $\mathfrak{u}(2)$  Lattice Gauge Theories with Ultracold Atoms in Optical Lattices”. In: *Nat. Phys.* 15.11 (11 Nov. 2019), pp. 1168–1173. issn: 1745-2481. doi: [10.1038/s41567-019-0649-7](https://doi.org/10.1038/s41567-019-0649-7).
- [843] R. Peierls. “Zur Theorie des Diamagnetismus von Leitungselektronen”. In: *Z. Phys.* 80.11 (Nov. 1, 1933), pp. 763–791. issn: 0044-3328. doi: [10.1007/BF01342591](https://doi.org/10.1007/BF01342591).

- 
- [844] D. R. Hofstadter. “Energy Levels and Wave Functions of Bloch Electrons in Rational and Irrational Magnetic Fields”. In: *Phys. Rev. B* 14.6 (Sept. 15, 1976), pp. 2239–2249. DOI: [10.1103/PhysRevB.14.2239](https://doi.org/10.1103/PhysRevB.14.2239).
- [845] J. Kwan et al. *Realization of 1D Anyons with Arbitrary Statistical Phase*. June 2, 2023. DOI: [10.48550/arXiv.2306.01737](https://doi.org/10.48550/arXiv.2306.01737). preprint.





# A

## Multi-Layer MCTDH Details

**D**UE to the recursive nature of the **ML-MCTDH** wave function ansatz, a general notation of the formalism is rather involved. Section 2.4 introduced the basic concepts of the method using an exemplary wave function tree. The present appendix provides a detailed general description of **ML-MCTDH** and employs the notation established by Manthe [421] including later refinements and modifications from Refs. [422, 547]. As a starting point, the **MCTDH** ansatz (2.16) is revisited and written as

$$\begin{aligned} |\Psi(t)\rangle &= \sum_{j_1=1}^{m_1^1} \cdots \sum_{j_{p^1}=1}^{m_{p^1}^1} A_{1;j_1,\dots,j_{p^1}}^1(t) \bigotimes_{\kappa_1=1}^{p^1} \left| \varphi_{j_{\kappa_1}}^{1;\kappa_1}(q_{\kappa_1}^1, t) \right\rangle \\ &= \sum_J A_{1;j}^1(t) \left| \Phi_J^1(t) \right\rangle \end{aligned} \quad (\text{A.1})$$

which also defines the top level configurations  $|\Phi_J^1(t)\rangle$  indexed by a multi-index  $J$  similar to Eq. (2.10). As before, the many-body wave function is expanded using time-dependent **SPFs** which in turn are represented with respect to time-independent primitive basis functions. Taking mode combination of the physical **DOFs** into account (see Section 2.3.4), the multidimensional **SPFs** are given by

$$\left| \varphi_i^{1;\kappa_1}(q_{\kappa_1}^1, t) \right\rangle = \sum_{j_1=1}^{n_1^{\kappa_1}} \cdots \sum_{j_{p^{2;\kappa_1}}=1}^{n_{p^{2;\kappa_1}}^{2;\kappa_1}} A_{i;j_1,\dots,j_{p^{2;\kappa_1}}}^{2;\kappa_1}(t) \bigotimes_{\kappa_2=1}^{p^{2;\kappa_1}} \left| \chi_{j_{\kappa_2}}^{2;\kappa_1,\kappa_2}(q_{\kappa_2}^{2;\kappa_1}) \right\rangle. \quad (\text{A.2})$$

The **ML-MCTDH** approach extends the construction of the wave function by representing the **SPFs** themselves using **MCTDH** wave functions, thus introducing more and more layers. In order to obtain a concise and consistent notation of this hierarchical ansatz, it is convenient to introduce the symbol

$$z = \ell; \kappa_1, \dots, \kappa_{\ell-1} \quad (\text{A.3})$$

to refer to a specific node in the wave function tree. Here,  $\ell$  denotes the layer of the tree and  $\kappa_1, \dots, \kappa_{\ell-1}$  the path from the root node to the node under consideration. For example,  $(3; 2, 4)$  denotes a node on the 3 layer of the tree that is the 4th child of the 2nd child of the root node. The parent node of the node  $z$  is then identified by

$$z - 1 = \ell; \kappa_1, \dots, \kappa_{\ell-2}. \quad (\text{A.4})$$

The SPFs associated with the  $\kappa_{\ell-1}$ th child of the node indexed by  $z-1$  are given by a MCTDH ansatz the SPFs of its child nodes<sup>1</sup>, i.e.,

$$\begin{aligned} \left| \varphi_i^{z-1, \kappa_{\ell-1}}(q_{\kappa_{\ell-1}}^{z-1}, t) \right\rangle &= \sum_{j_1=1}^{m_1^z} \cdots \sum_{j_{p^z}=1}^{m_{p^z}^z} A_{i; j_1, \dots, j_{p^z}}^z(t) \bigotimes_{\kappa_\ell=1}^{p^z} \left| \varphi_{j_{\kappa_\ell}}^{z, \kappa_\ell}(q_{\kappa_\ell}^z, t) \right\rangle \\ &= \sum_J A_{i; J}^z \left| \Phi_J^z(q_{\kappa_{\ell-1}}^{z-1}, t) \right\rangle \end{aligned} \quad (\text{A.5})$$

The corresponding logical coordinate  $q_{\kappa_{\ell-1}}^{z-1}$  can be viewed as a combined mode of the logical coordinates of the child nodes, i.e.,

$$q_{\kappa_{\ell-1}}^{z-1} = (q_1^z, \dots, q_{p^z}^z). \quad (\text{A.6})$$

Therefore, the construction of a ML-MCTDH wave function can be understood as successive combination of coordinates, starting from the primitive nodes at the leaves of the tree. Figure A.1 illustrates the wave function construction as well as the notation using a simple example that incorporates one additional layer compared to MCTDH.

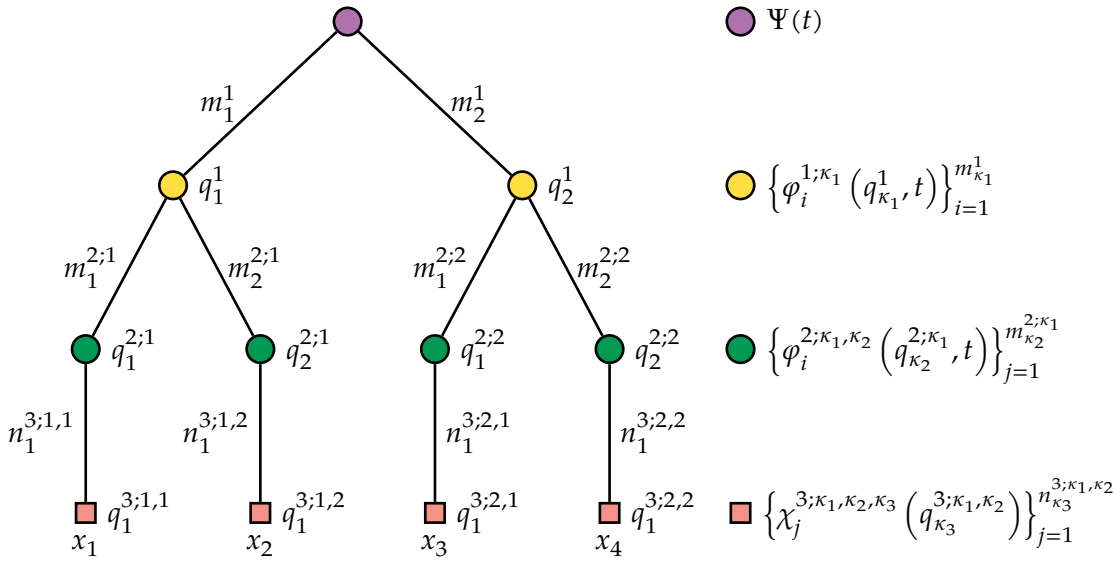


Figure A.1.: Detailed tree diagram of a ML-MCTDH wave function. This example employs one additional layer of SPFs compared to MCTDH in order to describe a system comprising four physical DOFs. The nodes of the tree are labeled by their corresponding logical coordinates while the edges indicate the numbers of SPFs and primitive basis functions, thus providing a unique recipe of how to construct the wave function.

The EOMs for the ML-MCTDH ansatz can be derived using the Dirac-Frenkel TDVP

<sup>1</sup>As in normal MCTDH, the different sets of SPFs are assumed to form orthonormal bases, i.e.,  $\left\langle \varphi_i^{z-1, \kappa_{\ell-1}}(q_{\kappa_{\ell-1}}^{z-1}, t) \middle| \varphi_j^{z-1, \kappa_{\ell-1}}(q_{\kappa_{\ell-1}}^{z-1}, t) \right\rangle = \delta_{ij}$ . This property is conserved under time propagation.

(2.4). Both the **EOM** for the top layer coefficients

$$i\partial_t A_{1;j}^1 = \sum_K \langle \Phi_j^1 | \hat{H} | \Phi_K^1 \rangle A_{1;K}^1 - \sum_{\kappa_1=1}^{p^1} \sum_{r=1}^{m_{\kappa_1}^1} g_{j\kappa_1 r}^{1,\kappa_1} A_{j_1 \dots r \dots j_{p^1}}^1 \quad (\text{A.7})$$

and for the **SPFs**

$$i\partial_t |\varphi_r^{z,\kappa_\ell}\rangle = (1 - P^{z,\kappa_\ell}) \sum_{j,n=1}^{m_{\kappa_\ell}^z} (\rho^{z,\kappa_\ell})_{rj}^{-1} \langle \hat{H} \rangle_{jn}^{z,\kappa_\ell} |\varphi_n^{z,\kappa_\ell}\rangle + \sum_{j=1}^{m_{\kappa_\ell}^z} g_{jr}^{z,\kappa_\ell} |\varphi_j^{z,\kappa_\ell}\rangle \quad (\text{A.8})$$

exhibit the same structure as in **MCTDH** (compare Eqs. (2.23) and (2.24)) highlighting the recursive construction of the wave function ansatz.<sup>2</sup> In Eq. (A.8),  $P^{z,\kappa_\ell} = \sum_{j=1}^{m_{\kappa_\ell}^z} |\varphi_j^{z,\kappa_\ell}\rangle \langle \varphi_j^{z,\kappa_\ell}|$  denotes the projector onto the space spanned by the **SPFs**  $\{|\varphi_j^{z,\kappa_\ell}\rangle\}$ . Similar to **MCTDH**, constraint operators

$$g_{jr}^{z,\kappa_\ell} = \langle \varphi_j^{z,\kappa_\ell} | \hat{g}^{z,\kappa_\ell} | \varphi_r^{z,\kappa_\ell} \rangle = i \langle \varphi_j^{z,\kappa_\ell} | \partial_t \varphi_r^{z,\kappa_\ell} \rangle \quad (\text{A.9})$$

are introduced for each node in order to remediate the ambiguity of the ansatz. In principle, a different Hermitian operator can be chosen for each set of **SPFs**, but a common choice is to use the standard gauge  $\hat{g}^{z,\kappa_\ell} = 0$  throughout the tree which leads to a simpler form of the **EOM**. The reduced one-body density matrix

$$\rho_{ij}^{z,\kappa_\ell} = \langle \Psi_i^{z,\kappa_\ell} | \Psi_j^{z,\kappa_\ell} \rangle \quad (\text{A.10})$$

and the mean fields<sup>3</sup>

$$\langle \hat{H} \rangle_{ij}^{z,\kappa_\ell} = \langle \Psi_i^{z,\kappa_\ell} | \hat{H} | \Psi_j^{z,\kappa_\ell} \rangle \quad (\text{A.11})$$

are determined by the single-hole functions which are obtained by projecting out a single **SPF** from the full wave function

$$|\Psi_j^{z,\kappa_\ell}\rangle = \langle \varphi_j^{z,\kappa_\ell} (q_{\kappa_\ell}^z) | \Psi \rangle. \quad (\text{A.12})$$

Since the **SPFs** are represented with respect to the **SPFs** or primitive basis functions of the layer beneath, in an actual implementation only the different coefficient tensors have to be propagated. The corresponding **EOMs** for non-top-level coefficients follow from the **SPFs EOMs** (A.8) by projecting onto the respective **SPFs** basis, i.e.,  $i\partial_t A_{r;j}^z = i \langle \Phi_j^z | \partial_t \varphi_r^{z-1,\kappa_{\ell-1}} \rangle$ . For the explicit form of this equation, which is here omitted for the sake of brevity, the reader is referred to Ref. [547].

<sup>2</sup>Again, the time-indices have been dropped for a more readable notation.

<sup>3</sup>As in a **MCTDH**, the Hamiltonian is assumed to be in sum-of-products form, see Section 2.3.3.



# B

## Natural Orbital Gauge for MCTDHB

IN this appendix, the derivation of the natural orbital gauge for MCTDHB is outlined. The goal is to find a constraint operator  $\hat{g}$ , such that the SPFs coincide with the natural orbitals, i.e., the eigenfunctions of the one-body density matrix. In order to be consistent with the current implementation, a different normalization of the one-body density matrix [729] compared to Eq. (2.57) is used in the following:

$$\rho_{jk}^{(1)}(t) = \frac{1}{N} \langle \Psi(t) | \hat{b}_j^\dagger \hat{b}_k | \Psi(t) \rangle, \quad (\text{B.1})$$

Since the difference is only an additional factor of  $1/N$  with  $N$  denoting the particle number, the derivation could readily be rewritten to be consistent with Eq. (2.57).

The natural orbital gauge is equivalent to the reduced one-body density matrix being diagonal at all times, which consequently must be fulfilled at  $t = 0$ , i.e.,

$$\rho_{jk}^{(1)}(0) = \delta_{jk} \rho_{jj}^{(1)}(0). \quad (\text{B.2})$$

The constraint operator can then be derived by demanding that the time derivative of the off-diagonal elements vanishes, i.e.,

$$i\partial_t \rho_{jk}^{(1)}(t) = 0 \quad \forall j \neq k. \quad (\text{B.3})$$

The time derivative of the one-body density matrix follows from Eqs. (2.49) and (B.1):

$$\begin{aligned} i\partial_t \rho_{jk}^{(1)} &= \frac{i}{N} \sum_{n,m} (\partial_t C_n^*) C_m \langle \mathbf{n} | \hat{b}_j^\dagger \hat{b}_k | \mathbf{m} \rangle \\ &+ \frac{i}{N} \sum_{n,m} C_n^* (\partial_t C_m) \langle \mathbf{n} | \hat{b}_j^\dagger \hat{b}_k | \mathbf{m} \rangle \\ &+ \frac{i}{N} \sum_{n,m} C_n^* C_m (\partial_t \langle \mathbf{n} |) \hat{b}_j^\dagger \hat{b}_k | \mathbf{m} \rangle \\ &+ \frac{i}{N} \sum_{n,m} C_n^* C_m \langle \mathbf{n} | \hat{b}_j^\dagger \hat{b}_k (\partial_t | \mathbf{m} \rangle) \\ &+ \frac{i}{N} \sum_{n,m} C_n^* C_m \langle \mathbf{n} | (\partial_t \hat{b}_j^\dagger) \hat{b}_k | \mathbf{m} \rangle \\ &+ \frac{i}{N} \sum_{n,m} C_n^* C_m \langle \mathbf{n} | \hat{b}_j^\dagger (\partial_t \hat{b}_k) | \mathbf{m} \rangle = 0 \end{aligned} \quad (\text{B.4})$$

As the derivative of the coefficients is determined by the corresponding EOM (2.54), the two remaining ingredients required are the derivatives of the number states as well as

the creation and annihilation operators.

The time derivative of the creation and annihilation operators can be obtained by expressing them as superposition of time-independent operators. The derivative can then be straightforwardly computed and subsequently written as

$$i\partial_t \hat{b}_j^\dagger = \sum_{k=1}^m g_{kj} \hat{b}_k^\dagger \quad (\text{B.5})$$

with respect to the matrix elements of the constraint operator (2.55). The time derivative of the number states given by Eq. (2.47) follows from (B.5):

$$i\partial_t |n\rangle = i \left[ \sum_{j=1}^m \left( \prod_{\substack{k=1 \\ j \neq k}}^m \frac{(\hat{b}_k^\dagger)^{n_k}}{\sqrt{n_k!}} \right) \frac{\sqrt{n_j}}{\sqrt{(n_j-1)!}} (\partial_t \hat{b}_j^\dagger) (\hat{b}_j^\dagger)^{n_j-1} \right] |\text{vac}\rangle \quad (\text{B.6})$$

$$= i \sum_{j=1}^m \sqrt{n_j} (\partial_t \hat{b}_j^\dagger) |n - e_j\rangle = \sum_{j=1}^m (i\partial_t \hat{b}_j^\dagger) \hat{b}_j |n\rangle \quad (\text{B.7})$$

$$\stackrel{(\text{B.5})}{=} \sum_{j,k=1}^m g_{jk} \hat{b}_j^\dagger \hat{b}_k |n\rangle \quad (\text{B.8})$$

Finally, the constraint operator for the natural orbital gauge of MCTDHB can be obtained by inserting Eqs. (2.54), (B.5) and (B.8) into Eq. (B.4) and reads

$$g_{kj} = \frac{1}{N} \frac{\langle \Psi | [\hat{H}, \hat{b}_j^\dagger \hat{b}_k] | \Psi \rangle}{\rho_{kk}^{(1)} - \rho_{jj}^{(1)}} \quad (\text{B.9})$$

or when exploiting the typical Hamiltonian structure of MCTDHB simulations (see Section 2.7.2)

$$g_{jk} = h_{jk} + (N-1) \sum_{p,q,r=1}^m \frac{W_{pqkr} \rho_{pqjr}^{(2)} - W_{jpqr} \rho_{kpqr}^{(2)}}{\rho_{jj}^{(1)} - \rho_{kk}^{(1)}}. \quad (\text{B.10})$$

It should be noted that only the off-diagonal elements of the constraint operator are determined, and the diagonal elements can be chosen as arbitrary real numbers to preserve its Hermiticity, e.g.,  $g_{jj} = 0$ .

Both Equation (B.9) and (B.10) have to be regularized in the event of a degeneracy of the natural populations

$$\frac{1}{\rho_{jj}^{(1)} - \rho_{kk}^{(1)}} \rightarrow \frac{\rho_{jj}^{(1)} - \rho_{kk}^{(1)}}{(\rho_{jj}^{(1)} - \rho_{kk}^{(1)})^2 + \varepsilon \exp\left(-\frac{1}{\varepsilon}(\rho_{jj}^{(1)} - \rho_{kk}^{(1)})^2\right)} \quad (\text{B.11})$$

where  $\varepsilon$  denotes a small positive regularization parameter.

Proper care has to be taken when deriving the natural orbital gauge for the imaginary time propagation used for energy relaxation (see Section 2.8.1). The corresponding

---

constraint operator reads

$$g_{kj}^{\text{relax}} = \frac{1}{N} \frac{\langle \Psi | \{ \hat{H}, \hat{b}_j^\dagger \hat{b}_k \} | \Psi \rangle}{\rho_{kk}^{(1)} - \rho_{jj}^{(1)}} = \frac{1}{N} \frac{\langle \Psi | [ \hat{H}, \hat{b}_j^\dagger \hat{b}_k ] | \Psi \rangle}{\rho_{kk}^{(1)} - \rho_{jj}^{(1)}} + \frac{2}{N} \frac{\langle \Psi | \hat{b}_j^\dagger \hat{b}_k \hat{H} | \Psi \rangle}{\rho_{kk}^{(1)} - \rho_{jj}^{(1)}} \quad (\text{B.12})$$

$$\stackrel{(\text{B.9})}{=} g_{kj} + \frac{2}{N} \frac{\langle \Psi | \hat{b}_j^\dagger \hat{b}_k \hat{H} | \Psi \rangle}{\rho_{kk}^{(1)} - \rho_{jj}^{(1)}} \quad (\text{B.13})$$

and follows from the imaginary time derivatives of the creation operator

$$\partial_\tau \hat{b}_j^\dagger = - \sum_{k=1}^m g_{kj} \hat{b}_k^\dagger \quad (\text{B.14})$$

and number states

$$\partial_\tau | \mathbf{n} \rangle = - \sum_{a,b=1}^m g_{ab} \hat{b}_a^\dagger \hat{b}_b | \mathbf{n} \rangle . \quad (\text{B.15})$$





## Diagonalization Gauge for MCTDHB

INSTEAD of a gauge that diagonalizes the one-body density matrix as in Appendix B, one can also find a gauge that diagonalizes an arbitrary, Hermitian one-body operator  $\hat{O}$  in SPF representation,<sup>1</sup>

$$O_{jk}(t) = \langle \varphi_j(t) | \hat{O} | \varphi_k(t) \rangle. \quad (\text{C.1})$$

Similar to Appendix B, the operator is assumed to be diagonal in the initial basis, i.e.,

$$O_{jk}(0) = \delta_{jk} O_{jj}(0). \quad (\text{C.2})$$

In order to derive a constraint operator that ensures that the diagonality persists during time propagation, we demand that

$$\partial_t O_{jk}(t) = 0 \quad \forall i \neq j. \quad (\text{C.3})$$

For the derivation of the diagonalization gauge it is instructive to rewrite the SPF EOM (2.56) as

$$i\partial |\varphi_j(t)\rangle = i\partial |\varphi_j^{(0)}(t)\rangle + \hat{P}(t)\hat{g} |\varphi_j(t)\rangle \quad (\text{C.4})$$

where  $i\partial |\varphi_j^{(0)}(t)\rangle$  denotes the time derivative of the  $j$ th SPF in standard gauge, i.e., for  $\hat{g} = 0$ , as given by Eq. (2.61). Inserting Eq. (C.4) into Eq. (C.3) yields<sup>2</sup>

$$\partial_t O_{jk} = \langle \partial_t \varphi_j | \hat{O} | \varphi_k \rangle + \langle \varphi_j | \hat{O} | \partial_t \varphi_k \rangle \quad (\text{C.5})$$

$$= \langle \partial_t \varphi_j^{(0)} | \hat{O} | \varphi_k \rangle + \langle \varphi_j | \hat{O} | \partial_t \varphi_k^{(0)} \rangle + i \langle \varphi_j | \hat{g}^\dagger \hat{P}^\dagger \hat{O} | \varphi_k \rangle - i \langle \varphi_j | \hat{O} \hat{P} \hat{g} | \varphi_k \rangle$$

$$\stackrel{\hat{g}^\dagger = \hat{g}}{\stackrel{\hat{P}^\dagger = \hat{P}}{=}} \langle \dot{\varphi}_j^{(0)} | \hat{O} | \varphi_k \rangle + \langle \varphi_j | \hat{O} | \dot{\varphi}_k^{(0)} \rangle + i \langle \varphi_j | \hat{g} \hat{P} \hat{O} | \varphi_k \rangle - i \langle \varphi_j | \hat{O} \hat{P} \hat{g} | \varphi_k \rangle$$

$$= \langle \dot{\varphi}_j^{(0)} | \hat{O} | \varphi_k \rangle + \langle \varphi_j | \hat{O} | \dot{\varphi}_k^{(0)} \rangle + i \sum_{\ell=1}^m \frac{\langle \varphi_j | \hat{g} | \varphi_\ell \rangle}{g_{j\ell}} \frac{\langle \varphi_\ell | \hat{O} | \varphi_k \rangle}{O_{\ell k} = \delta_{\ell k} O_{kk}}$$

$$- i \sum_{\ell=1}^m \frac{\langle \varphi_j | \hat{O} | \varphi_\ell \rangle}{O_{j\ell} = \delta_{j\ell} O_{jj}} \frac{\langle \varphi_\ell | \hat{g} | \varphi_k \rangle}{g_{\ell k}}$$

$$= \langle \partial_t \varphi_j^{(0)} | \hat{O} | \varphi_k \rangle + \langle \varphi_j | \hat{O} | \partial_t \varphi_k^{(0)} \rangle + i g_{jk} O_{kk} - i g_{jk} O_{jj} = 0 \quad (\text{C.6})$$

<sup>1</sup>It should be noted that the following deductions are compatible with traditional MCTDH as well.

<sup>2</sup>Omitting the time argument in the following for the sake of readability.

such that the constraint operator reads

$$g_{jk} = i \frac{\langle \hat{\varphi}_j^{(0)} | \hat{O} | \varphi_k \rangle + \langle \varphi_j | \hat{O} | \hat{\varphi}_k^{(0)} \rangle}{O_{kk} - O_{jj}}. \quad (\text{C.7})$$

The diagonal elements of  $\hat{g}$  remain undetermined and can be set to arbitrary real values, e.g.,  $g_{jj} = 0$  or  $g_{jj} = h_{jj}$ . Again, as in Appendix B, the constraint operator has to be regularized in order to avoid singularities in case of degenerate eigenvalues of  $\hat{O}$ . This can be achieved in the same manner as for the natural orbital gauge by replacing

$$\frac{1}{O_{jj} - O_{kk}} \rightarrow \frac{O_{jj} - O_{kk}}{(O_{jj} - O_{kk})^2 + \varepsilon \exp\left(-\frac{1}{\varepsilon}(O_{jj} - O_{kk})^2\right)} \quad (\text{C.8})$$

where  $\varepsilon$  is a small regularization parameter. Analogously, the off-diagonal elements of the constraint operator for imaginary time propagation are given by

$$g_{jk}^{\text{relax}} = \frac{\langle \hat{\varphi}_j^{(0)} | \hat{O} | \varphi_k \rangle + \langle \varphi_j | \hat{O} | \hat{\varphi}_k^{(0)} \rangle}{O_{jj} - O_{kk}}. \quad (\text{C.9})$$

Instead of demanding that the off-diagonal of the one-body operator  $\hat{O}$  in SPF representation strictly vanish, one can also demand that they decay over time, e.g., exponentially. This is helpful when starting with a state whose SPFs do not diagonalize  $\hat{O}$  or to recover from the errors introduced by the regularization.<sup>3</sup> By introducing a parameter  $c$  that determines the decay rate of the off-diagonal elements of  $\hat{O}$ , a modified constraint operator can be derived<sup>4</sup>:

$$\begin{aligned} \partial_t O_{jk} &= \langle \partial_t \varphi_j^{(0)} | \hat{O} | \varphi_k \rangle + \langle \varphi_j | \hat{O} | \partial_t \varphi_k^{(0)} \rangle + i g'_{jk} O_{kk} - i g'_{jk} O_{jj} = c O_{jk} \quad \forall j \neq k \\ \Leftrightarrow g'_{jk} &= i \frac{\langle \partial_t \varphi_j^{(0)} | \hat{O} | \varphi_k \rangle + \langle \varphi_j | \hat{O} | \partial_t \varphi_k^{(0)} \rangle}{O_{kk} - O_{jj}} + \frac{ic O_{jk}}{O_{kk} - O_{jj}} = g_{jk} + \frac{ic O_{jk}}{O_{kk} - O_{jj}}. \end{aligned} \quad (\text{C.10})$$

The corresponding constraint operator for imaginary time propagation reads

$$g'_{jk, \text{relax}} = g_{jk}^{\text{relax}} + \frac{c O_{jk}}{O_{jj} - O_{kk}}. \quad (\text{C.11})$$

---

<sup>3</sup>We applied this approach when investigating whether different gauges can improve the dynamical pruning approach proposed in Ref. [FK1] by yielding a more sparse coefficient vector. For this purpose it is not necessary that the SPFs exactly match the eigenfunctions of  $\hat{O}$ .

<sup>4</sup>It should be noted that a similar derivation can be performed for the natural orbital gauge.

# Acknowledgements

Pursuing my PhD has been a long and challenging journey, but it was also very rewarding and fulfilling. I would not want to miss this experience for anything in the world. I am filled with tremendous gratitude for the incredible people who have made this quest possible and enjoyable.

First and foremost, I would like to express my deepest appreciation for my supervisor Prof. Dr. Peter Schmelcher. Thank you for giving me the opportunity to pursue my PhD in your research group but also for your unwavering guidance, support, and mentorship throughout the years. Your expertise and insights have been invaluable, and I am grateful for your encouragement to follow my own ideas.

I am also immensely thankful to the entire research group. Your camaraderie and the vibrant atmosphere you created made my time in the group truly joyful. The countless discussions and conversations, often leading to prolonged coffee breaks, were not only intellectually stimulating but also a source of inspiration. I want to extend special thanks Dr. Rick Mukherjee for all his (life) advice and reigniting my curiosity and passion for physics as well as for helping to push the spin project much further than anticipated. Hopefully, we will be able to continue our collaboration in the future. Prof. Dr. Hans-Dieter Meyer shared his incredibly deep knowledge of numerical methods and [ML-MCTDH](#) with me on numerous occasions, and I am grateful for his advice and support. Furthermore, I want to thank Dr. Maxim Pyzh, Dr. Rick Mukherjee, Friethjof Theel, Daniel Bosworth and my brother Daniel for proofreading this thesis and providing valuable feedback.

Beyond the academic realm, I owe a profound debt of gratitude to my family. They have been a constant source of support and allowed me to pursue my dreams and receive such a great education. To my life companion, Erica, your presence in my life truly has been a blessing. Thank you for your patience, understanding, and encouragement.

To everyone who has played a part, no matter how big or small, in my journey towards this achievement, I am deeply grateful. This thesis would not have been possible without your collective contributions, encouragement, and belief in my potential. Thank you all from the bottom of my heart.



# Eidesstattliche Versicherung/Declaration on Oath

Hiermit versichere ich an Eides statt, die vorliegende Dissertationsschrift selbst verfasst und keine anderen als die angegebenen Hilfsmittel verwendet zu haben.

*Hamburg, den 5.9.2023*



---

Fabian Köhler